DISCOVERY OF PROTEINS AND PATHWAYS CONTRIBUTING TO TDP-43-MEDIATED NEURODEGENERATION IN A NOVEL TRANSGENIC MOUSE MODEL OF DISEASE.

MACQUARIE
University

Hossai Gul

A Thesis in the Field of Biomedical Science

for the Degree of Master of Research in Neurobiology

Macquarie University

Supervisor:

Dr. Adam Walker

Centre for MND Research

Department of Biomedical Sciences

Faculty of Medicine and Health Sciences

November 2017

Abstract

Background

Motor neuron disease (MND)/amyotrophic lateral sclerosis (ALS) is an incurable and fatal neurodegenerative disease caused by progressive loss of motor neurons controlling movement. The main pathology exhibited by 97% of ALS cases is the aggregation of the RNA/DNA-binding protein TDP-43 within the cytoplasm of affected neurons. Although ALS pathology is characterised by TDP-43 accumulation, it is not understood how this dysfunction causes disease, meaning that it has not been possible to design disease-modifying therapeutics. To combat this issue, a new transgenic mouse model was created to develop the disease as presented in humans which exhibits both pathology as well as a disease phenotype very similar to human ALS.

Methods

Using the new transgenic mouse model, a large-scale advanced quantitative mass spectrometry (SWATH-MS) study was performed to discover the protein changes involved in TDP-43-mediated pathogenesis. Mass spectrometry results were analysed using several methods ranging from singular protein analysis (Uniprot), to comprehensive analyses (Ingenuity Pathway Analysis). Quantitative immunoblotting and immunofluorescence was used to validate mass spectrometry results.

Results

Identified the proteins and pathways which changed during disease course within rNLS TDP-43 mice model of ALS. Two key proteins, COQ9 and IMA3, which are involved in known mechanisms of ALS pathogenesis were validated using immunoblotting. In addition, the canonical pathways, upstream regulators and biological

function involved in rNLS TDP-43 pathology were comprehensively identified. This study provides important insights into TDP-43-mediated ALS neurodegeneration.

Conflict of interest

The author declares no competing conflicts of interest, financial or otherwise, while conducting this study.

Declaration of originality

I declare that the thesis titled *"Discovery of proteins and pathways contributing to TDP-43-mediated neurodegeneration in a novel transgenic mouse model of disease"* has not been submitted for a degree in any other university or institution other than Macquarie University. I would like to acknowledge the following assistance with the study outlined in this thesis:

- The protein extraction for the initial proteomics and some validations studies were conducted by Dr. Prachi Mehta
- The proteomics was conducted at the Australian Proteomic Analysis Facility under Assoc. Prof. Mark Molloy and Dr. Christoph Krisp
- Tissue extraction was conducted with assistance of Dr. Adam Walker and Dr. Sheng Le

All other project design, experiments, analyses, and subsequent writing of this thesis was conducted by me.

Hossai Gul

Student number 43899218

9th Nov 2017

Research outputs arising from this work

DISCOVERY OF PROTEINS AND PATHWAYS CONTRIBUTING TO TDP-43-MEDIATED NEURODEGENERATION IN A NOVEL TRANSGENIC MOUSE MODEL OF DISEASE.

Gul H[1], Mehta P[1], Hedl T[1], Le S[1], Wright A[1], Berning B[1], Riddell W[1], Lee A[1], Krisp C[2], Molloy MP[2], Walker AK[1].

1. Centre for MND Research, Department of Biomedical Sciences, Macquarie University, NSW, Australia. 2. Australian Proteome Analysis Facility, Macquarie University, NSW, Australia.

Accepted for poster presentation at following conferences:

1. **3rd Proteostasis and Disease Symposium**, Nov 2017, Wollongong, Australia

2. **37th Annual Meeting of the Australasian Society for Neuroscience (ANS)**, Dec 2017, Sydney, Australia

Table of Contents

List of Tables

List of Figures

1. INTRODUCTION

Amyotrophic lateral sclerosis (ALS) is a progressive neurodegenerative motor neuron disorder that affects the brain and spinal cord resulting in neuronal cell death and muscular paralysis. The life time risk of ALS is approximately 1 in 400 with average survival of 3-5 years from symptom onset [1, 2]. The main cause of death is muscle weakness within the diaphragm leading to respiratory failure [3]. The disease is foremost categorised into two main forms, sporadic ALS (sALS) and familial ALS (fALS). Sporadic ALS (sALS) occurs in 95% of patients and is classified as having no family history of the disease, while 5% of patients with family history of ALS are assigned as fALS [4]. ALS incidence is predicted to increase, mainly due to better screening and aging populations [5, 6]. There is a sex difference in prevalence for sALS with a male to female ratio of almost 2:1, while no sex differences have been observed for fALS [2, 7].

1.1 Clinical features of ALS

The main clinical manifestation that differentiates ALS from other motor neuron diseases is the involvement of both upper motor neurons (brain) and lower (spinal cord) motor neurons and their subsequent dysfunction [7]. Clinical heterogeneity is a hallmark of ALS due to several factors: age of onset, sit of onset, rate of progression, and association of ALS with other conditions [8].

Age of Onset

The mean age of ALS onset is 65 years of age, however in less than 5% of cases onset occurs before the age of 30 and is known as juvenile ALS 9, 10. The younger onset of disease has a male predominance, and is divided into two subgroups of long survival (more than 5 years) and short survival (mean of 1.9 years) 10. Incidence under 40 years of age is 1.5/100,000 per year, and highest during the 60-79 age group with 10-15/100,000 per year as shown in population based studies 11. This age-related incidence curve suggests that ALS is dependent on both genetic and environmental risk factors that occur over time.

Site of Onset

ALS usually begins in one focal point within the body and progressively spreads throughout the motor system 8. This initial region of focality is known as the site of onset and is highly variable, occurring in any region of the neuroaxis 12. Site of onset is often used to classify patients, such as bulbar onset ALS or spinal onset ALS 13. The clinical features and pattern of disease progression is highly heterogeneous. For example, in spinal onset ALS, symptoms can initially present as muscle weakness in the focal point of a limb on one side of the body but eventually progresses to both sides, then to the bulbar region, and finally spread to the respiratory system (which is the main cause of death) 13. In contrast, the initial symptoms of bulbar onset ALS include slurred or slow speech (dysarthria) and limb symptoms can occur simultaneously or progressively within 1-2 years 13. A small portion of ALS patients present with respiratory weakness at onset without any limb or bulbar involvement 14, 15.

Upper and lower motor involvement

In conjunction with site of onset, the degree of upper motor neuron (UMN) and lower motor neuron (LMN) involvement presents yet another layer of heterogeneity to ALS. Due to the variable mixtures of UMN and LMN signs within ALS patients, it is believed that motor neuron involvement lies within a continuum 13. The most common motor phenotype (70-90%) is referred to as the classic ALS and it presents with predominate LMN signs and slight-to-moderate UMN signs as the disease progresses 8. Approximately 5-10% of ALS patients exhibit only LMN signs without any UMN involvement and are diagnosed as having progressive muscular atrophy (PMA) 16. Another LMN dominate variant of ALS is known as 'flail arm' or 'flail leg'17, 18. These patients present with symmetrical onset in either proximal upper limb (flail arm) or distal lower limb (flail leg) with UMN signs such as weakness in swallowing and diaphragm seen only late in disease 19, 20. In contrast to the LMN dominant variants of ALS, primary lateral sclerosis (PLS) patients exhibit pure UMN symptoms with only some patients developing classic ALS signs 21. PLS is also referred to as UMN-dominate (UMN-D) ALS and has different onset, sex ratio, and better prognosis compared to typical ALS 8, 21, 22.

The large variance in motor phenotype led to hypotheses that these motor neuron variants maybe distinct conditions to ALS. However, evidence from clinical and genetic studies show large overlap between these motor phenotype variants and ALS 23, 24. In addition, post-mortem pathological hallmarks of ALS, such as ubiquitinated inclusions, have been seen in PLS and PMA patients 13, 21. While these variants share hallmarks of

disease, it is vital to determine involvement of UMN and LMU for diagnosis and prognosis.

Rate of progression

In conjunction with the above mentioned clinical diversity, ALS is further differentiated by the rate of disease progression. While the average survival rate is approximately 3 years from symptom onset, there is a large variance in disease duration amongst individuals, ranging from several months to over a decade 25. Disease end-stage is generally marked by respiratory failure, however disease progression rates cannot be determined by testing respiratory function due to a lack of reliable, non-invasive measurement tools 26. As such other clinical features that have shown associations with disease rates are used for prognosis. For example, longer survival is linked with younger age of onset, UMN-D forms of ALS, and symmetrical patterns as seen in flail arm ALS 27. However, the greatest indicator of slow disease progression is a long interval between symptom onset and time of diagnosis because it is the only clinical feature that indicates overall disease progression 28. On the other hand, shorter survival is associated with cognitive impairment (e.g. executive dysfunction, rapid weight loss, and early involvement of the respiratory system 29-32.

1.2 ALS genetics

Many ALS genes and mutations have been identified, of those describe below are the top four genetic causes of ALS.

SOD1

Superoxide dismutase 1 (*SOD1)* was the first genetic cause of ALS identified in 1993 [33]. Since that time, more than 150 mutations have been discovered, covering every exon of the gene [34]. *SOD1* Mutations that have been proven to be the cause of ALS account for approximately 12% of fALS cases, and 1-2% of sALS cases [35]. Phenotypically, mutant SOD1 ALS cases present with variance in age of onset, disease progression, and severity of disease [36].

The SOD1 protein is a Cu, Zn superoxide dismutase cytoplasmic enzyme that is a scavenger of free radical superoxide (O_2^-) [37]. The exact causal mechanism of *SOD1*-associated ALS remains unknown, although evidence from transgenic *SOD1* mice support a toxic gain of function of SOD1 that increases the generation of damaging superoxide, leading to the development of motor neuron degeneration [38]. In addition, studies have linked *SOD1* mutations with many pathogenic pathways of ALS and other novel SOD1 functions such as glucose signalling and RNA-binding [36, 39, 40].

TARDBP

The first ALS-related mutations within the TAR DNA binding protein (*TARDBP*) gene was discovered in 2008 [41]. Currently, there are over 40 mutations reported with an

incidence rate of approximately 4-5% in fALS and up to 2% in sALS [36, 42]. The phenotypic features of of *TARDBP*-associated ALS cases are broad and indistinguishable compared to other forms of ALS [43]. Nevertheless, studies have reported some trends with respect to age of onset, level of upper and lower motor neuron involvement, and survival rates; though these are only present in aggregated cohorts of affected patients [44, 45].

TARDBP codes for the protein TAR DNA binding protein-43 (TDP-43) which is primarily a DNA-/RNA-binding protein [46]. TDP-43 is ubiquitously expressed within the nucleus of most cells but is also capable of translocating into the cytoplasm at times of increased activity and stress [47, 48]. Within the nucleus, TDP-43 regulates RNA splicing and microRNA biogenesis, and autoregulates TDP-43 protein levels by regulating the stability of its own RNA [49-51]. In ALS cases, TDP-43 protein translocates from the nucleus, is phosphorylated, ubiquitinated, and forms cytoplasmic inclusions that are the pathological hallmark of ALS [52]. However, the underlying mechanism by which the genetic mutations of *TARDBP* gene cause ALS pathogenesis is not yet known [53].

FUS

ALS mutations in fused in sarcoma (*FUS*) were discovered shortly after *TARDBP* finding as the FUS protein shares functional homology with TDP-43 [54]. Over 50 *FUS* mutation have been identified with a low incidence of approximately 4% of fALS cases, and less than 1% of sALS cases [55-57]. Clinical features of *FUS*-related ALS resemble other ALS of known and unknown genetics and are characterised with a wide range of age of onset, and disease duration [36].

The FUS protein is very similar to TDP-43 both in role and location: FUS is in the nucleus and is involved in RNA binding, splicing and transport [55, 56]. *FUS* mutations cause pathology in the form of FUS protein aggregates in the cytoplasm of neurons without the presence of TDP-43 and ubiquitin [58]. It is hypothesised that this may be due to FUS acting downstream of TDP-43 within the same pathway [59].

C9ORF72

Chromosome 9 open reading frame 72 (*C9ORF72*) is a hexanucleotide (GGGGCC) repeat expansion mutation within intron 1 of the C9ORF72 gene [60, 61]. The *C9ORF72* mutation is the most frequent cause of ALS, accounting for 40% of fALS cases and around 25% of sALS [62]. Many patients with these mutations in C9ORF72 have also been found in 25% of patients with FTD without signs of ALS [63]. A high percentage of *C9ORF72*associated ALS cases present with bulbar onset ALS compared to other genetically caused ALS subgroups [64].

C9ORF72-ALS inclusions include both ubiquitin and TDP-43 with both the loss- and gain-of function of the C9ORF72 protein proposed as possible pathological mechanisms [65]. Other pathogenic pathways related to C9ORF72 pathogenesis include - RNA toxicity which has been associated with nucleocytoplasmic trafficking defects and nuclear stress [65].

1.3 Molecular mechanisms of pathogenesis

ALS pathogenesis affects most cell processes. The proposed ALS pathogenic mechanisms within literature include: mitochondrial dysfunction, glutamate excitotoxicity, oxidative stress, impaired proteostasis, cytoskeletal and axonal transport dysfunction, neuroinflammation, RNA metabolism disruption, and nuclear transport alterations. Described below are the commonly studied pathogenic mechanisms.

Mitochondrial dysfunction

Mitochondria play an important role in several vital cellular processes, such as energy production, cellular respiration, and calcium homeostasis [66]. Additionally, mitochondria produce high amounts of reactive oxygen species (ROS) and can activate apoptosis via the caspase cascade by releasing cytochrome c into the cytoplasm [67]. Due to these functions, mitochondrial damage has been linked to many facets of ALS pathogenesis and other neurodegenerative diseases [66, 68].

Abnormalities in both mitochondrial morphology and biochemistry have been reported in ALS patients. Mitochondrial morphological changes have been observed within the skeletal muscle and spinal motor neurons of sALS and fALS patients and SOD1 mouse models [69-73]. These abnormalities include, the formation of vacuoles, disorganisation of cristae and membranes, fragmented networks, and dilated mitochondria [72, 74, 75].

The main mitochondrial biochemical changes include: 1) a decrease in ATP production, 2) imbalance of Ca^{2+} homeostasis, 3) altered mitochondrial transport along axons, 4) release of ROS into the cytoplasm, and 5) apoptosis triggering.

Glutamate excitotoxicity

Glutamate is an excitatory neurotransmitter that is produced in the presynaptic terminal [76]. During neurotransmission glutamate diffuses across the synaptic cleft and activates specific receptors on the dendrites of the postsynaptic motor neuron and generates action potentials [76]. The two most common glutamate receptors are α-amino-3-hydroxyl-5-methyl-4-isoxazole-propionate (AMPA) and N-methyl-D-aspartate (NMDA) [76, 77]. Activation of these receptors results in the depolarisation of the neuronal membrane, which in effect opens the voltage-dependent calcium ion channels, thus permitting the entry of Ca^{2+} into the cell [76, 78].

Once the neurotransmission process is complete, glutamate is cleared from the synaptic cleft by glial and neuronal cells that contain excitatory amino acid transporters (EAATs) [76, 78]. The concentration of glutamate within the synaptic cleft is regulated by its constant release and removal by EAATs to maintain a balance and avoid the excessive or extended activation of glutamate receptors which can lead to excitotoxicity [79]. However, within the motor cortex and spinal cord of ALS patients and SOD1 mouse models, there is a decrease in the astroglial EAAT isoform 2 (EAAT2) and glutamate is not rapidly cleared from the synaptic cleft [80-82]. This glutamate mediated excitotoxicity within neurons causes an increased influx of calcium and sodium ions, and leads to the formation of reactive oxygen species (ROS) [68, 82]. These intracellular shifts lead to enzymatic and mitochondrial damage and trigger biochemical pathways related to neuronal degeneration and apoptosis as seen in sporadic and familial ALS [83-86].

Oxidative stress

Normal oxygen metabolism results in the formation of reactive oxygen species as free radicals [87]. When the rate of ROS production is higher than the rate of ROS removal within a neuron, it leads to oxidative stress [68]. This build-up of ROS causes permanent damage to cell structure and function, leading to cell death [88]. This oxidative damage has been reported in biopsies of ALS cases, while elevated ROS was found in the cerebrospinal fluid (CSF), serum, and urine samples of ALS patients [89-91].

Oxidative stress can be caused by mutations in the SOD1 (the main intracellular antioxidant defence) gene altering SOD1 enzyme activity, and thus leading to cytotoxicity [88, 92]. However, ROS induced oxidative stress is not always linked with SOD1 mutation, it can be linked to other pathogenic mechanisms, such as glutamate excitotoxicity, mitochondrial dysfunction, and defective oxidative phosphorylation [82, 93, 94].

1.4 ALS proteomics

Proteomics have been widely used to understand the mechanisms of neurodegenerative diseases. A comparison of previous studies using proteomics to study ALS have been outlined in **Table 1.1**. This shows that most of the recent ALS proteomics studies have been performed using human post-mortem tissue, cell lines, or SOD1 mouse models (**Table 1.1**). There are no proteomic studies using TDP-43 mice models, despite TDP-43 pathology being a hallmark of most ALS cases[52]. The various methods and stages of using proteomics to study neurodegenerative diseases including the type of sample source used, proteomic techniques, the type of methods applied to analyse the proteomic data, and the type of methods used to validate proteomic data has been assessed and compared to the current study in section 5.2 of this thesis.

Table 1.1 A comparison of proteomic studies of ALS.

Tissue	Proteomic Technology	Bioinformatic Analysis	Validation	Findings	Year	Citation
Spinal cord *Human -post-mortem*	Fluorescent 2D-DIGE LC-MS/MS	Functional annotation (*Uniprot)*	Western immunoblotting	-Downregulation of ATP5D and calmodulin -Mitochondrial dysfunction in synaptic clefts may be involved in pathogenesis	2017	[95]
SH-SY5Y Neuroblastoma cell line *Human*	2D-DIGE LC-MS/MS	Enrichment analysis *(STRING)*	Western immunoblotting	-FUS interacting partners associated with multiple pathways -mRNA transport and stress granule regulations most important in ALS pathogenesis	2016	[96]
Neuronal cells N2A *Mouse*	Biotin-streptavidin pull down In-gel analysis LC-MS/MS	Enrichment analysis *(PANTHER)*	Western immunoblotting	-Common proteins involved in ALS congregate within a limited number of molecular pathways -FMRP an interactor of ATXN2, FUS, and TDP-43 can reverse pathogenic effects and is a potential therapeutic target for ALS	2016	[97]
Cerebrospinal fluid (CSF) *Human*	2D LC‑MS/MS	Functional annotation *(DAVID)*	Western immunoblotting	-GRIA4 expression may be related to ALS severity	2016	[98]

				-IGF-2 a possible biomarker of ALS		
Spinal cord *Human -post-mortem*	Matrix-assisted laser desorption/ionization (MALDI) imaging mass spectrometry (IMS)	Data processing statistical tests only	Western immunoblotting	-Reduction in truncated ubiquitin with grey matter of ALS patients -Region-specific change in protease activity	2013	99
Ventral root and Lumbar spinal cord *Mouse (Transgenic, human WT SOD1)*	LC-MS/MS	Data processing statistical tests only	Western immunoblotting	-Galectin-3 elevation in spinal cord shown in mice spinal cord, and in human spinal cord and CSF -Galectin-3 a potential biomarker for ALS	2010	100
Spinal cord *Mouse (G127X hSOD1 mutation)*	Fluorescent 2D-DIGE LC-MS/MS	Enrichment and network analysis *(IPA)*	Western immunoblotting	-Characterisation of ALS spinal cord proteome -Pathways and networks revealed	2009	101

Acronyms:
DIGE: Difference gel electrophoresis
LC-MS/MS: Liquid chromatography (LC) with mass spectrometry (MS)
ATP5D: ATP synthase subunit delta, mitochondrial
FUS: Fused in Sarcoma
FMRP: Fragile X mental retardation 1
ATXN2: Ataxin-2
GRIA4: Glutamate receptor 4
IGF-2: Insulin-like growth factor 2
TDP-43: TAR DNA-binding protein 43
CSF: Cerebrospinal fluid
WT: Wilde type
SOD1: superoxide dismutase 1

2. STUDY TOPIC AND AIMS

ALS is an incurable and fatal neurodegenerative disease as the early biochemical pathways and proteins involved in ALS onset and progression remain unclear. As such it has not been possible to design disease-modifying therapeutics [102, 103]. This is mainly because it is not possible to directly study, in biochemical detail, the brain and spinal cord of human patients in early stages of ALS. And until recently, there was also a lack of comparable *in vivo* animal models that develop the disease as presented in human patients [104-107]. To combat this issue, a new transgenic mouse model (named rNLS TDP-43 mice) was created to express the main pathological protein found in ALS patients, the RNA-binding protein TDP-43; these mice exhibit both pathology as well as a disease phenotype very similar to human ALS [108]. As such, it is now possible to investigate and identify the proteins and pathways involved in ALS onset and progression. To do this, a large scale proteomic study was undertaken to examine the protein changes within the cortex and spinal cord of diseased mice in comparison to control before symptom onset and during different stages of disease.

The *aim* of this study was to analyse and validate the proteomic data from the cortex and spinal cord of rNLS TDP-43 mice to identify the proteins and pathways involved in TDP-43-mediated pathogenesis. More specifically the study had the following aims:

Aim 1: Analyse proteomic data using *singular* bioinformatic analysis methods to narrow down key proteins for validation.

Aim 2: Validate the proteins selected using singular bioinformatic analyses.

Aim 3: Analyse proteomic data using *comprehensive* bioinformatic analysis methods to place proteomic data into biological context and select key pathways for validation.

Aim 4: Validate the proteins and pathways selected using comprehensive bioinformatic analyses.

3. METHODS AND MATERIALS

Experimental design

The experimental design within this study has been illustrated in **Figure 3.1**. Protein was extracted from the cortex and lumbar spinal cord of rNLS mice at 2-, 4-, and 6-week timepoints of disease. SWATH proteomics was conducted to identify and quantify protein changes between rNLS TDp-43 mice compared to control mice. The subsequent proteomic data was analysed via two methods: singular analyses and comprehensive analyses. Proteins were selected from each bioinformatic analysis method for validation by western blotting and immunofluorescence imaging.

Animal ethics

All studies involving mice were conducted in accordance to Macquarie University ethics protocols under two Animal Research Authority (ARA) approvals: ARA Reference Number 2016/026-2 and ARA Reference Number 2015/042-3.

Mice monitoring

Mice phenotype was monitored three times per week using a neurological scoring assessment that consisted of checking for hindlimb clasping and measuring weight.

Protein extraction

Bicarb (5x) buffer was added to the cortex and spinal cord tissue, sonicated and spun. The supernatant was the extracted soluble protein using for both mass spectrometry and western blotting. To measure the quantity of protein within the extract, a standard BCA assay was performed.

Western blotting

For western blotting 10ug of 1/10 dilution of the soluble bicarb protein fraction was loaded into 4–15% Criterion™ TGX™ Precast Midi Protein Gel (Bio-Rad). Gels were run for 1 hour at 120V. Transfers were conducted for 20 minutes using the Bio-Rad Transblot turbo system. Membranes were then blocked using LiCor Blocking buffer for 1 hour and subsequently incubated in primary antibody overnight. The next day, the membrane was washed with a series of 1x TBST and 1x TBS and incubated in secondary antibody for 2 hours, and the washes repeated. Blots were visualised using the LiCor Image Studio software using 2 different channels together with GAPDH and target (680 and 800 channels) and then re-probed for TDP-43 to confirm the genotype of the mice and show TDP-43 expression level difference.

Antibodies

The antibodies used in this study include: rabbit polyclonal anti-CNKR2 (Bioss), rabbit polyclonal anti-CHCHD2 (Bioss), rabbit polyclonal anti-COQ9 (Abcam), rabbit polyclonal anti-VADC (Bioss), rabbit polyclonal anti-IPO4 (Bioss), rabbit polyclonal anti-PCP (ProteinTech), rabbit polyclonal anti-EMB (ProteinTech).

Tissue staining

Paraffin-embedded tissue was deparaffinized in 100% xylene and hydrated through a series of ethanol washes (100%-70%) and then washed in 0.1M Tris. Slides were then heated with 1x citrate buffer in a microwave to reach 90-95C. Slides were washed again with 0.1M Tris buffer pH 7.6 for 5 minutes and blocked for 30 minutes (2% FBS in 0.1M Tris). Primary antibodies were applied to slides and incubated overnight. The next day slides were washed with 0.1M Tris buffer and blocked (2% FBS in 0.1M Tris) for 5

minutes. Secondary antibodies were applied, and slides incubated at room temperature for 2 hours. Finally slides were washed in 0.1M Tris buffer for 5 minutes (this was repeated 3 times). Imaging was conducted at 40x magnification, using the same exposure time for control and rNLS via the Zeiss Axiolmager upright fluorescence microscope.

Bioinformatic analyses

Singular analysis was conducted via UniProt database searching of each individual protein to identify functions. All other singular analysis was conducted using JVenn as reported in the results.

Comprehensive analyses were conducted using Ingenuity Pathway analysis- IPA (Qiagen). The analysis settings were as follows: reference set included genes only looking at both direct and indirect relationships, at the experimentally observed confidence level, and included human, mouse, and rate curations. The rational for each analysis has been reported alongside results.

Statistical analysis

All statistical analysis was carried out using GraphPad Prism version 7.02.

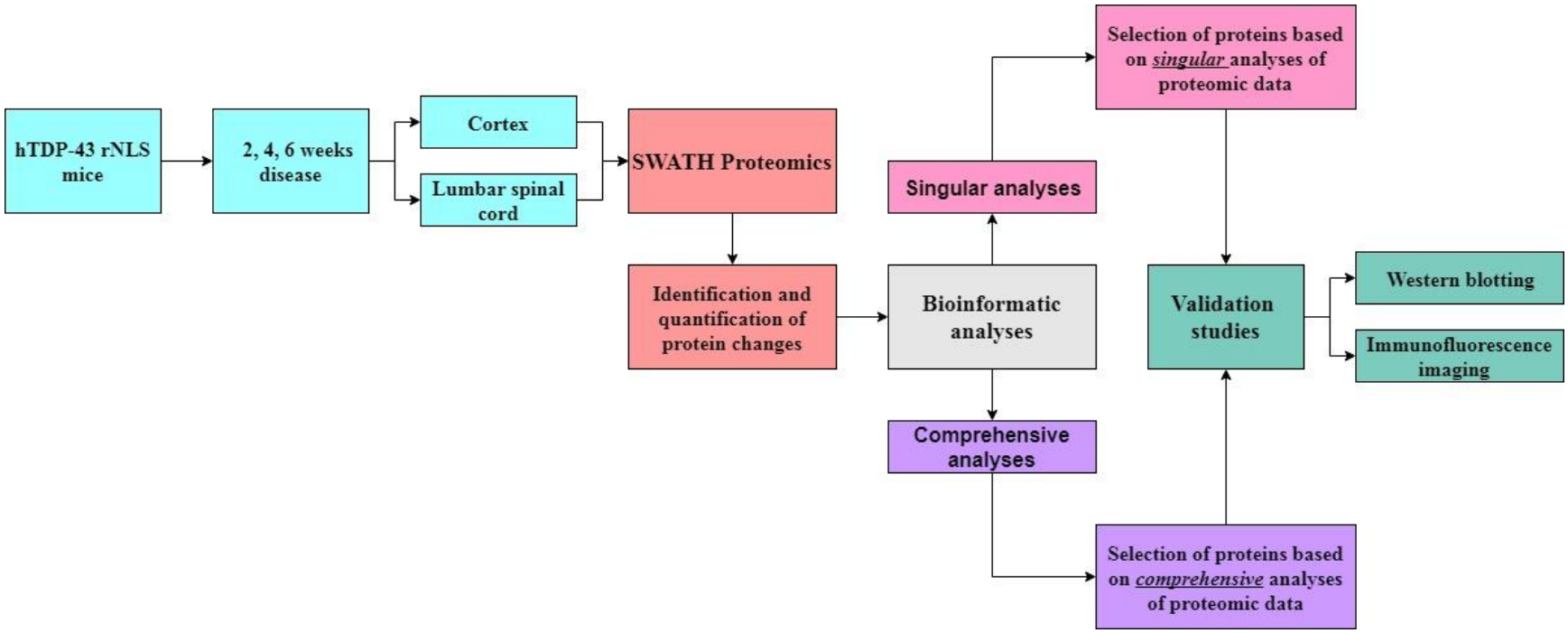

Figure 3.1 Pipeline for discovering proteins involved in TDP-43 pathogenesis.

Protein was extracted from the cortex and lumbar spinal cord of rNLS mice at several timepoints of disease (blue). SWATH proteomics was conducted to identify and quantify protein changes (red) between rNLS TDp-43 mice compared to control mice. The subsequent proteomic data was analysed via two methods: singular analyses (pink) and comprehensive analyses (purple). Proteins were selected from each bioinformatic analysis method for validation by western blotting and immunofluorescence imaging (green). Diagram illustrated using draw.io (https://www.draw.io/).

4. RESULTS

4.1 Identification of individual protein changes over disease course in the rNLS TDP-43 mouse model: Singular bioinformatic analysis

4.1.1 Large-scale proteomics on rNLS TDP-43 mice

TDP-43 inclusions are a hallmark of ALS pathology and are present in the brain and spinal cord of 97% of ALS cases[106]. A new TDP-43 mouse model (known as rNLS mice) has been generated which exhibits both pathology and phenotype resembling human ALS[108]. To investigate the proteins and pathways that drive TDP-43 pathology, prior to this thesis a large-scale proteomics study was conducted on the soluble protein extracts from the hippocampus, cortex, and spinal cord of the rNLS mice during several timepoints of disease (2 week – disease onset, 4 weeks – early-disease, and 6 weeks – mid-late-disease symptoms) alongside litter- and sex-matched non-transgenic control mice (Walker laboratory, unpublished data). SWATH MS resulted in the identification and quantification of >2500 proteins per timepoint for each anatomical region. Across all timepoints and regions, a total of 190 proteins were either significantly ($p<0.05$ or $q<0.1$) increased or decreased by ≥1.5-fold in rNLS mice compared to litter-matched, sex-matched and time-matched control mice (n=3-5) (**Appendix Table 1.1**). The first stage of this thesis project was the UniProt searching, analysis and interpretation following generation of the SWATH MS dataset, with the goal of identifying the most promising increased and decreased proteins for further study.

4.1.2 Individual functions of top altered proteins

The first aim was to determine the function(s) for each of the 190 proteins which changed across the three anatomical regions. This was done by searching within the UniProt[109] protein database using the codes generated by MS identification. This revealed that the changed proteins encompass a diverse range of functions and subcellular localisations (**Appendix Table 1.1**). The top 10 increased and decreased proteins for 2, 4, and 6-week timepoints within the cortex have been listed in **Tables 4.1.1-4.13.** These proteins are involved in various potential neurodegenerative- and ALS-related pathogenic mechanisms. For example, the top increased protein within the cortex at the 2-week timepoint (other than TDP-43) was DnaJ homolog subfamily B member 5-heat shock protein Hsp40-3 (DNJB5) which is involved in chaperone and unfolded protein binding[109]; whereas the top decreased at the same timepoint was SLIT-ROBO Rho GTPase-activating protein 3 (SRGP3) which is involved in negative regulation of cell migration and signal transduction[109] (**Table 4.1.1**).

Table 4.1.1 Top increased and decreased in the cortex at 2-week timepoint.

Protein was extracted from the cortex of rNLS mice at 2-week timepoint. SWATH MS was conducted (n=3-5 mice) to identify and quantify proteins that changed in TDP-43 mice compared to control non-bigenic mice. Proteins that were statistically significantly changed (q<0.1 or p<0.05, ≥1.5-fold-change) in 2-week cortex samples are shown Listed are the top increased (red) and decreased (green).

Protein ID (MOUSE)	Protein name	Fold change (disease/control)	p-value	q-value	Subcellular location	Uniprot functions summary	Uniprot code
TADBP	**TAR DNA-binding protein 43 (TDP-43)**	7.00	2.25E-06	2.60E-02	**Nucleus (mislocated to cytoplasm in rNLS mice)**	**DNA and RNA-binding protein which regulates transcription and splicing.**	**Q921F2**
DNJB5	DnaJ homolog subfamily B member 5 (Heat shock protein Hsp40-3)	2.92	7.47E-04	3.56E-02	Cytosol, Nucleus	Chaperone binding.	O89114
DHYS	Deoxyhypusine synthase (DHS)	2.83	2.40E-04	2.36E-02	Cytoplasm	Enzyme. Catalyses the NAD-dependent oxidative cleavage of spermidine to form the intermediate deoxyhypusine residue.	Q3TXU5
THEM6	Protein THEM6	2.34	1.88E-03	4.70E-02	Secreted	Function unknown.	Q80ZW2
LRC40	Leucine-rich repeat-containing protein 40	2.32	4.12E-04	2.93E-02	Membrane	Leucine-rich repeat-containing protein 40	Q9CRC8

ERGI1	Endoplasmic reticulum-Golgi intermediate compartment protein 1	2.06	5.26E-03	7.05E-02	Endoplasmic reticulum, Golgi intermediate compartment membrane	Possible role in transport between endoplasmic reticulum and Golgi.	Q9DC16
PLAK	Junction plakoglobin (Desmoplakin III)	2.04	7.97E-03	8.60E-02	Cell junction, adherens junction	Common junctional plaque protein.	Q02257
PLBL2	Putative phospholipase B-like 2	1.75	1.11E-03	4.09E-02	Lysosome lumen	Enzyme. Lipid catabolic process	Q3TCN2
MBB1A	Myb-binding protein 1A	1.71	2.27E-03	5.50E-02	Nucleolus, Cytoplasm	May activate or repress transcription via interactions with sequence specific DNA-binding proteins.	Q7TPV4
LYAG	Lysosomal alpha-glucosidase	1.69	8.66E-04	3.98E-02	Lysosome	Enzyme. Essential for the degradation of glycogen to glucose in lysosomes.	P70699
SRGP3	SLIT-ROBO Rho GTPase-activating protein 3 (srGAP3)	0.49	4.14E-04	2.86E-02	cytoplasm	GTPase-activating protein for RAC1 and perhaps CDC42, but not for RhoA small GTPase.	Q812A2
CHCH2	Coiled-coil-helix-coiled-coil-helix domain-containing protein 2	0.50	5.35E-04	2.78E-02	Nucleus, Mitochondrion	Transcription factor- binds to oxygen responsive element of COX4I2 and activates its transcription under hypoxia conditions.	Q9D1L0
PURB	Transcriptional activator protein Pur-beta	0.50	6.84E-05	1.77E-02	Nucleus	Transcriptional activator protein. Has capacity to bind repeated elements in single-stranded DNA.	O35295
STRBP	Spermatid perinuclear RNA-binding protein	0.50	7.51E-03	8.40E-02	Cytoplasm, cytoskeleton	Spermatid perinuclear RNA-binding protein	Q91WM1

KKCC2	Calcium/calmodulin-dependent protein kinase kinase 2 (CaM-KK 2)	0.51	2.52E-05	1.30E-02	Nucleus, Cytoplasm, Cell projection	May play a role in neurite growth. Isoform 2 may promote neurite elongation, while isoform 1 may promoter neurite branching. May be involved in hippocampal activation of CREB1.	Q8C078
DGKB	Diacylglycerol kinase beta	0.52	1.84E-03	4.64E-02	Cytoplasm	Enzyme. Exhibits high phosphorylation activity for long-chain diacylglycerols.	Q6NS52
VDAC3	Voltage-dependent anion-selective channel protein 3 (VDAC-3)	0.53	7.25E-03	8.42E-02	Mitochondrion outer membrane	Forms a channel through the mitochondrial outer membrane that allows diffusion of small hydrophilic molecules.	Q60931
CNKR2	Connector enhancer of kinase suppressor of ras 2	0.55	6.51E-03	7.82E-02	Cytoplasm, Membrane	May function as an adapter protein or regulator of Ras signalling pathways.	Q80YA9
SNP25	Synaptosomal-associated protein 25 (SNAP-25)	0.61	2.71E-03	5.56E-02	Cytoplasm, perinuclear region	t-SNARE involved in the molecular regulation of neurotransmitter release. May play an important role in the synaptic function of specific neuronal systems.	P60879
PLXA2	Plexin-A2 (Plex 2)	0.61	5.91E-03	7.59E-02	Cell membrane	Plays a role in axon guidance, invasive growth and cell migration.	P70207

At 4 weeks disease in cortex, dynactin subunit 6 (DCTN6) was the top increased protein and is involved in dynein (cellular transport protein) binding, while the top decreased protein was splicing factor 1 (SF01) and is part of the first step in mRNA splicing[109] (**Table 4.1.2**). At 6 weeks disease the top increased protein in the cortex was a protein of unknown function called UPF0600 protein C5orf51 homolog (CE051)[109] (**Table 4.1.3**). The second top increased protein was glial fibrillary acidic protein (GFAP) which is a cell-specific marker that distinguishes astrocytes from other glial cells, and increased levels indicate reactive astrogliosis[109]. The top decreased protein in the cortex at the 6-week timepoint was HECT, C2 and WW domain containing E3 ubiquitin-protein ligase 2 (HECW2), which is part of the proteasomal ubiquitin-dependent protein breakdown pathway[109] (**Table 4.1.3**).

Table 4.1.2 Top increased and decreased in the cortex at 4-week timepoint.

Protein was extracted from the cortex of rNLS mice at 4-week timepoint. SWATH MS was conducted (n=3-5 mice) to identify and quantify proteins that changed in TDP-43 mice compared to control non-bigenic mice. Proteins that were statistically significantly changed (q<0.1 or p<0.05, ≥1.5-fold-change) in cortex at 4-week samples are shown Listed are the top to increased (red) and decreased (green).

Protein ID (MOUSE)	Protein name	Fold change (disease/control)	p-value	q-value	Subcellular location	Uniprot functions summary	Uniprot code
DCTN6	Dynactin subunit 6	4.05	1.21E-03	3.21E-02	Cytoskeleton	May be involved in Dynein binding.	Q9WUB4
TADBP	**TAR DNA-binding protein 43 (TDP-43)**	3.96	1.08E-04	2.18E-04	**Nucleus (dissocialised into cytoplasm in rNLS mice).**	**DNA and RNA-binding protein which regulates transcription and splicing.**	**Q921F2**
CCD53	WASH complex subunit 3	3.80	1.38E-03	3.59E-02	Early endosome	Activity in recruiting and activating the Arp2/3 complex to induce actin polymerization. Regulation of the fission of tubules that serve as transport intermediates during endosome sorting.	Q9CR27
TY3H	Tyrosine 3-monooxygenase	2.79	1.96E-02	9.32E-02	Axon	Enzyme. Plays an important role in the physiology of adrenergic neurons.	P24529

PSME3	Proteasome activator complex subunit 3	2.65	6.57E-04	3.75E-02	Nucleus, Cytoplasm	Proteasome activator complex. proteasome regulator.	P61290
THEM6	Protein THEM6	2.63	8.80E-03	6.08E-02	Secreted	Function unknown.	Q80ZW2
GOT1B	Vesicle transport protein GOT1B (Golgi transport 1 homolog B)	2.53	1.28E-02	7.57E-02	Golgi apparatus membrane	May be involved in fusion of ER-derived transport vesicles with the Golgi complex.	Q9CR60
ASSY	Argininosuccinate synthase	2.11	1.59E-03	3.63E-02	Myelin sheath, extracellular exosome, mitochondrion	Enzyme. Involved in step 2 of the subpathway that synthesizes L-arginine.	P16460
GFAP	Glial fibrillary acidic protein	2.09	6.02E-03	4.82E-02	Cytoplasm	GFAP, a class-III intermediate filament, is a cell-specific marker that, during the development of the central nervous system, distinguishes astrocytes from other glial cells.	P03995
PLBL2	Putative phospholipase B-like 2	2.04	1.32E-02	7.61E-02	Lysosome lumen	Enzyme. Lipid catabolic process	Q3TCN2
SF01	Splicing factor 1	0.42	3.92E-03	4.12E-02	Nucleus	Necessary for the ATP-dependent first step of spliceosome assembly.	Q64213
AMPN	Aminopeptidase N	0.49	2.15E-02	9.66E-02	Membrane, Single-pass type II membrane protein	Enzyme. May be involved in the metabolism of regulatory peptides of neuropeptides.	P97449
RIMB2	RIMS-binding protein 2 (RIM-BP2)	0.51	1.41E-02	8.01E-02	Cell membrane, synapse	Plays a role in the synaptic transmission as bifunctional linker that interacts simultaneously with RIMS1, RIMS2, CACNA1D and CACNA1B.	Q80U40

DGKB	Diacylglycerol kinase beta	0.52	6.36E-03	5.18E-02	Cytoplasm	Enzyme. Exhibits high phosphorylation activity for long-chain diacylglycerols.	Q6NS52
SNP25	Synaptosomal-associated protein 25 (SNAP-25)	0.54	2.88E-03	4.05E-02	Cytoplasm, perinuclear region	t-SNARE involved in the molecular regulation of neurotransmitter release. May play an important role in the synaptic function of specific neuronal systems.	P60879
KPCB	Protein kinase C beta type (PKC-B)	0.54	7.98E-04	3.45E-02	Cytoplasm, cell membrane, nucleus	Enzyme. Protein kinase C. Depending on the cell type, is involved in many cell functions.	P68404
FAK1	Focal adhesion kinase 1 (FADK 1)	0.55	1.21E-04	1.96E-02	Cell junction, focal adhesion	Enzyme. Regulates axon growth and neuronal cell migration, axon branching and synapse formation; required for normal development of the nervous system.	P34152
PP2BB	Serine/threonine-protein phosphatase 2B catalytic subunit beta isoform	0.55	4.36E-03	4.09E-02	Calcineurin complex, cytosol	Enzyme. Calcium-dependent, calmodulin-stimulated protein phosphatase.	P48453
CNKR2	Connector enhancer of kinase suppressor of ras 2	0.55	1.33E-02	7.59E-02	Cytoplasm, Membrane	May function as an adapter protein or regulator of Ras signalling pathways.	Q80YA9
BRK1	Protein BRICK1	0.58	1.35E-02	7.69E-02	Cytoskeleton	Involved in regulation of actin and microtubule organization.	Q91VR8

Table 4.1.3 Top increased and decreased in the cortex at 6-week timepoint.

Protein was extracted from the cortex of rNLS mice at 6-week timepoint. SWATH MS was conducted (n=3-5 mice) to identify and quantify proteins that changed in TDP-43 mice compared to control non-bigenic mice. Proteins that were statistically significantly changed (q<0.1 or p<0.05, ≥1.5-fold-change) in 6-week cortex samples are shown Listed are the top to increased (red) and decreased (green).

Protein ID (MOUSE)	Protein name	Fold change (disease/control)	p-value	q-value	Subcellular location	Uniprot functions summary	Uniprot code
TADBP	**TAR DNA-binding protein 43 (TDP-43)**	3.92	4.71E-06	0	**Nucleus (dissocialised into cytoplasm in rNLS mice).**	**DNA and RNA-binding protein which regulates transcription and splicing.**	**Q921F2**
CE051	UPF0600 protein C5orf51 homolog	3.62	5.24E-04	6.33E-03	Unknown	Function unknown.	Q8BR90
GFAP	Glial fibrillary acidic protein	3.38	4.76E-04	5.20E-03	Cytoplasm	GFAP, a class-III intermediate filament, is a cell-specific marker that, during the development of the central nervous system, distinguishes astrocytes from other glial cells.	P03995

IFIT3	Interferon-induced protein with tetratricopeptide repeats 3 (IFIT-3)	3.35	1.60E-02	3.65E-02	Cytoplasm, Mitochondrion	Interferon-induced protein with tetratricopeptide repeats 3	Q64345
C1QA	Complement C1q subcomponent subunit A	3.28	4.18E-03	1.71E-02	Secreted	Complement activation pathway.	P98086
TPSN	Tapasin (TPN)	3.17	7.59E-03	2.37E-02	Endoplasmic reticulum membrane	Involved in the association of MHC class I with transporter associated with antigen processing (TAP) and in the assembly of MHC class I with peptide (peptide loading).	Q9R233
GOT1B	Vesicle transport protein GOT1B (Golgi transport 1 homolog B)	2.97	3.21E-02	6.87E-02	Golgi apparatus membrane	May be involved in fusion of ER-derived transport vesicles with the Golgi complex.	Q9CR60
VIME	Vimentin	2.30	9.23E-04	8.33E-03	Cytoplasm	Vimentin is attached to the nucleus, endoplasmic reticulum, and mitochondria, either laterally or terminally.	P20152
APOD	Apolipoprotein D	2.25	1.96E-03	9.92E-03	Secreted	Able to transport a variety of ligands in a number of different contexts.	P51910
HMGA1	High mobility group protein	2.20	1.28E-03	8.43E-03	Nucleus, Chromosome	Binds preferentially to the minor groove of A+T rich regions in double-stranded DNA.	P17095
HECW2	HECT, C2 and WW domain containing E3 ubiquitin-protein ligase 2	0.46	2.71E-02	5.89E-02	Cytoplasm	Enzyme. E3 ubiquitin-protein ligase that mediates ubiquitination of TP73.	Q6I6G8
FPPS	Farnesyl pyrophosphate synthase (FPP synthase)	0.48	3.65E-02	7.52E-02	Cytoplasm	Enzyme. Key enzyme in isoprenoid biosynthesis	Q920E5

KCC4	Calcium/calmodulin-dependent protein kinase type IV	0.49	5.62E-04	6.00E-03	Cytoplasm, Nucleus	Operates in the calcium-triggered CaMKK-CaMK4 signalling cascade and regulates, mainly by phosphorylation, the activity of several transcription activators.	P08414
VTI1B	Vesicle transport through interaction with t-SNAREs homolog 1B	0.50	1.55E-03	8.37E-03	Late endosome membrane	V-SNARE that mediates vesicle transport pathways through interactions with t-SNAREs on the target membrane.	O88384
KPCB	Protein kinase C beta type (PKC-B)	0.53	4.22E-06	0	Cytoplasm, cell membrane, nucleus	Enzyme. Protein kinase C. Depending on the cell type, is involved in many cell functions.	P68404
NSMA2	Sphingomyelin phosphodiesterase 3	0.53	1.90E-04	4.63E-03	Lipid-anchor in membranes	Enzyme. Involved in the pathway sphingolipid metabolism, which is part of Lipid metabolism.	Q9JJY3
CDS1	Phosphatidate cytidylyltransferase 1	0.53	3.08E-03	1.32E-02	Endoplasmic reticulum membrane	Enzyme. Provides CDP-diacylglycerol, an important precursor for the synthesis of phosphatidylinositol. May play an important role in the signal transduction mechanism of retina and neural cells.	P98191
KCNA1	Potassium voltage-gated channel subfamily A member 1 (MBK1)	0.53	6.79E-04	7.18E-03	Cell membrane, axon, dendrite, synapse	Contributes to the regulation of the membrane potential and nerve signalling, and prevents neuronal hyperexcitability.	P16388
MACD2	O-acetyl-ADP-ribose deacetylase MACROD2	0.54	4.34E-04	5.74E-03	Nucleus	Enzyme. Removes ADP-ribose from glutamate residues in proteins bearing a single ADP-ribose moiety.	Q3UYG8
PCP4	Calmodulin regulator protein PCP4 (Brain-specific antigen PCP-4)	0.55	3.95E-05	8.14E-03	Cytosol, nucleus	Probable regulator of calmodulin signalling. Maybe involved in synaptic plasticity.	P63054

At 2-week spinal cord timepoint, the only alteration within the proteome was the increase of 3 proteins (including TDP-43; over-expressed within rNLS mice) with no decreased proteins at more than 1.5-fold. The top increased protein was ubiquinone biosynthesis protein (COQ9) which is an essential mitochondrial lipid-soluble electron transporter for aerobic cellular respiration[109] (Table 4.1.4). At the 6-week timepoint, again only 3 proteins were increased including TDP-43, of the remaining two, the greatest increased was shown by myoglobin (MYG); an oxygen-binding protein which classically functions as an auxiliary supply of oxygen and enables the movement of oxygen within muscles[109] (Table 4.1.4). At the 6-week timepoint, 10 proteins were statistically significantly decreased at more than 1.5-fold, with the top decreased protein being ATPase inhibitor (ATIF1). ATIF1 limits ATP depletion when the mitochondrial membrane potential is no longer in a steady state (mitochondrial depolarisation)[109](Table 4.1.4).

Table 4.1.4 Protein changes within the spinal cord.

Protein was extracted from the spinal cord of rNLS mice at 2 and 6-week timepoints. SWATH MS was conducted (n=3-5 mice) to identify and quantify proteins that changed in TDP-43 mice compared to control non-bigenic mice. Proteins that were statistically significantly changed (q<0.1 or p<0.05, ≥1.5-fold-change) in spinal cord samples are shown. Red: increased; green: decreased.

Protein ID (MOUSE)	Protein name	Fold change (disease/control)	p-value	Subcellular location	Uniprot functions summary	Uniprot code
2 Weeks						
COQ9	Ubiquinone biosynthesis protein COQ9	4.30	7.58E-04	Mitochondrion	An essential lipid-soluble electron transporter for aerobic cellular respiration.	Q8K1Z0
TADBP	**TAR DNA-binding protein 43 (TDP-43)**	2.79	1.30E-03	**Nucleus (dissocialised into cytoplasm in rNLS mice).**	**DNA and RNA-binding protein which regulates transcription and splicing.**	**Q921F2**
MYEF2	Myelin expression factor 2 (MEF-2)	2.41	5.42E-03	Nucleus	Transcriptional repressor of the myelin basic protein gene (MBP).	Q8C854
6 weeks						
TADBP	**TAR DNA-binding protein 43 (TDP-43)**	2.62	5.30E-06	**Nucleus (dissocialised into cytoplasm in rNLS mice).**	**DNA and RNA-binding protein which regulates transcription and splicing.**	**Q921F2**

MYG	Myoglobin	2.14	8.61E-03	Extracellular exosome	Reserve supply of oxygen and facilitates the movement of oxygen within muscles.	P04247
VPS35	Vacuolar protein sorting-associated protein 35	1.58	2.99E-03	Cytoplasm	Vacuolar protein sorting-associated protein	Q9EQH3
ATIF1	ATPase inhibitor	0.57	3.88E-03	Mitochondrion	Limiting ATP depletion when the mitochondrial membrane potential falls below a threshold.	O35143
NFH	Neurofilament heavy polypeptide (NF-H)	0.58	1.79E-04	Cytoplasm	Important function in mature axons that is not subserved by the two smaller NF proteins.	P19246
PCP4	Calmodulin regulator protein PCP4 (Brain-specific antigen PCP-4)	0.58	6.09E-04	Cytosol, nucleus	Probable regulator of calmodulin signalling. Maybe involved in synaptic plasticity.	P63054
CHM4B	Charged multivesicular body protein 4b	0.60	3.46E-03	Cytosol, Late endosome membrane	Core component of the endosomal sorting.	Q9D8B3
EMB	Embigin	0.63	0.00174117	Cell membrane, synapse	Plays a role in the outgrowth of motoneurons and in the formation of neuromuscular junctions.	P21995
FPPS	Farnesyl pyrophosphate synthase (FPP synthase)	0.64	2.53E-05	Cytoplasm	Enzyme. Key enzyme in isoprenoid biosynthesis	Q920E5
SV2A	Synaptic vesicle glycoprotein 2A	0.64	9.13E-03	Cell junction, synapse	Plays a role in the control of regulated secretion in neural and endocrine cells, enhancing selectively low-frequency neurotransmission.	Q9JIS5
SYUA	Alpha-synuclein (Non-A beta component of AD amyloid)	0.65	6.79E-04	Cytoplasm › cytosol	May be involved in the regulation of dopamine release and transport.	O55042

DENR	Density-regulated protein (DRP)	0.66	1.50E-03	Translation initiation complex	May be involved in the translation of target mRNAs by scanning and recognition of the initiation codon.	Q9CQJ6
NFM	Neurofilament medium polypeptide (NF-M)	0.66	8.50E-04	Axon, myelin sheath, neurofilament	Neurofilament medium polypeptide	P08553

Hippocampus tissue was also analysed for two reasons: to optimise the initial protein extraction protocol using less-precious samples and to determine if over-expression of TDP-43 leads to proteome changes in non-cortical regions of the brain. Excluding TDP-43, SWATH MS showed only 29 proteins as increased or decreased within the hippocampus at any of the 3 timepoints analysed (2, 4 and 6 weeks), of which 22 proteins were changed at the relatively late stage of 6 weeks disease (**Appendix Table 1.1**). Due to the small number of changes and the minimal involvement of hippocampus within ALS disease, it has been excluded from further investigation within this study. However, it is noteworthy that the some of the proteins that were changed within the hippocampus were also changed within the cortex and spinal cord (**Table 4.1.5**). For example, heat shock protein 105 kDa (HS105), which prevents the aggregation of denatured proteins in cells under severe stress[109], was decreased at the 6-week timepoint in both the hippocampus and the cortex (**Table 4.1.5**). While calmodulin regulator protein (PCP4) was the only protein which overlapped across all 3 anatomical regions exhibiting a decrease at 6 weeks disease (**Table 4.1.5**).

Table 4.1.5 Protein changes in hippocampus that overlap with cortex and spinal cord.

Protein was extracted from the hippocampus, cortex, and spinal cord of rNLS mice at 2, 4 and 6-week timepoints. SWATH MS was conducted (n=3-5 mice) to identify and quantify proteins that changed in TDP-43 mice compared to control non-bigenic mice. Listed are all the proteins that were changed (q<0.1 or p<0.05, ≥1.5-fold-change) in the hippocampus that overlap with proteins that were also changed in the cortex or spinal cord. NC: no change, ND: not detected; red: increased; green: decreased.

Protein ID (MOUSE)	Protein name	Fold change (disease/control)								Subcellular location	Uniprot functions summary	Uniprot code
		Hippocampus			Cortex			Spinal cord				
		2 weeks	4 weeks	6 weeks	2 weeks	4 weeks	6 weeks	2 weeks	6 weeks			
DCLK1	Serine/threonine-protein kinase DCLK1	NC	NC	0.64	0.67	0.61	0.64	NC	NC	Postsynaptic density	Enzyme. May be involved in a calcium-signalling pathway controlling neuronal migration in the developing brain	Q9JLM8
DHB11	Estradiol 17-beta-dehydrogenase 11	NC	1.59	NC	NC	NC	1.59	NC	NC	Secreted, Cytoplasm	Enzyme. May participate in androgen metabolism during steroidogenesis.	Q9EQ06
GFAP	Glial fibrillary acidic protein	NC	NC	3.78	1.52	2.09	3.38	NC	NC	Cytoplasm	GFAP, a class-III intermediate filament, is a cell-specific marker that, during the development of the central nervous system, distinguishes astrocytes from other glial cells.	P03995

HS105	Heat shock protein 105 kDa (42 degrees C-HSP) (Heat shock 110 kDa protein)	NC	NC	0.63	NC	NC	0.63	NC	NC	Cytoplasm, Nucleus	Prevents the aggregation of denatured proteins in cells under severe stress.	Q61699
IP3KA	Inositol-trisphosphate 3-kinase A	NC	NC	0.46	NC	0.62	0.58	ND	ND	Dendritic spine	Enzyme. ATP + 1D-myo-inositol 1,4,5-trisphosphate = ADP + 1D-myo-inositol 1,3,4,5-tetrakisphosphate.	Q8R071
KPCB	Protein kinase C beta type (PKC-B)	NC	NC	0.55	0.64	0.54	0.53	NC	NC	Cytoplasm, cell membrane, nucleus	Enzyme. Protein kinase C. Depending on the cell type, is involved in many cell functions.	P68404
PCP4	Calmodulin regulator protein PCP4 (Brain-specific antigen PCP-4)	NC	NC	0.58	NC	NC	0.55	NC	0.58	Cytosol, nucleus	Probable regulator of calmodulin signalling. Maybe involved in synaptic plasticity.	P63054
PGM2L	Glucose 1,6-bisphosphate synthase	NC	NC	0.56		0.63		NC	NC	Cytosol	Enzyme. Glucose metabolism pathway.	Q8CAA7
PP2BA	Serine/threonine-protein phosphatase 2B catalytic subunit alpha isoform	NC	0.61	0.54	NC	0.66	0.64	NC	NC	Cell membrane, sarcolemma, nucleus	Enzyme. Calcium-dependent, calmodulin-stimulated protein phosphatase.	P63328
PP2BB	Serine/threonine-protein phosphatase 2B catalytic subunit beta isoform	NC	NC	0.57	NC	0.55	NC	NC	NC	Calcineurin complex, cytosol	Enzyme. Calcium-dependent, calmodulin-stimulated protein phosphatase.	P48453

SNP25	Synaptosomal-associated protein 25 (SNAP-25)	NC	0.49	NC	0.61	0.54	0.58	NC	NC	Cytoplasm, perinuclear region	t-SNARE involved in the molecular regulation of neurotransmitter release. May play an important role in the synaptic function of specific neuronal systems.	P60879
SRGP3	SLIT-ROBO Rho GTPase-activating protein 3 (srGAP3)	NC	0.53	NC	0.49	0.63	NC	NC	NC	cytoplasm	GTPase-activating protein for RAC1 and perhaps CDC42, but not for RhoA small GTPase.	Q812A2
TADBP	**TAR DNA-binding protein 43 (TDP-43)**	9.24	5.98	4.78	7.00	3.96	3.92	2.79	2.62	**Nucleus (mislocated to cytoplasm in rNLS mice)**	**DNA and RNA-binding protein which regulates transcription and splicing.**	**Q921F2**

4.1.3 Individual protein change patterns in rNLS mice during disease progression

The protein changes within the cortex (2, 4, 6 weeks disease) and spinal cord (2 and 6 weeks) were selected for singular bioinformatic analysis. Data for spinal cord at 4 weeks disease is currently being generated. Visualisation of the protein changes at all timepoints and regions revealed that there were more changed proteins in the cortex than the spinal cord (**Figure 4.1.1**). The number of proteins that were changed within cortex increased with disease progression, with most changes occurring at 6 weeks disease (115 proteins) (**Figure 4.1.1**). Excluding TDP-43, only 14 proteins changed within the spinal cord, of those 12 changes occurred at 6 weeks disease. Three proteins overlap both the cortex and spinal cord (excluding TDP-43 over-expression): calmodulin regulator protein (Purkinje cell protein-PCP4), Neurofilament medium polypeptide (NFM), and Farnesyl pyrophosphate synthase (FPPS) (**Table 4.1.6**)[109]. All three proteins decreased at 6 weeks disease within both regions and are involved in different functions as summarised in **Table 4.1.6**[109]. Despite the small number of proteins that were changed within the spinal cord (**Table 4.1.4**), the data has been included for further analysis within this study due to the important involvement of spinal cord motor neurons in ALS disease.

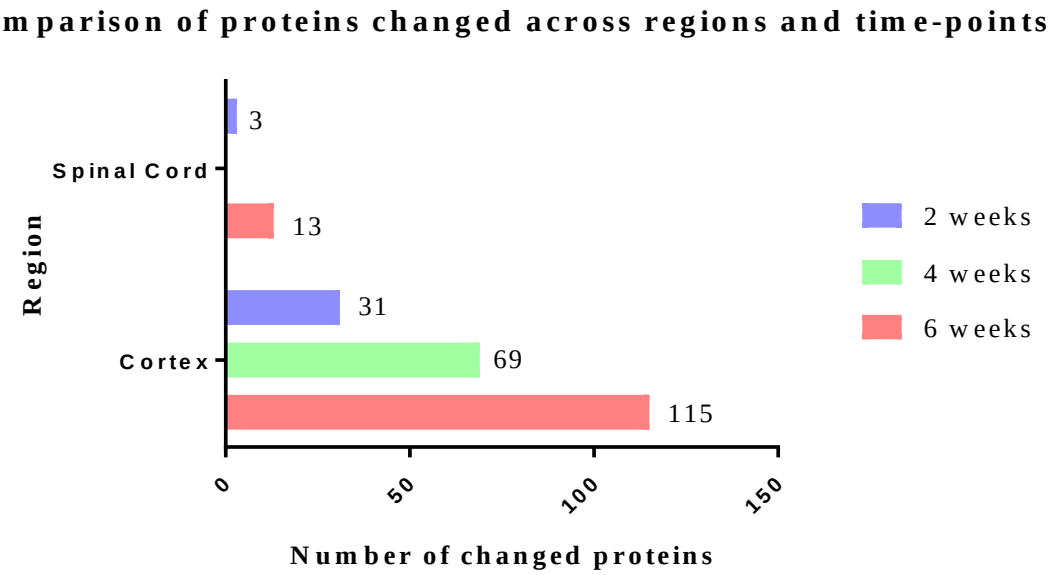

Figure 4.1.1 Most protein changes occur within the cortex of rNLS mice.

Protein was extracted from the cortex, and lumbar spinal cord of rNLS TDP43 mice and litter-, sex-, time-matched non-bigenic controls at 2, 4, and 6-week timepoints. SWATH MS was conducted (n=3-5 mice) to identify and quantify proteins that changed in rNLS mice compared to control. Proteins which showed a fold change which was determined to be significant ($p<0.05$ or $q<0.1$) were selected for singular analysis. When comparing the protein changes (increased and decreased) within each timepoint, most changes occur within the cortex. Data for spinal cord at 4 weeks disease is currently being generated. GraphPad Prism version 7.02 was used to generate graph.

Table 4.1.6 Changed proteins that overlap between cortex and spinal cord.

Protein was extracted from the cortex, and lumbar spinal cord of rNLS TDP43 mice and litter-, sex-, time-matched non-bigenic controls at 2, 4, and 6-week timepoints. SWATH MS was conducted (n=3-5 mice) to identify and quantify proteins that changed in rNLS mice compared to control. Within the list of changed proteins, three proteins overlapped between the cortex and spinal cord (excluding TDP-43). All three proteins have decreased at 6 weeks disease at both regions. Proteins that were statistically significantly changed (q<0.1 or p<0.05, ≥1.5-fold-change) at least one timepoint in both cortex and spinal cord are shown. Green: decreased, NC: no change.

Protein ID (MOUSE)	Protein name	Fold change (disease/control)					Subcellular location	Uniprot functions summary[109]	Uniprot code
		Cortex			Spinal cord				
		2 weeks	4 weeks	6 weeks	2 weeks	6 weeks			
FPPS	Farnesyl pyrophosphate synthase (FPP synthase)	NC	NC	0.48	NC	0.64	Cytoplasm	Enzyme. Key enzyme in isoprenoid biosynthesis	Q920E5
NFM	Neurofilament medium polypeptide (NF-M)	NC	NC	0.63	NC	0.66	Axon, myelin sheath, neurofilament	Neurofilament medium polypeptides which are involved in the maintenance of neuronal caliber.	P08553
PCP4	Calmodulin regulator protein PCP4 (Brain-specific antigen PCP-4)	NC	NC	0.55	NC	0.58	Cytosol, nucleus	Probable regulator of calmodulin signalling. Maybe involved in synaptic plasticity.	P63054

To determine the overlap between the changed proteins specifically within each region, JVenn[110] was used to examine any intersections. Not surprisingly, this revealed no overlap between the increased and decreased proteins within the cortex (**Figure 4.1.2**). Most protein changes occurred at 6 weeks disease with 67 increased proteins and 48 decreased proteins (**Figure 4.1.2**). The numbers of both increased and decreased protein changes were higher at later timepoints in disease progression. The number of increased proteins rose from 16 changes at 2 weeks disease, to 39 changes at 4 weeks disease, and 67 changes at 6 weeks disease (**Figure 4.1.2**). Similarly, with the decreased proteins, there are 15 proteins decreased at 2 weeks, 30 proteins decreased at 4 weeks, and 48 proteins decreased at 6 weeks disease (**Figure 4.1.2**). All proteins that changed at 2 and 4 weeks of disease, also changed at the 6-week timepoint in the cortex (**Figure 4.1.2**). The only exception was one protein that changed at both 2 and 4-week timepoint which *did not* change at the 6-week timepoint was SRGP3 (described above) (**Table 4.1.1**), which is important for early-stage disease. Most protein changes within the spinal cord occurred during week 6 and the only overlap between changed proteins across the two timepoints in the spinal cord was the increase in TDP-43, which is over-expressed in rNLS TDP-43 mice (**Figure 4.1.3**).

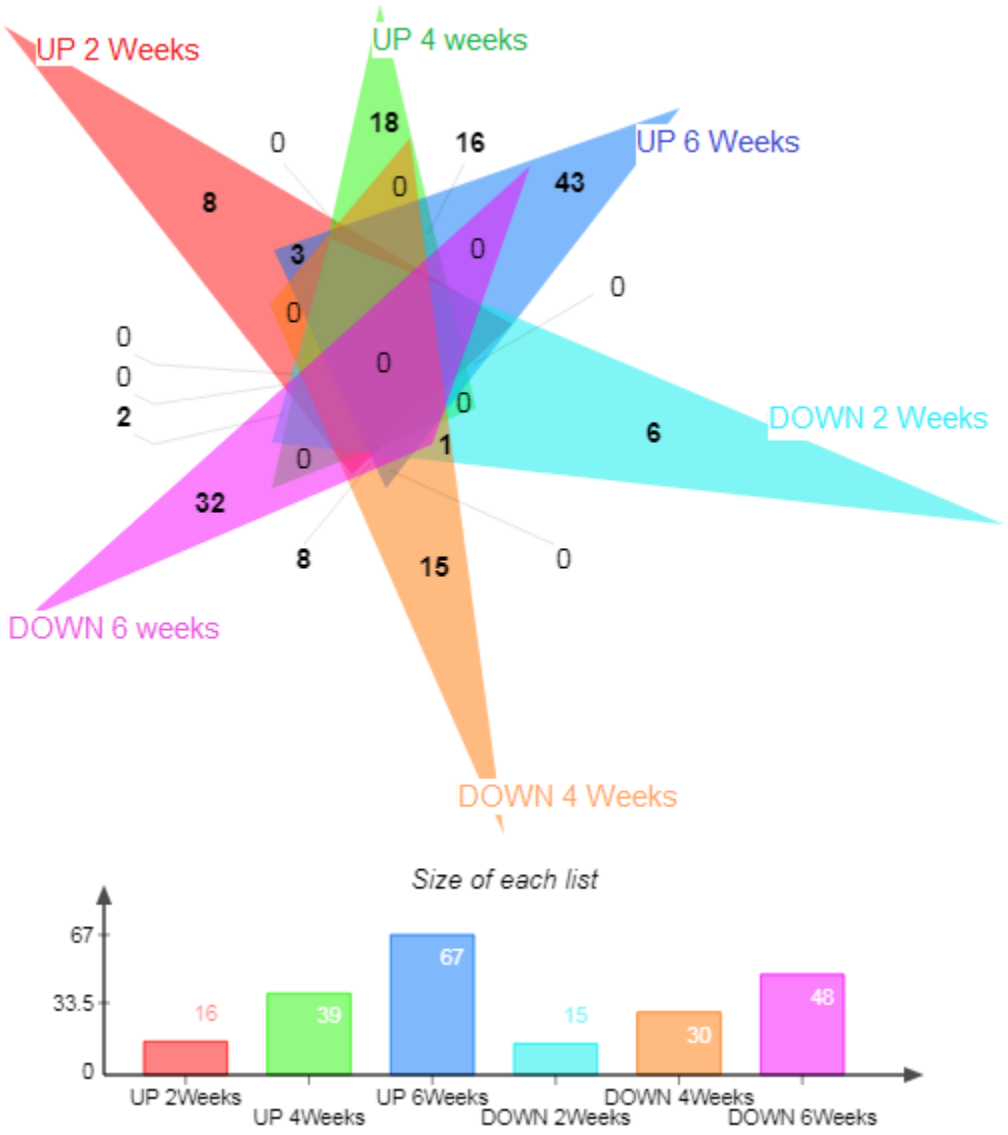

Figure 4.1.2 Comparison of the sets of proteins changed within the cortex at different time points.

Protein was extracted from the lumbar spinal cord of rNLS TDP43 mice and litter-, sex-, time-matched non-bigenic controls at 2, 4, and 6-week timepoints. SWATH MS was conducted (n=3-5 mice) to identify and quantify proteins that changed in rNLS mice compared to control. No protein changes overlap between increased and decreased at all timepoints. JVenn was used to generate diagram (http://jvenn.toulouse.inra.fr/app/index.html).

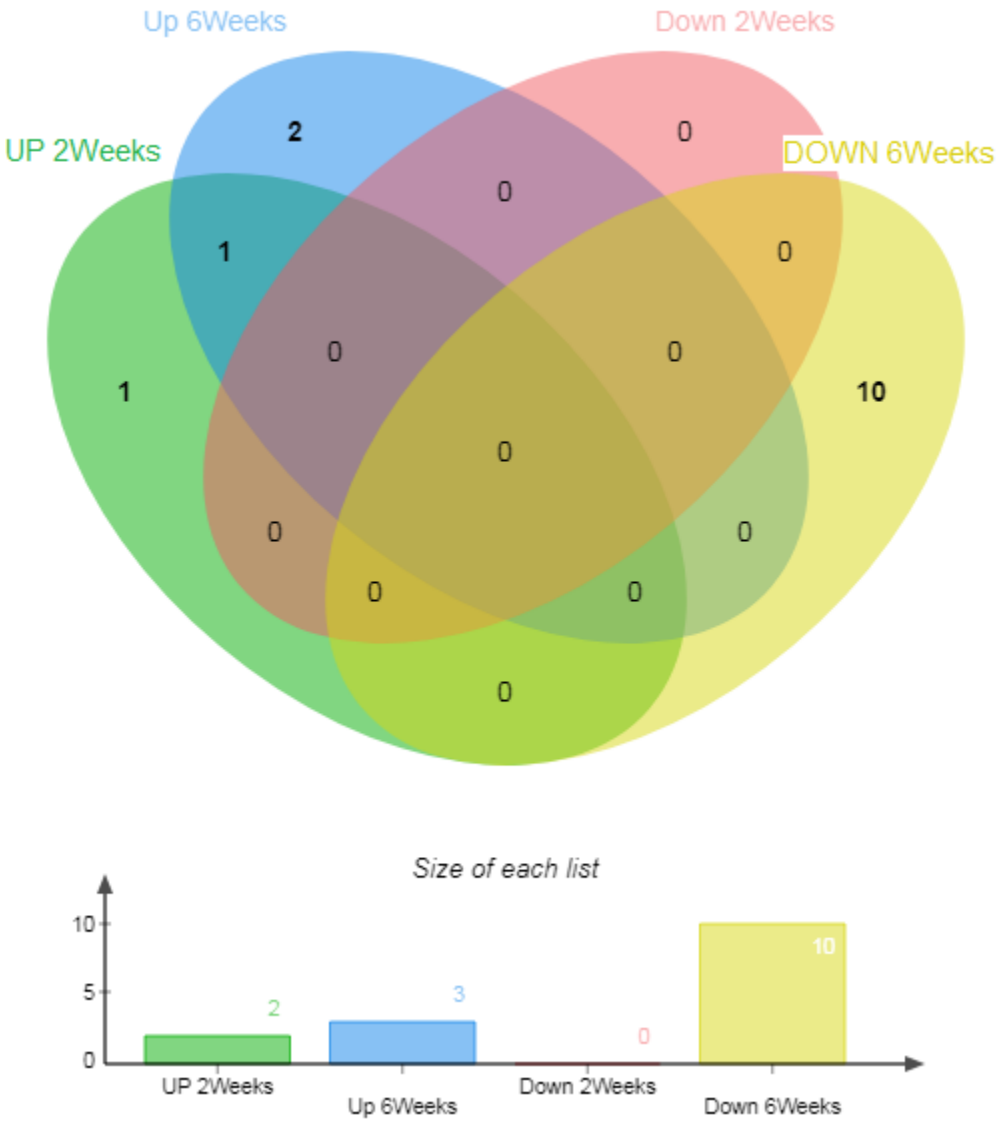

Figure 4.1.3 Comparison of the sets of proteins changed within the spinal cord at different time points.

Protein was extracted from the cortex of rNLS TDP43 mice and litter-, sex-, time-matched non-bigenic controls at 2, 4, and 6-week timepoints. SWATH MS was conducted (n=3-5 mice) to identify and quantify proteins that changed in rNLS mice compared to control. SWATH MS was conducted (n=3-5 mice) to identify and quantify proteins that changed in disease compared to control. No overlap between changed proteins at 2 weeks or 6 weeks disease at spinal cord. JVenn was used to generate diagram (http://jvenn.toulouse.inra.fr/app/index.html).

Due to most variations occurring within the cortex, the altered proteins were categorised into *increased* proteins and *decreased* proteins. JVenn[110] was used to gain additional insight into the overlap between the proteins within the two categories, and this revealed *four* main protein change patterns during disease progression. First, when analysing the *increased* proteins, five proteins overlapped across all timepoints within the cortex (**Figure 4.1.4**). Excluding TDP-43, the four overlapping *increased* proteins were Argininosuccinate synthase (ASSY), Putative phospholipase B-like 2 (PLBL2), Glial fibrillary acidic protein (GFAP), and Protein THEM6 (THEM6) (**Table 4.1.7**). ASSY and PLBL2 are enzymes; ASSY is involved in the synthesis of L-arginine, and PLBL2 is part of lipid catabolic pathway (**Table 4.1.7**)[109]. GFAP is a cell-specific marker that distinguishes astrocytes from other glial cells, and an increased level indicates astrogliosis in the rNLS TDP-43 mice, as previously demonstrated (**Table 4.1.7**)[108, 109]. THEM6 is a protein of unknown function reported in following section (**Table 4.1.11**)[109].

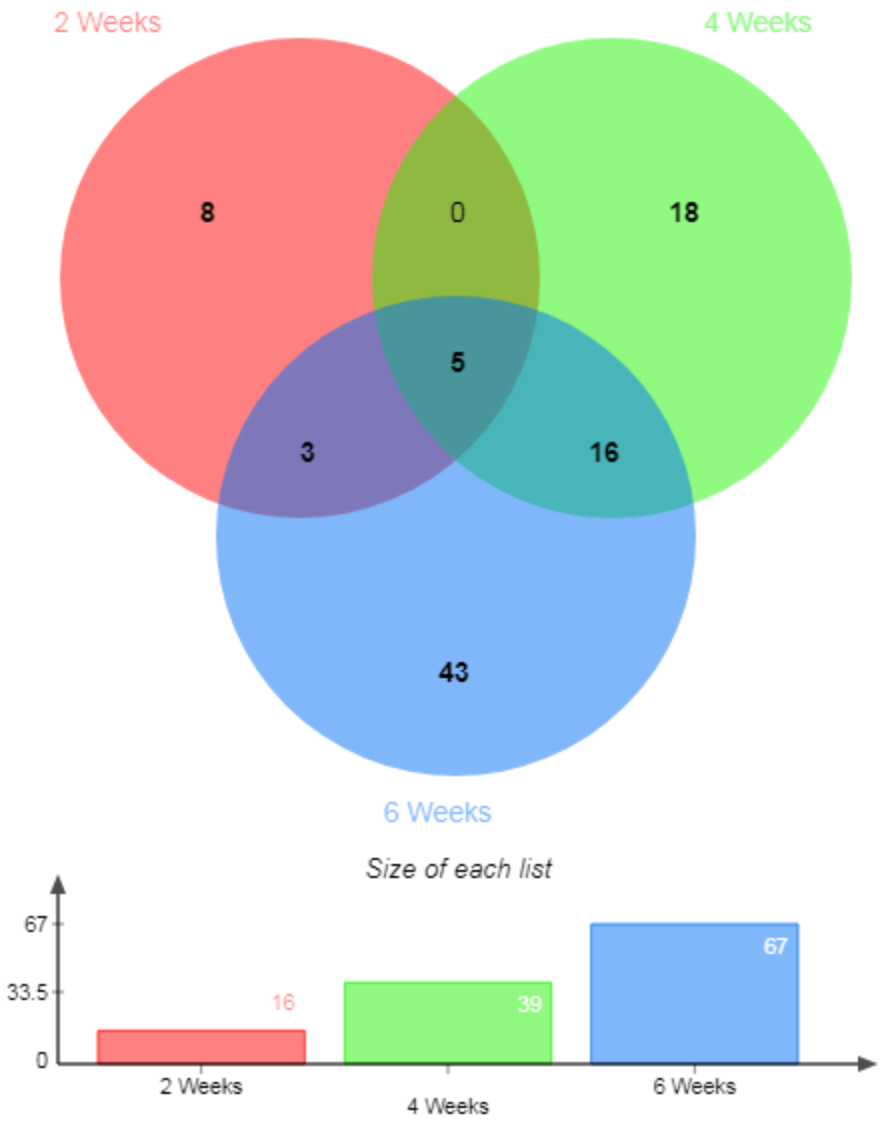

Figure 4.1.4 Overlap of increased proteins within the cortex.

Protein was extracted from the cortex of rNLS TDP43 mice and litter-, sex-, time-matched non-bigenic controls at 2, 4, and 6-week timepoints. SWATH MS was conducted (n=3-5 mice) to identify and quantify proteins that changed in rNLS mice compared to control. Five proteins increase across all timepoints while most proteins increase at 6 weeks disease. JVenn was used to generate diagram (http://jvenn.toulouse.inra.fr/app/index.html).

Table 4.1.7 Proteins increased at all timepoints within cortex.

Protein was extracted from the cortex of rNLS TDP43 mice and litter-, sex-, time-matched non-bigenic controls at 2, 4, and 6-week timepoints. SWATH MS was conducted (n=3-5 mice) to identify and quantify proteins that changed in rNLS mice compared to control. Five proteins increased across all timepoints within the cortex, including TDP-43 (over-expressed within rNLS mice). Red: decreased.

Protein ID (Mouse)	Protein name	Fold change			Subcellular location	Functions summary	Uniprot code
		Cortex					
		2 weeks	4 weeks	6 weeks			
ASSY	Argininosuccinate synthase	1.52	2.11	1.99	Myelin sheath, extracellular exosome, mitochondrion	Involved in step 2 of the subpathway that synthesizes L-arginine.	P16460
GFAP	Glial fibrillary acidic protein	1.52	2.09	3.38	Cytoplasm	A class-III intermediate filament, is a cell-specific marker that, during the development of the central nervous system, distinguishes astrocytes from other glial cells.	P03995
PLBL2	Putative phospholipase B-like 2	1.75	2.04	1.55	Lysosome lumen	Enzyme. Lipid catabolic process.	Q3TCN2
TADBP	**TAR DNA-binding protein 43 (TDP-43)**	7.00	3.96	3.92	**Nucleus (mislocalised into cytoplasm in rNLS mice).**	**DNA and RNA-binding protein which regulates transcription and splicing.**	**Q921F2**
THEM6	Protein THEM6	2.34	2.63	1.77	Secreted	Functions unknown.	Q80ZW2

Second, the analysis of the *decreased* proteins within the cortex revealed six proteins intersected across all time points (**Figure 4.1.5**). Three of these decreased proteins are the kinase enzymes Serine/Threonine-protein kinase (DCLK1), Diacylglycerol kinase beta (DGKB), and Protein kinase C beta type (PKC-B) (**Table 4.1.8**). These kinases are involved in distinct functions including calcium signalling of neuronal migration, phosphorylation of diacylglycerols, and oxidative stress-induced apoptosis respectively (**Table 4.1.8**)[109]. The remaining three overlapping *decreased* proteins were: coiled-coil-helix-coiled-coil-helix domain-containing protein 2 (CHCH2), connector enhancer of kinase suppressor of ras 2 (CNKR2), and synaptosomal-associated protein 25 (SNAP25) (**Table 4.1.8**)[109]. CHCH2 is a mitochondrial protein that acts as transcription factor in the nucleus under conditions of cellular stress, and which activates COX4I2 (Cytochrome c oxidase, the terminal oxidase in mitochondrial electron transport)[109] under hypoxia conditions (**Table 4.1.8**)[109]. CNKR2 may function as an adapter protein or regulator of Ras signalling pathways (**Table 4.1.8**)[109]. SNAP25 is a vesicle fusion meditator (with a targeted receptor associated with nerve terminal membranes)[111] that is involved in regulation of neurotransmitter release and may play a role in synaptic function of specific neurons (**Table 4.1.8**)[109].

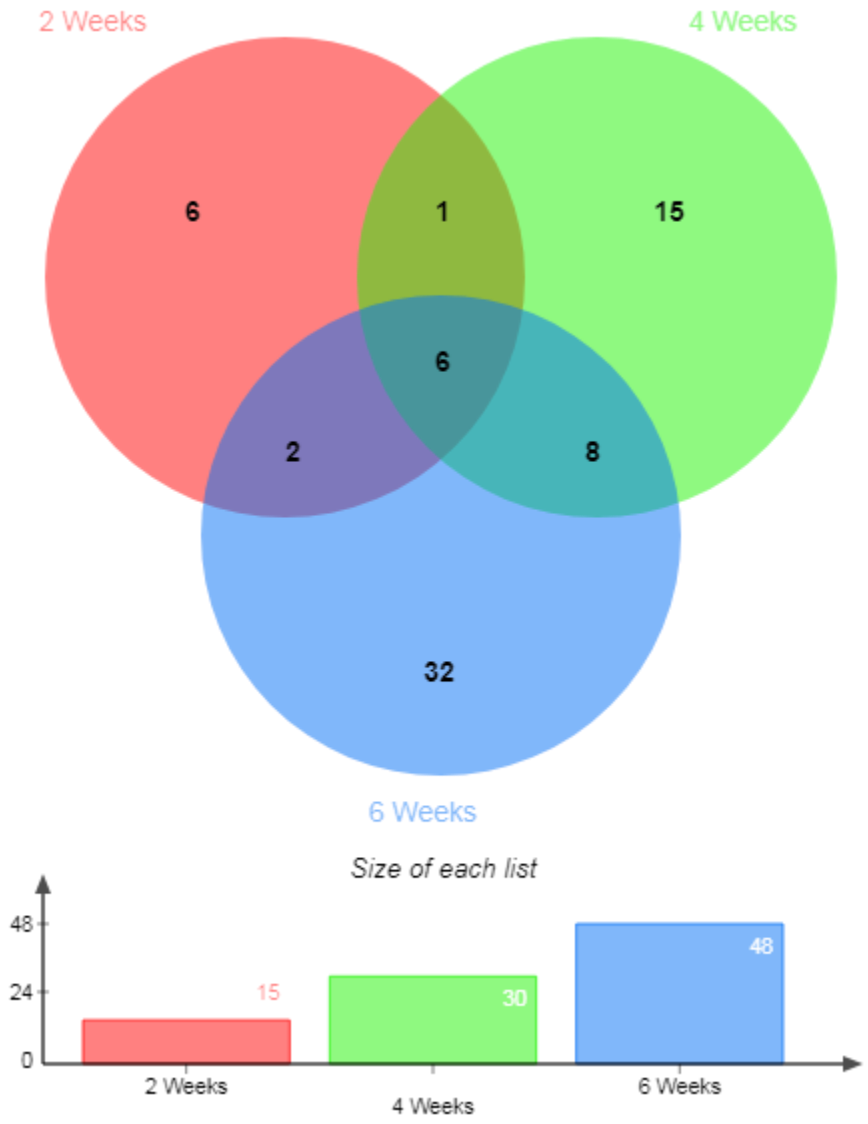

Figure 4.1.5 Overlap of decreased proteins within the cortex.

Protein was extracted from the cortex of rNLS TDP43 mice and litter-, sex-, time-matched non-bigenic controls at 2, 4, and 6-week timepoints. SWATH MS was conducted (n=3-5 mice) to identify and quantify proteins that changed in rNLS mice compared to control. Six proteins decrease across all timepoints while most proteins decrease at 6 weeks disease. JVenn was used to generate diagram (http://jvenn.toulouse.inra.fr/app/index.html).

Table 4.1.8 Proteins decreased at all time points within cortex.

Protein was extracted from the cortex of rNLS TDP43 mice and litter-, sex-, time-matched non-bigenic controls at 2, 4, and 6-week timepoints. SWATH MS was conducted (n=3-5 mice) to identify and quantify proteins that changed in rNLS mice compared to control. Six proteins decreased across all timepoints within the cortex. Green: decreased.

Protein ID (Mouse)	Protein name	Fold change (disease/control)			Subcellular location	UniProt functions summary[109]	Uniprot code
		Cortex					
		2 weeks	4 weeks	6 weeks			
CHCH2	Coiled-coil-helix-coiled-coil-helix domain-containing protein 2	0.50	0.63	0.64	Nucleus, Mitochondrion	Transcription factor- binds to oxygen responsive element of COX4I2 and activates its transcription under hypoxia conditions.	Q9D1L0
CNKR2	Connector enhancer of kinase suppressor of ras 2	0.55	0.55	0.67	Cytoplasm, Membrane	May function as an adapter protein or regulator of Ras signalling pathways.	Q80YA9
DCLK1	Serine/threonine-protein kinase DCLK1	0.67	0.61	0.64	Postsynaptic density	May be involved in a calcium-signalling pathway controlling neuronal migration in the developing brain.	Q9JLM8
DGKB	Diacylglycerol kinase beta	0.52	0.52	0.57	Cytoplasm	Enzyme. Exhibits high phosphorylation activity for long-chain diacylglycerols.	Q6NS52
KPCB	Protein kinase C beta type (PKC-B)	0.64	0.54	0.53	Cytoplasm, cell membrane, nucleus	Enzyme. Depending on the cell type, is involved in many cell functions.	P68404
SNP25	Synaptosomal-associated protein 25 (SNAP-25)	0.61	0.54	0.58	Cytoplasm, perinuclear region	t-SNARE involved in the molecular regulation of neurotransmitter release. May play an important role in the synaptic function of specific neuronal systems.	P60879

Third, within both the increased and decreased proteins of the cortex, five proteins demonstrated a 'change-skip-change' pattern whereby they displayed a change in 2 weeks disease, no change at 4 weeks disease, and change in 6 weeks disease (Table 4.1.9). Two proteins, calcium/calmodulin-dependent protein kinase kinase 2 (KKCC2) and voltage-dependent anion-selective channel protein 3 (VDAC3), showed a decrease-no change-decrease pattern across the three timepoints (Table 4.1.9). KKCC2 may play a role in neurite (axon or dendrite) growth, whereas VDAC3 is an outer mitochondrial membrane channel that allows the diffusion of small hydrophilic molecules (Table 4.1.9)[109]. In addition, three proteins, namely deoxyhypusine synthase (DHS), myb-binding protein 1A (MBB1A), and junction plakoglobin (PLAK) all displayed an increase-no change-increase pattern (Table 4.1.9). DHS is an enzyme that catalyses the oxidative cleavage of spermidine (numerous metabolic functions), MBB1A may be involved in the repression or activation of DNA-binding proteins, and PLAK is a cell junction protein involved in cell-to-cell communication (Table 4.1.9)[109].

Table 4.1.9 Proteins that exhibit a 'change-skip-change' pattern within cortex.

Protein was extracted from the cortex of rNLS TDP43 mice and litter-, sex-, time-matched non-bigenic controls at 2, 4, and 6-week timepoints. SWATH MS was conducted (n=3-5 mice) to identify and quantify proteins that changed in rNLS mice compared to control. Five proteins demonstrate a 'change-skip-change' pattern whereby change is seen in 2 weeks disease, no change (NC) at 4 weeks disease, and change again at 6 weeks disease. These proteins were either not detected or not changed within spinal cord. Green: decreased, red: increased.

Protein ID (Mouse)	Protein name	Fold change (disease/control)			Subcellular location	Uniprot functions summary[109]	Uniprot code
		Cortex					
		2 weeks	4 weeks	6 weeks			
KKCC2	Calcium/calmodulin-dependent protein kinase kinase 2 (CaM-KK 2)	0.51	NC	0.63	Nucleus, Cytoplasm, Cell projection	May play a role in neurite growth. Isoform 2 may promote neurite elongation, while isoform 1 may promote neurite branching. May be involved in hippocampal activation of CREB1.	Q8C078
VDAC3	Voltage-dependent anion-selective channel protein 3 (VDAC-3)	0.53	NC	0.61	Mitochondrion outer membrane	Forms a channel through the mitochondrial outer membrane that allows diffusion of small hydrophilic molecules.	Q60931
DHYS	Deoxyhypusine synthase (DHS)	2.83	NC	1.87	Cytoplasm	Enzyme. Catalyses the NAD-dependent oxidative cleavage of spermidine to form the intermediate deoxyhypusine residue.	Q3TXU5
MBB1A	Myb-binding protein 1A	1.71	NC	1.50	Nucleolus, Cytoplasm	May activate or repress transcription via interactions with sequence specific DNA-binding proteins.	Q7TPV4
PLAK	Junction plakoglobin (Desmoplakin III)	2.04	NC	1.53	Cell junction, adherens junction	Common cell junctional plaque protein.	Q02257

Lastly, the fourth pattern of protein change is in direct contrast with the *'change-skip-change'* pattern where the protein change occurs only at 4 weeks disease and no change is observed at 2 and 6-week timepoints. Thirty-two proteins showed the '*skip-change-skip*' pattern of change (**Table 4.1.10**). More specifically, 14 proteins exhibited the '*no change-decrease-no change*' pattern. For example, focal adhesion kinase 1 (FADK 1), which regulates axon growth and neuronal cell migration, was decreased at 4 weeks disease, but was unchanged at 2 and 6-week timepoints (**Table 4.1.10**)[109]. The remaining 18 proteins showed a '*no change-increase-no change*' pattern. For example, FUN14 domain-containing protein 1 and 2 (FUND1 and FUND2)-,which are involved in mitophagy (selective autophagy of damaged mitochondria), were increased at 4 weeks disease but were not changed during 2 and 6- timepoints (**Table 4.1.10**)[109]

Table 4.1.10 Proteins that exhibit a 'skip-change-skip' pattern within cortex.

Protein was extracted from the cortex of rNLS TDP43 mice and litter-, sex-, time-matched non-bigenic controls at 2, 4, and 6-week timepoints. SWATH MS was conducted (n=3-5 mice) to identify and quantify proteins that changed in rNLS mice compared to control. Thirty-two proteins demonstrate a 'skip-change-skip' pattern whereby no change (NC) is seen in 2 weeks disease, change at 4 weeks disease, and no change (NC) again at 6 weeks disease. These proteins were either not detected or not changed within spinal cord. Green: decreased, red: increased.

Protein ID (MOUSE)	Protein name	Fold change (disease/control)			Subcellular location	Functions summary	Uniprot code
		Cortex					
		2 weeks	4 weeks	6 weeks			
1433F	14-3-3 protein eta	NC	0.67	NC	Cytoplasm	Adapter protein implicated in the regulation of a large spectrum of both general and specialized signaling pathways.	P68510
AMPN	Aminopeptidase N	NC	0.49	NC	Membrane, Single-pass type II membrane protein	Enzyme. May be involved in the metabolism of regulatory peptides of neuropeptides.	P97449
BRK1	Protein BRICK1	NC	0.58	NC	Cytoskeleton	Involved in regulation of actin and microtubule organization.	Q91VR8
CA2D1	Voltage-dependent calcium channel subunit alpha-2/delta-1	NC	0.61	NC	Membrane	Activation/inactivation kinetics of the calcium channel.	O08532
FAK1	Focal adhesion kinase 1	NC	0.55	NC	Cell junction, focal adhesion	Enzyme. Regulates axon growth and neuronal cell migration, axon branching and synapse formation; required for normal development of the nervous system.	P34152
NOE1	Noelin (Neuronal olfactomedin-related ER localized protein)	NC	0.65	NC	Secreted, synapse, Endoplasmic reticulum, axon, Perikaryon	Contributes to the regulation of axonal growth in the embryonic and adult central nervous system by inhibiting interactions between RTN4R and LINGO1.	O88998

NPY	Pro-neuropeptide Y	NC	0.62		Secreted	NPY is implicated in the control of feeding and in secretion of gonadotrophin-release hormone.	P57774
PGM2L	Glucose 1,6-bisphosphate synthase		0.63		Cytosol	Enzyme. Glucose metabolism pathway.	Q8CAA7
PP2BB	Serine/threonine-protein phosphatase 2B catalytic subunit beta isoform	NC	0.55	NC	Calcineurin complex , cytosol	Enzyme. Calcium-dependent, calmodulin-stimulated protein phosphatase.	P48453
PSD3	PH and SEC7 domain-containing protein 3	NC	0.65	NC	Postsynaptic cell membrane	Guanine nucleotide exchange factor for ARF6.	Q2PFD7
RIMB2	RIMS-binding protein 2 (RIM-BP2)	NC	0.51	NC	Cell membrane, synapse	Plays a role in the synaptic transmission as bifunctional linker that interacts simultaneously with RIMS1, RIMS2, CACNA1D and CACNA1B.	Q80U40
S4A10	Sodium-driven chloride bicarbonate exchanger	NC	0.62	NC	Cell membrane	Electrogenic sodium/bicarbonate cotransporter in exchange for intracellular chloride	Q5DTL9
Sep-08	Septin-8	NC	0.66		Cytoplasm, cytoskeleton	Filament-forming cytoskeletal GTPase .	Q8CHH9
SF01	Splicing factor 1	NC	0.42		Nucleus	Necessary for the ATP-dependent first step of spliceosome assembly.	Q64213
STMN1	Stathmin (Leukemia-associated gene protein)	NC	0.66	NC	Cytoplasm, cytoskeleton	Involved in the regulation of the microtubule (MT) filament system by destabilizing microtubules. Phosphorylation at Ser-16 may be required for axon formation during neurogenesis.	P54227
3HIDH	3-hydroxyisobutyrate dehydrogenase	NC	1.60	NC	Mitochondrion	Enzyme. 3-hydroxyisobutyrate dehydrogenase.	Q99L13

ARHL2	Poly(ADP-ribose) glycohydrolase ARH3	NC	1.51	NC	Nucleus, cytoplasm	Poly(ADP-ribose) synthesized after DNA damage is rapidly degraded by poly(ADP-ribose) glycohydrolase. Poly(ADP-ribose) metabolism may be required for maintenance of the normal function of neuronal cells.	Q8CG72
CK5P3	CDK5 regulatory subunit-associated protein 3	NC	1.81	NC	Nucleus, Centrosome	Tumor suppressor initially identified as a CDK5R1 interactor controlling cell proliferation.	Q99LM2
COMT	Catechol O-methyltransferase	NC	1.57	NC	Cytoplasm (Soluble), Cell membrane (membrane-bound)	Enzyme. Catalyzes the O-methylation, and thereby the inactivation, of catecholamine neurotransmitters and catechol hormones. Also shortens the biological half-lives of certain neuroactive drugs, like L-DOPA, alpha-methyl DOPA and isoproterenol.	O88587
DCTN6	Dynactin subunit 6	NC	4.05	NC	Cytoskeleton	Dynactin subunit 6. May be involved in Dynein binding.	Q9WUB4
FUCM	Fucose mutarotase	NC	1.63	NC	Unknown	Enzyme. Interconversion between alpha- and beta-L-fucoses.	Q8R2K1
FUND1	FUN14 domain-containing protein 1	NC	1.55	NC	Mitochondrion outer membrane	Acts as an activator of hypoxia-induced mitophagy, an important mechanism for mitochondrial quality control.	Q9DB70
FUND2	FUN14 domain-containing protein 2	NC	1.51	NC	Integral component of mitochondrial outer membrane	FUN14 domain-containing protein 2. Mitophagy.	Q9D6K8
ISCA2	Iron-sulfur cluster assembly 2 homolog	NC	1.53	NC	Mitochondrion	Involved in the maturation of mitochondrial 4Fe-4S proteins functioning late in the iron-sulfur cluster assembly pathway.	Q9DCB8
KS6C1	Ribosomal protein S6 kinase delta-1	NC	1.71		Cytoplasm, Membrane	Enzyme. Maybe involved in transmitting sphingosine-1 phosphate (SPP)-mediated signaling into the cell.	Q8BLK9

MAAI	Maleylacetoacetate isomerase (MAAI)	NC	1.52	NC	Cytoplasm	Enzyme. This protein is involved in step 5 of the subpathway that synthesizes acetoacetate and fumarate from L-phenylalanine.	Q9WVL0
NHP2	H/ACA ribonucleoprotein complex subunit 2	NC	1.52	NC	Nucleolus, Cajal body	Required for ribosome biogenesis and telomere maintenance.	Q9CRB2
NOP58	Nucleolar protein 58	NC	1.52	NC	Nucleolus, nucleoplasm	Required for the biogenesis of box C/D snoRNAs.	Q6DFW4
PPGB	Lysosomal protective protein	NC	1.57	NC	Lysosome	Protective protein appears to be essential for both the activity of beta-galactosidase and neuraminidase.	P16675
PREB	Prolactin regulatory element-binding protein	NC	1.57	NC	Endoplasmic reticulum membrane	Guanine nucleotide exchange factor that specifically activates the small GTPase SAR1B.	Q9WUQ2
PSME3	Proteasome activator complex subunit 3	NC	2.65	NC	Nucleus, Cytoplasm	Proteasome activator complex. proteasome regulator.	P61290
RAP2C	Ras-related protein Rap-2c	NC	1.69	NC	Cytoplasm	Small GTP-binding protein which cycles between a GDP-bound inactive and a GTP-bound active form.	Q8BU31
TY3H	Tyrosine 3-monooxygenase	NC	2.79	NC	Axon	Enzyme. Plays an important role in the physiology of adrenergic neurons.	P24529

4.1.4 Detection of proteins with unknown function

Overall, three proteins of unknown function were observed, all of which changed within the cortex: Ankyrin repeat domain-containing protein 63 (ANR63)- increased at 6 weeks disease, UPF0600 protein C5orf51 homolog (CE051)- increased at 6 weeks disease, and Protein THEM6 (THEM6) increased at all timepoints (**Table 4.1.11**). These unknown proteins were either not detected (ND) or not changed (NC) within the hippocampus and spinal cord (**Appendix Table 1.1**)[109].

Table 4.1.11. Changed proteins with unknown functions.

Protein was extracted from the hippocampus, cortex, and lumbar spinal cord of rNLS TDP43 mice and litter-, sex-, time-matched non-bigenic controls at 2, 4, and 6-week timepoints. SWATH MS was conducted (n=3-5 mice) to identify and quantify proteins that changed in rNLS mice compared to control. To determine the function of changed proteins, a Uniprot[109] database search as performed for each protein. The biological function of three changed proteins is currently unknown. These proteins were either not changed or not detected within hippocampus and spinal cord. Green: decreased, red: increased, NC: no change.

Protein ID (MOUSE)	Protein name	Fold change (disease/control)			Subcellular location	UniProt functions summary[109]	Uniprot code
		Cortex					
		2 weeks	4 weeks	6 weeks			
ANR63	Ankyrin repeat domain-containing protein 63	NC	NC	0.56	Unknown	Function unknown.	A2ARS0
CE051	UPF0600 protein C5orf51 homolog	NC	NC	3.62	Unknown	Function unknown.	Q8BR90
THEM6	Protein THEM6	2.34	2.63	1.77	Secreted	Function unknown.	Q80ZW2

4.1.5 Selection of proteins for validation studies based on singular analyses

Singular bioinformatic analysis of proteins examined the individual protein functions and the patterns of change displayed by each protein within the cortex and spinal cord during three timepoints of disease progression. The next objective was to use the information obtained from singular analysis to select proteins for validation studies. Protein selection was based on the pattern of change, protein functions, and interpretation of literature pertinent to ALS disease mechanisms. As a result, an initial 30 proteins were selected based on display of diverse range of protein change patterns during disease progression and possible implications for ALS. It is important to note that while 30 proteins were selected, only 5 proteins have been reported within this study and additional selected proteins will be the focus of further additional studies (**Table 4.1.12**). The proteins selected for validation from singular analysis within this study are: coiled-coil-helix-coiled-coil-helix domain-containing protein 2 (CHCH2), connector enhancer of kinase suppressor of ras 2 (CNKR2), embigin, (EMB), calmodulin regulator protein (Purkinje cell protein PCP-4), and mitochondrial import receptor subunit -translocase of outer membrane 34 kDa subunit- (TOM34). The selection process for each protein is reported below as this was an integral result from the singular bioinformatic analysis.

CHCH2 is transcription factor that activates COX4I2 (cytochrome c oxidase, the terminal oxidase in mitochondrial electron transport) transcription under hypoxia conditions[109]. CHCHD2 mutations have been previously implicated in late-onset Parkinson's disease[112]. In addition, CHCH2 is a gene paralog of CHCHD10, and mutations within the *CHCHD10* gene have been reported as pathogenic in ALS[113, 114]. It has also been shown that CHCHD10 plays a protective role in mitochondrial dysfunction,

synaptic integrity, and maintenance of nuclear TDP-43[115]. As such it was hypothesised that CHCH2 may play a similar role in rNLS mice as its counterpart CHCHD10 does in ALS. Due to this and the decrease at all timepoints within the cortex, CHCH2 was selected for validation studies (**Table 4.1.12**).

CNKR2 is part of the Ras signalling pathways and has also been described as a synaptic protein involved in signalling[109, 116]. The decrease of CNKR2 or loss of its gene *CNKRS2* has been implicated in numerous human neurological disorders related to synaptic dysfunction such as seizures and intellectual deficits[116, 117]. In rNLS mice CNKR2 was decreased at all timepoints within the cortex (**Table 4.1.12**). Therefore, CNKR2 was selected for further validation due to its change pattern and implication in disease.

EMB is involved in the outgrowth of motor neurons and in the formation of neuromuscular junctions (NMJ)[109]. More specifically, EMB promotes NMJ development after nerve damage via muscle re-innervation[118]. As such, it has been suggested that EMB overexpression in muscle may lead to formation of new nerve terminals in denervated muscle[118]. Having direct involvement in NMJ and being decreased within the spinal cord at 6 weeks disease within rNLS mice, resulted in the selection of EMB for validation.

PCP4 (also known as PEP19) is a protein originally characterised in Purkinje cells that is involved in regulating calcium-modulated signalling, positive regulating of neuroendocrine cell differentiation, promotes acetylcholine and dopamine release, and which prevents apoptosis induced by reactive oxygen species[119-121]. PCP4 is decreased in

brain of patients with neurodegenerative diseases such as Alzheimer's disease, Huntington's disease, and Parkinson's disease[122, 123]. More specifically in ALS, previous studies have found the PCP4 is downregulated in the ALS motor cortex, and the gene *PCP4* is downregulated in the spinal cords of ALS patients[122, 124]. In rNLS mice PCP4 was decreased at 6 weeks disease within the cortex, spinal cord and hippocampus (**Table 4.1.5** and **4.1.12**). Once more, the combination of function, protein-change pattern, and interpreting current literature led to the selection of PCP4 for validation studies.

TOM34 exhibits a chaperone-like function and is involved in importing precursor-proteins into mitochondria[109]. Mitochondrial dysfunction is a common feature of neurodegenerative disorders because of Mitochondria's role in ATP production, response to reactive oxygen species, and activates a major apoptotic pathway[125, 126]. TOM34 was decreased at the 2-week timepoint in rNLS mice and this may suggest a decrease in the import of pre-proteins into mitochondria and initiation of mitochondrial dysfunction at an early timepoint of disease (**Table 4.1.12**). As such TOM34 was also selected for validation studies.

Table 4.1.12 Proteins selected from singular analysis for validation studies.

Protein was extracted from the cortex, and lumbar spinal cord of rNLS TDP43 mice and litter-, sex-, time-matched non-bigenic controls at 2, 4, and 6-week timepoints. SWATH MS was conducted (n=3-5 mice) to identify and quantify proteins that changed in rNLS mice compared to control. Changed proteins at all tested timepoints of cortex and spinal cord were selected for singular bioinformatic analysis. Five proteins were selected based on singular analyses for further validation for this study. Green: decreased, red; increased, NC: no change, ND: not detected.

Protein ID (Mouse)	Protein name	Fold change					Subcellular location	UniProt functions summary	Reasoning for selection
		Cortex			Spinal cord				
		2 weeks	4 weeks	6 weeks	2 weeks	6 weeks			
CHCH2	Coiled-coil-helix-coiled-coil-helix domain-containing protein 2	0.50	0.63	0.64	ND	ND	Nucleus, Mitochondrion	Transcription factor- binds to oxygen responsive element of COX4I2 and activates its transcription under hypoxia conditions.	• CHCH2 decreased at all timepoints within cortex. • Human *CHCHD10*gene causative for many neurological disorders including ALS.
CNKR2	Connector enhancer of kinase suppressor of ras 2	0.55	0.55	0.67	ND	ND	Cytoplasm, Membrane	May function as an adapter protein or regulator of Ras signalling pathways.	• CNKR decreased at all timepoints within cortex. • Synaptic protein; decrease of protein or loss of gene implicated in numerous human neurological disorders.

EMB	Embigin	NC	NC	NC	NC	0.63	Cell membrane, synapse	Plays a role in the outgrowth of motoneurons and in the formation of neuromuscular junctions. Following muscle denervation, promotes nerve terminal sprouting and the formation of additional acetylcholine receptor clusters at synaptic sites without affecting terminal Schwann cell number or morphology.	• EMB decreased at week 6 within the spinal cord and no change within the cortex. • Due to its role in motor neurons and neuromuscular junctions.
PCP4	Calmodulin regulator protein (Purkinje cell protein PCP-4)	NC	NC	0.55	NC	0.58	Cytosol, nucleus	Probable regulator of calmodulin Signalling. Maybe involved in synaptic plasticity.	• Decreased in 6 weeks disease for both cortex an spinal cord. • Invovled in many neurodegeneraive diseaes including ALS.

TOM34	Mitochondrial import receptor subunit TOM34 (Translocase of outer membrane 34 kDa subunit)	1.62	NC	NC	NC	NC	Cytoplasm	Plays a role in the import of cytosolically synthesized preproteins into mitochondria. May be a chaperone-like protein that helps to keep newly synthesized precursors in an unfolded import compatible state.	• TOM43 increased only in week 2 cortex. • Role in protein transport and possible role in early disease mitochondrial dysfunction.

4.1.6 Validation of proteins selected from singular bioinformatic analysis

Prior to validation of proteins selected via singular analysis, immunofluorescence validation of TDP-43 mislocalisation within the brain and spinal cord of rNLS mice used for the proteomics experiment was performed. To do this, immunofluorescence imaging of cortex and spinal cord of mice from the same cohort that was used for proteomics was conducted using specific TDP-43 antibody. This showed the over-expression and mislocalisation of TDP-43 within the cortex and spinal cord of rNLS mice compared to control (**Figure 4.1.6**). In both the cortex and spinal cord of non-bigenic littermate controls, TDP-43 was detected within its normal nuclear location, while in rNLS mice TDP-43 was present in the cytoplasm and formed intense puncta reminiscent of the protein inclusions seen in ALS tissues (**Figure 4.1.6**).

To validate the protein changes shown by proteomics, antibodies were first optimised using several concentrations for both western blotting and immunofluorescence (**Table 4.1.13**). The only antibody that showed a visible band by western blotting at the expected molecular weight was anti-CNKR2 at the concentration of 1 in 500. Similarly, in immunofluorescence optimisation, anti-CNKR2 was the only antibody successful (**Table 4.1.13**). As such validation studies could only be carried out for one selected protein: CNKR2.

Western blot experiments were conducted on two different cohorts of mice: cohort one was the *same* exact cohort used for the SWATH MS proteomics and cohort two was a *different* cohort of mice. All experiments were conducted using litter-matched, sex-matched mice pairs of n=3 for cohort 1 (proteomics cohort) and n=4 for cohort 2 (new cohort). SWATH MS showed that CNKR2 was decreased at all timepoints in the

cortex and was not detected in the spinal cord (**Table 4.1.12**). Western blots using the *same* cohort of mice revealed a trend towards decreased levels of CNKR2 in the cortex at 4 and 6-week timepoints, although the difference was not statistically significant (**Figure 4.1.7** and **Table 4.1.14**). At the 2-week timepoint no band was detected for CNKR2 (**Appendix Figure 2.1**). Validation with *different* cohort of mice showed a trend towards a decrease in CNKR2 at 4-week timepoint, although the change was not statistically significant (**Figure 4.1.8** and **Table 4.1.14**). The *different* cohort showed no difference at 2- and 6-week timepoints in the cortex (**Figure 4.1.8** and **Table 4.1.14**). The same antibody was used to visualise CNKR2 in the cortex at 4-week timepoint. This revealed that there may be a decrease of CNKR2 in rNLS mice, although further optimisation and quantification of the immunofluorescence staining is required (**Figure 4.1.9**).

Overall, western blotting did not show the same results as the proteomics for CNKR2 changes within the cortex. However, the blots from both cohorts and the microscopy results show non-specific binding by the CNKR2 antibody (**Figure 4.1.9**, **Appendix Figure 2.1 and 3.2**). As such a different antibody is required for CNKR2 validation, as well as the other candidate proteins selected via singular analysis.

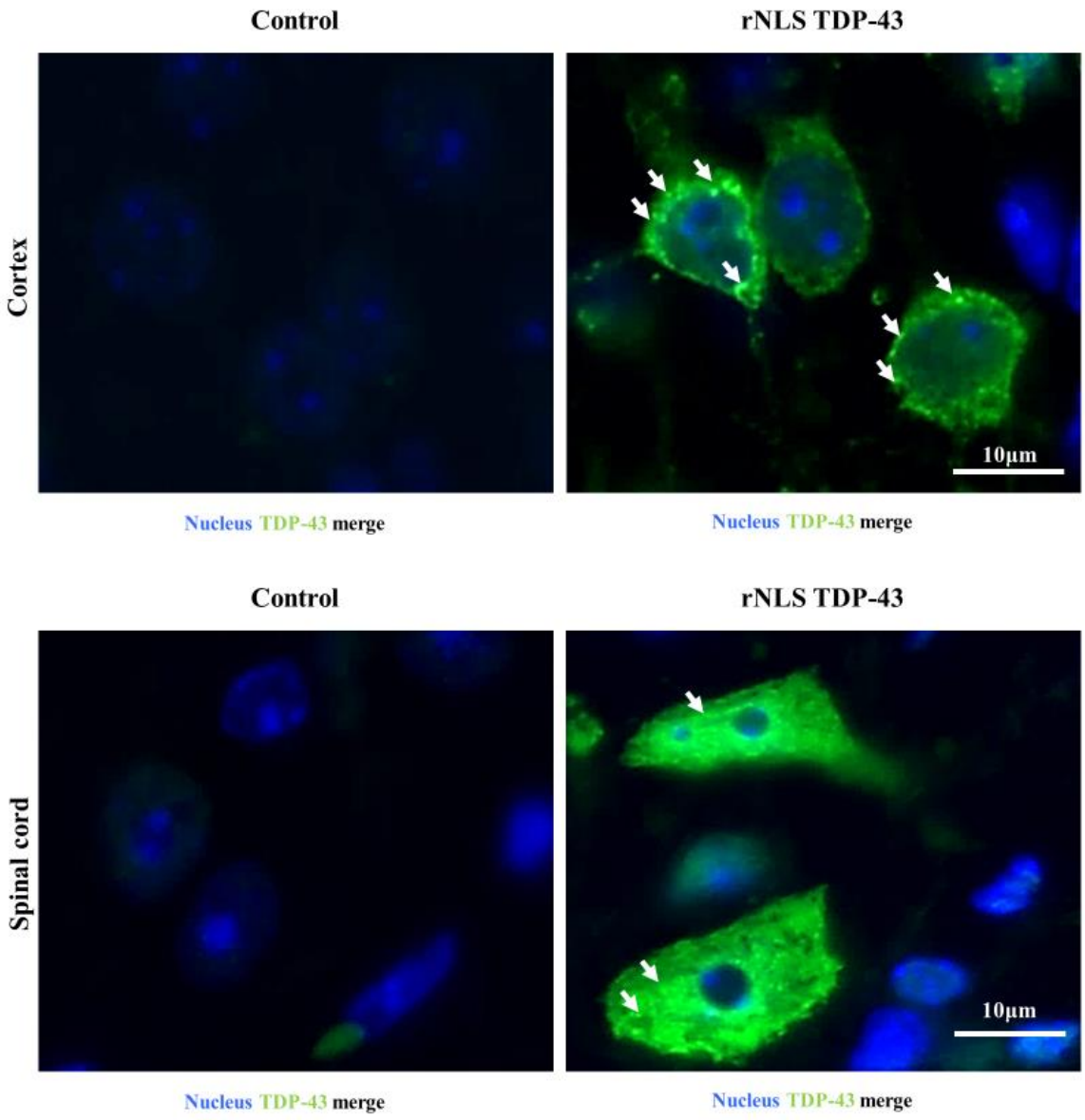

Figure 4.1.6 TDP-43 mislocalisation within the cortex and spinal cord.

Specific TDP-43 antibody was used to visualise the mislocalisation of TDP-43 from the nucleus into the cytoplasm using immunofluorescence imaging of cortex and spinal cord tissue from litter-matched, sex-matched pairs for control and rNLS at 4-week timepoint (2 technical replicates). Imaging was conducted at 40x magnification, using the same exposure time for control and rNLS via the Zeiss Axiolmager upright fluorescence microscope. Blue: nuclear stain DAPI; green: TDP-43; arrow: TDP-43 intense puncta reminiscent of the protein inclusions seen in ALS tissues.

Table 4.1.13 Antibody validation for proteins selected via singular analysis.

Antibodies were validated using cortex tissue from control and rNLS at 4-week timepoint. For western blots 3 concentrations were used and 2 different concentrations for immunofluorescence imaging. CNKR2 was the only antibody that resulted in visible band for western blotting and immunofluorescence.

Antibody	Successful/Unsuccessful				
	Western Blot (conc.)			Immunofluorescence imaging (conc.)	
	1/2000	1/1000	1/500	1/500	1/100
anti-CHCH2	Unsuccessful	Unsuccessful	Unsuccessful	Unsuccessful	Unsuccessful
anti-CNKR2	Unsuccessful	Unsuccessful	Successful	Successful	Successful
anti-EMB	Unsuccessful	Unsuccessful	Unsuccessful	Unsuccessful	Unsuccessful
Anti-PCP4	Unsuccessful	Unsuccessful	Unsuccessful	Unsuccessful	Unsuccessful
anti-TOM34	Unsuccessful	Unsuccessful	Unsuccessful	Unsuccessful	Unsuccessful

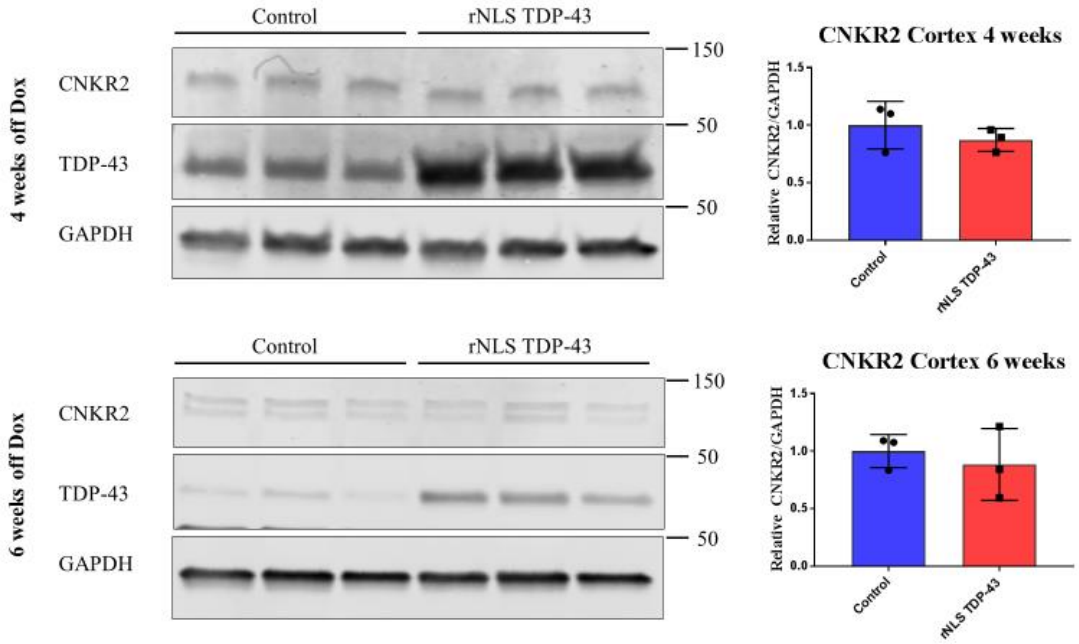

Figure 4.1.7 Validation of CNKR2 within *same* mice cohort used for proteomics.

Specific CNKR2 antibody was used to validate protein changes using cortex tissue from the same cohort that was used for SWATH MS (litter-matched, sex-matched pairs for

control and rNLS) at 2,4 and 6-week timepoints (n=3). Blots were visualised and quantified using the LI-COR Image Studio software. Statistical analysis was conducted using a Paired T-test via GraphPad Prism version 7.02 (not significant=P > 0.05). The molecular weight for CNKR2 is 120kDa. Week 2 blot did not show a band for CNKR2, for full blots refer to ***Appendix figure 2.1****. For p-values refer to* ***Table 4.1.9****.*

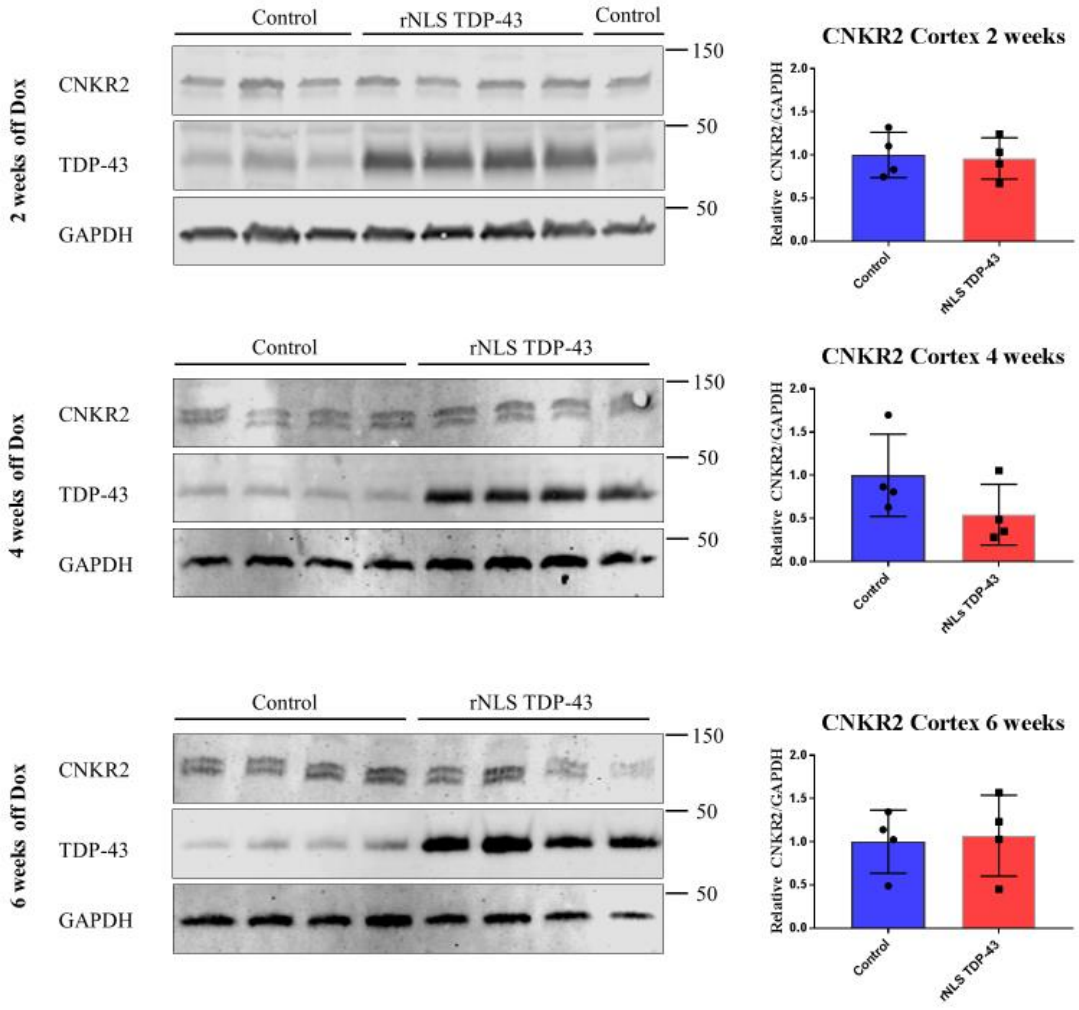

Figure 4.1.8 Validation of CNKR2 within *different* cohort of mice.

Specific CNKR2 antibody was used to validate protein changes using cortex tissue from a different cohort of mice to that used for SWATH MS (litter-matched, sex-matched pairs for control and rNLS) at 2,4 and 6-week timepoints (n=4). Blots were visualised and quantified using the LI-COR Image Studio software. Statistical analysis was conducted using a Paired T-test via GraphPad Prism version 7.02 (not significant=P > 0.05). The

molecular weight for CNKR2 is 120kDa. For p-values refer to ***Table 4.1.9*** *and for full blots refer to* ***Appendix figure 2.2****.*

Table 4.1.14 P-values generated from western blot quantification of CNKR2

Western blotting using a specific CNKR2 antibody was used to validate the decrease of CNKR2 in two cohorts of mice: Proteomic cohort and a second different cohort of mice. Blots were visualised and quantified using the LI-COR Image Studio software. Statistical analysis was conducted using a Paired T-test via GraphPad Prism version 7.02. ND: not detected.

Cohort of mice	p-value (Western blots)		
	Week 2	Week 4	Week 6
Proteomics cohort (n=3)	ND	0.5294	0.4576
Second cohort (n=4)	0.8546	0.2307	0.6939

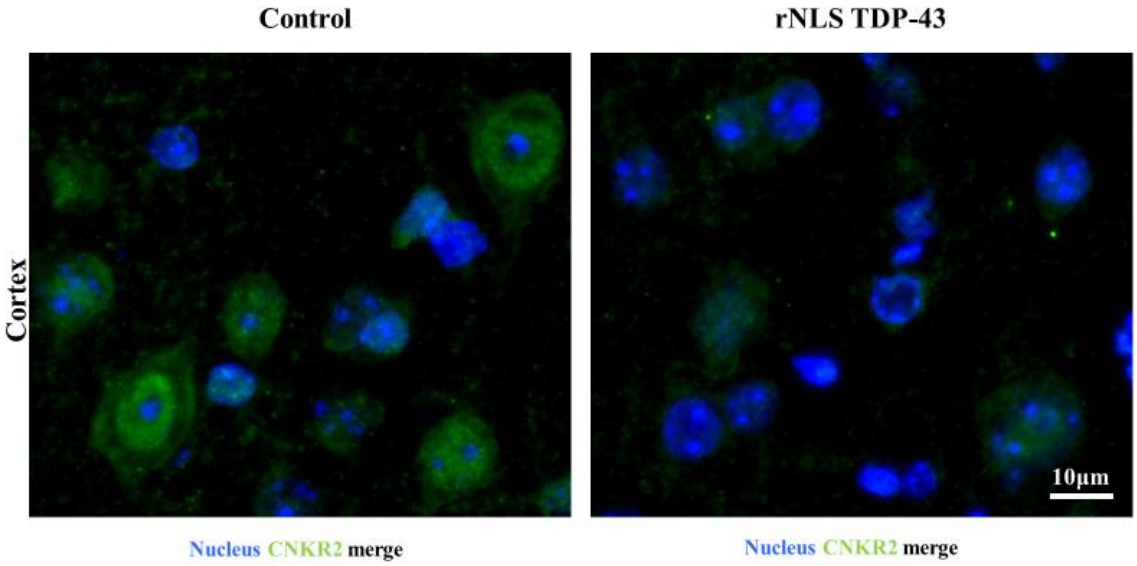

Figure 4.1.9 Visualisation of CNKR2 within the cortex.

Specific CNKR2 antibody (1/100 concentration) was used to visualise the candidate protein using immunofluorescence imaging of cortex tissue from litter-matched, sex-matched pairs for control and rNLS at 4-week timepoint (2 technical replicates). Imaging

was conducted at 40x magnification, using the same exposure time for control and rNLS via the Zeiss Axiolmager upright fluorescence microscope. Blue: nuclear stain DAPI; green: CNKR2.

4.2 Identification of pathways, upstream regulators, and biological functions over disease course in the rNLS TDP-43 mouse model: Comprehensive bioinformatic analysis

4.2.1 Ingenuity Pathway Analysis (IPA)

Singular analyses of differentiated proteins provided insight into individual protein change patterns and functions. The next aim was to place the proteomic data into biological context to gain a more comprehensive view of TDP-43 pathogenesis within rNLS mice. This was done by using the Ingenuity Pathway Analysis (IPA) software, which relies on a manually curated Ingenuity Knowledge Base (http://www.ingenuity.com/) to analyse and interpret large complex 'omics data. For this analysis the complete list of all proteins identified and quantified were used in IPA analyses, as opposed to singular analyses that only examined altered proteins. Three main analyses were performed using IPA Core analysis: identification of canonical pathways (activated, inhibited, enriched), prediction of upstream regulators (activated and inhibited), and prediction of downstream effects of proteomic changes during disease progression. These analyses were performed for all available timepoints for cortex (2, 4, and 6 weeks) and spinal cord (2 and 6 weeks). The parameters for each analysis were kept consistent and have been reported within the methods and materials.

4.2.2 Canonical pathways activated and inhibited during disease course

Pathway analysis within IPA compares the overlap between the proteins within the experimental dataset *with* the proteins of each pathway within the IPA reference database which is curated based on literature findings. This is known as enrichment

analysis. Then, to determine the significance of the overlap (or significance of enrichment), a Fisher's exact test (right-tailed) is performed which indicates the probability of the overlap by random chance alone (significance is set at a p-value of 0.05 or less). Subsequently, an algorithm within IPA generates z-scores to predict the activation or inhibition of a pathway. The algorithm considers the directional effect of one protein on another protein or on a pathway, *and* the direction of protein changes within the experimental dataset to predict activation (z-score of 2 or more) or inhibition (z-score of -2 or less). Reported here are the most activated, inhibited, and most significantly enriched pathways within each timepoint in the cortex and spinal cord.

At the *2-week* time point within the *cortex*, there were 4 activated pathways and 48 inhibited pathways (**Table 4.2.1**). The most activated pathway with the highest z-score was apoptosis signalling with 9% of the proteins within the pathway being upregulated (**Table 4.2.1, Figure 4.2.1, Figure 4.2.2**). While the activated pathway with the most significant enrichment was EIF2 (eukaryotic initiation factor-2) signalling (involved in protein synthesis) with 37% of proteins within the pathway being upregulated (**Table 4.2.1, Figure 4.2.1, Figure 4.2.2**). The inhibited pathway with the lowest z-score was Rac Signalling with 30% of proteins within the pathway being down-regulated (**Table 4.2.1, Figure 4.2.1, Figure 4.2.2**). The inhibited pathway with the most significant enrichment was signalling by Rho Family GTPases with 28% of proteins within the pathway being down-regulated (**Table 4.2.1, Figure 4.2.1, Figure 4.2.2**).

Table 4.2.1 Activated and inhibited pathways at 2 weeks cortex.

Protein was extracted from the cortex of rNLS mice at 2, 4, and 6-week timepoints. SWATH MS was conducted (n=3-5 mice) to identify and quantify proteins that changed in TDP-43 mice compared to control non-bigenic mice. Ingenuity Pathway Analysis (IPA) software was used to determine the most activated (orange) and inhibited (blue) pathways. An algorithm within IPA, called z-scores, considers the directional effect of one protein on another protein or on a pathway, and the direction of protein changes within the experimental dataset to predict activation (z-score of 2 or more) or inhibition (z-score of -2 or less). The significance is calculated by a Fisher's exact test right-tailed (-log[p-value 0.05]=1.3). Reported are all the activated and inhibited pathways that also generated a p-value of ≤ 0.05 at 2 weeks cortex.

Activated and inhibited pathways Cortex - 2 weeks					
Canonical pathway	**z-score**	**Overall Predicted State**	**p-value**	**-log(p-value)**	**Percentage of dataset proteins within pathway**
Apoptosis Signalling	2.68	Activated	0.004	2.41	22.2
RhoGDI Signalling	2.50	Activated	2.51E-23	22.60	41.6
HIPPO Signalling	2.31	Activated	5.25E-06	5.28	29.9
EIF2 Signalling	2.10	Activated	1.0E-39	39.00	47.5
Rac Signalling	-4.32	Inhibited	3.16E-12	11.50	36.8
fMLP Signalling in Neutrophils	-4.22	Inhibited	5.01E-14	13.30	38.2
RhoA Signalling	-3.68	Inhibited	2.00E-17	16.70	41.9
Signalling by Rho Family GTPases	-3.54	Inhibited	5.01E-27	26.30	38.3
Ephrin Receptor Signalling	-3.50	Inhibited	1.26E-19	18.90	38.5
PAK Signalling	-3.40	Inhibited	3.31E-05	4.48	26.7
CD28 Signalling in T Helper Cells	-3.40	Inhibited	0.012	1.93	18.9
Cdc42 Signalling	-3.14	Inhibited	0.001	2.96	20.4
LPS-stimulated MAPK Signalling	-3.13	Inhibited	0.003	2.59	23
Integrin Signalling	-3.05	Inhibited	4.0E-17	16.40	33.3
Regulation of Actin-based Motility by Rho	-3.00	Inhibited	3.16E-13	12.50	42.2
Fcγ Receptor-mediated Phagocytosis in Macrophages and Monocytes	-3.00	Inhibited	3.16E-11	10.50	38.7
Renin-Angiotensin Signalling	-3.00	Inhibited	1.29E-07	6.89	29.5
HGF Signalling	-3.00	Inhibited	0.002	2.73	21.7
Actin Cytoskeleton Signalling	-2.87	Inhibited	6.31E-18	17.20	33.5
GDNF Family Ligand-Receptor Interactions	-2.84	Inhibited	0.015	1.81	21.1
Agrin Interactions at Neuromuscular Junction	-2.84	Inhibited	8.71E-06	5.06	31.9
CXCR4 Signalling	-2.83	Inhibited	1.26E-15	14.90	35.8
UVC-Induced MAPK Signalling	-2.83	Inhibited	6.46E-07	6.19	41.9

Actin Nucleation by ARP-WASP Complex	-2.71	Inhibited	8.71E-10	9.06	44.6
IL-3 Signalling	-2.71	Inhibited	6.76E-05	4.17	27.7
Fc Epsilon RI Signalling	-2.71	Inhibited	0.012	1.92	19.3
Cholecystokinin/Gastrin-mediated Signalling	-2.69	Inhibited	3.55E-07	6.45	30.7
Antiproliferative Role of Somatostatin Receptor 2	-2.67	Inhibited	5.13E-08	7.29	36
Renal Cell Carcinoma Signalling	-2.67	Inhibited	0.0005	3.27	25.3
Phospholipase C Signalling	-2.65	Inhibited	6.46E-10	9.19	26.2
NGF Signalling	-2.60	Inhibited	0.002	2.80	21.7
SAPK/JNK Signalling	-2.52	Inhibited	0.036	1.44	18.3
Thrombopoietin Signalling	-2.50	Inhibited	0.003	2.49	24.6
Paxillin Signalling	-2.48	Inhibited	1.70E-06	5.77	28.3
Gα12/13 Signalling	-2.45	Inhibited	0.020	1.70	18.3
Corticotropin Releasing Hormone Signalling	-2.41	Inhibited	3.39E-06	5.47	27.9
IL-8 Signalling	-2.41	Inhibited	5.8E-09	8.24	26.9
Gαq Signalling	-2.40	Inhibited	7.59E-10	9.12	29.8
14-3-3-mediated Signalling	-2.40	Inhibited	7.94E-13	12.10	35.9
B Cell Receptor Signalling	-2.40	Inhibited	0.009	2.03	17.9
Prolactin Signalling	-2.36	Inhibited	0.008	2.11	21.7
Role of NFAT in Regulation of the Immune Response	-2.34	Inhibited	3.16E-07	6.50	25.3
Aryl Hydrocarbon Receptor Signalling	-2.33	Inhibited	0.004	2.43	20
IL-2 Signalling	-2.31	Inhibited	0.007	2.16	23.4
Ephrin B Signalling	-2.18	Inhibited	7.94E-18	17.10	53.4
ErbB4 Signalling	-2.18	Inhibited	0.004	2.41	23.6
Non-Small Cell Lung Cancer Signalling	-2.14	Inhibited	0.035	1.45	19.5
P2Y Purigenic Receptor Signalling Pathway	-2.14	Inhibited	6.31E-12	11.20	34.6
Chemokine Signalling	-2.04	Inhibited	5.37E-10	9.27	40.8
Relaxin Signalling	-2.04	Inhibited	1.58E-09	8.80	29.9
CREB Signalling in Neurons	-2.02	Inhibited	2.51E-17	16.60	35.7
NF-κB Activation by Viruses	-2.00	Inhibited	0.049	1.31	18.4

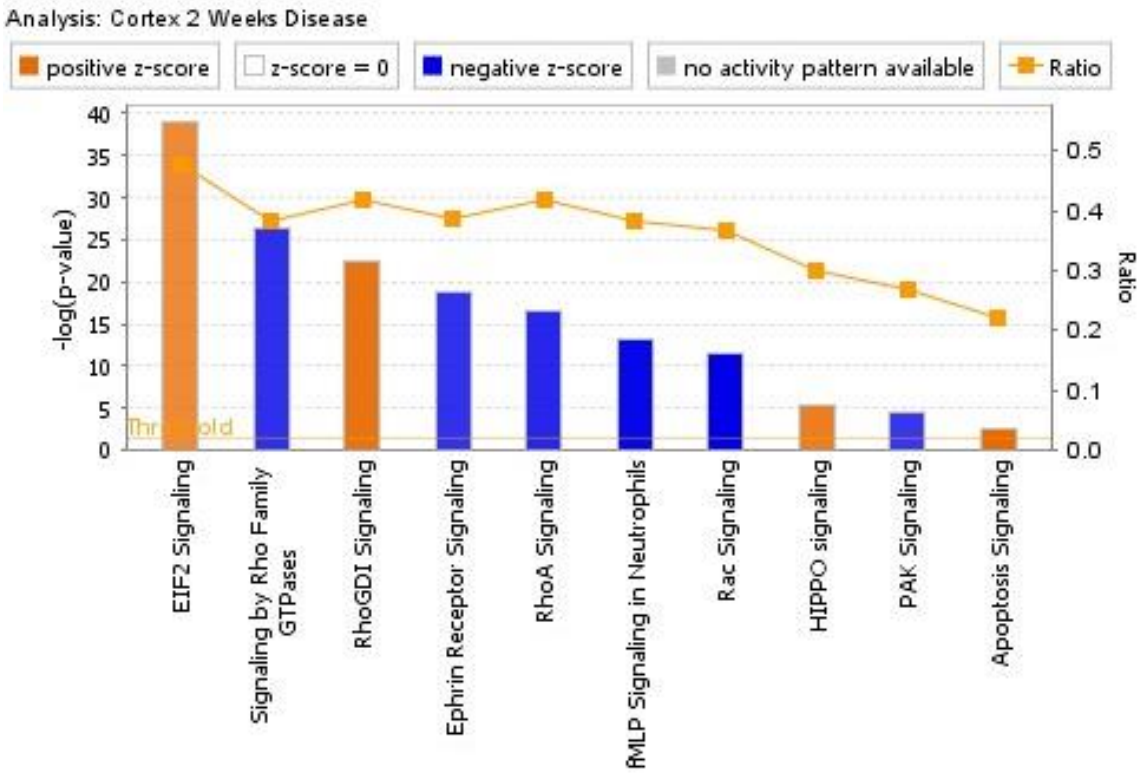

Figure 4.2.1 Top activated and inhibited pathways at 2 weeks cortex.

Protein was extracted from the cortex of rNLS mice at 2, 4, and 6-week timepoints. SWATH MS was conducted (n=3-5 mice) to identify and quantify proteins that changed in TDP-43 mice compared to control non-bigenic mice. Ingenuity Pathway Analysis (IPA) software was used to determine the most activated (orange) and inhibited (blue) pathways. An algorithm within IPA, called z-scores, considers the directional effect of one protein on another protein or on a pathway, and the direction of protein changes within the experimental dataset to predict activation (z-score of 2 or more) or inhibition (z-score of -2 or less). The left y-axis displays the -log of p-value calculated by a Fisher's exact test right-tailed (-log[p-value 0.05]=1.3). The right y-axis displays the ratio (orange line) of proteins within experimental dataset divided by the total number of proteins within that pathway that are curated within the reference set. Reported are the top activated and inhibited pathways that also generated a p-value of ≤ 0.05 at 2 weeks cortex.

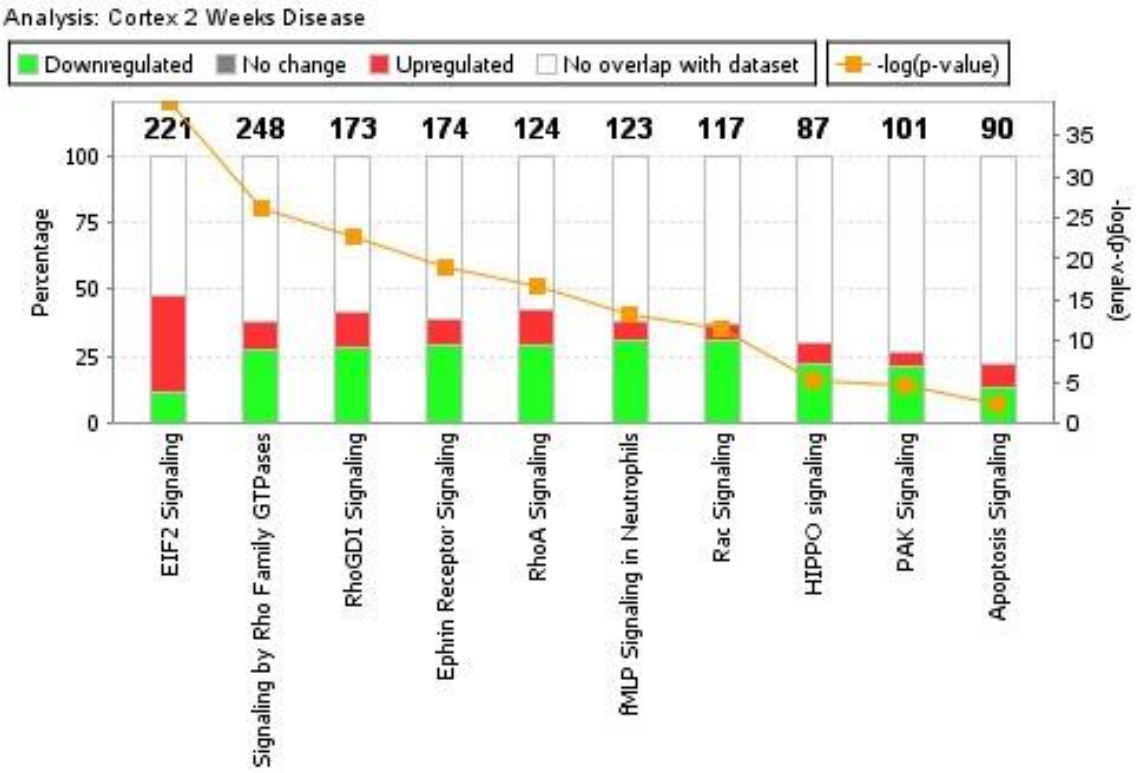

Figure 4.2.2 Top activated and inhibited pathways at 2 weeks cortex- percentage of proteins changed.

Protein was extracted from the cortex of rNLS mice at 2, 4, and 6-week timepoints. SWATH MS was conducted (n=3-5 mice) to identify and quantify proteins that changed in TDP-43 mice compared to control non-bigenic mice. Ingenuity Pathway Analysis (IPA) software was used to determine the most activated and inhibited pathways. This stacked bar chart displays the percentage of up- and down-regulated proteins within each pathway shown in ***Figure 4.2.1****. The right y-axis displays the percentage of proteins within experimental dataset that have up regulated (red) or down-regulated (green). The left y-axis displays the -log of p-value (orange line) calculated by a Fisher's exact test right-tailed (-log[p-value 0.05]=1.3). Reported are the top activated and inhibited pathways that also generated a p-value of ≤ 0.05 at 2 weeks cortex.*

At the *4-week* timepoint within the *cortex*, IPA predicted 4 pathways as activated and 57 pathways as inhibited (**Table 4.2.2**). The top activated pathway (highest z-score) was apoptosis signalling with 6% of proteins within the pathway being upregulated (**Table 4.2.2, Figure 4.2.3, Figure 4.2.4**). Of all the activated pathways, the most significantly enriched was HIPPO Signalling with 6% of proteins within the pathway being upregulated (**Table 4.2.2, Figure 4.2.3, Figure 4.2.4**). The top inhibited pathway (lowest z-score) was fMLP signalling in neutrophils with 30% of proteins within the pathway being down regulated (**Table 4.2.2, Figure 4.2.3, Figure 4.2.4**). The most significantly enriched inhibited pathway was CREB signalling in neurons with 25% of proteins within the pathway being upregulated (**Table 4.2.2, Figure 4.2.3, Figure 4.2.4**).

Table 4.2.2 Activated and inhibited pathways at 4 weeks cortex.

Protein was extracted from the cortex of rNLS mice at 2, 4, and 6-week timepoints. SWATH MS was conducted (n=3-5 mice) to identify and quantify proteins that changed in TDP-43 mice compared to control non-bigenic mice. Ingenuity Pathway Analysis (IPA) software was used to determine the most activated (orange) and inhibited (blue) pathways. An algorithm within IPA, called z-scores, considers the directional effect of one protein on another protein or on a pathway, and the direction of protein changes within the experimental dataset to predict activation (z-score of 2 or more) or inhibition (z-score of -2 or less). The significance is calculated by a Fisher's exact test right-tailed (-log[p-value 0.05]=1.3). Reported are all the activated and inhibited pathways that also generated a p-value of ≤ 0.05 at 4 weeks cortex.

Activated and inhibited pathways Cortex - 4 weeks					
Pathway name	**z-score**	**Overall Predicted State**	**p-value**	**-log(p-value)**	**Percentage of dataset proteins within pathway**
Apoptosis Signalling	2.68	Activated	0.004	2.41	22.2
Antioxidant Action of Vitamin C	2.67	Activated	0.028	1.55	18.5
HIPPO Signalling	2.31	Activated	5.25E-06	5.28	29.9

PTEN Signalling	2.04	Activated	0.003	2.52	21
fMLP Signalling in Neutrophils	-3.89	Inhibited	5.01E-14	13.30	38.2
CD28 Signalling in T Helper Cells	-3.80	Inhibited	0.012	1.93	18.9
Rac Signalling	-3.70	Inhibited	3.16E-12	11.50	36.8
PI3K Signalling in B Lymphocytes	-3.66	Inhibited	0.001	2.92	21.5
GNRH Signalling	-3.65	Inhibited	3.98E-13	12.40	36.4
CREB Signalling in Neurons	-3.46	Inhibited	2.51E-17	16.60	35.7
B Cell Receptor Signalling	-3.43	Inhibited	0.009	2.03	17.9
14-3-3-mediated Signalling	-3.43	Inhibited	7.94E-13	12.10	35.9
Cholecystokinin/Gastrin-mediated Signalling	-3.41	Inhibited	3.55E-07	6.45	30.7
IL-8 Signalling	-3.32	Inhibited	5.75E-09	8.24	26.9
Neuregulin Signalling	-3.27	Inhibited	5.75E-07	6.24	31.8
Glioma Signalling	-3.27	Inhibited	8.91E-05	4.05	25
Synaptic Long-Term Potentiation	-3.27	Inhibited	2.51E-20	19.60	45.5
LPS-stimulated MAPK Signalling	-3.13	Inhibited	0.003	2.59	23
Actin Nucleation by ARP-WASP Complex	-3.13	Inhibited	8.71E-10	9.06	44.6
Thrombin Signalling	-3.11	Inhibited	1.26E-16	15.90	33.8
Renin-Angiotensin Signalling	-3.00	Inhibited	1.29E-07	6.89	29.5
Glutamate Receptor Signalling	-3.00	Inhibited	4.27E-08	7.37	40.4
Synaptic Long-Term Depression	-2.95	Inhibited	2.88E-10	9.54	31.3
Neuropathic Pain Signalling in Dorsal Horn Neurons	-2.85	Inhibited	1.17E-10	9.93	34.8
CXCR4 Signalling	-2.83	Inhibited	1.26E-15	14.90	35.8
UVC-Induced MAPK Signalling	-2.83	Inhibited	6.46E-07	6.19	41.9
Chemokine Signalling	-2.79	Inhibited	5.37E-10	9.27	40.8
Cdc42 Signalling	-2.75	Inhibited	0.001	2.96	20.4
Fc Epsilon RI Signalling	-2.71	Inhibited	0.012	1.92	19.3
IL-3 Signalling	-2.71	Inhibited	6.76E-05	4.17	27.7
ErbB4 Signalling	-2.67	Inhibited	0.004	2.41	23.6
p70S6K Signalling	-2.67	Inhibited	9.55E-10	9.02	31.8
Phospholipase C Signalling	-2.65	Inhibited	6.46E-10	9.19	26.2
α-Adrenergic Signalling	-2.61	Inhibited	1.26E-19	18.90	51.7
PAK Signalling	-2.60	Inhibited	3.31E-05	4.48	26.7
mTOR Signalling	-2.53	Inhibited	2.51E-26	25.60	41.3
Type II Diabetes Mellitus Signalling	-2.50	Inhibited	0.015	1.82	18.8
Thrombopoietin Signalling	-2.50	Inhibited	0.003	2.49	24.6
Calcium-induced T Lymphocyte Apoptosis	-2.50	Inhibited	0.0209	1.68	21.2
Gαq Signalling	-2.40	Inhibited	7.59E-10	9.12	29.8
Agrin Interactions at Neuromuscular Junction	-2.40	Inhibited	8.71E-06	5.06	31.9
Remodelling of Epithelial Adherens Junctions	-2.40	Inhibited	2.00E-25	24.70	65.2
Prolactin Signalling	-2.36	Inhibited	0.008	2.11	21.7

Macropinocytosis Signalling	-2.36	Inhibited	0.0001	3.87	27.2
Signalling by Rho Family GTPases	-2.36	Inhibited	5.01E-27	26.30	38.3
Oncostatin M Signalling	-2.33	Inhibited	0.015	1.82	26.5
nNOS Signalling in Neurons	-2.33	Inhibited	6.17E-07	6.21	40.4
Glioblastoma Multiforme Signalling	-2.27	Inhibited	0.0129	1.89	18.1
UVA-Induced MAPK Signalling	-2.24	Inhibited	0.0123	1.91	19.8
HGF Signalling	-2.20	Inhibited	0.002	2.73	21.7
Leukocyte Extravasation Signalling	-2.19	Inhibited	1.82E-07	6.74	24.6
Renal Cell Carcinoma Signalling	-2.18	Inhibited	0.0005	3.27	25.3
GM-CSF Signalling	-2.18	Inhibited	0.0002	3.63	27.4
Non-Small Cell Lung Cancer Signalling	-2.14	Inhibited	0.0355	1.45	19.5
P2Y Purigenic Receptor Signalling Pathway	-2.14	Inhibited	6.31E-12	11.20	34.6
Sperm Motility	-2.12	Inhibited	9.12E-06	5.04	26
Paxillin Signalling	-2.12	Inhibited	1.70E-06	5.77	28.3
SAPK/JNK Signalling	-2.07	Inhibited	0.036	1.44	18.3
VEGF Signalling	-2.04	Inhibited	5.75E-06	5.24	28.2
Endothelin-1 Signalling	-2.03	Inhibited	9.77E-05	4.01	21.6
NF-κB Activation by Viruses	-2.00	Inhibited	0.049	1.31	18.4
Calcium Signalling	-2.00	Inhibited	4.27E-10	9.37	29.1

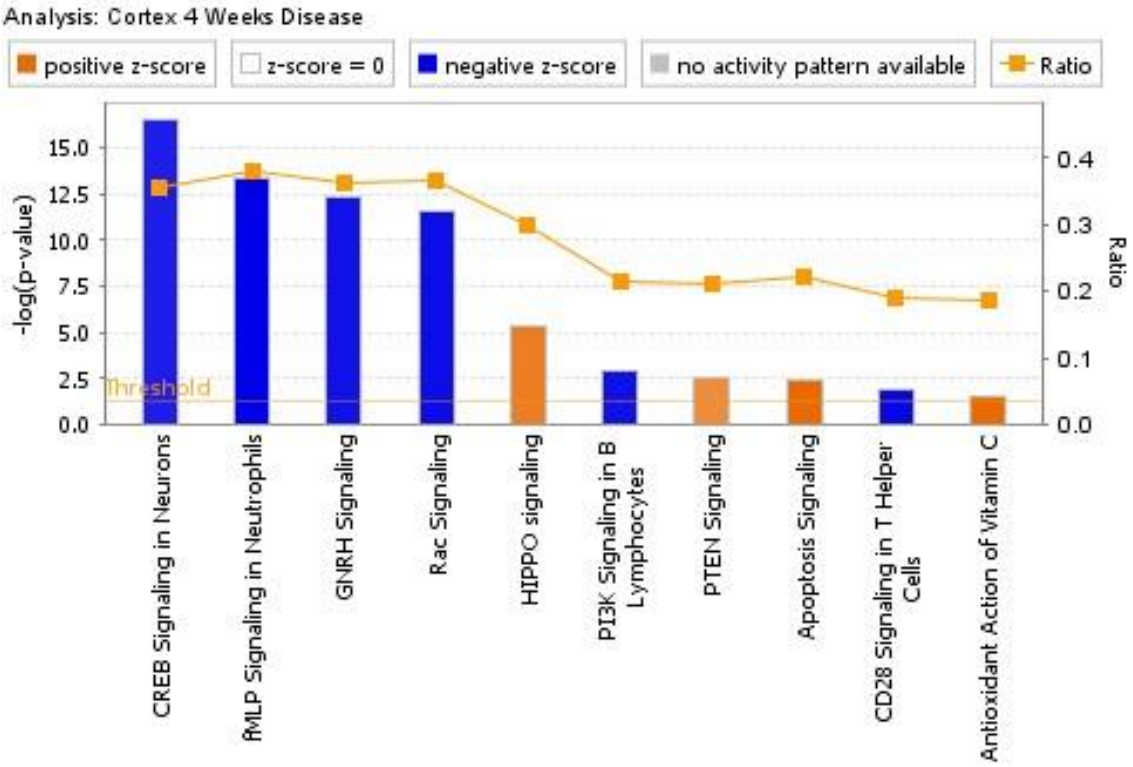

Figure 4.2.3 Top activated and inhibited pathways at 4 weeks cortex.

Protein was extracted from the cortex of rNLS mice at 2, 4, and 6-week timepoints. SWATH MS was conducted (n=3-5 mice) to identify and quantify proteins that changed in TDP-43 mice compared to control non-bigenic mice. Ingenuity Pathway Analysis (IPA) software was used to determine the most activated (orange) and inhibited (blue) pathways. An algorithm within IPA, called z-scores, considers the directional effect of one protein on another protein or on a pathway, and the direction of protein changes within the experimental dataset to predict activation (z-score of 2 or more) or inhibition (z-score of -2 or less). The left y-axis displays the -log of p-value calculated by a Fisher's exact test right-tailed (-log[p-value 0.05]=1.3). The right y-axis displays the ratio (orange line) of proteins within experimental dataset divided by the total number of proteins within that pathway that are curated within the reference set. Reported are the top activated and inhibited pathways that also generated a p-value of ≤ 0.05 at 4 weeks cortex.

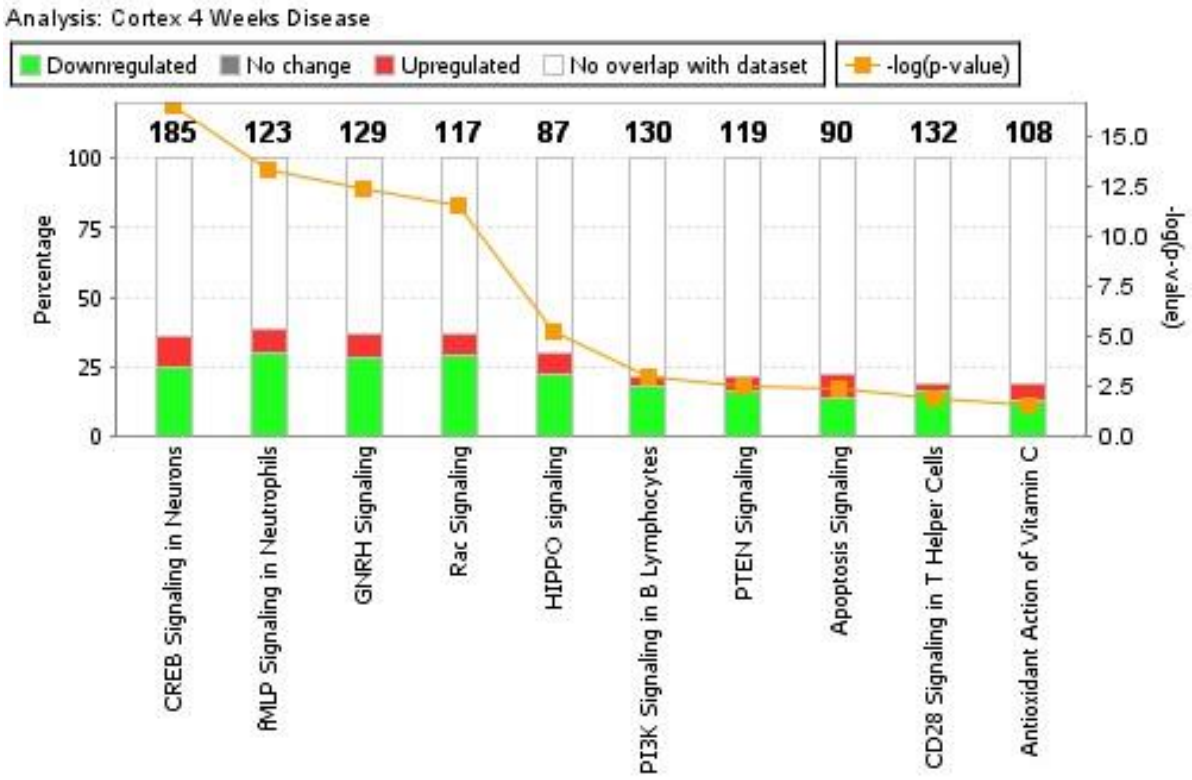

Figure 4.2.4 Top activated and inhibited pathways at 4 weeks cortex- percentage of proteins changed.

Protein was extracted from the cortex of rNLS mice at 2, 4, and 6-week timepoints. SWATH MS was conducted (n=3-5 mice) to identify and quantify proteins that changed in TDP-43 mice compared to control non-bigenic mice. Ingenuity Pathway Analysis (IPA) software was used to determine the most activated and inhibited pathways. This stacked bar chart displays the percentage of up- and down-regulated proteins within each pathway shown in ***Figure 4.2.3****. The right y-axis displays the percentage of proteins within experimental dataset that have up regulated (red) or down-regulated (green). The left y-axis displays the -log of p-value (orange line) calculated by a Fisher's exact test right-tailed (-log[p-value 0.05]=1.3). Reported are the top activated and inhibited pathways that also generated a p-value of ≤ 0.05 at 4 weeks cortex.*

At the *6-week* timepoint within the *cortex* IPA predicted 2 activated pathways and 10 inhibited pathways. The two activated pathways were aryl hydrocarbon receptor (AHR) signalling and AMPK signalling (**Table 4.2.3, Figure 4.2.5**). AHR signalling had 15% of proteins upregulated within the pathway and is involved in multiple signalling pathways, such as apoptosis, cell cycle regulation, and nuclear receptor signalling (**Figure 4.2.6**). AMPK signalling had 13% of proteins upregulated within the pathway and is involved in inhibiting key enzymes of ATP consuming pathways and activation of pathways that generate ATP (**Figure 4.2.6**). The top inhibited pathway is Rac signalling, with 28% of proteins within the pathway being down-regulated (**Table 4.2.3, Figure 4.2.5, Figure 4.2.6**). The inhibited pathway with the most significant enrichment was signalling by Rho Family GTPases with 25% of proteins within the pathway being down-regulated (**Table 4.2.3, Figure 4.2.5, Figure 4.2.6**).

Table 4.2.3 Activated and inhibited pathways at 6 weeks cortex.

Protein was extracted from the cortex of rNLS mice at 2, 4, and 6-week timepoints. SWATH MS was conducted (n=3-5 mice) to identify and quantify proteins that changed in TDP-43 mice compared to control non-bigenic mice. Ingenuity Pathway Analysis (IPA) software was used to determine the most activated (orange) and inhibited (blue) pathways. An algorithm within IPA, called z-scores, considers the directional effect of one protein on another protein or on a pathway, and the direction of protein changes within the experimental dataset to predict activation (z-score of 2 or more) or inhibition (z-score of -2 or less). The significance is calculated by a Fisher's exact test right-tailed (-log[p-value 0.05]=1.3). Reported are all the activated and inhibited pathways that also generated a p-value of ≤ 0.05 at 6 weeks cortex.

Activated and inhibited pathways Cortex - 6 weeks					
Pathway name	**z-score**	**Overall Predicted State**	**p-value**	**-log(p-value)**	**Percentage of dataset proteins within pathway**
Aryl Hydrocarbon Receptor Signalling	2.33	Activated	0.004	2.43	20

AMPK Signalling	2.00	Activated	7.76E-07	6.11	24.1
Rac Signalling	-3.70	Inhibited	3.16E-12	11.5	36.8
CD28 Signalling in T Helper Cells	-3.40	Inhibited	0.012	1.93	18.9
RhoA Signalling	-3.11	Inhibited	2.00E-17	16.7	41.9
fMLP Signalling in Neutrophils	-2.92	Inhibited	5.01E-14	13.3	38.2
CREB Signalling in Neurons	-2.60	Inhibited	2.51E-17	16.6	35.7
Cdc42 Signalling	-2.35	Inhibited	0.001	2.96	20.4
nNOS Signalling in Neurons	-2.33	Inhibited	6.17E-07	6.21	40.4
GNRH Signalling	-2.19	Inhibited	3.98E-13	12.4	36.4
Signalling by Rho Family GTPases	-2.12	Inhibited	5.01E-27	26.3	38.3
PI3K Signalling in B Lymphocytes	-2.12	Inhibited	0.001	2.92	21.5
B Cell Receptor Signalling	-2.06	Inhibited	0.009	2.03	17.9

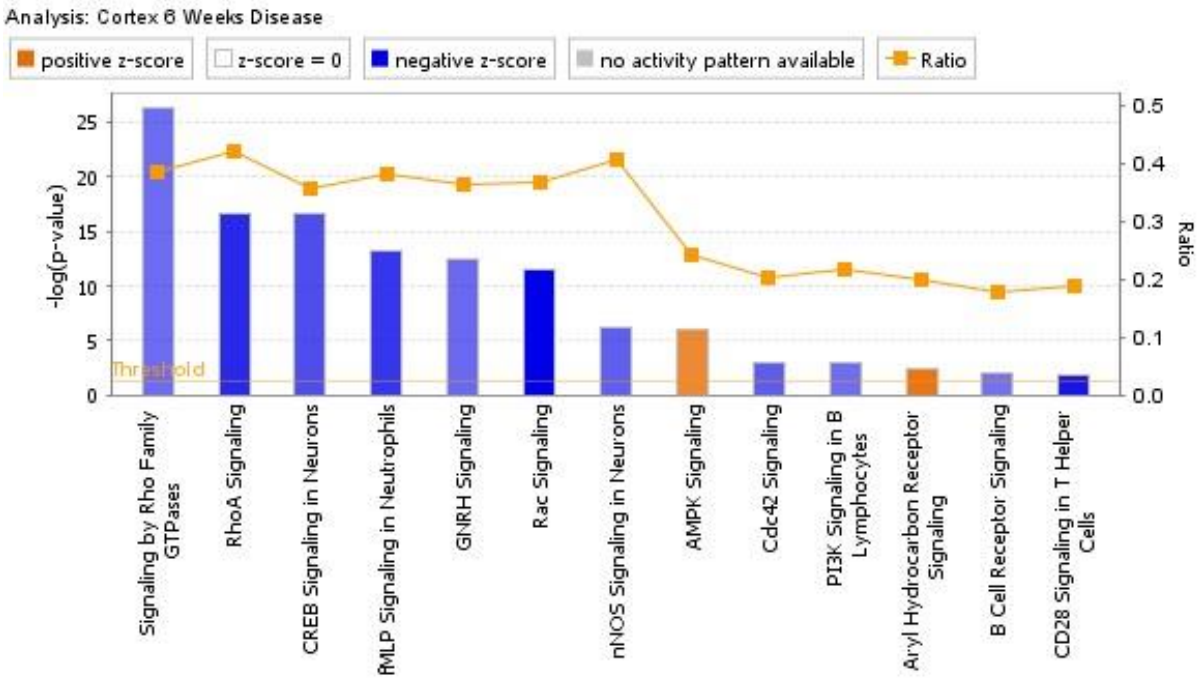

Figure 4.2.5 Activated and inhibited pathways at 6 weeks cortex.

Protein was extracted from the cortex of rNLS mice at 2, 4, and 6-week timepoints. SWATH MS was conducted (n=3-5 mice) to identify and quantify proteins that changed in TDP-43 mice compared to control non-bigenic mice. Ingenuity Pathway Analysis (IPA) software was used to determine the most activated (orange) and inhibited (blue) pathways. An algorithm within IPA, called z-scores, considers the directional effect of one protein on another protein or on a pathway, and the direction of protein changes within the experimental dataset to predict activation (z-score of 2 or more) or inhibition

(z-score of -2 or less). The left y-axis displays the -log of p-value calculated by a Fisher's exact test right-tailed (-log[p-value 0.05]=1.3). The right y-axis displays the ratio (orange line) of proteins within experimental dataset divided by the total number of proteins within that pathway that are curated within the reference set. Reported are the activated and inhibited pathways that also generated a p-value of ≤ 0.05 at 6 weeks cortex.

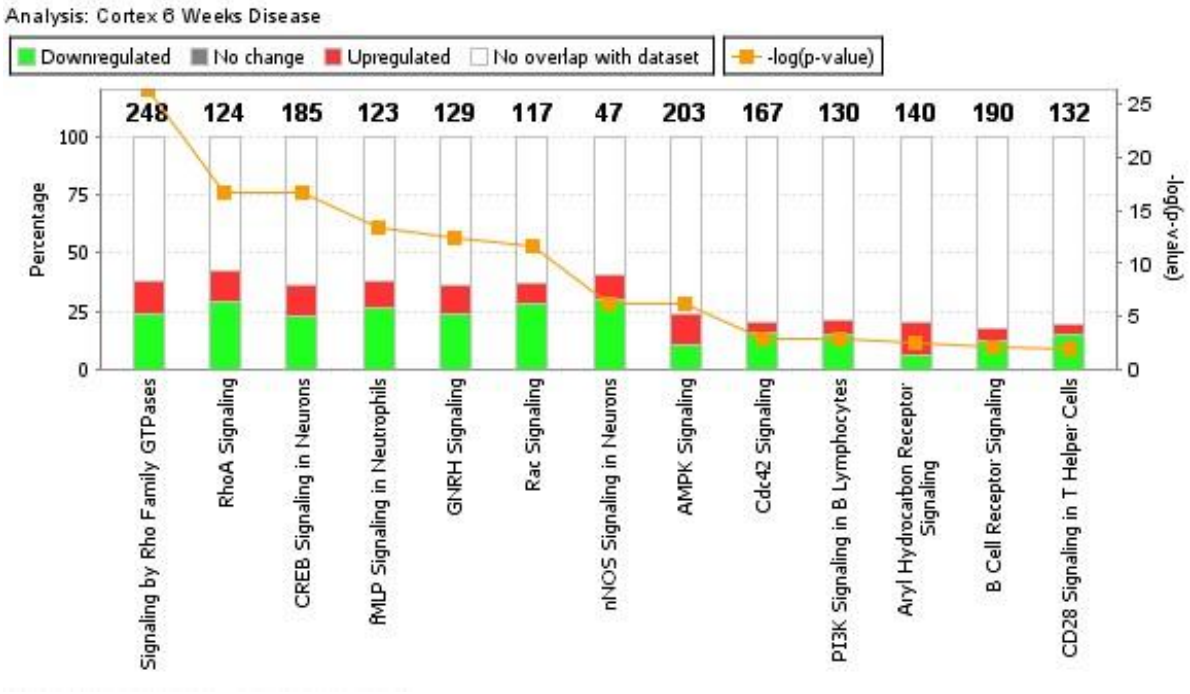

Figure 4.2.6 Activated and inhibited pathways at 6 weeks cortex- percentage of proteins changed.

Protein was extracted from the cortex of rNLS mice at 2, 4, and 6-week timepoints. SWATH MS was conducted (n=3-5 mice) to identify and quantify proteins that changed in TDP-43 mice compared to control non-bigenic mice. Ingenuity Pathway Analysis (IPA) software was used to determine the most activated and inhibited pathways. This stacked bar chart displays the percentage of up- and down-regulated proteins within each pathway shown in ***Figure 4.2.5****. The right y-axis displays the percentage of proteins within experimental dataset that have up regulated (red) or down-regulated (green). The left y-axis displays the -log of p-value (orange line) calculated by a Fisher's exact test right-tailed (-log[p-value 0.05]=1.3). Reported are the activated and inhibited pathways that also generated a p-value of ≤ 0.05 at 6 weeks cortex.*

To examine the *intersection* of the activated and inhibited pathways during disease progression within the *cortex*, JVenn was used to visualise the overlap between the 3 timepoints for both the activated and inhibited pathways. This revealed that there were no activated pathways that overlapped across all timepoints within the cortex (**Figure 4.2.7**). Two pathways were activated at both 2- and 4-weeks disease: apoptosis signalling and HIPPO signalling (**Figure 4.2.7**). When analysing the inhibited pathways, 7 pathways overlapped across all 3 timepoints: Rac signalling, fMLP signalling in Neutrophils, signalling by Rho Family GTPases, CD28 signalling in T Helper Cells, Cdc42 signalling, B Cell Receptor signalling, and CREB signalling in Neurons (**Figure 4.2.8**).

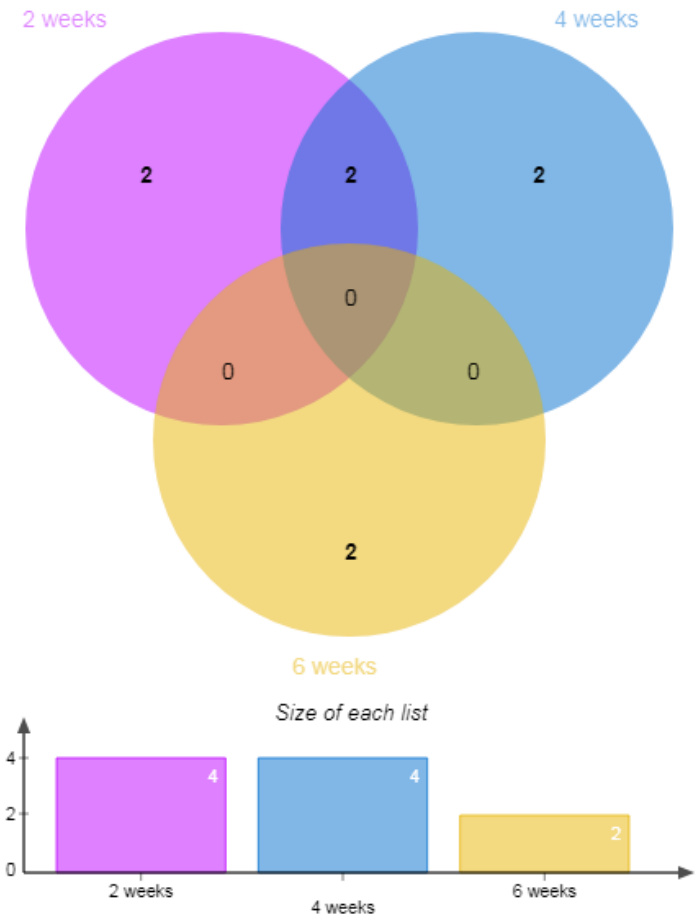

Figure 4.2.7 Overlap of activated pathways within the cortex at 2, 4, and 6-weeks.

Protein was extracted from the cortex of rNLS mice at 2, 4, and 6-week timepoints. SWATH MS was conducted (n=3-5 mice) to identify and quantify proteins that changed in TDP-43 mice compared to control non-bigenic mice. Ingenuity Pathway Analysis (IPA) software was used to determine the most activated pathways. JVenn was used to determine the overlap of activated pathways at 2, 4, and 6-week timepoints (http://jvenn.toulouse.inra.fr/app/index.html).

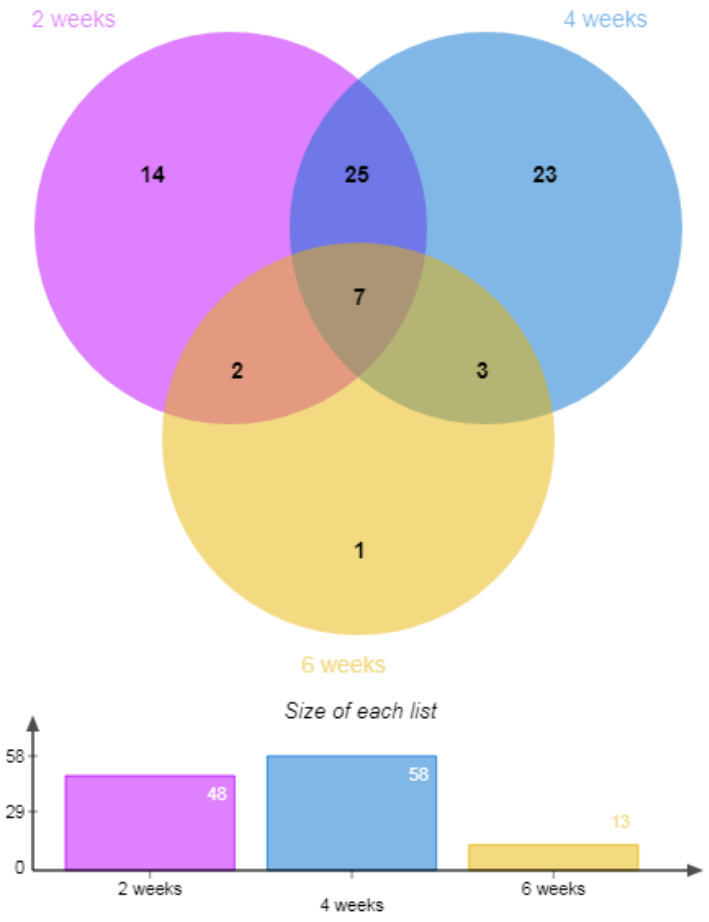

Figure 4.2.8 Overlap of inhibited pathways within the cortex at 2,4, and 6-weeks.

Protein was extracted from the cortex of rNLS mice at 2, 4, and 6-week timepoints. SWATH MS was conducted (n=3-5 mice) to identify and quantify proteins that changed in TDP-43 mice compared to control non-bigenic mice. Ingenuity Pathway Analysis (IPA) software was used to determine the most inhibited pathways. JVenn was used to

determine the overlap of inhibited pathways at 2, 4, and 6-week timepoints (http://jvenn.toulouse.inra.fr/app/index.html).

To identify which pathways were the *most significant enrichment* by proteins from the experimental dataset (regardless of the activation state), the top 15 enriched pathways based on p-value were extracted (**Table 4.2.4, Figure 4.2.9**). The top 3 significantly enriched pathways, at all timepoints within the *cortex* include EIF2 signalling, mitochondrial dysfunction, and signalling by Rho Family GTPases (**Table 4.2.4, Figure 4.2.9**). For most of the significantly enriched pathways IPA could not generate an activity pattern due to lack of information about the pathway activation state within the IPA reference database. For example, mitochondrial dysfunction is highly significantly enriched across all timepoints (p-value of enrichment 7.94E-31) with a 47.7% overlap between proteins within the pathway and experimental dataset (**Table 4.2.4, Figure 4.2.9**). However, the overall activity state of mitochondrial dysfunction cannot be determined by IPA (hence no z-score) due to lack of available information within the reference set.

Table 4.2.4 Top 15 most significantly enriched pathways within cortex during disease course.

Protein was extracted from the cortex of rNLS mice at 2, 4, and 6-week timepoints. SWATH MS was conducted (n=3-5 mice) to identify and quantify proteins that changed in TDP-43 mice compared to control non-bigenic mice. Ingenuity Pathway Analysis (IPA) software was used to determine the most significantly enriched pathways (pathways with that show most significant overlap of proteins within dataset and IPA reference set). The significance was calculated by a Fisher's exact test right-tailed (-log[p-value 0.05]=1.3), shown by the left y-axis. An algorithm within IPA, called z-scores, considers the directional effect of one protein on another protein or on a pathway, and the direction of protein changes within the experimental dataset to predict activation (z-score of 2 or more) or inhibition (z-score of -2 or less). IPA does not contain activity information for all pathways, and these pathways are shown in grey as

'no activity pattern available' (NAPA). The right y-axis displays the ratio (orange line) of proteins within experimental dataset divided by the total number of proteins within that pathway that are curated within the reference set. Reported are the top significantly enriched pathways that also generated a p-value of ≤ 0.05 at 2, 4, and 6-weeks in the cortex.

Pathway name	z-score			p-value	-log(p-value)	Ratio
	Week 2	Week 4	Week 6			
EIF2 Signalling	2.10	0.14	-1.54	1.00E-39	39	105/221 (0.475)
Mitochondrial Dysfunction	NAPA	NAPA	NAPA	7.94E-31	30.1	81/171 (0.474)
Signalling by Rho Family GTPases	-3.54	-2.36	-2.12	5.01E-27	26.3	94/248 (0.383)
mTOR Signalling	0.32	-2.53	0.32	2.51E-26	25.6	83/201 (0.413)
Regulation of eIF4 and p70S6K Signalling	0.22	-1.09	1.09	1.26E-25	24.9	71/157 (0.452)
Remodelling of Epithelial Adherens Junctions	-1.09	-2.40	-1.09	2.00E-25	24.7	45/69 (0.652)
Breast Cancer Regulation by Stathmin1	NAPA	NAPA	NAPA	1.26E-24	23.9	81/203 (0.399)
Clathrin-mediated Endocytosis Signalling	NAPA	NAPA	NAPA	7.94E-24	23.1	79/199 (0.397)
RhoGDI Signalling	2.50	1.39	1.11	2.51E-23	22.6	72/173 (0.416)
Huntington's Disease Signalling	-1.18	-1.52	-0.51	1.58E-22	21.8	87/243 (0.358)
Oxidative Phosphorylation	NAPA	NAPA	NAPA	2.00E-20	19.7	52/109 (0.477)
Synaptic Long-Term Potentiation	-1.63	-3.27	-1.63	2.51E-20	19.6	55/121 (0.455)
Protein Ubiquitination Pathway	NAPA	NAPA	NAPA	3.16E-20	19.5	88/265 (0.332)
Axonal Guidance Signalling	NAPA	NAPA	NAPA	7.94E-20	19.1	124/452 (0.274)
α-Adrenergic Signalling	-1.92	-2.61	-1.22	1.26E-19	18.9	45/87 (0.517)

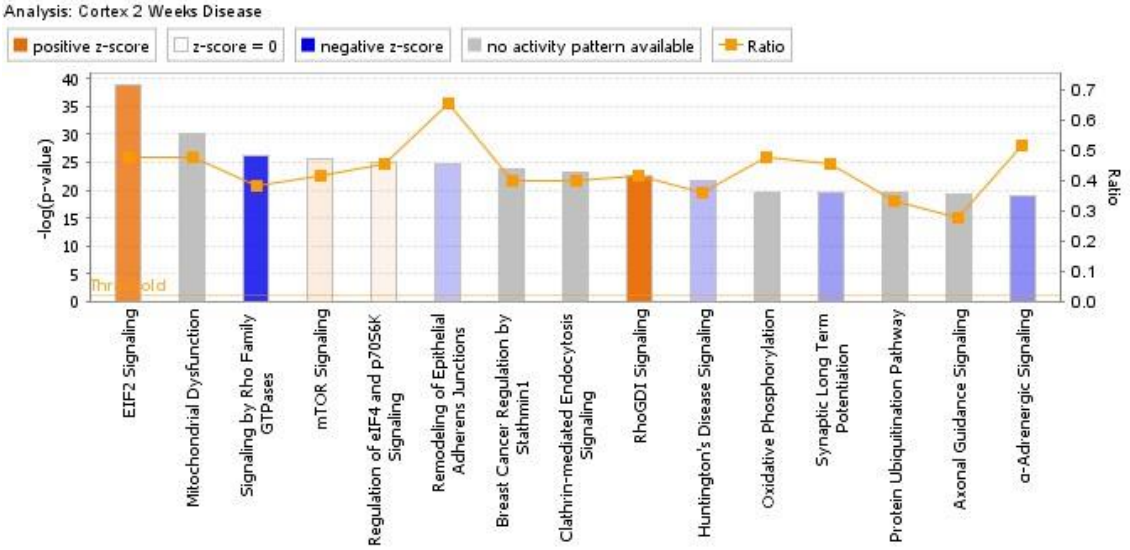
Analysis: Cortex 2 Weeks Disease
positive z-score
z-score = 0
negative z-score
no activity pattern available
Ratio
-log(p-value)
Ratio
EIF2 Signaling
Mitochondrial Dysfunction
Signaling by Rho Family GTPases
mTOR Signaling
Regulation of eIF4 and p70S6K Signaling
Remodeling of Epithelial Adherens Junctions
Breast Cancer Regulation by Stathmin1
Clathrin-mediated Endocytosis Signaling
RhoGDI Signaling
Huntington's Disease Signaling
Oxidative Phosphorylation
Synaptic Long Term Potentiation
Protein Ubiquitination Pathway
Axonal Guidance Signaling
α-Adrenergic Signaling

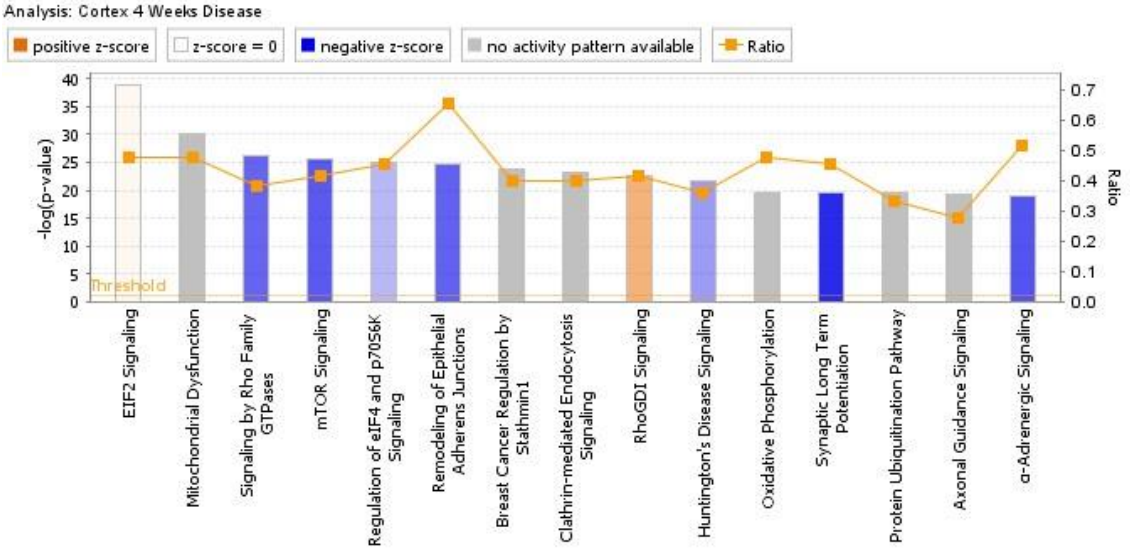
Analysis: Cortex 4 Weeks Disease
positive z-score
z-score = 0
negative z-score
no activity pattern available
Ratio
-log(p-value)
Ratio
Threshold
EIF2 Signaling
Mitochondrial Dysfunction
Signaling by Rho Family GTPases
mTOR Signaling
Regulation of eIF4 and p70S6K Signaling
Remodeling of Epithelial Adherens Junctions
Breast Cancer Regulation by Stathmin1
Clathrin-mediated Endocytosis Signaling
RhoGDI Signaling
Huntington's Disease Signaling
Oxidative Phosphorylation
Synaptic Long Term Potentiation
Protein Ubiquitination Pathway
Axonal Guidance Signaling
α-Adrenergic Signaling

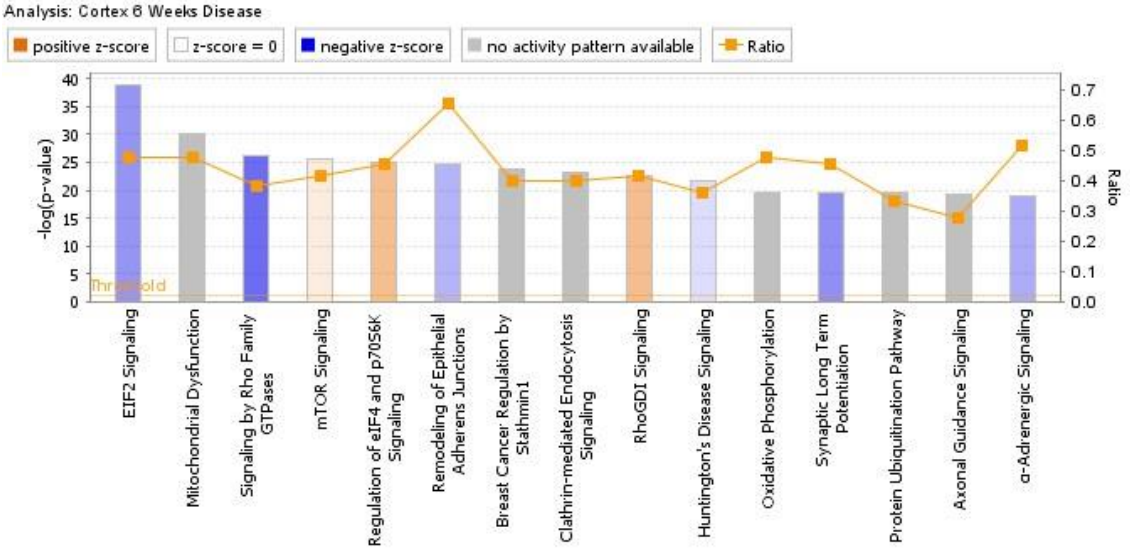
Analysis: Cortex 6 Weeks Disease
positive z-score
z-score = 0
negative z-score
no activity pattern available
Ratio
-log(p-value)
Ratio
EIF2 Signaling
Mitochondrial Dysfunction
Signaling by Rho Family GTPases
mTOR Signaling
Regulation of eIF4 and p70S6K Signaling
Remodeling of Epithelial Adherens Junctions
Breast Cancer Regulation by Stathmin1
Clathrin-mediated Endocytosis Signaling
RhoGDI Signaling
Huntington's Disease Signaling
Oxidative Phosphorylation
Synaptic Long Term Potentiation
Protein Ubiquitination Pathway
Axonal Guidance Signaling
α-Adrenergic Signaling

Figure 4.2.9 Top 15 most significantly enriched pathways within cortex during disease course.

Protein was extracted from the cortex of rNLS mice at 2, 4, and 6-week timepoints. SWATH MS was conducted (n=3-5 mice) to identify and quantify proteins that changed in TDP-43 mice compared to control non-bigenic mice. Ingenuity Pathway Analysis (IPA) software was used to determine the most significantly enriched pathways (pathways with that show most significant overlap of proteins within dataset and IPA reference set). The significance was calculated by a Fisher's exact test right-tailed (-log[p-value 0.05]=1.3), shown by the left y-axis. An algorithm within IPA, called z-scores, considers the directional effect of one protein on another protein or on a pathway, and the direction of protein changes within the experimental dataset to predict activation (z-score of 2 or more) or inhibition (z-score of -2 or less). IPA does not contain activity information for all pathways, and these pathways are shown in grey as 'no activity pattern available'. The right y-axis displays the ratio (orange line) of proteins within experimental dataset divided by the total number of proteins within that pathway that are curated within the reference set. Reported are the top significantly enriched pathways that also generated a p-value of ≤ 0.05 at 2, 4, and 6-weeks in the cortex.

At the *2-week* timepoint within the *spinal cord* there was 1 activated pathway and 2 inhibited pathways (**Table 4.2.5**). The activated pathway was RhoGDI signalling with 10% of the proteins within the pathway being upregulated (**Table 4.2.5, Figure 4.2.10, Figure 4.2.11**). The two inhibited pathways were regulation of actin-based motility by Rho (20% of proteins down-regulated within pathway) and RhoA Signalling (18% of proteins down-regulated within the pathway) (**Table 4.2.5, Figure 4.2.10, Figure 4.2.11**).

Table 4.2.5 Activated and inhibited pathways at 2 weeks spinal cord.

Protein was extracted from the spinal cord of rNLS mice at 2 and 6-week timepoints. SWATH MS was conducted (n=3-5 mice) to identify and quantify proteins that changed in TDP-43 mice compared to control non-bigenic mice. Ingenuity Pathway Analysis (IPA) software was used to determine the most activated (orange) and inhibited (blue) pathways. An algorithm within IPA, called z-scores, considers the directional effect of one protein on another protein or on a pathway, and the direction of protein changes within the experimental dataset to predict activation (z-score of 2 or more) or inhibition (z-score of -2 or less). The significance is calculated by a Fisher's exact test right-tailed (-log[p-value 0.05]=1.3). Reported are all the activated and inhibited pathways that also generated a p-value of ≤ 0.05 at 2 weeks spinal cord.

Activated and inhibited pathways spinal cord - 2 weeks					
Canonical pathway	**z-score**	**Overall Predicted State**	**p-value**	**-log(p-value)**	**Percentage of dataset proteins within pathway**
RhoGDI Signalling	2.191	Activated	5.01E-19	18.3	26.0
Regulation of Actin-based Motility by Rho	-2.449	Inhibited	1.00E-12	12.0	28.9
RhoA Signalling	-2.263	Inhibited	2.00E-15	14.7	27.4

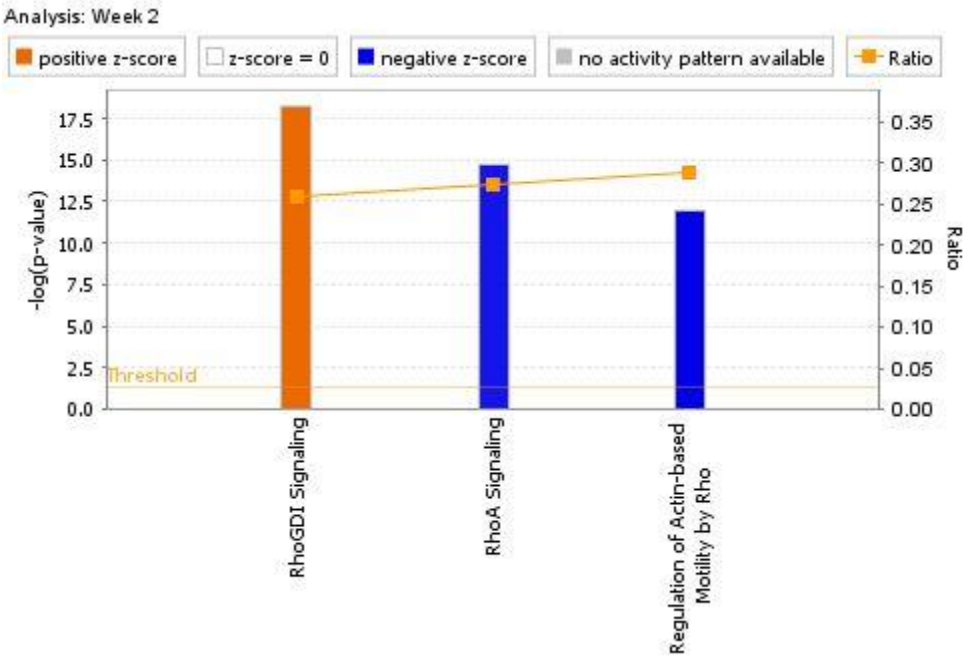

Figure 4.2.10 Activated and inhibited pathways at 2 weeks spinal cord.

Protein was extracted from the spinal cord of rNLS mice at 2 and 6-week timepoints. SWATH MS was conducted (n=3-5 mice) to identify and quantify proteins that changed in TDP-43 mice compared to control non-bigenic mice. Ingenuity Pathway Analysis (IPA) software was used to determine the most activated (orange) and inhibited (blue) pathways. An algorithm within IPA, called z-scores, considers the directional effect of one protein on another protein or on a pathway, and the direction of protein changes within the experimental dataset to predict activation (z-score of 2 or more) or inhibition (z-score of -2 or less). The left y-axis displays the -log of p-value calculated by a Fisher's exact test right-tailed (-log[p-value 0.05]=1.3). The right y-axis displays the ratio (orange line) of proteins within experimental dataset divided by the total number of proteins within that pathway that are curated within the reference set. Reported are the activated and inhibited pathways that also generated a p-value of ≤ 0.05 at 2 weeks spinal cord.

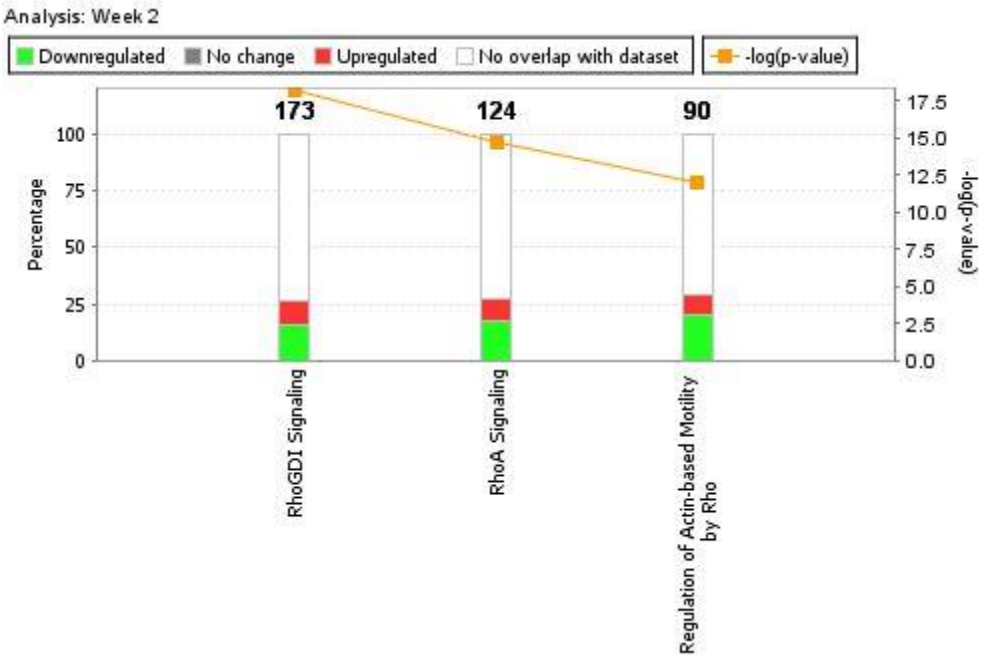

Figure 4.2.11 Activated and inhibited pathways at 2 weeks spinal cord- percentage of proteins changed.

Protein was extracted from the spinal cord of rNLS mice at 2 and 6-week timepoints. SWATH MS was conducted (n=3-5 mice) to identify and quantify proteins that changed in TDP-43 mice compared to control non-bigenic mice. Ingenuity Pathway Analysis (IPA) software was used to determine the most activated and inhibited pathways. This stacked bar chart displays the percentage of up- and down-regulated proteins within each pathway shown in ***Figure 4.2.10****. The right y-axis displays the percentage of proteins within experimental dataset that have up regulated (red) or down-regulated (green). The left y-axis displays the -log of p-value (orange line) calculated by a Fisher's exact test right-tailed (-log[p-value 0.05]=1.3). Reported are the top activated and inhibited pathways that also generated a p-value of ≤ 0.05 at 2 weeks spinal cord.*

At the *6-week* timepoint within the *spinal cord* there were no predications about activated pathways while 12 pathways were inhibited (**Table 4.2.6**). The top inhibited pathway (lowest z-score) was telomerase signalling with 6% of proteins within the pathway being down-regulated (**Table 4.2.6, Figure 4.2.12, Figure 4.2.13**). The most significantly enriched inhibited pathway was ILK signalling with 12% of proteins within the pathway being down-regulated (**Table 4.2.6, Figure 4.2.12, Figure 4.2.13**).

There were no *intersections* between the activated and inhibited pathways within the spinal cord across the two timepoints.

Table 4.2.6 Inhibited pathways at 6 weeks spinal cord.

Protein was extracted from the spinal cord of rNLS mice at 2 and 6-week timepoints. SWATH MS was conducted (n=3-5 mice) to identify and quantify proteins that changed in TDP-43 mice compared to control non-bigenic mice. Ingenuity Pathway Analysis (IPA) software was used to determine the most activated (orange) and inhibited (blue) pathways. An algorithm within IPA, called z-scores, considers the directional effect of one protein on another protein or on a pathway, and the direction of protein changes within the experimental dataset to predict activation (z-score of 2 or more) or inhibition (z-score of -2 or less). The significance is calculated by a Fisher's exact test right-tailed (-log[p-value 0.05]=1.3). Reported are all the activated and inhibited pathways that also generated a p-value of ≤ 0.05 at 6 weeks spinal cord. There was no activated pathway prediction for 6-weeks spinal cord.

Activated and inhibited pathways spinal cord - 6 weeks					
Pathway name	**z-score**	**Overall Predicted State**	**p-value**	**-log(p-value)**	**Percentage of dataset proteins within pathway**
Telomerase Signalling	-2.89	Inhibited	7.24E-03	2.14	11.7
Agrin Interactions at Neuromuscular Junction	-2.71	Inhibited	1.17E-03	2.93	15.9
p70S6K Signalling	-2.67	Inhibited	6.76E-07	6.17	17.4
PI3K/AKT Signalling	-2.40	Inhibited	3.80E-06	5.42	16.8
Regulation of eIF4 and p70S6K Signalling	-2.33	Inhibited	3.63E-07	6.44	16.6
mTOR Signalling	-2.32	Inhibited	1.55E-06	5.81	14.4
ILK Signalling	-2.27	Inhibited	2.82E-07	6.55	15.3

Renin-Angiotensin Signalling	-2.14	Inhibited	6.61E-03	2.18	11.5
Renal Cell Carcinoma Signalling	-2.12	Inhibited	3.63E-02	1.44	10.8
B Cell Receptor Signalling	-2.07	Inhibited	7.76E-03	2.11	10
ERK/MAPK Signalling	-2.04	Inhibited	1.26E-06	5.90	14.6
P2Y Purigenic Receptor Signalling Pathway	-2.00	Inhibited	7.76E-07	6.11	17.3

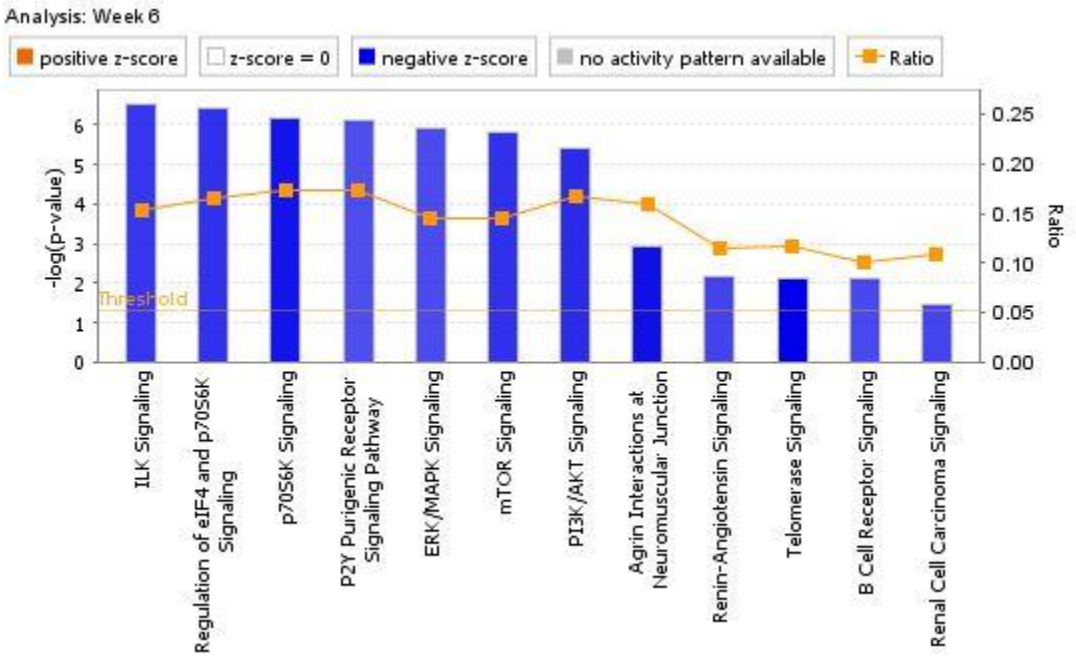

Figure 4.2.12 Top inhibited pathways at 6 weeks spinal cord.

Protein was extracted from the spinal cord of rNLS mice at 2 and 6-week timepoints. SWATH MS was conducted (n=3-5 mice) to identify and quantify proteins that changed in TDP-43 mice compared to control non-bigenic mice. Ingenuity Pathway Analysis (IPA) software was used to determine the most activated (orange) and inhibited (blue) pathways. An algorithm within IPA, called z-scores, considers the directional effect of one protein on another protein or on a pathway, and the direction of protein changes within the experimental dataset to predict activation (z-score of 2 or more) or inhibition (z-score of -2 or less). The left y-axis displays the -log of p-value calculated by a Fisher's exact test right-tailed (-log[p-value 0.05]=1.3). The right y-axis displays the ratio (orange line) of proteins within experimental dataset divided by the total number of proteins within that pathway that are curated within the reference set. Reported are the inhibited pathways that also generated a p-value of ≤ 0.05 at 6 weeks spinal cord. There was no activated pathway prediction for 6-weeks spinal cord.

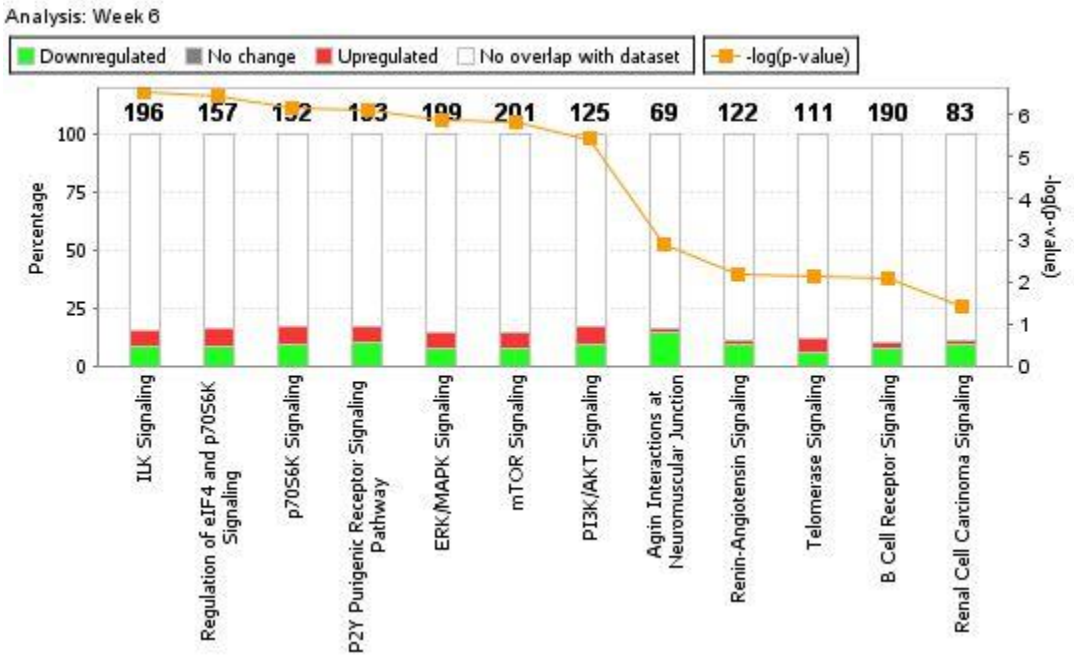

Figure 4.2.13 Inhibited pathways at 6 weeks spinal cord- percentage of proteins changed.

Protein was extracted from the spinal cord of rNLS mice at 2 and 6-week timepoints. SWATH MS was conducted (n=3-5 mice) to identify and quantify proteins that changed in TDP-43 mice compared to control non-bigenic mice. Ingenuity Pathway Analysis (IPA) software was used to determine the most activated and inhibited pathways. This stacked bar chart displays the percentage of up- and down-regulated proteins within each pathway shown in ***Figure 4.2.12****. The right y-axis displays the percentage of proteins within experimental dataset that have up regulated (red) or down-regulated (green). The left y-axis displays the -log of p-value (orange line) calculated by a Fisher's exact test right-tailed (-log[p-value 0.05]=1.3). Reported are the top inhibited pathways that also generated a p-value of ≤ 0.05 at 6 weeks spinal cord. There was no activated pathway prediction for 6-weeks spinal cord.*

The 15 top *most significantly enriched* pathways within the *spinal cord* were extracted according to p-value with the top 3 pathways being mitochondrial dysfunction, oxidative phosphorylation, and signalling by Rho Family GTPases (**Table 4.2.7, Figure 4.2.14**). Here, again for most significantly enriched pathways IPA does not contain enough information to predict activation or inhibition (**Table 4.2.7, Figure 4.2.14**).

Table 4.2.7 Top 15 most significantly enriched pathways within spinal during disease course.

Protein was extracted from the cortex of rNLS mice at 2, 4, and 6-week timepoints. SWATH MS was conducted (n=3-5 mice) to identify and quantify proteins that changed in TDP-43 mice compared to control non-bigenic mice. Ingenuity Pathway Analysis (IPA) software was used to determine the most significantly enriched pathways (pathways with that show most significant overlap of proteins within dataset and IPA reference set). The significance was calculated by a Fisher's exact test right-tailed (-log[p-value 0.05]=1.3), shown by the left y-axis. An algorithm within IPA, called z-scores, considers the directional effect of one protein on another protein or on a pathway, and the direction of protein changes within the experimental dataset to predict activation (z-score of 2 or more) or inhibition (z-score of -2 or less). IPA does not contain activity information for all pathways, and these pathways are shown in grey as 'no activity pattern available' (NAPA). The right y-axis displays the ratio (orange line) of proteins within experimental dataset divided by the total number of proteins within that pathway that are curated within the reference set. Reported are the top significantly enriched pathways that also generated a p-value of ≤ 0.05 at 2 and 6-weeks in the spinal.

Pathway name	z-score#		p-value	-log(p-value)*	Ratio^
	Week 2	Week 6			
Mitochondrial Dysfunction	NAPA	NAPA	3.98E-41	40.4	0.398
Oxidative Phosphorylation	NAPA	NAPA	1.58E-29	28.8	0.422
Signalling by Rho Family GTPases	-1.51	-1.21	6.31E-24	23.2	0.246
Clathrin-mediated Endocytosis Signalling	NAPA	NAPA	1.26E-22	21.9	0.266
Remodelling of Epithelial Adherens Junctions	0.54	1.07	5.01E-19	18.3	0.420
RhoGDI Signalling	2.19	0	5.01E-19	18.3	0.260
Protein Ubiquitination Pathway	NAPA	NAPA	2.51E-17	16.6	0.204
Breast Cancer Regulation by Stathmin1	NAPA	NAPA	7.94E-17	16.1	0.227
Protein Kinase A Signalling	-0.27	0.54	3.16E-16	15.5	0.167
TCA Cycle II (Eukaryotic)	NAPA	NAPA	1.00E-15	15	0.696

Huntington's Disease Signalling	0.28	-0.83	1.26E-15	14.9	0.202
RhoA Signalling	-2.26	-1.22	2.00E-15	14.7	0.274
Phagosome Maturation	NAPA	NAPA	3.16E-15	14.5	0.250
Ephrin B Signalling	-1.27	0	3.98E-15	14.4	0.356
Actin Cytoskeleton Signalling	-1.23	0	1.26E-13	12.9	0.194

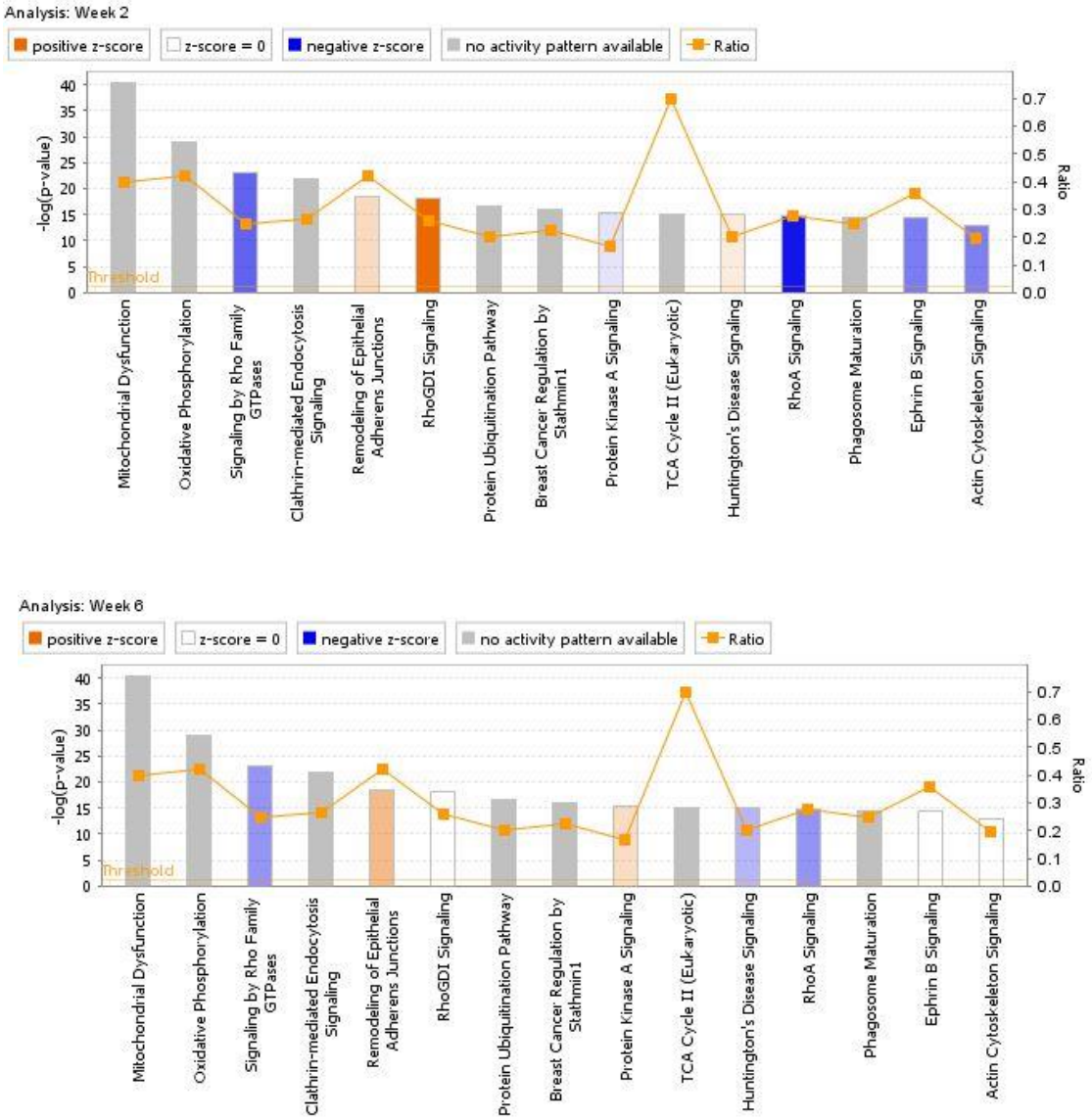

Figure 4.2.14 Top 15 most significantly enriched pathways within spinal cord during disease course.

Protein was extracted from the spinal cord of rNLS mice at 2 and 6-week timepoints. SWATH MS was conducted (n=3-5 mice) to identify and quantify proteins that changed in TDP-43 mice compared to control non-bigenic mice. Ingenuity Pathway Analysis (IPA) software was used to determine the most significantly enriched pathways (pathways with that show most significant overlap of proteins within dataset and IPA reference set). The significance was calculated by a Fisher's exact test right-tailed (-log[p-value 0.05]=1.3), shown by the left y-axis. An algorithm within IPA, called z-scores, considers the directional effect of one protein on another protein or on a pathway, and the direction of protein changes within the experimental dataset to predict activation (z-score of 2 or more) or inhibition (z-score of -2 or less). IPA does not contain activity information for all pathways, and these pathways are shown in grey as 'no activity pattern available'. The right y-axis displays the ratio (orange line) of proteins within experimental dataset divided by the total number of proteins within that pathway that are curated within the reference set. Reported are the top significantly enriched pathways that also generated a p-value of ≤ 0.05 at 2 and 6-weeks in the spinal cord.

4.2.3 Mapping pathways across disease course

To gain more detailed insight into the top activated, inhibited, and enriched pathways, each pathway was first mapped using IPA. A tool within IPA called Molecule Activity Predictor (MAP) was then used to compare the predicted activity pattern observed in the experimental proteomic dataset to the expected pattern within IPA reference set for each pathway. MAP predicts both the upstream and downstream effects of protein changes *and* the increase or decrease of diseases and/or functional end-points associated each canonical pathway. The activity pattern of each pathway is determined by the curation of key regulator proteins within each pathway that must be in a known state for the pathway to be activated or inhibited. The causal relationships that create the pathways are based on both direct and indirect protein interactions.

At two *2 weeks* disease within the *cortex* the top *activated* pathway was apoptosis signalling. The pathway MAP prediction revealed that while apoptosis was not activated, there was an activation of cell shrinkage and an inhibition of DNA repair (**Figure 4.2.15**). In addition, DNA fragmentation was both activated and inhibited by two different cascades within the apoptosis pathway (**Figure 4.2.15**). The top *inhibited* pathway at cortex 2-weeks was Rac signalling pathway which resulted in the predicted *inhibition* of actin polymerisation (via two cascades), protein translation, cell-cell adhesion, and transcription (**Figure 4.2.16**). At the same timepoint, the top *enriched* pathway was EIF2 signalling which revealed an integrated stress response with the *activation* of ER stress response, assembly of stress granules, translation elongation, and amino acid biosynthesis and transport (**Figure 4.2.17**).

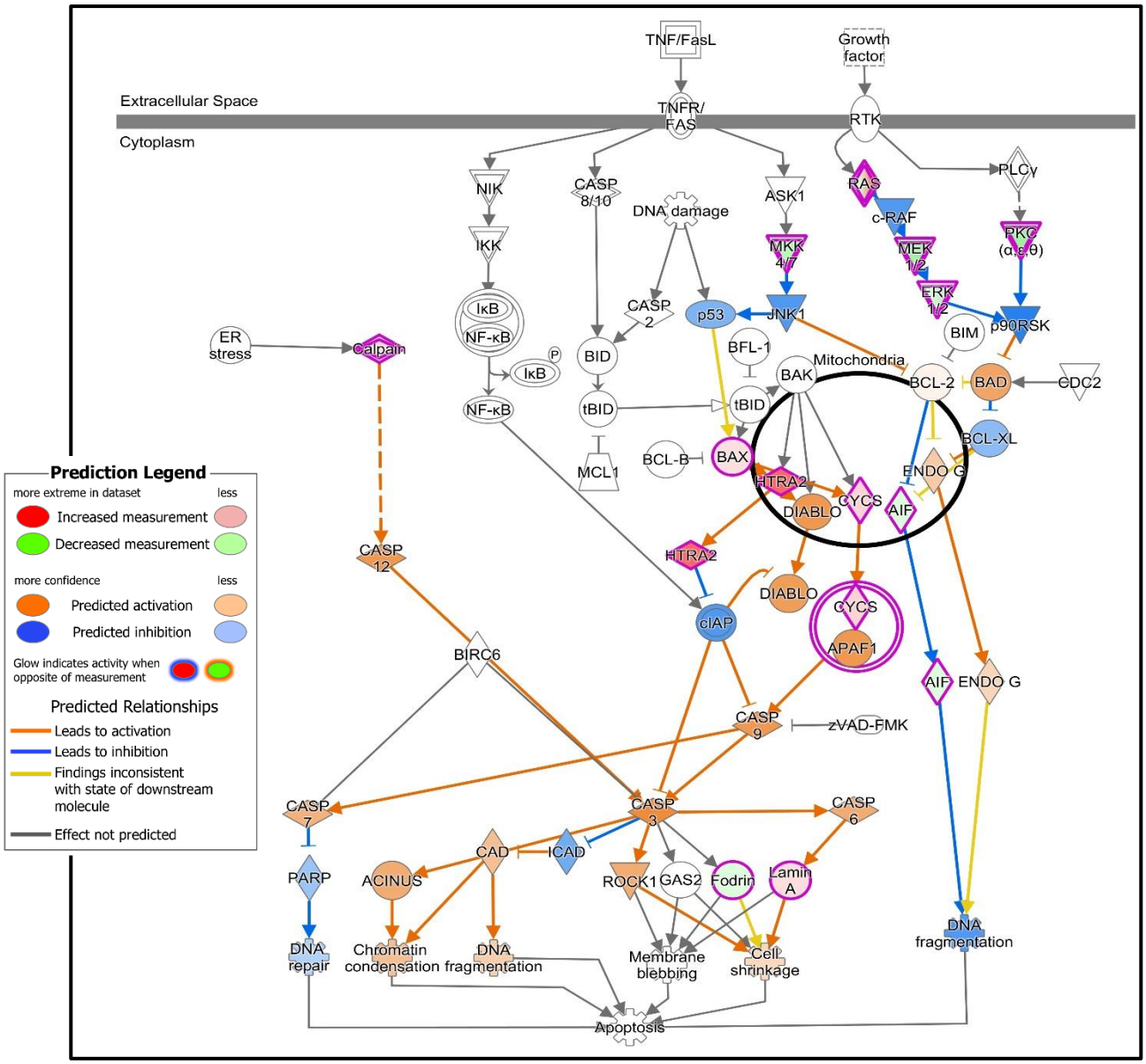

Figure 4.2.15 Top activated pathway at 2-weeks disease within cortex- apoptosis signalling.

Protein was extracted from the cortex of rNLS mice at 2, 4, and 6-week timepoints. SWATH MS was conducted (n=3-5 mice) to identify and quantify proteins that changed in TDP-43 mice compared to control non-bigenic mice. Ingenuity Pathway Analysis (IPA) software was used to map the most activated, inhibited, and enriched pathways at each timepoint. A tool within IPA called Molecule Activity Predictor (MAP) was then used to compare the predicted activity pattern observed in the experimental proteomic dataset to the expected pattern within IPA reference set for each pathway. MAP also predicted the increase/decrease of diseases and/or functional end points within each canonical pathway. Pink: experimental dataset proteins that overlap with pathway; red:

upregulation; green: down regulation; double bordered: group or complex; white: protein within pathway that do not overlap with experimental dataset.

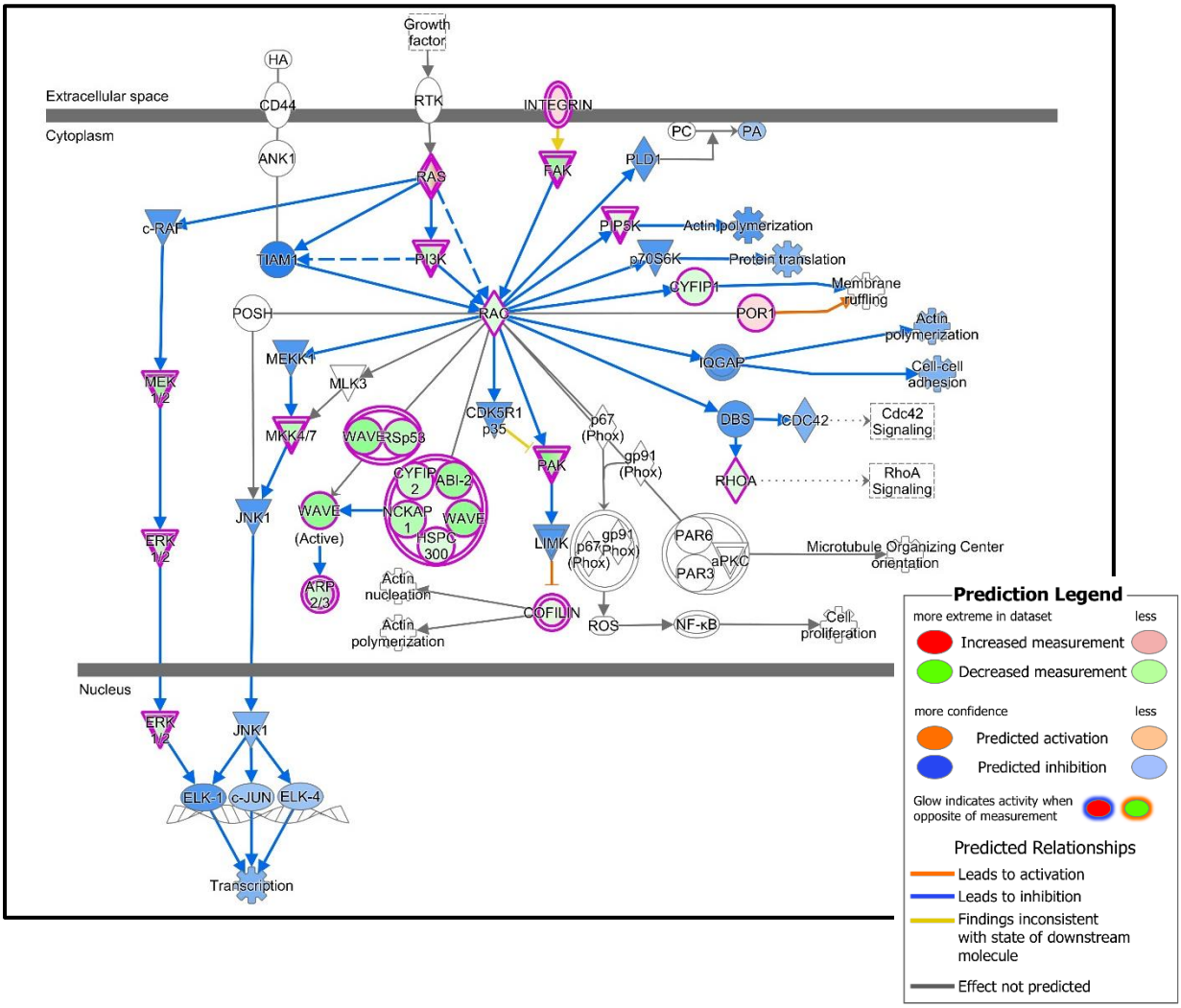

Figure 4.2.16 Top inhibited pathway at 2-weeks disease within cortex- Rac Signaling.

Protein was extracted from the cortex of rNLS mice at 2, 4, and 6-week timepoints. SWATH MS was conducted (n=3-5 mice) to identify and quantify proteins that changed in TDP-43 mice compared to control non-bigenic mice. Ingenuity Pathway Analysis (IPA) software was used to map the most activated, inhibited, and enriched pathways at each timepoint. A tool within IPA called Molecule Activity Predictor (MAP) was then used to compare the predicted activity pattern observed in the experimental proteomic dataset to the expected pattern within IPA reference set for each pathway. MAP also predicted the increase/decrease of diseases and/or functional end points within each

canonical pathway. Pink: experimental dataset proteins that overlap with pathway; red: upregulation; green: down regulation; double bordered: group or complex; white: protein within pathway that do not overlap with experimental dataset.

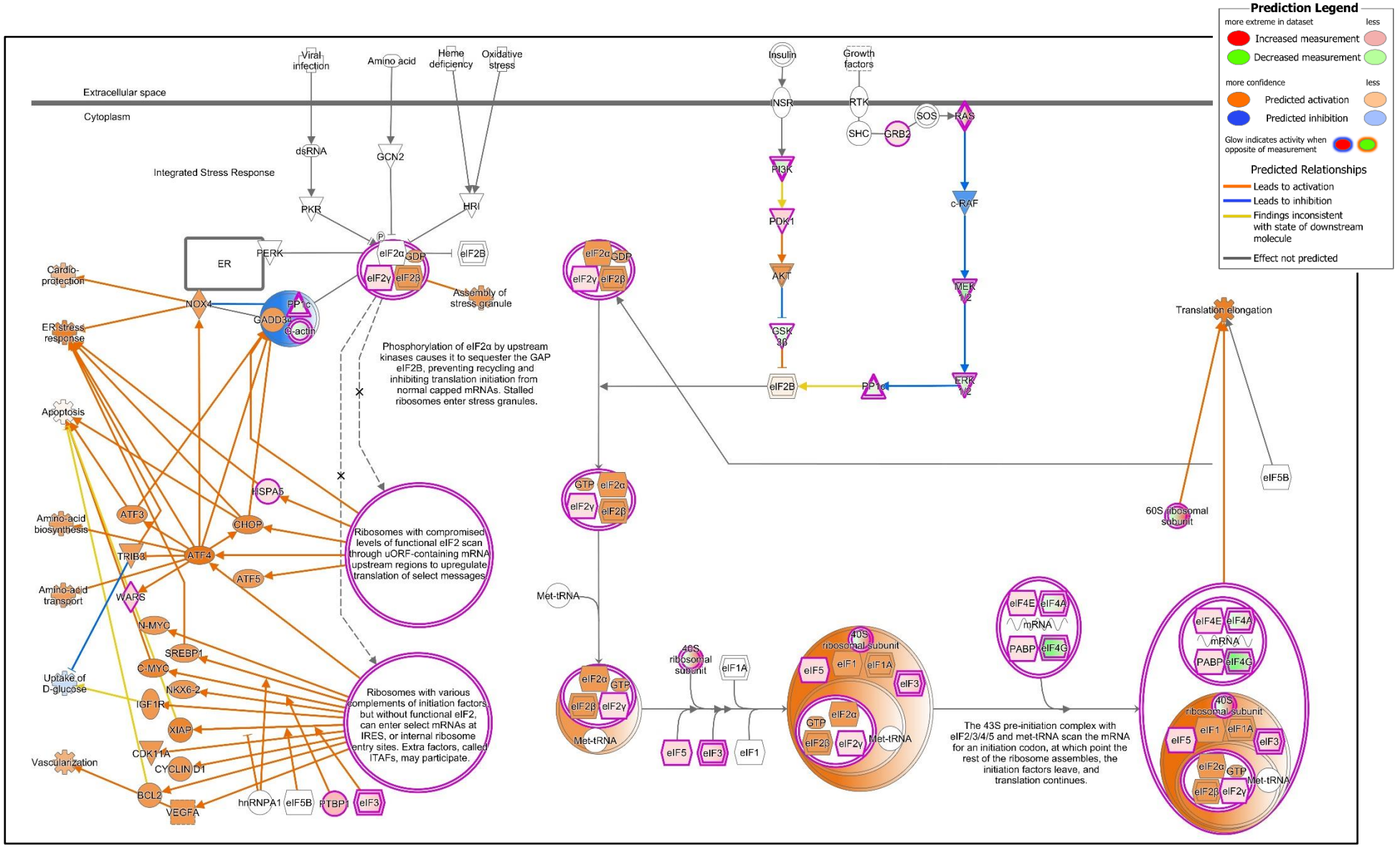

Figure 4.2.17 Top enriched pathway at 2-weeks disease within cortex- EIF2 Signalling.

Protein was extracted from the cortex of rNLS mice at 2, 4, and 6-week timepoints. SWATH MS was conducted (n=3-5 mice) to identify and quantify proteins that changed in TDP-43 mice compared to control non-bigenic mice. Ingenuity Pathway Analysis (IPA) software was used to map the most activated, inhibited, and enriched pathways at each timepoint. A tool within IPA called Molecule Activity Predictor (MAP) was then used to compare the predicted activity pattern observed in the experimental proteomic dataset to the expected pattern within IPA reference set for each pathway. MAP also predicted the increase/decrease of diseases and/or functional end points within each canonical pathway. Pink: experimental dataset proteins that overlap with pathway; red: upregulation; green: down regulation; double bordered: group or complex; white: protein within pathway that do not overlap with experimental dataset.

.

At the *4-week* timepoint within the *cortex*, the top *activated* pathway was again apoptosis signalling. However, in contrast to 2-weeks disease, at 4 weeks disease DNA fragmentation is only activated via one cascade (same cascade that showed an inhibition of DNA fragmentation at 2-weeks cortex) (**Figure 4.2.18**). The top *inhibited* pathway, fMLP signalling in neutrophils, revealed an inhibition of chemokine gene expression and actin organization (**Figure 4.2.19**). The top *enriched* pathway at 4-weeks cortex was also EIF2 signalling, however MAP prediction revealed a complete contrast in in integrated stress response to 2-weeks disease (**Figure 4.2.20**). All the *activated* proteins and functions from 2-weeks have been *inhibited* at 4 weeks disease (**Figure 4.2.17** compared to **Figure 4.2.20**). The inhibited functions within the EIF2 signalling pathway at 4-weeks include ER stress response, amino acid biosynthesis and transport, while assembly of stress granules remained activated (**Figure 4.2.20**).

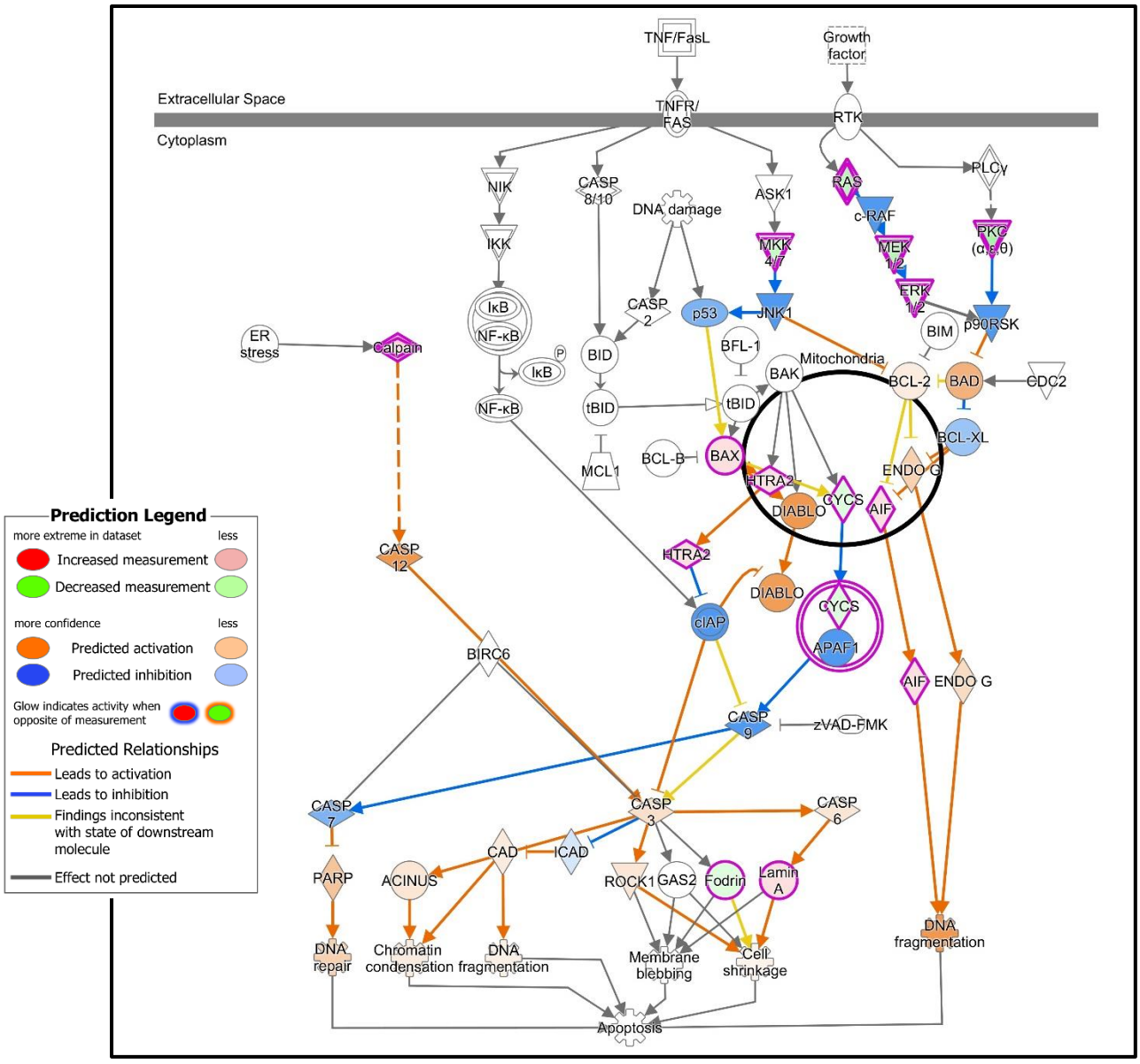

Figure 4.2.18 Top activated pathway at 4-weeks disease within cortex- Apoptosis Signaling.

Protein was extracted from the cortex of rNLS mice at 2, 4, and 6-week timepoints. SWATH MS was conducted (n=3-5 mice) to identify and quantify proteins that changed in TDP-43 mice compared to control non-bigenic mice. Ingenuity Pathway Analysis (IPA) software was used to map the most activated, inhibited, and enriched pathways at each timepoint. A tool within IPA called Molecule Activity Predictor (MAP) was then used to compare the predicted activity pattern observed in the experimental proteomic

dataset to the expected pattern within IPA reference set for each pathway. MAP also predicted the increase/decrease of diseases and/or functional end points within each canonical pathway. Pink: experimental dataset proteins that overlap with pathway; red: upregulation; green: down regulation; double bordered: group or complex; white: protein within pathway that do not overlap with experimental dataset.

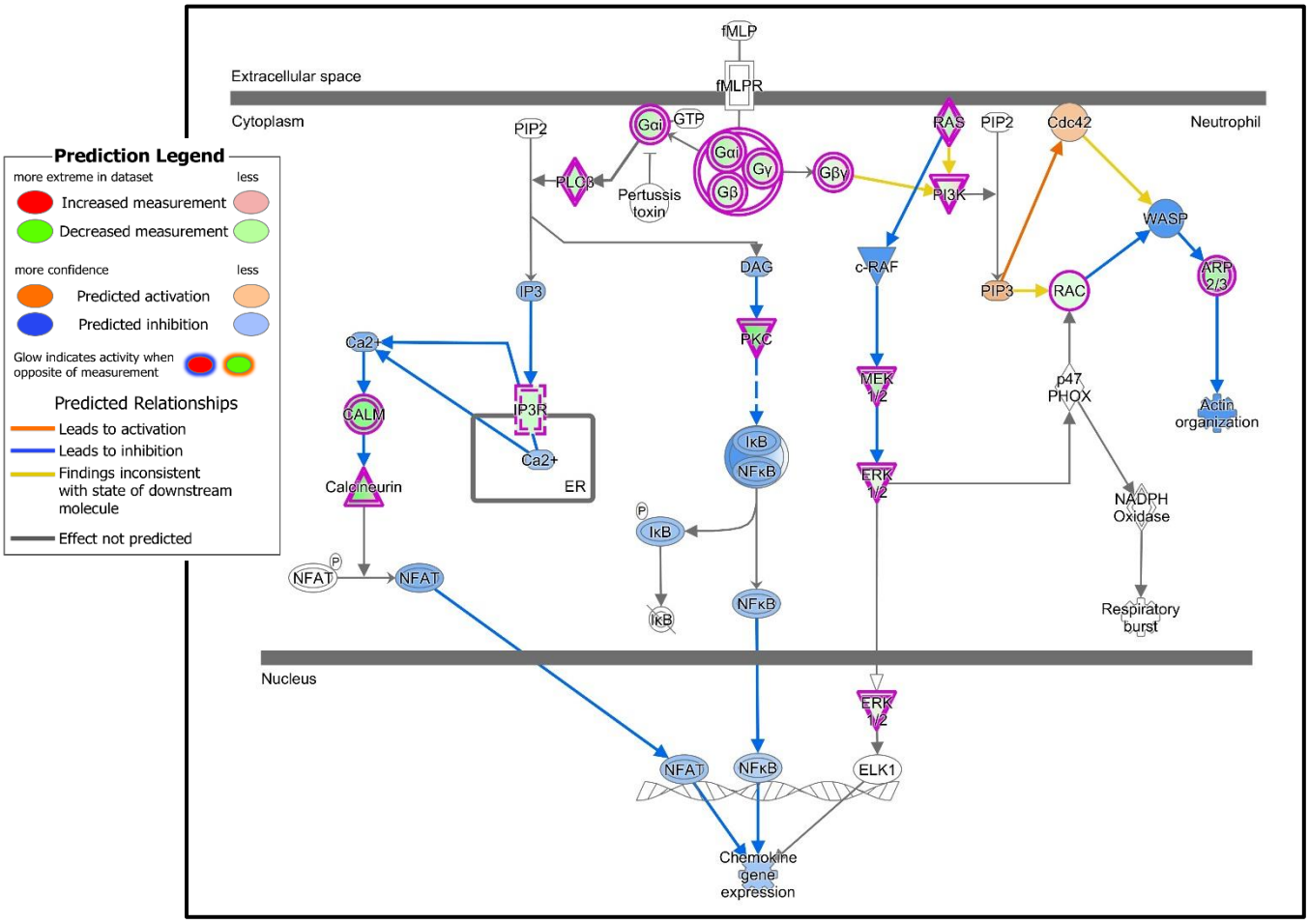

Figure 4.2.19 Top inhibited pathway at 4-weeks disease within cortex- fMLP

Signaling in Neutrophils.

Protein was extracted from the cortex of rNLS mice at 2, 4, and 6-week timepoints. SWATH MS was conducted (n=3-5 mice) to identify and quantify proteins that changed in TDP-43 mice compared to control non-bigenic mice. Ingenuity Pathway Analysis (IPA) software was used to map the most activated, inhibited, and enriched pathways at each timepoint. A tool within IPA called Molecule Activity Predictor (MAP) was then

used to compare the predicted activity pattern observed in the experimental proteomic dataset to the expected pattern within IPA reference set for each pathway. MAP also predicted the increase/decrease of diseases and/or functional end points within each canonical pathway. Pink: experimental dataset proteins that overlap with pathway; red: upregulation; green: down regulation; double bordered: group or complex; white: protein within pathway that do not overlap with experimental dataset.

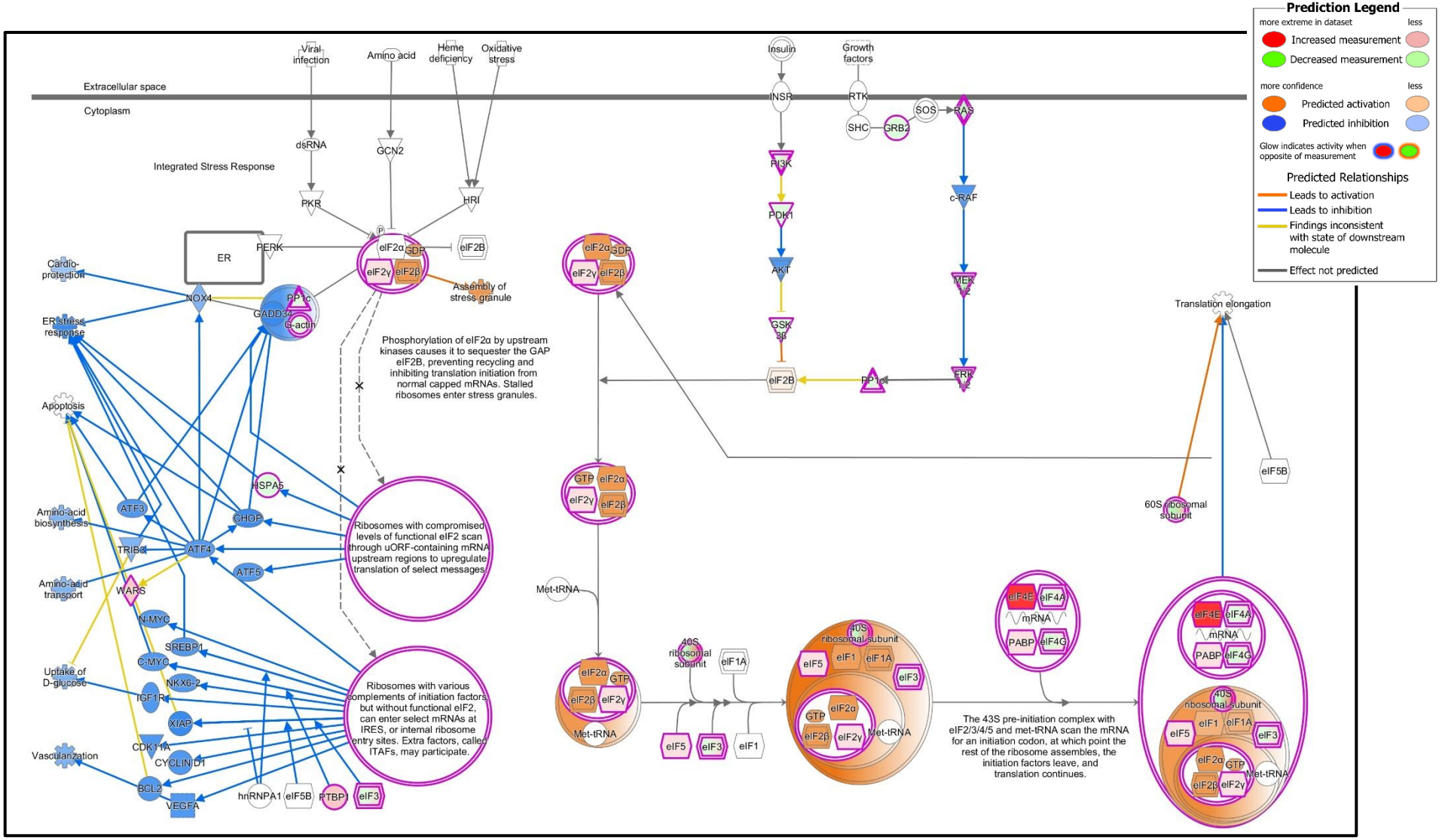

Figure 4.2.20 Top enriched pathway at 4-weeks disease within the cortex- EIF2 Signalling.

Protein was extracted from the cortex of rNLS mice at 2, 4, and 6-week timepoints. SWATH MS was conducted (n=3-5 mice) to identify and quantify proteins that changed in TDP-43 mice compared to control non-bigenic mice. Ingenuity Pathway Analysis (IPA) software was used to map the most activated, inhibited, and enriched pathways at each timepoint. A tool within IPA called Molecule

Activity Predictor (MAP) was then used to compare the predicted activity pattern observed in the experimental proteomic dataset to the expected pattern within IPA reference set for each pathway. MAP also predicted the increase/decrease of diseases and/or functional end points within each canonical pathway. Pink: experimental dataset proteins that overlap with pathway; red: upregulation; green: down regulation; double bordered: group or complex; white: protein within pathway that do not overlap with experimental dataset.

At the *6-week* timepoint within the *cortex*, the top *activated* pathway was Aryl Hydrocarbon Receptor (AHR) signalling which is a large pathway involved in many signalling cascades. As such reported here is the most enriched fraction of the pathway (**Figure 4.2.21**). At this fraction MAP revealed the end functions of the pathway as inhibition of cell cycle and G1/S transition, inhibition of apoptosis, while fatty acid synthesis and estrogen metabolism were activated (**Figure 4.2.21**). The top *inhibited* pathway at 6-weeks disease was Rac signalling, which was also the most inhibited at 2 weeks disease. Similar to 2-weeks, at 6 weeks there was the inhibition of most actin organization related functions, inhibition of cell-cell adhesion, and inhibition of protein translation (**Figure 4.2.22**). However, the notable difference being at 6-weeks disease transcription was activated while at 2-weeks disease it was inhibited (**Figure 4.2.16** compared to **Figure 4.2.22**). Again, like 2-, and 4-weeks, the top *enriched* pathway at 6-weeks cortex was again EIF2 signalling. The integrated stress response within the pathway showed a dynamic pattern of activity: at 2-weeks ER and integrated stress response was activated (**Figure 4.2.17**), in contrast at 4-weeks disease it was inhibited (**Figure 4.2.20**), while at 6-weeks disease it reverted again to an active state (**Figure 4.2.23**).

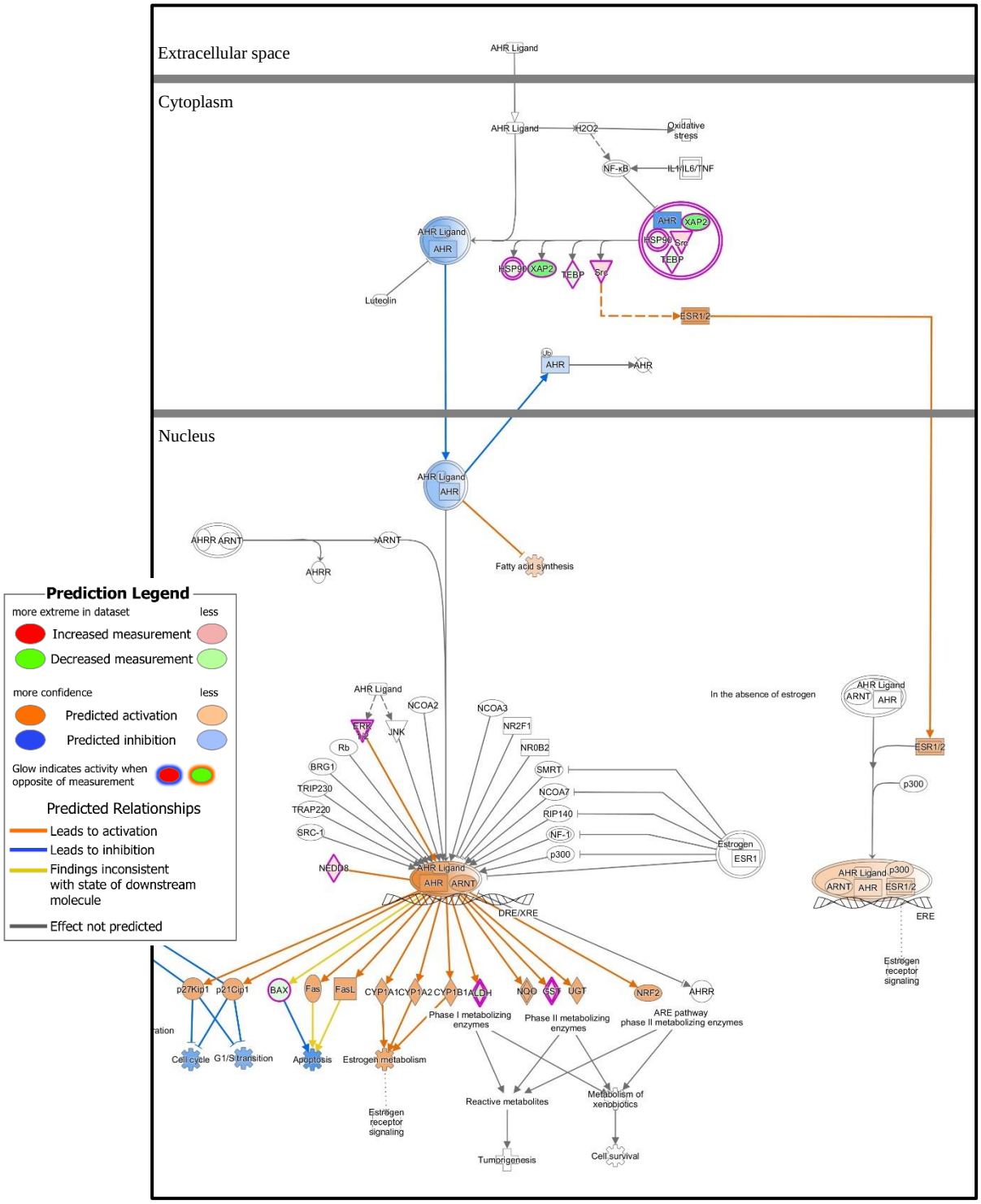

Figure 4.2.21 Top activated pathway at 6-weeks disease within cortex- Aryl Hydrocarbon Receptor Signalling.

Protein was extracted from the cortex of rNLS mice at 2, 4, and 6-week timepoints. SWATH MS was conducted (n=3-5 mice) to identify and quantify proteins that changed in TDP-43 mice compared to control non-bigenic mice. Ingenuity Pathway Analysis (IPA) software was used to map the most activated, inhibited, and enriched pathways at each timepoint. A tool within IPA called Molecule Activity Predictor (MAP) was then used to compare the predicted activity pattern observed in the experimental proteomic dataset to the expected pattern within IPA reference set for each pathway. MAP also predicted the increase/decrease of diseases and/or functional end points within each canonical pathway. Pink: experimental dataset proteins that overlap with pathway; red: upregulation; green: down regulation; double bordered: group or complex; white: protein within pathway that do not overlap with experimental dataset. Only most enriched fraction of pathway is shown as entire pathway is large and could not be depicted here in detail.

.

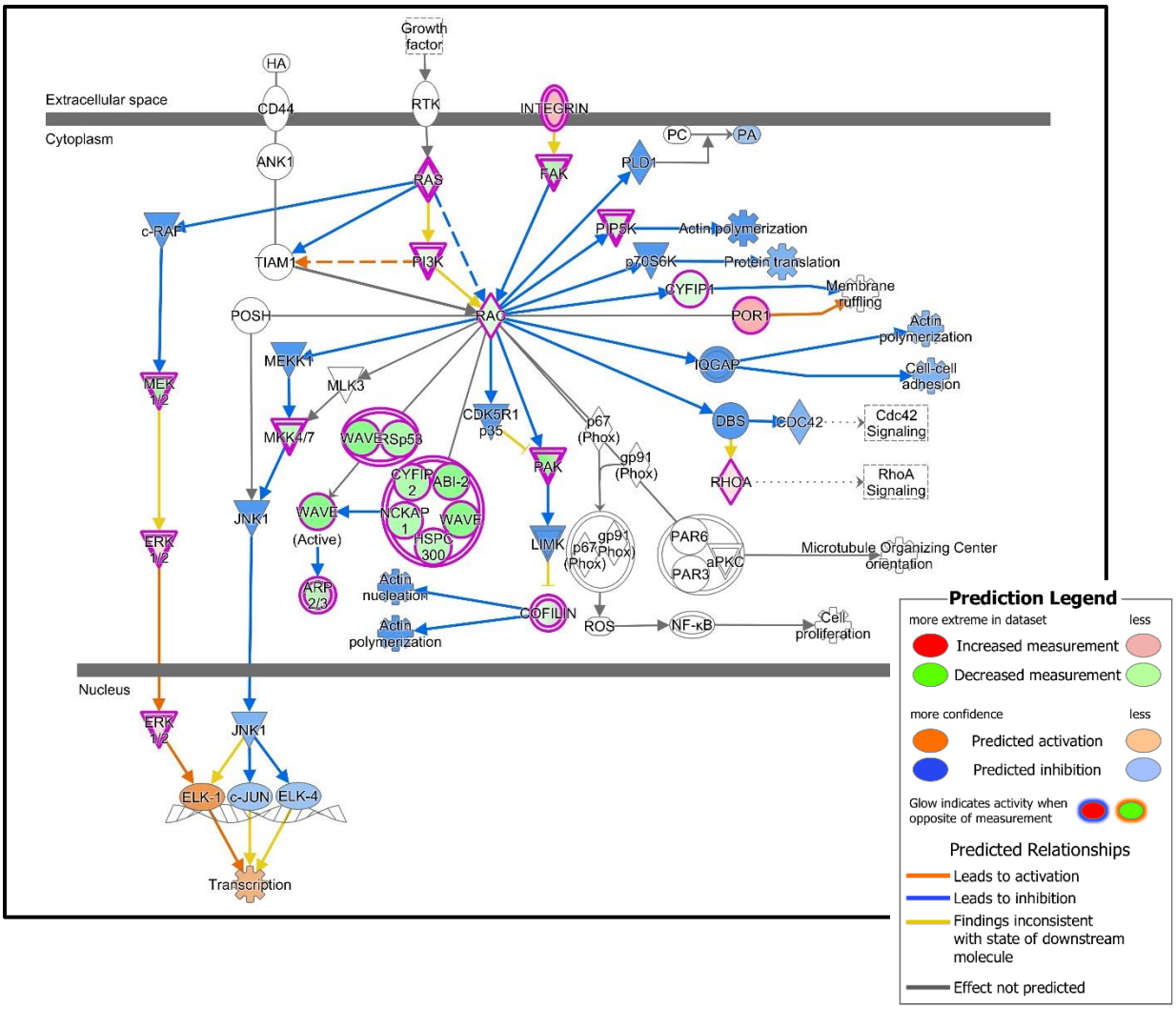

Figure 4.2.22 Top inhibited pathway at 6-weeks disease within cortex- CD28

Signaling in T Helper Cells.

Protein was extracted from the cortex of rNLS mice at 2, 4, and 6-week timepoints. SWATH MS was conducted (n=3-5 mice) to identify and quantify proteins that changed in TDP-43 mice compared to control non-bigenic mice. Ingenuity Pathway Analysis (IPA) software was used to map the most activated, inhibited, and enriched pathways at each timepoint. A tool within IPA called Molecule Activity Predictor (MAP) was then used to compare the predicted activity pattern observed in the experimental proteomic dataset to the expected pattern within IPA reference set for each pathway. MAP also predicted the increase/decrease of diseases and/or functional end points within each canonical pathway. Pink: experimental dataset proteins that overlap with pathway; red: upregulation; green: down regulation; double bordered: group or complex; white: protein within pathway that do not overlap with experimental dataset.

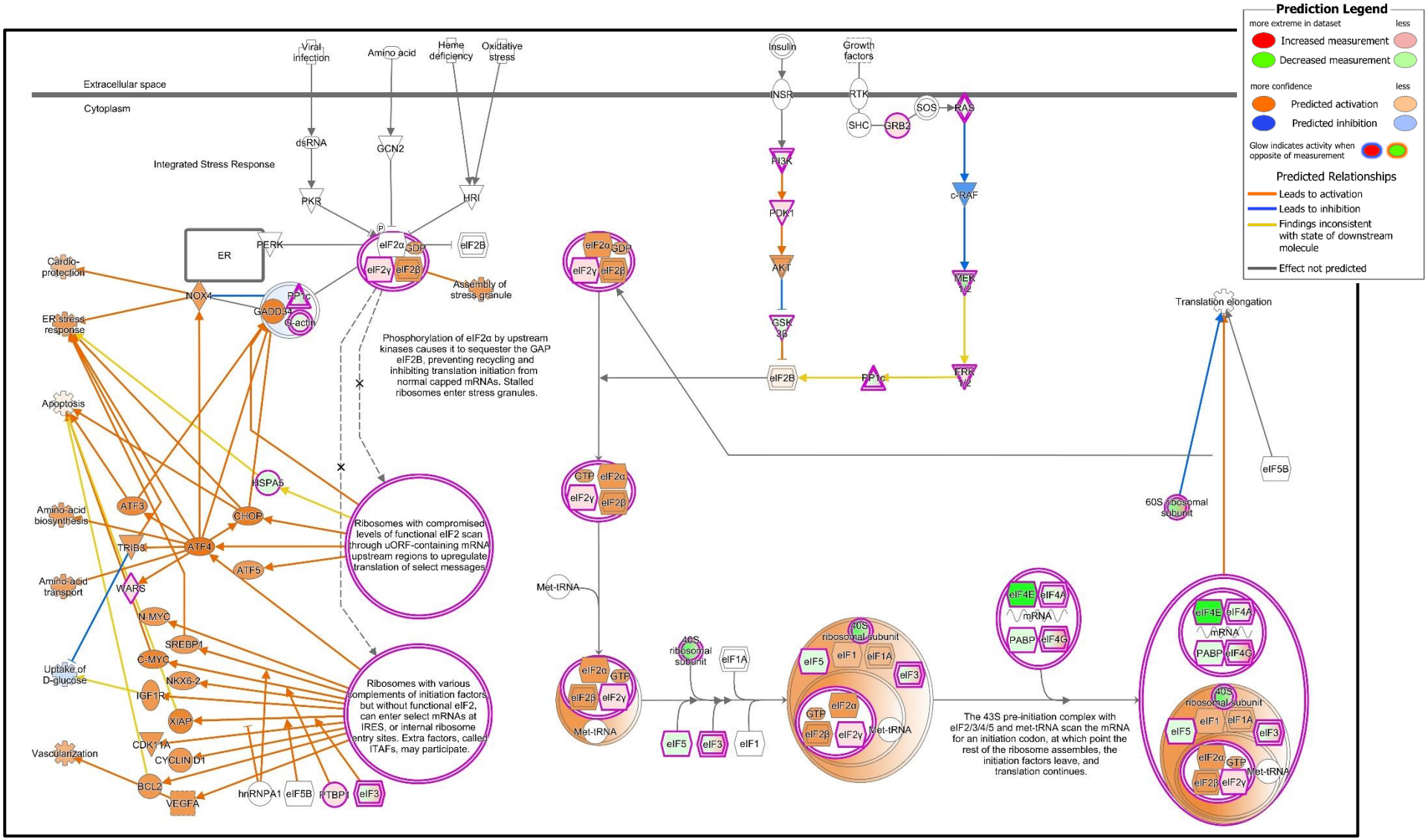

Figure 4.2.23 Top enriched pathway at 6-weeks disease within cortex- EIF2 Signalling.

Protein was extracted from the cortex of rNLS mice at 2, 4, and 6-week timepoints. SWATH MS was conducted (n=3-5 mice) to identify and quantify proteins that changed in TDP-43 mice compared to control non-bigenic mice. Ingenuity Pathway Analysis (IPA) software was used to map the most activated, inhibited, and enriched pathways at each timepoint. A tool within IPA called Molecule Activity Predictor (MAP) was then used to compare the predicted activity pattern observed in the experimental proteomic dataset to the expected pattern within IPA reference set for each pathway. MAP also predicted the increase/decrease of diseases and/or functional end points within each canonical pathway. Pink: experimental dataset proteins that overlap with pathway; red: upregulation; green: down regulation; double bordered: group or complex; white: protein within pathway that do not overlap with experimental dataset.

.

At *2 weeks* of disease within the *spinal cord* the top *activated* pathway was RhoGDI signalling. MAP predictions revealed that the functional end-point of this pathway was the inhibition of actin linkage, actin polymerization, and cytoskeletal reorganisation (**Figure 4.2.24**). The top *inhibited* pathway was regulation of actin-based motility by Rho which also revealed actin related functions being inhibited including: inhibition of actin polymerisation and nucleation, an inhibition of cell motility and contraction, inhibition of stress fiber and focal adhesion formation (**Figure 4.2.25**). However, there was also the activation of actin filament stabilisation and relaxation of contractile forces (**Figure 4.2.25**). The top *enriched* pathway was mitochondrial dysfunction and the MAP prediction revealed an inhibition of ROS mediated mitochondrial dysfunction, inhibition of amyloid β mediated mitochondrial fragmentation, and inhibition of cytochrome C triggered apoptosis (**Figure 4.2.26**). While there was activation of oxidative stress in both the intermembrane space and mitochondrial matrix, there was also the inhibition of oxidative stress via different signalling cascades (**Figure 4.2.26**).

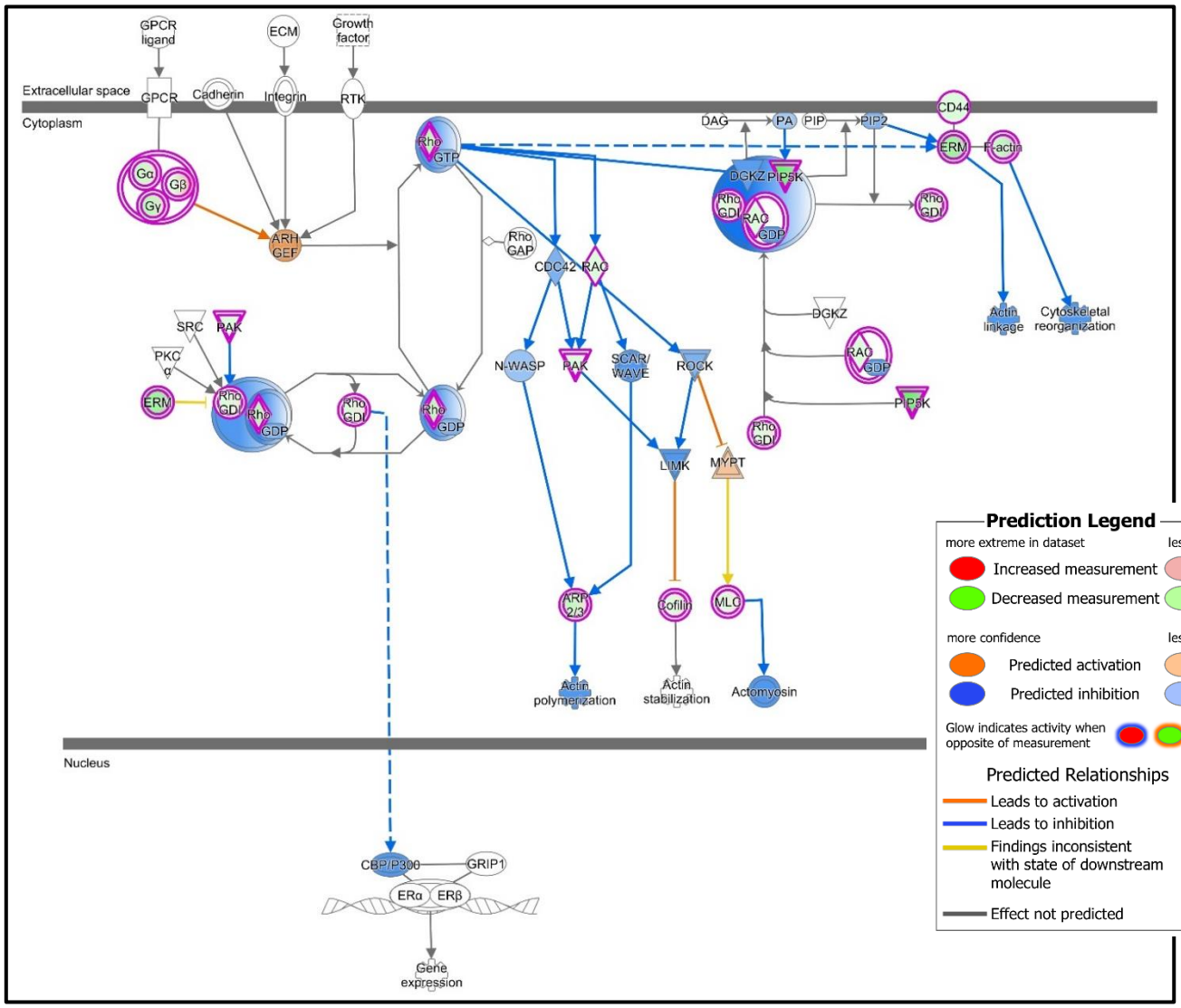

Figure 4.2.24 Top activated pathway at 2-weeks disease within spinal cord- RhoGDI Signalling.

Protein was extracted from the spinal cord of rNLS mice at 2 and 6-week timepoints. SWATH MS was conducted (n=3-5 mice) to identify and quantify proteins that changed in TDP-43 mice compared to control non-bigenic mice. Ingenuity Pathway Analysis (IPA) software was used to map the most activated, inhibited, and enriched pathways at each timepoint. A tool within IPA called Molecule Activity Predictor (MAP) was then used to compare the predicted activity pattern observed in the experimental proteomic dataset to the expected pattern within IPA reference set for each pathway. MAP also predicted the increase/decrease of diseases and/or functional end points within each canonical pathway. Pink: experimental dataset proteins that overlap with pathway; red: upregulation; green: down regulation; double bordered: group or complex; white: protein within pathway that do not overlap with experimental dataset.

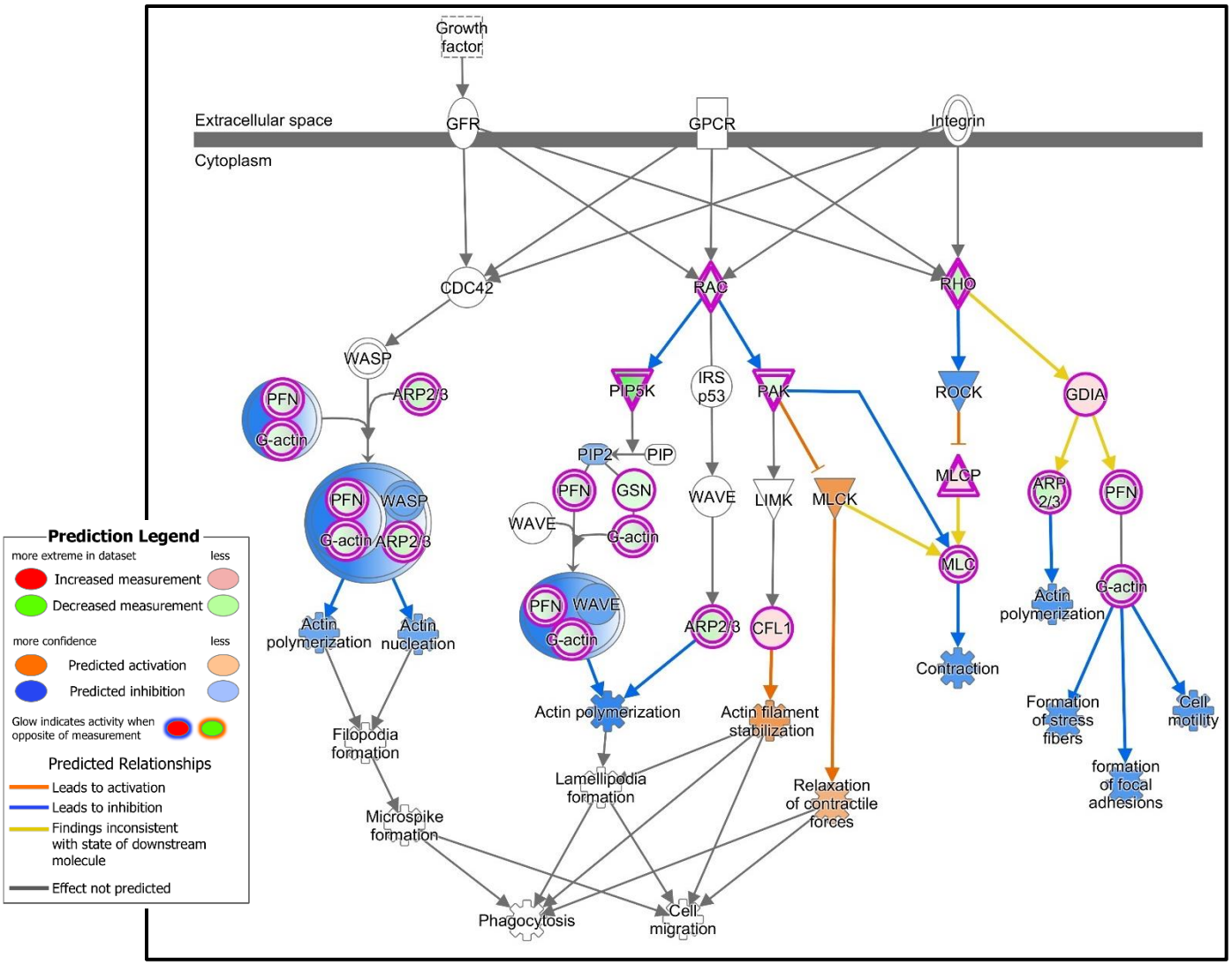

Figure 4.2.25 Top inhibited pathway at 2-weeks disease within spinal cord-

Regulation of Actin-based Motility by Rho.

Protein was extracted from the spinal cord of rNLS mice at 2 and 6-week timepoints. SWATH MS was conducted (n=3-5 mice) to identify and quantify proteins that changed in TDP-43 mice compared to control non-bigenic mice. Ingenuity Pathway Analysis (IPA) software was used to map the most activated, inhibited, and enriched pathways at each timepoint. A tool within IPA called Molecule Activity Predictor (MAP) was then used to compare the predicted activity pattern observed in the experimental proteomic dataset to the expected pattern within IPA reference set for each pathway. MAP also predicted the increase/decrease of diseases and/or functional end points within each canonical pathway. Pink: experimental dataset proteins that overlap with pathway; red:

upregulation; green: down regulation; double bordered: group or complex; white: protein within pathway that do not overlap with experimental dataset.

.

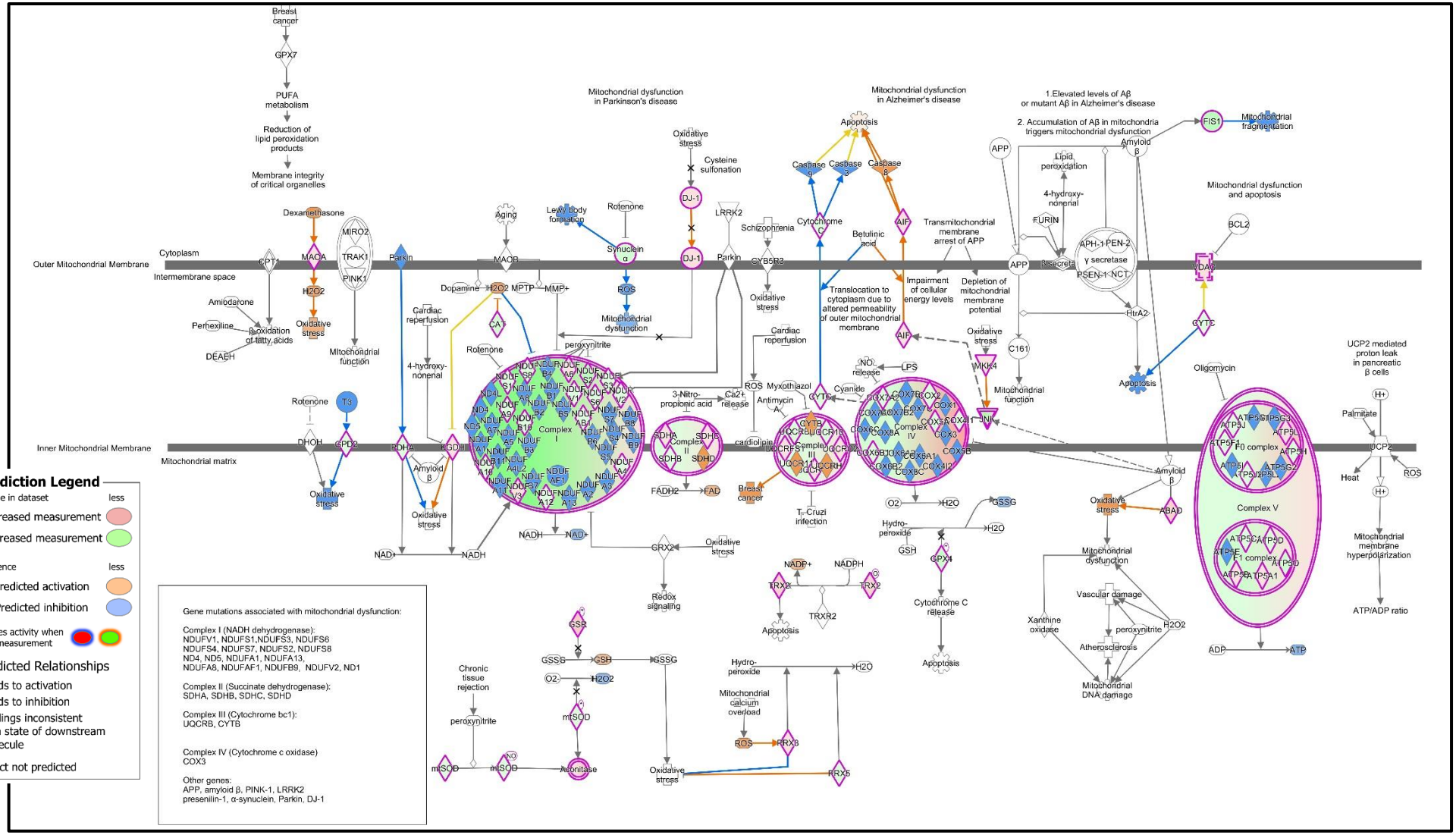

4.2.26 Top enriched pathway at 2-weeks disease within spinal cord- Mitochondrial Dysfunction.

Protein was extracted from the spinal cord of rNLS mice at 2 and 6-week timepoints. SWATH MS was conducted (n=3-5 mice) to identify and quantify proteins that changed in TDP-43 mice compared to control non-bigenic mice. Ingenuity Pathway Analysis (IPA) software was used to map the most activated, inhibited, and enriched pathways at each timepoint. A tool within IPA called Molecule Activity Predictor (MAP) was then used to compare the predicted activity pattern observed in the experimental proteomic dataset to the expected pattern within IPA reference set for each pathway. MAP also predicted the increase/decrease of diseases and/or functional end points within each canonical pathway. Pink: experimental dataset proteins that overlap with pathway; red: upregulation; green: down regulation; double bordered: group or complex; white: protein within pathway that do not overlap with experimental dataset.

At the *6-week* timepoint within the *spinal cord*, no *activated* pathways were detected by IPA. The top *inhibited* pathway was telomerase signalling which showed an inhibition for the pathway overall (and protein specific changes), however there were no specific functional endpoint changes predicted by MAP analysis (**Figure 4.2.26**). The top *enriched* pathway was again mitochondrial dysfunction (same at 2-weeks spinal cord). The major difference in the activity of the mitochondrial dysfunction pathway between 2- and 6-weeks disease was the activation of apoptosis (**Figure 4.2.27**). At 6-weeks disease cytochrome C translocated to cytoplasm potentially due to altered permeability of the outer mitochondrial membrane, triggering caspase-mediated apoptosis (**Figure 4.2.27**). At the 6-week disease mitochondrial dysfunctional and fragmentation continued to be inhibited while oxidative stress was both inhibited and activated depending on specific signalling cascades (**Figure 4.2.27**).

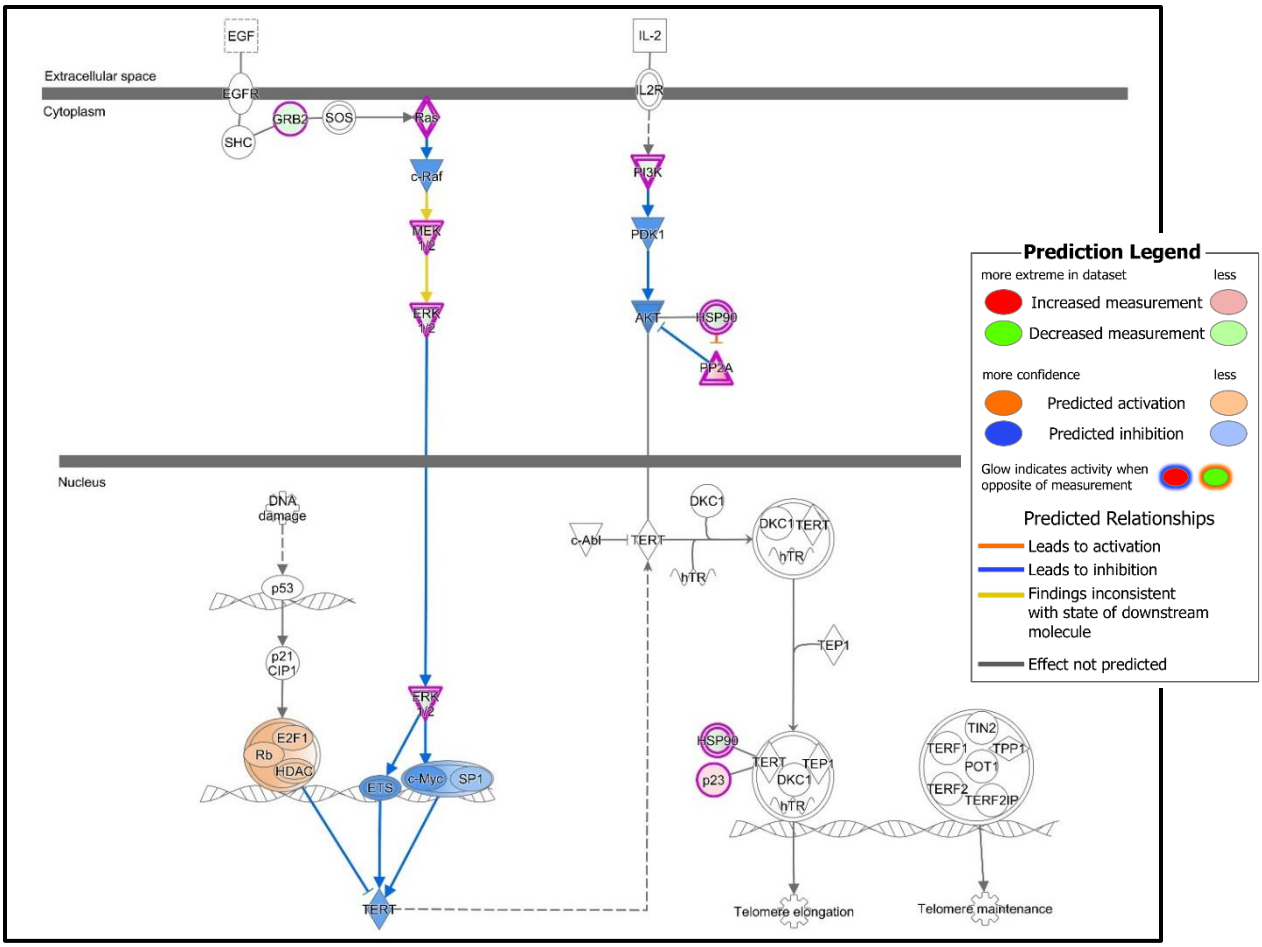

Figure 4.2.26 Top inhibited pathway at 6-weeks disease within spinal cord-

Telomerase Signalling.

Protein was extracted from the spinal cord of rNLS mice at 2 and 6-week timepoints. SWATH MS was conducted (n=3-5 mice) to identify and quantify proteins that changed in TDP-43 mice compared to control non-bigenic mice. Ingenuity Pathway Analysis (IPA) software was used to map the most activated, inhibited, and enriched pathways at each timepoint. A tool within IPA called Molecule Activity Predictor (MAP) was then used to compare the predicted activity pattern observed in the experimental proteomic dataset to the expected pattern within IPA reference set for each pathway. MAP also predicted the increase/decrease of diseases and/or functional end points within each canonical pathway. Pink: experimental dataset proteins that overlap with pathway; red: upregulation; green: down regulation; double bordered: group or complex; white: protein within pathway that do not overlap with experimental dataset.

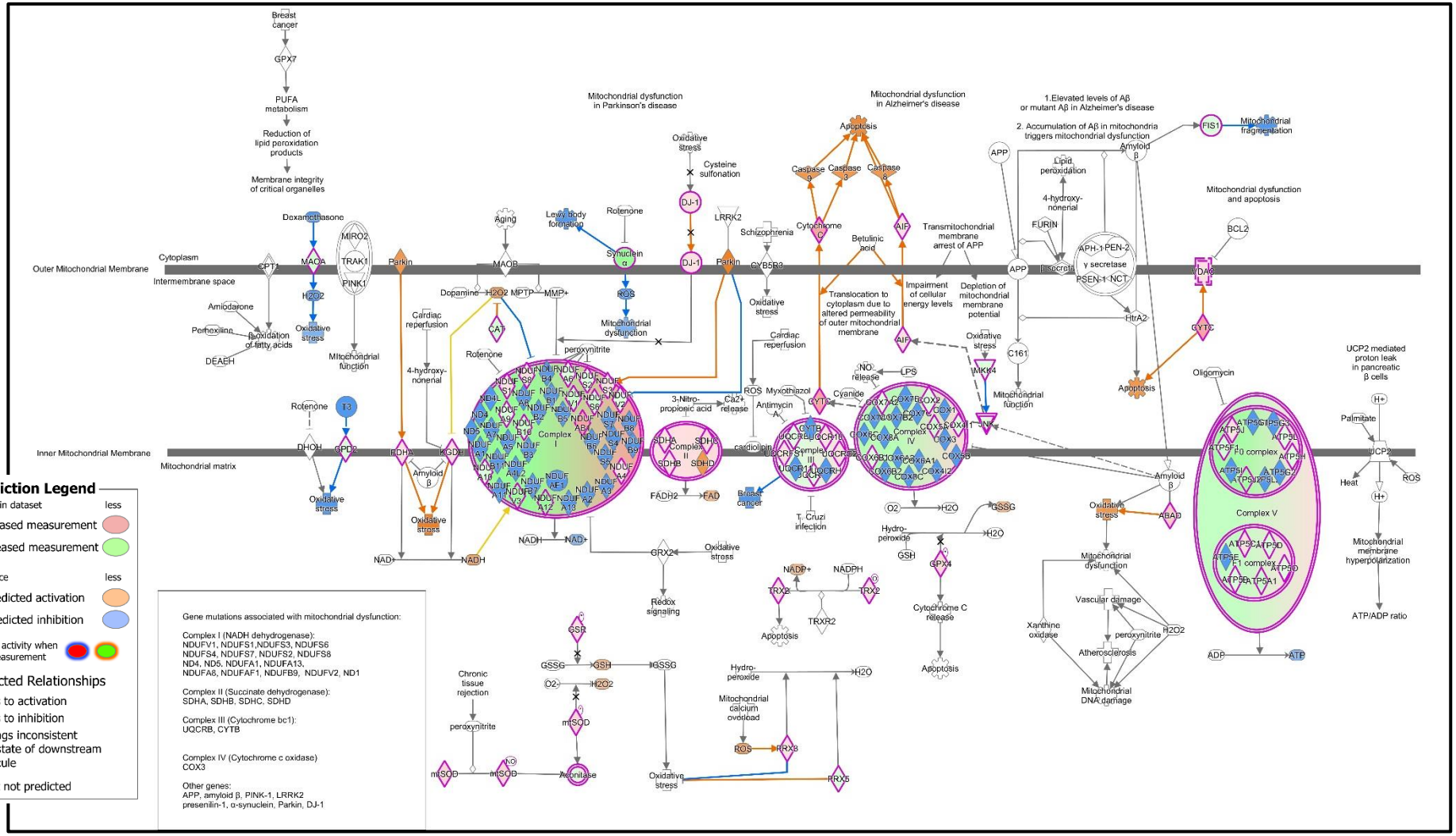

Figure 4.2.27 Top enriched pathway at 6-weeks disease within spinal cord- Mitochondrial Dysfunction.

Protein was extracted from the spinal cord of rNLS mice at 2 and 6-week timepoints. SWATH MS was conducted (n=3-5 mice) to identify and quantify proteins that changed in TDP-43 mice compared to control non-bigenic mice. Ingenuity Pathway Analysis (IPA) software was used to map the most activated, inhibited, and enriched pathways at each timepoint. A tool within IPA called Molecule Activity Predictor (MAP) was then used to compare the predicted activity pattern observed in the experimental proteomic dataset to the expected pattern within IPA reference set for each pathway. MAP also predicted the increase/decrease of diseases and/or functional end points within each canonical pathway. Pink: experimental dataset proteins that overlap with pathway; red: upregulation; green: down regulation; double bordered: group or complex; white: protein within pathway that do not overlap with experimental dataset.

4.2.4 Prediction of upstream regulators affecting protein changes over disease course in rNLS TDP-43 mice

To identify the upstream regulators that may be responsible for the proteomic changes within the experimental dataset, an Upstream Regulator analysis was carried out using IPA. The aim of the Upstream Regulator (UR) analytic tool within IPA is to first identify potential upstream regulators and then predict the regulators state of activity (activated or inhibited). To identify upstream regulators, the UR tool examines the experimental dataset for known targets of regulators (based on literature findings) and then statistically determines the significance of the overlap (Fisher's Exact p-value<0.01). IPA has a broad definition of the type of molecule that can be classified as an upstream regulator. As such the description of an 'upstream regulator; is any molecule (regulator) that can affect the expression of another molecule (target).

To determine the activity state of each regulator, UR tool *compares* the causal effects between identified upstream regulators and target proteins that are known within literature *to* the target proteins actual fold change within the experimental dataset. The exact z-score (state of activity) is measured relative to a control (model with random regulator directions and causal relationships). Activation is defined as z-score of 2 or more and inhibition is defined as z-score of -2 or less

The predicted activated and inhibited *upstream regulators* during disease course within the *cortex* are listed in **Tables 4.2.8-10.** JVenn was used to examine the overlap across the timepoints. This revealed 2 *activated* upstream regulators overlapped across all timepoints: UCP1 and ATF4 (**Figure 4.2.28**). UCP1 is a mitochondrial carrier protein that is involved in the transfer and return of ions from the inner to the outer mitochondrial

membrane and regulate mitochondrial membrane potential [127]. ATF4 is transcription activator that is also known as CREB-2 and is part of many canonical pathways[127]. The analysis of the *inhibited* upstream regulators also revealed the overlap of 2 upstream regulators across all timepoints within the cortex: Calmodulin and SLC30A3 (**Figure 4.2.29**). Calmodulin is the intracellular target for a Ca^{2+} and facilitates the regulation of enzymes, ion channels, aquaporins and other proteins via calcium-binding[109] and has been implicated in Alzheimer disease [128]. SLC30A3 is a solute carrier that is involved in the accumulation of zinc in synaptic vesicles[109] and has also been implicated in Alzheimer disease[129].

Table 4.2.8 Activated and inhibited upstream regulators at 2-weeks cortex.

Protein was extracted from the cortex of rNLS mice at 2, 4, and 6-week timepoints. SWATH MS was conducted (n=3-5 mice) to identify and quantify proteins that changed in TDP-43 mice compared to control non-bigenic mice. Ingenuity Pathway Analysis (IPA) software was used to identify the upstream regulators which may be responsible for the proteomic changes within the experimental dataset at each timepoint. The Upstream Regulator analysis tool within IPA provides two statistical measures: 1) identifies upstream regulators and calculates significance using Fisher's Exact Test ($p<0.01$); 2) infers the likely activation state of each regulator using the z-score algorithm to predict activation (z-score of 2 or more) or inhibition (z-score of -2 or less). IPA defines any molecule (regulator) that can affect the expression of another molecule (target) as an 'upstream regulator'. Listed are the significantly activated and inhibited up-stream regulators at 2-weeks disease within cortex. Orange: activated; blue: inhibited.

Upstream regulators- Cortex 2 weeks					
Upstream Regulator	**Molecule Type**	**Predicted Activation State**	**Activation Z-score**	**Target proteins in dataset**	**p-value**
PSEN1	peptidase	Activated	2.50	173	4.76E-64
NFE2L2	transcription regulator	Activated	2.23	135	3.01E-38

HTT	transcription regulator	Activated	2.07	158	1.09E-35
TCR	complex	Activated	2.40	75	1.3E-12
KRAS	enzyme	Activated	2.51	71	1.5E-11
IGF1R	transmembrane receptor	Activated	2.08	63	2.9E-09
UCP1	transporter	Activated	2.90	40	7.48E-09
NFE2L1	transcription regulator	Activated	2.31	12	3.24E-06
PDGF (family)	group	Activated	2.45	6	1.79E-04
ATF4	transcription regulator	Activated	2.61	30	1.85E-04
FBXO2	enzyme	Activated	2.19	5	4.20E-04
VBP1	other	Activated	2.00	4	9.32E-04
MYOC	other	Activated	2.98	19	3.82E-03
PRNP	other	Activated	2.07	13	4.16E-03
PAX7	transcription regulator	Activated	2.14	15	0.0197
RICTOR	other	Inhibited	-2.49	146	4.4E-66
MKNK1	kinase	Inhibited	-2.18	54	1.47E-24
mir-122	microrna	Inhibited	-2.92	43	1.06E-17
TRAP1	enzyme	Inhibited	-2.86	18	8.09E-09
PHF21A	enzyme	Inhibited	-2.80	8	3.40E-07
Calmodulin	group	Inhibited	-2.29	19	7.25E-06
ERG	transcription regulator	Inhibited	-2.41	38	3.78E-05
AIFM1	enzyme	Inhibited	-2.22	6	1.79E-04
SLC30A3	transporter	Inhibited	-2.00	4	9.67E-03
VCAN	other	Inhibited	-2.20	22	0.0252
HIST1H1T	other	Inhibited	-2.67	17	0.0253
SLC13A1	transporter	Inhibited	-2.18	17	0.0452

Table 4.2.9 Activated and inhibited upstream regulators at 4-weeks cortex.

Protein was extracted from the cortex of rNLS mice at 2, 4, and 6-week timepoints. SWATH MS was conducted (n=3-5 mice) to identify and quantify proteins that changed in TDP-43 mice compared to control non-bigenic mice. Ingenuity Pathway Analysis (IPA) software was used to identify the upstream regulators which may be responsible for the proteomic changes within the experimental dataset at each timepoint. The Upstream Regulator analysis tool within IPA provides two statistical measures: 1) identifies upstream regulators and calculates significance using Fisher's Exact Test ($p<0.01$); 2) infers the likely activation state of each regulator using the z-score algorithm to predict activation (z-score of 2 or more) or inhibition (z-score of -2 or less). IPA defines any molecule (regulator) that can affect the expression of another molecule (target) as an

'upstream regulator'. Listed are the significantly activated and inhibited up-stream regulators at 4-weeks disease within cortex. Orange: activated; blue: inhibited.

Upstream regulators- Cortex 4 weeks					
Upstream Regulator	**Molecule Type**	**Predicted Activation State**	**Activation Z-score**	**Target proteins in dataset**	**p-value**
TSC1	other	Activated	2.61	8	0.0441
mir-137	microRNA	Activated	2.24	5	3.69E-03
REST	transcription regulator	Activated	2.57	16	3.57E-03
SGPP2	phosphatase	Activated	2.83	9	2.33E0-03
RAB1B	other	Activated	2.14	11	1.12E-03
SPP1	cytokine	Activated	2.11	24	9.57E-04
ATF4	transcription regulator	Activated	2.77	30	1.85E-04
PPARA	ligand-dependent nuclear receptor	Activated	2.56	83	4.77E-07
TCF7L2	transcription regulator	Activated	2.66	71	1.32E-07
UCP1	transporter	Activated	3.97	40	7.48E-09
TFAM	transcription regulator	Activated	2.32	15	1.26E-10
INSR	kinase	Activated	2.02	102	5.32E-15
FMR1	translation regulator	Activated	2.81	33	1.02E-18
MAPT	other	Activated	2.37	169	4.19E-96
MDM4	enzyme	Inhibited	-2.22	5	0.0263
Calmodulin	group	Inhibited	-3.18	19	7.25E-07
MKNK1	kinase	Inhibited	-2.99	54	1.47E-24
PHF21A	enzyme	Inhibited	-2.80	8	3.40E-07
MAP4K4	kinase	Inhibited	-2.76	50	1.28E-16
BDNF	growth factor	Inhibited	-2.16	33	2.79E-07
BARX2	transcription regulator	Inhibited	-2.00	4	9.67E-03
SLC30A3	transporter	Inhibited	-2.00	4	9.67E-03

Table 4.2.10 Activated and inhibited upstream regulators at 6-weeks cortex.

Protein was extracted from the cortex of rNLS mice at 2, 4, and 6-week timepoints. SWATH MS was conducted (n=3-5 mice) to identify and quantify proteins that changed

in TDP-43 mice compared to control non-bigenic mice. Ingenuity Pathway Analysis (IPA) software was used to identify the upstream regulators which may be responsible for the proteomic changes within the experimental dataset at each timepoint. The Upstream Regulator analysis tool within IPA provides two statistical measures: 1) identifies upstream regulators and calculates significance using Fisher's Exact Test ($p<0.01$); 2) infers the likely activation state of each regulator using the z-score algorithm to predict activation (z-score of 2 or more) or inhibition (z-score of -2 or less). IPA defines any molecule (regulator) that can affect the expression of another molecule (target) as an 'upstream regulator'. Listed are the significantly activated and inhibited up-stream regulators at 6-weeks disease within cortex. Orange: activated; blue: inhibited.

Upstream regulators- Cortex 6 weeks					
Upstream Regulator	**Molecule Type**	**Predicted Activation State**	**Activation Z-score**	**Target proteins in dataset**	**p-value**
SPP1	cytokine	Activated	3.40	24	9.57E-04
INSR	kinase	Activated	3.39	102	5.32E-15
UCP1	transporter	Activated	3.38	40	7.48E-09
TP53	transcription regulator	Activated	3.18	290	9.72E-31
HNF4A	transcription regulator	Activated	2.64	56	0.0235
ATF4	transcription regulator	Activated	2.61	30	1.85E-04
REST	transcription regulator	Activated	2.57	16	0.00357
PPARA	ligand-dependent nuclear receptor	Activated	2.44	83	4.77E-07
HTT	transcription regulator	Activated	2.42	158	1.09E-35
MAPT	other	Activated	2.37	169	4.19E-96
TCF7L2	transcription regulator	Activated	2.34	71	1.32E-07
SGPP2	phosphatase	Activated	2.12	9	2.33E-03
IPMK	kinase	Activated	2.11	11	1.43E-05
IGF1R	transmembrane receptor	Activated	2.08	63	2.9E-09
PFDN6	other	Activated	2.00	4	9.32E-05
Calmodulin	group	Inhibited	-2.74	19	7.25E-07
mir-122	microrna	Inhibited	-2.61	43	1.06E-17
TRAP1	enzyme	Inhibited	-2.41	18	8.09E-09
MTOR	kinase	Inhibited	-2.24	74	1.4E-23
HIST1H1T	other	Inhibited	-2.18	17	0.0253
SLC30A3	transporter	Inhibited	-2.00	4	9.67E-03

Figure 4.2.28 Overlap of activated upstream regulators across disease course within the cortex.

Protein was extracted from the cortex of rNLS mice at 2, 4, and 6-week timepoints. SWATH MS was conducted (n=3-5 mice) to identify and quantify proteins that changed in TDP-43 mice compared to control non-bigenic mice. Ingenuity Pathway Analysis (IPA) software was used to identify the upstream regulators which may be responsible for the proteomic changes within the experimental dataset at each timepoint. JVenn was subsequently used to determine the overlap of activated upstream regulators across the 3 timepoints within the cortex (http://jvenn.toulouse.inra.fr/app/index.html).

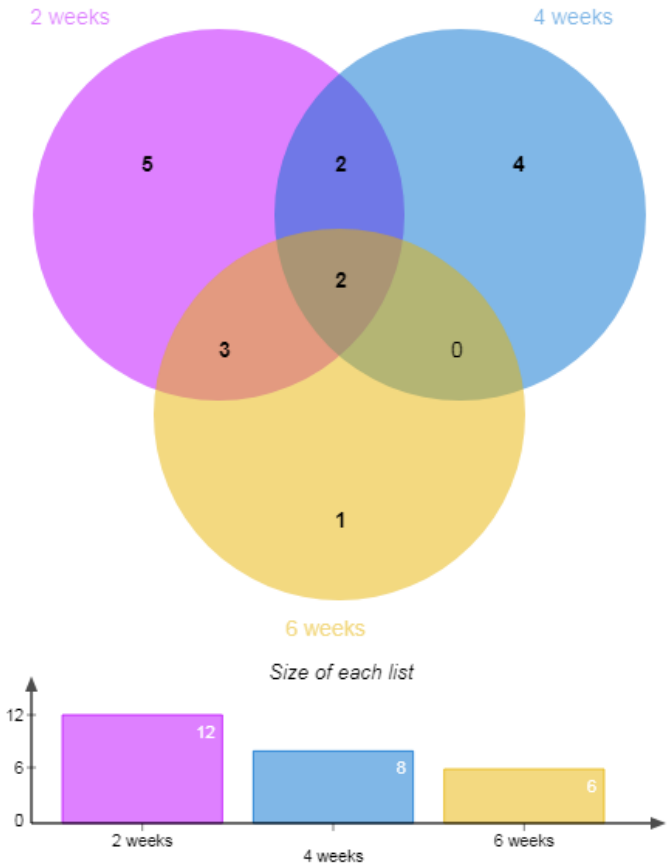

Figure 4.2.29 Overlap of inhibited upstream regulators across disease course within the cortex.

Protein was extracted from the cortex of rNLS mice at 2, 4, and 6-week timepoints. SWATH MS was conducted (n=3-5 mice) to identify and quantify proteins that changed in TDP-43 mice compared to control non-bigenic mice. Ingenuity Pathway Analysis (IPA) software was used to identify the upstream regulators which may be responsible for the proteomic changes within the experimental dataset at each timepoint. JVenn was subsequently used to determine the overlap of inhibited upstream regulators across the 3 timepoints within the cortex (http://jvenn.toulouse.inra.fr/app/index.html).

The activated and inhibited *upstream regulators* at 2- and 6-weeks disease within the *spinal cord* have been listed in **Tables 4.2.11-12**. When analysing the overlap, only one upstream regulator intersected the two timepoints: the inhibition of DIO2 at both 2- and 6-week disease. DIO2 is iodothyronine deiodinase 2, and is involved in the catalysis of thyroid hormone T3 which is vital for the brain during development[109]. Downregulation of DIO2 mRNA has been shown to be associated with Huntington disease[130].

Table 4.2.11 Activated and inhibited upstream regulators at 2-weeks spinal cord.

Protein was extracted from the spinal cord of rNLS mice at 2 and 6-week timepoints. SWATH MS was conducted (n=3-5 mice) to identify and quantify proteins that changed in TDP-43 mice compared to control non-bigenic mice. Ingenuity Pathway Analysis (IPA) software was used to identify the upstream regulators which may be responsible for the proteomic changes within the experimental dataset at each timepoint. The Upstream Regulator analysis tool within IPA provides two statistical measures: 1) identifies upstream regulators and calculates significance using Fisher's Exact Test ($p<0.01$); 2) infers the likely activation state of each regulator using the z-score algorithm to predict activation (z-score of 2 or more) or inhibition (z-score of -2 or less). IPA defines any molecule (regulator) that can affect the expression of another molecule (target) as an 'upstream regulator'. Listed are the significantly activated and inhibited up-stream regulators at 2-weeks disease within the spinal cord. Orange: activated; blue: inhibited.

Upstream regulators- spinal cord 2 weeks					
Upstream Regulator	**Molecule Type**	**Predicted Activation State**	**Activation Z-score**	**Target proteins in dataset**	**p-value**
RICTOR	other	Activated	2.82	88	8.69E-46
FMR1	translation regulator	Activated	2.34	26	7.49E-20
mir-144	microrna	Activated	2.00	4	4.25E-03
VBP1	other	Activated	2.00	4	4.23E-05
IL15	cytokine	Inhibited	-2.74	23	2.75E-05
PPARGC1A	transcription regulator	Inhibited	-2.72	48	2.80E-20

NFE2L2	transcription regulator	Inhibited	-2.54	87	3.21E-34
AR	ligand-dependent nuclear receptor	Inhibited	-2.46	30	1.90E-02
DIO2	enzyme	Inhibited	-2.45	6	9.45E-03
LEP	growth factor	Inhibited	-2.41	34	4.68E-05
PPARGC1B	transcription regulator	Inhibited	-2.36	10	1.19E-05
PCGEM1	other	Inhibited	-2.36	25	3.86E-22
FSH	complex	Inhibited	-2.35	39	2.75E-06
ADIPOR1	transmembrane receptor	Inhibited	-2.24	5	2.27E-03
NRF1	transcription regulator	Inhibited	-2.14	12	8.10E-08
CYP1B1	enzyme	Inhibited	-2.12	8	8.58E-03
MTOR	kinase	Inhibited	-2.08	60	1.30E-31

Table 4.2.12 Activated and inhibited upstream regulators at 6-weeks spinal cord.

Protein was extracted from the spinal cord of rNLS mice at 2 and 6-week timepoints. SWATH MS was conducted (n=3-5 mice) to identify and quantify proteins that changed in TDP-43 mice compared to control non-bigenic mice. Ingenuity Pathway Analysis (IPA) software was used to identify the upstream regulators which may be responsible for the proteomic changes within the experimental dataset at each timepoint. The Upstream Regulator analysis tool within IPA provides two statistical measures: 1) identifies upstream regulators and calculates significance using Fisher's Exact Test ($p<0.01$); 2) infers the likely activation state of each regulator using the z-score algorithm to predict activation (z-score of 2 or more) or inhibition (z-score of -2 or less). IPA defines any molecule (regulator) that can affect the expression of another molecule (target) as an 'upstream regulator'. Listed are the significantly activated and inhibited up-stream regulators at 6-weeks disease within the spinal cord. Orange: activated; blue: inhibited.

Upstream regulators- spinal cord 6 weeks					
Upstream Regulator	**Molecule Type**	**Predicted Activation State**	**Activation Z-score**	**Target proteins in dataset**	**p-value**
TSC2	other	Activated	2.65	16	3.09E-04
ERG	transcription regulator	Activated	2.50	16	0.02
POR	enzyme	Activated	2.14	28	5.34E-07
REST	transcription regulator	Activated	2.08	11	7.26E-04

ERN1	kinase	Inhibited	-2.99	11	0.0472
DIO2	enzyme	Inhibited	-2.45	6	9.45E-03
MTOR	kinase	Inhibited	-2.36	60	1.30E-31
SREBF1	transcription regulator	Inhibited	-2.17	27	7.02E-08
PRL	cytokine	Inhibited	-2.02	25	1.56E-04

4.2.5 Activation and inhibition of biological functions over disease course in rNLS TDP-43 mice

To determine the downstream effects of the proteomic changes and identify which biological functions, processes, and diseases are affected, a downstream analysis was carried out using IPA. Henceforth, these downstream effects will be referred to as biofunctions. Here again the z-score algorithm was used to make predictions about the expected increase or decrease of biofunctions given the proteomic changes within the experimental dataset.

The increased and decreased *biofunctions* across the timepoints within the *cortex* are listed in **Tables 4.2.13-15**. To examine the number of changes across disease duration, GraphPad Prism was used to visualise the comparison of increased and decreased biofunctions within 2, 4, and 6 weeks in the cortex (**Figure 4.2.30**). This revealed that most biological changes occurred at 4-weeks disease, with more decreased biofunctions compared to increased biofunctions at each timepoint (**Figure 4.2.30**). The overlap of the biofunctions was visualised using JVenn and this revealed that there are 4 *increased* biofunctions that intersect 2, 4, and 6-weeks of disease and all were seizure-related: seizure disorder, seizures, generalized seizures, and tonic-clonic seizure (**Figure 4.2.31** and **Tables 4.2.13-15)**. Three increased biofunctions were exclusive to the 2-week timepoint (associated to early disease stage): paired-pulse facilitation, oligomerization, and localization of protein (**Figure 4.2.31** and **Tables 4.2.13-15)**. When analysing the overlap within the *decreased* biofunctions, 13 biofunctions intersected all timepoints (**Figure 4.2.32**). Of the 13-overlapping decreased biofunctions, 10 were related to

neurotransmission or transmission within the synapse and cortex, while the remaining 3 biofunctions were receptor-mediated endocytosis, coordination, and long-term depression (**Figure 4.2.32** and **Tables 4.2.13-15)**. Again, three decreased biofunctions were exclusive to the 2-week timepoint (associated to early disease stage): transport of vesicles, cell-cell contact, docking of vesicles (**Figure 4.2.32** and **Tables 4.2.13-15)**.

Table 4.2.13 Increased and decreased biological functions at 2-weeks disease within the cortex.

Protein was extracted from the cortex of rNLS mice at 2, 4, and 6-week timepoints. SWATH MS was conducted (n=3-5 mice) to identify and quantify proteins that changed in TDP-43 mice compared to control non-bigenic mice. Ingenuity Pathway Analysis (IPA) software was used to identify the downstream effects given the proteomic changes within the experimental dataset at each timepoint. The downstream regulator analysis tool within IPA provides two statistical measures: 1) identifies downstream biological functions and calculates significance using Fisher's Exact Test ($p<0.05$); 2) infers the likely increase (z-score of 2 or more) or decrease (z-score of -2 or less) of downstream effect using the z-score algorithm. Listed are the significantly increased and decreased downstream effects at 2-weeks disease within the cortex. Red: increased; blue: decreased.

Biological functions- Cortex 2 weeks				
Diseases or Functions Annotation	**p-value**	**Number of proteins within dataset**	**Predicted activation state**	**z-score[#]**
Increased				
seizure disorder	1.48E-29	185	Increased	3.79
seizures	1.83E-26	155	Increased	3.69
generalized seizures	3.67E-09	33	Increased	3.29
tonic-clonic seizure	8.03E-08	28	Increased	3.21
paired-pulse facilitation	1.71E-14	31	Increased	2.47
oligomerization	1.83E-14	88	Increased	2.21
localization of protein	6.70E-08	59	Increased	2.16
Decreased				
cell death of osteosarcoma cells	8.02E-54	91	Decreased	-4.51
synaptic transmission	2.49E-34	141	Decreased	-3.46

synaptic transmission of cerebral cortex cells	4.66E-13	28	Decreased	-3.36
neurotransmission	5.50E-37	168	Decreased	-3.30
synaptic transmission of brain cells	8.96E-15	31	Decreased	-3.25
neurotransmission of cerebral cortex cells	2.18E-14	30	Decreased	-3.25
neurotransmission of brain cells	1.64E-16	34	Decreased	-3.15
synaptic transmission of nervous tissue	2.17E-13	44	Decreased	-3.13
cell death of tumour cells	4.68E-24	132	Decreased	-2.95
necrosis of tumour	2.14E-23	133	Decreased	-2.95
synaptic transmission of cells	2.26E-22	57	Decreased	-2.87
neurotransmission of hippocampal cells	9.46E-08	17	Decreased	-2.77
transport of vesicles	3.58E-27	63	Decreased	-2.74
cell death of cancer cells	1.50E-27	124	Decreased	-2.57
receptor-mediated endocytosis	1.87E-15	58	Decreased	-2.54
coordination	5.14E-16	81	Decreased	-2.44
endocytosis of synaptic vesicles	5.68E-09	15	Decreased	-2.42
endocytosis of vesicles	7.49E-11	20	Decreased	-2.40
prepulse inhibition	2.44E-08	31	Decreased	-2.37
cell-cell contact	9.84E-23	190	Decreased	-2.32
release of neurotransmitter	1.06E-10	42	Decreased	-2.28
formation of focal adhesions	1.62E-19	61	Decreased	-2.20
formation of filopodia	4.63E-10	49	Decreased	-2.16
docking of vesicles	7.60E-08	16	Decreased	-2.14
long term depression	3.43E-24	64	Decreased	-2.05
cancer	3.81E-37	2283	Decreased	-2.03

Table 4.2.14 Increased and decreased biological functions at 4-weeks disease within the cortex.

Protein was extracted from the cortex of rNLS mice at 2, 4, and 6-week timepoints. SWATH MS was conducted (n=3-5 mice) to identify and quantify proteins that changed in TDP-43 mice compared to control non-bigenic mice. Ingenuity Pathway Analysis (IPA) software was used to identify the downstream effects given the proteomic changes within the experimental dataset at each timepoint. The downstream regulator analysis tool within IPA provides two statistical measures: 1) identifies downstream biological functions and calculates significance using Fisher's Exact Test ($p<0.05$); 2) infers the likely increase (z-score of 2 or more) or decrease (z-score of -2 or less) of downstream effect using the z-score algorithm. Listed are the significantly increased and decreased downstream effects at 4-weeks disease within the cortex. Red: increased; blue: decreased.

Biological functions- Cortex 4 weeks				
Diseases or Functions Annotation	**p-value**	**Number of proteins within dataset**	**Week 4**	**z-score[#]**
Increased				
seizure disorder	1.48E-29	185	Increased	3.24
perinatal death	4.81E-10	154	Increased	3.21
tonic-clonic seizure	8.03E-08	28	Increased	3.21
seizures	1.83E-26	155	Increased	2.98
generalized seizures	3.67E-09	33	Increased	2.82
epilepsy	6.29E-15	109	Increased	2.82
neonatal death	3.53E-10	120	Increased	2.81
motor dysfunction or movement disorder	1.05E-94	483	Increased	2.42
contraction of heart	7.07E-11	58	Increased	2.17
paired-pulse facilitation of synapse	3.13E-13	27	Increased	2.16
action potential of cells	1.62E-14	58	Increased	2.16
Movement Disorders	6.02E-93	475	Increased	2.12
emotional behaviour	9.88E-19	100	Increased	2.10
heart rate	1.58E-10	82	Increased	2.06
Decreased				
synaptic transmission of cerebral cortex cells	4.66E-13	28	Decreased	-3.61
endocytosis by eukaryotic cells	6.65E-09	79	Decreased	-3.56
synaptic transmission of brain cells	8.96E-15	31	Decreased	-3.49
neurotransmission of cerebral cortex cells	2.18E-14	30	Decreased	-3.49
synaptic transmission of nervous tissue	2.17E-13	44	Decreased	-3.47
receptor-mediated endocytosis	1.87E-15	58	Decreased	-3.45

neurotransmission of brain cells	1.64E-16	34	Decreased	-3.38
synaptic transmission	2.49E-34	141	Decreased	-3.26
endocytosis	7.64E-27	162	Decreased	-3.25
engulfment of tumour cell lines	3.71E-10	46	Decreased	-3.17
secretion of neurotransmitter	3.66E-10	49	Decreased	-3.08
cell death of cancer cells	1.50E-27	124	Decreased	-3.07
synaptic transmission of cells	2.26E-22	57	Decreased	-2.87
cell death of osteosarcoma cells	8.02E-54	91	Decreased	-2.83
long term depression	3.43E-24	64	Decreased	-2.82
long term depression of synapse	9.10E-15	35	Decreased	-2.80
neurotransmission	5.50E-37	168	Decreased	-2.70
cell death of tumour cells	4.68E-24	132	Decreased	-2.69
necrosis of tumour	2.14E-23	133	Decreased	-2.69
release of neurotransmitter	1.06E-10	42	Decreased	-2.68
secretion of molecule	2.40E-12	139	Decreased	-2.67
long-term potentiation	1.76E-42	133	Decreased	-2.56
long term depression of hippocampus	7.27E-09	21	Decreased	-2.51
memory	4.02E-14	88	Decreased	-2.48
coordination	5.14E-16	81	Decreased	-2.48
gastrointestinal neoplasia	6.85E-18	1714	Decreased	-2.46
plasticity of synapse	1.52E-23	64	Decreased	-2.37
formation of cellular protrusions	3.76E-49	333	Decreased	-2.37
migration of cells	2.47E-12	426	Decreased	-2.36
engulfment of cells	4.49E-16	122	Decreased	-2.34
learning	1.41E-32	170	Decreased	-2.34
aciduria	1.67E-11	30	Decreased	-2.31
cancer	3.81E-37	2283	Decreased	-2.25
formation of lamellipodia	7.76E-10	45	Decreased	-2.20
potentiation of synapse	1.28E-43	135	Decreased	-2.18
neurotransmission of hippocampal cells	9.46E-08	17	Decreased	-2.17
cell movement	1.40E-17	505	Decreased	-2.12
formation of focal adhesions	1.62E-19	61	Decreased	-2.08
formation of filopodia	4.63E-10	49	Decreased	-2.02
folding of protein	3.35E-17	40	Decreased	-2.01

Table 4.2.15 Increased and decreased biological functions at 4-weeks disease within the cortex.

Protein was extracted from the cortex of rNLS mice at 2, 4, and 6-week timepoints. SWATH MS was conducted (n=3-5 mice) to identify and quantify proteins that changed in TDP-43 mice compared to control non-bigenic mice. Ingenuity Pathway Analysis (IPA) software was used to identify the downstream effects given the proteomic changes within the experimental dataset at each timepoint. The downstream regulator analysis tool within IPA provides two statistical measures: 1) identifies downstream biological functions and calculates significance using Fisher's Exact Test ($p<0.05$); 2) infers the likely increase (z-score of 2 or more) or decrease (z-score of -2 or less) of downstream effect using the z-score algorithm. Listed are the significantly increased and decreased downstream effects at 6-weeks disease within the cortex. Red: increased; blue: decreased.

Biological functions- Cortex 6 weeks				
Diseases or Functions Annotation	**p-value**	**Number of proteins within dataset**	**Week 4**	**z-score[#]**
Increased				
generalized seizures	3.67E-09	33	Increased	2.94
tonic-clonic seizure	8.03E-08	28	Increased	2.80
contraction of heart	7.07E-11	58	Increased	2.77
seizure disorder	1.48E-29	185	Increased	2.67
hyperactive behaviour	1.25E-12	56	Increased	2.59
heart rate	1.58E-10	82	Increased	2.42
seizures	1.83E-26	155	Increased	2.40
epilepsy	6.29E-15	109	Increased	2.29
Decreased				
synaptic transmission of brain cells	8.96E-15	31	Decreased	-3.25
coordination	5.14E-16	81	Decreased	-3.05
receptor-mediated endocytosis	1.87E-15	58	Decreased	-3.05
neurotransmission	5.50E-37	168	Decreased	-3.02
synaptic transmission	2.49E-34	141	Decreased	-2.99
synaptic transmission of cerebral cortex cells	4.66E-13	28	Decreased	-2.99
synaptic transmission of cells	2.26E-22	57	Decreased	-2.87
neurotransmission of brain cells	1.64E-16	34	Decreased	-2.79
synaptic transmission of nervous tissue	2.17E-13	44	Decreased	-2.78
prepulse inhibition	2.44E-08	31	Decreased	-2.62
release of neurotransmitter	1.06E-10	42	Decreased	-2.60
neurotransmission of cerebral cortex cells	2.18E-14	30	Decreased	-2.52

migration of neurons	8.62E-12	74	Decreased	-2.49
endocytosis	7.64E-27	162	Decreased	-2.45
endocytosis of synaptic vesicles	5.68E-09	15	Decreased	-2.42
endocytosis of vesicles	7.49E-11	20	Decreased	-2.40
learning	1.41E-32	170	Decreased	-2.40
endocytosis by eukaryotic cells	6.65E-09	79	Decreased	-2.37
neurotransmission of hippocampal cells	9.46E-08	17	Decreased	-2.32
long-term potentiation	1.76E-42	133	Decreased	-2.30
secretion of molecule	2.40E-12	139	Decreased	-2.30
autosomal recessive disease	1.37E-08	266	Decreased	-2.17
fragmentation of mitochondria	1.67E-11	24	Decreased	-2.16
engulfment of tumour cell lines	3.71E-10	46	Decreased	-2.15
memory	4.02E-14	88	Decreased	-2.12
long term depression of neurons	1.88E-13	26	Decreased	-2.10
tumorigenesis of malignant tumour	4.78E-14	1399	Decreased	-2.10
migration of cerebral cortex cells	3.84E-08	18	Decreased	-2.09
synaptic depression	5.62E-35	85	Decreased	-2.09
long term depression	3.43E-24	64	Decreased	-2.09
secretion of neurotransmitter	3.66E-10	49	Decreased	-2.08
neurodegeneration of brain	2.91E-13	47	Decreased	-2.06
neurodegeneration of central nervous system	3.98E-14	49	Decreased	-2.00
engulfment of cells	4.49E-16	122	Decreased	-2.00

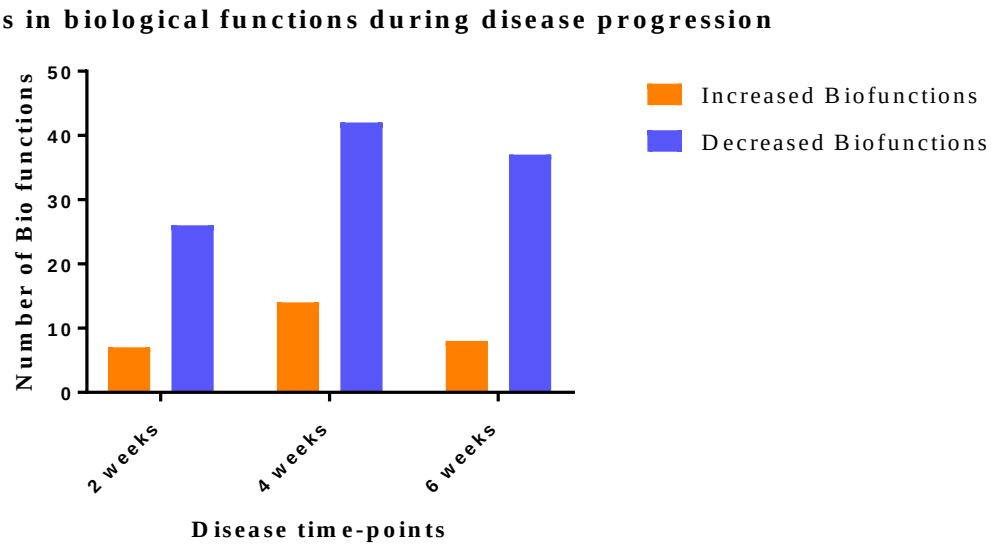

Figure 4.2.30 Changes in biological functions across disease progression within the cortex.

Protein was extracted from the cortex of rNLS mice at 2, 4, and 6-week timepoints. SWATH MS was conducted (n=3-5 mice) to identify and quantify proteins that changed in TDP-43 mice compared to control non-bigenic mice. Ingenuity Pathway Analysis (IPA) software was used to identify the downstream effects (biological functions) given the proteomic changes within the experimental dataset at each timepoint. The increased and decreased biofunctions were compared across disease timepoints using GraphPad Prism version 7.02. Orange: increased; blue: decreased.

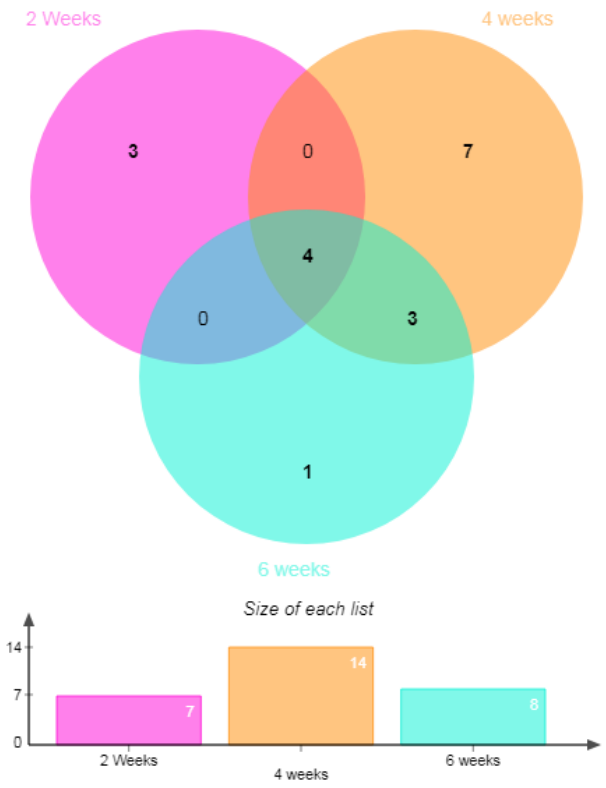

Figure 4.2.31 Overlap of increased biological functions across disease progression within the cortex.

Protein was extracted from the cortex of rNLS mice at 2, 4, and 6-week timepoints. SWATH MS was conducted (n=3-5 mice) to identify and quantify proteins that changed in TDP-43 mice compared to control non-bigenic mice. Ingenuity Pathway Analysis (IPA) software was used to identify the downstream effects (biological functions) given the proteomic changes within the experimental dataset at each timepoint. The increased biofunctions were compared across disease timepoints using JVenn (http://jvenn.toulouse.inra.fr/app/index.html).

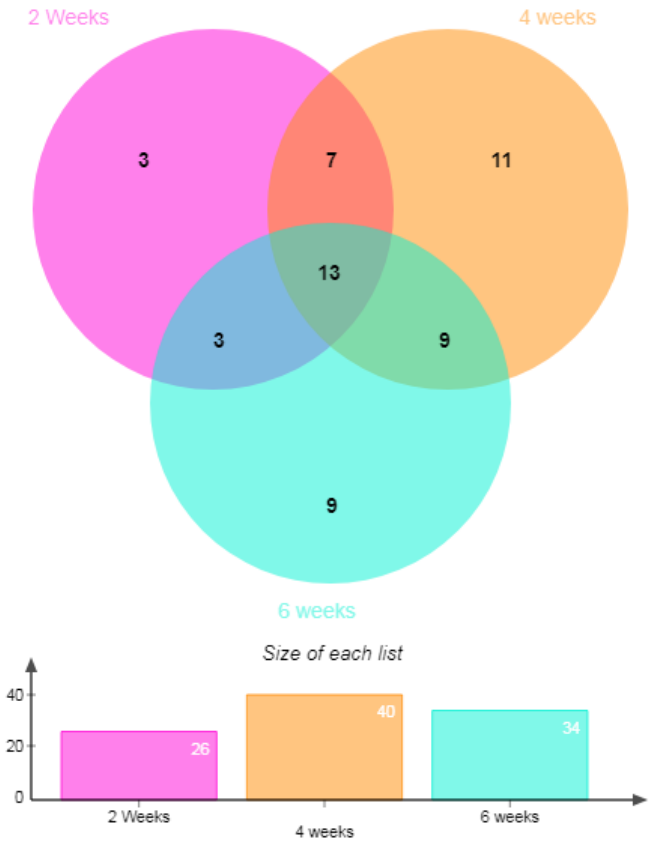

Figure 4.2.32 Overlap of decreased biological functions across disease progression within the cortex.

Protein was extracted from the cortex of rNLS mice at 2, 4, and 6-week timepoints. SWATH MS was conducted (n=3-5 mice) to identify and quantify proteins that changed in TDP-43 mice compared to control non-bigenic mice. Ingenuity Pathway Analysis (IPA) software was used to identify the downstream effects (biological functions) given the proteomic changes within the experimental dataset at each timepoint. The decreased biofunctions were compared across disease timepoints using JVenn (http://jvenn.toulouse.inra.fr/app/index.html).

The increased and decreased *biofunctions* within the *spinal cord* across two timepoints of are listed in **Tables 4.2.16-17.** More biofunctions changed at 6-weeks disease compared to 2-weeks, and more biofunctions decreased at both timepoints (**Tables 4.2.16-17**). There were only 2 biofunctions that overlapped the two timepoints within the cortex: migration of connective tissue cells and migration of fibroblasts were both decreased at both 2- and 6-weeks disease.

Table 4.2.16 Increased and decreased biological functions at 2-weeks disease within the spinal cord.

Protein was extracted from the spinal cord of rNLS mice at 2 and 6-week timepoints. SWATH MS was conducted (n=3-5 mice) to identify and quantify proteins that changed in TDP-43 mice compared to control non-bigenic mice. Ingenuity Pathway Analysis (IPA) software was used to identify the downstream effects given the proteomic changes within the experimental dataset at each timepoint. The downstream regulator analysis tool within IPA provides two statistical measures: 1) identifies downstream biological functions and calculates significance using Fisher's Exact Test ($p<0.05$); 2) infers the likely increase (z-score of 2 or more) or decrease (z-score of -2 or less) of downstream effect using the z-score algorithm. Listed are the significantly increased and decreased downstream effects at 2-weeks disease within the spinal cord. Red: increased; blue: decreased.

Biological functions- spinal cord 2 weeks				
Diseases or Functions Annotation	**p-value**	**Number of proteins within dataset**	**Predicted activation state**	**z-score[#]**
Increased				
apoptosis of muscle cells	1.76E-06	35	Increased	2.53
cell death of cervical cancer cell lines	4.87E-10	62	Increased	2.17
hydrolysis of nucleotide	1.20E-09	20	Increased	2.14
cell death of muscle cells	4.91E-07	45	Increased	2.12
stabilization of microtubules	9.91E-07	18	Increased	2.04
Decreased				
migration of connective tissue cells	1.32E-06	27	Decreased	-2.72
organization of organelle	1.50E-18	101	Decreased	-2.69
organization of filaments	7.25E-14	45	Decreased	-2.69

fatty acid metabolism	3.77E-15	92	Decreased	-2.58
cell movement of fibroblasts	1.64E-06	27	Decreased	-2.28
transmembrane potential	7.27E-08	43	Decreased	-2.17
brain atrophy	5.74E-08	17	Decreased	-2.16
organization of actin filaments	3.11E-07	20	Decreased	-2.12
concentration of ATP	2.67E-07	24	Decreased	-2.12
migration of fibroblasts	1.96E-06	23	Decreased	-2.07
transmembrane potential of mitochondria	1.73E-08	37	Decreased	-2.03
synthesis of fatty acid	4.85E-06	40	Decreased	-2.03
neurodegeneration of central nervous system	5.92E-07	23	Decreased	-2.01

Table 4.2.17 Increased and decreased biological functions at 6-weeks disease within the spinal cord.

Protein was extracted from the spinal cord of rNLS mice at 2 and 6-week timepoints. SWATH MS was conducted (n=3-5 mice) to identify and quantify proteins that changed in TDP-43 mice compared to control non-bigenic mice. Ingenuity Pathway Analysis (IPA) software was used to identify the downstream effects given the proteomic changes within the experimental dataset at each timepoint. The downstream regulator analysis tool within IPA provides two statistical measures: 1) identifies downstream biological functions and calculates significance using Fisher's Exact Test ($p<0.05$); 2) infers the likely increase (z-score of 2 or more) or decrease (z-score of -2 or less) of downstream effect using the z-score algorithm. Listed are the significantly increased and decreased downstream effects at 6-weeks disease within the spinal cord. Red: increased; blue: decreased.

Biological functions- spinal cord 6 weeks				
Diseases or Functions Annotation	**p-value**	**Number of proteins within dataset**	**Predicted activation state**	**z-score[#]**
Increased				
paired-pulse facilitation	1.98E-06	14	Increased	2.56
paired-pulse facilitation of synapse	1.44E-06	13	Increased	2.38
apoptosis of tumour cell lines	5.42E-13	169	Increased	2.20
cell death	3.77E-41	459	Increased	2.14
morbidity or mortality	1.38E-28	345	Increased	2.13
organization of actin filaments	3.11E-07	20	Increased	2.12
organismal death	2.43E-29	344	Increased	2.11
digestive organ tumour	4.32E-07	869	Increased	2.11

modification of reactive oxygen species	1.07E-08	8	Increased	2.08
cell death of tumour cell lines	6.03E-19	223	Increased	2.03
quantity of metal	1.72E-06	61	Increased	2.02
Decreased				
internalization by tumour cell lines	2.60E-07	22	Decreased	-3.13
secretion of neurotransmitter	7.74E-07	26	Decreased	-3.13
engulfment of tumour cell lines	2.77E-08	27	Decreased	-2.99
endocytosis by eukaryotic cells	2.20E-08	46	Decreased	-2.89
maximal conduction velocity	3.32E-06	8	Decreased	-2.79
metabolism of carbohydrate	4.52E-07	74	Decreased	-2.63
branching of neurites	6.57E-14	58	Decreased	-2.61
Clathrin mediated endocytosis	4.34E-07	16	Decreased	-2.58
branching of neurons	2.32E-14	60	Decreased	-2.37
migration of connective tissue cells	1.32E-06	27	Decreased	-2.32
endocytosis	2.87E-20	91	Decreased	-2.29
sprouting	1.95E-12	68	Decreased	-2.23
development of neurons	9.76E-27	150	Decreased	-2.23
haemolysis	2.59E-06	19	Decreased	-2.2
engulfment of cells	2.39E-11	65	Decreased	-2.219
size of body	2.63E-14	131	Decreased	-2.2
quantity of reactive oxygen species	4.37E-09	32	Decreased	-2.1
dendritic growth/branching	2.27E-11	46	Decreased	-2.0
migration of fibroblasts	1.96E-06	23	Decreased	-2.0
receptor-mediated endocytosis	1.69E-12	35	Decreased	-2.01

4.2.6 Selection of proteins for validation studies based on comprehensive analyses

Comprehensive bioinformatic analysis of proteomic data placed the protein changes from SWATH MS into biological context and the predictions enabled the formation of mechanistic hypotheses regarding proteins and pathways involvement in ALS disease. The objective was to use the information obtained from the comprehensive analyses to select pathways for validation studies. As a result, a large number of proteins, pathways, and upstream regulators were selected based on IPA predictions regarding activation, inhibition, and significant enrichment patterns during disease progression. The

possible implications of each candidate protein, pathway or regulator in ALS disease was considered. It is important to note that while many proteins, pathways, and regulators were selected, the protein and pathway selection within *this current* study was based on pathway enrichment and mapping. The additional selected proteins, pathways, and regulators will be the focus of further additional studies.

In the current study, two pathways were selected: mitochondrial dysfunctional and RAN signalling. Mitochondrial dysfunction was the top most enriched pathway within spinal cord and second most enriched within the cortex with 40% and 47% of pathway proteins identified within the experimental dataset respectively. Mitochondrial dysfunction is a major, multifaceted pathological pathway within ALS and is implicated in energy deficit, calcium dysregulation and oxidative stress[131]. Within the mitochondrial dysfunction pathway, two proteins were selected for validation: COQ9 and VDAC3 (**Table 4.2.18**).

RAN signalling was a significantly enriched pathway within the cortex with 58% of pathway proteins being identified within experimental dataset. However, RAN signalling was not detected within the spinal cord. RAN signalling is involved in the nucleo-cytoplasmic transport of proteins and due to mislocalisation of TDP-43 being a hallmark of ALS pathology, it was important to validate protein changes within this pathway. The two proteins selected for validation from the RAN signalling pathway were IMA3 and IPO4 (**Table 4.2.18**).

Table 4.2.18 Selection of pathways and proteins vis comprehensive bioinformatic analysis for validation.

Protein was extracted from the cortex and spinal cord of rNLS mice at 2, 4, and 6-week timepoints. SWATH MS was conducted (n=3-5 mice) to identify and quantify proteins that changed in TDP-43 mice compared to control non-bigenic mice. Ingenuity Pathway Analysis (IPA) software was used to perform a comprehensive bioinformatics analyses to place proteins within biological context and select proteins and pathways for validation studies. List are the proteins and pathways selected for validation via comprehensive analysis.

Protein ID (Mouse)	Protein name	Fold change					Subcellular location	Uniprot functions summary[109]	Reasons for selections
		Cortex			Spinal cord				
		2 weeks	4 weeks	6 weeks	2 weeks	6 weeks			
COQ9	Ubiquinone biosynthesis protein COQ9	NC	NC	NC	4.30	NC	Mitochondrion	An essential lipid-soluble electron transporter for aerobic cellular respiration.	Mitochondrial dysfunction top enriched pathway within spinal cord and second most enriched within cortex. Mitochondrial dysfunction a major pathological pathway within ALS. COQ9 part of the 'motor dysfunction and movement disorder' biofunction increased at 4 weeks cortex.

VDAC3	Voltage-dependent anion-selective channel protein 3 (VDAC-3)	0.53	NC	0.61	ND	ND	Mitochondrion outer membrane	Forms a channel through the mitochondrial outer membrane that allows diffusion of small hydrophilic molecules.	Mitochondrial dysfunction most enriched pathway within spinal cord and second most enriched within cortex. Mitochondrial dysfunction a major pathological pathway within ALS. VDAC3 involved in BCL2-mediated apoptosis and as per pathway mapping in in both cortex and spinal cord.
IMA3	Importin subunit alpha-3 (Importin alpha Q1)	NC	1.73	1.74	ND	ND	Cytoplasm, Nucleus	Functions in nuclear protein import as an adapter protein.	IMA3 part of the RAN signalling pathway which plays a critical role in nucleo-cytoplasmic transport of macromolecules through the nuclear pore complex. RAN signalling significantly enriched within cortex. Nucleo-cytoplasmic transport of proteins critical for ALS pathology.
IPO4	Importin-4 (Imp4) (Importin-4a)	NC	1.91	1.61	ND	ND	Cytoplasm, Nucleus	Functions in nuclear protein import as a nuclear transport receptor.	IPO4 involved in NLS-bearing substrate import into nucleus as part of RAN GTPase binding. Nucleo-cytoplasmic transport of proteins critical for ALS pathology.

4.2.7 Validation of proteins selected from comprehensive analyses

To validate the proteins selected by comprehensive analysis, antibodies were first optimised using several concentrations for both western blotting and immunofluorescence (**Table 4.2.19**). The only antibody that was unsuccessful in forming visible bands was anti-IPO4 (**Table 4.2.19**). Similarly, in immunofluorescence optimisation, anti-IPO4 was the only antibody unsuccessful (**Table 4.2.19**). As such validation studies could only be carried out for the three proteins: COQ9, VDAC3, and IMA3.

Similar to the validation of singular analysis, western blot experiments were conducted on two different cohorts of mice: cohort one was the *same* exact cohort used for the SWATH MS proteomics and cohort two was a *different* cohort of mice. All experiments were conducted using litter-matched, sex-matched mice pairs of n=3 for cohort 1 (proteomics cohort) and n=4 for cohort 2 (new cohort).

SWATH MS showed that *COQ9* was unchanged at all timepoints within the cortex, however western blot analysis using a specific antibody revealed significant decrease in COQ9 at 2, 4, and 6-week disease in both the *same* and *different* cohorts of mice (**Table 4.2.18, Figure 4.2.33-34**). Immunofluorescence imaging using the same antibody at 4-weeks cortex tissue did reveal a reduction in COQ9 staining, however a large amount of non-specific binding was also visible and thus imaging needs to be repeated with tissue from the same and different timepoints. COQ9 also needs to be validated using spinal cord tissue as SWATH MS showed an increase at the 2-week time-point.

Table 4.2.19 Antibody validation for proteins selected via comprehensive analysis.

Antibodies were validated using cortex tissue from control and rNLS at 4-week timepoint. For western blots 3 concentrations were used and 2 different concentrations for immunofluorescence imaging. IPO4 was the only antibody that was unsuccessful in forming a visible band for western blotting and immunofluorescence.

Antibody	Successful/Unsuccessful				
	Western Blot (conc.)			Immunofluorescence imaging (conc.)	
	1/2000	1/1000	1/500	1/500	1/100
anti-COQ9	Unsuccessful	Unsuccessful	Successful	Successful	Successful
anti-VDAC3	Unsuccessful	Unsuccessful	Successful	Successful	Successful
Anti-KPNA4 (IMA3)	Unsuccessful	Unsuccessful	Successful	Successful	Successful
anti-IPO4	Unsuccessful	Unsuccessful	Unsuccessful	Unsuccessful	Unsuccessful

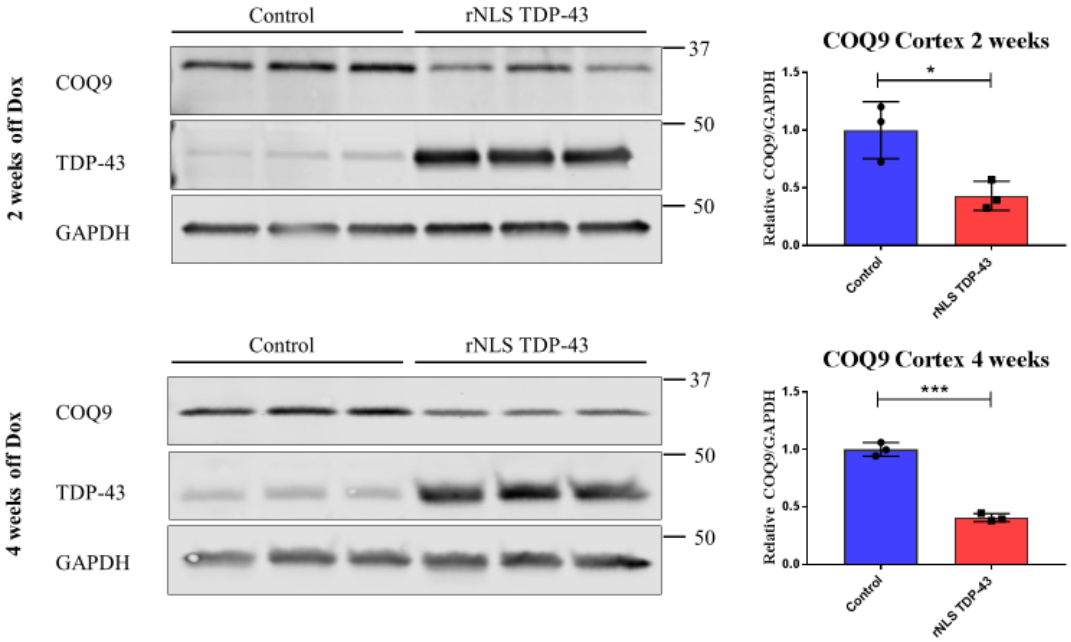

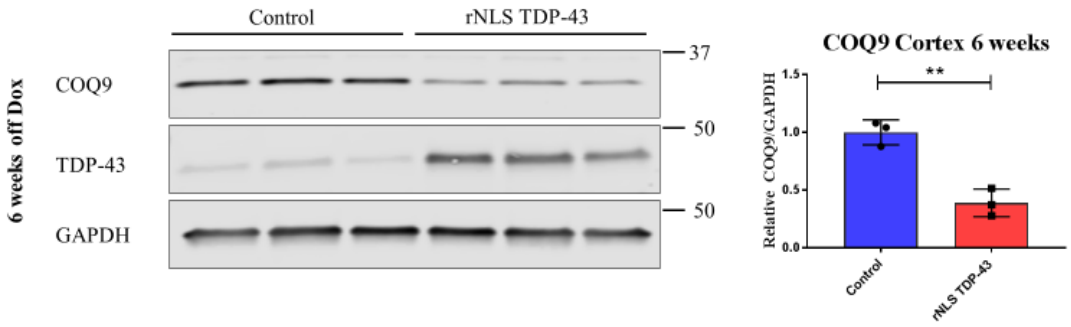

Figure 4.2.33 Validation of COQ9 within *same* mice cohort used for proteomics.

Specific COQ9 antibody was used to validate protein changes using cortex tissue from the same cohort that was used for SWATH MS (litter-matched, sex-matched pairs for control and rNLS) at 2,4 and 6-week timepoints (n=3). Blots were visualised and quantified using the LI-COR Image Studio software. Statistical analysis was conducted using a Paired T-test via GraphPad Prism version 7.02 (not significant=P > 0.05). The molecular weight for COQ9 is 35kDa. For full blots refer to ***Appendix figure 2.3****. For p-values refer to* ***Table 4.2.20****.*

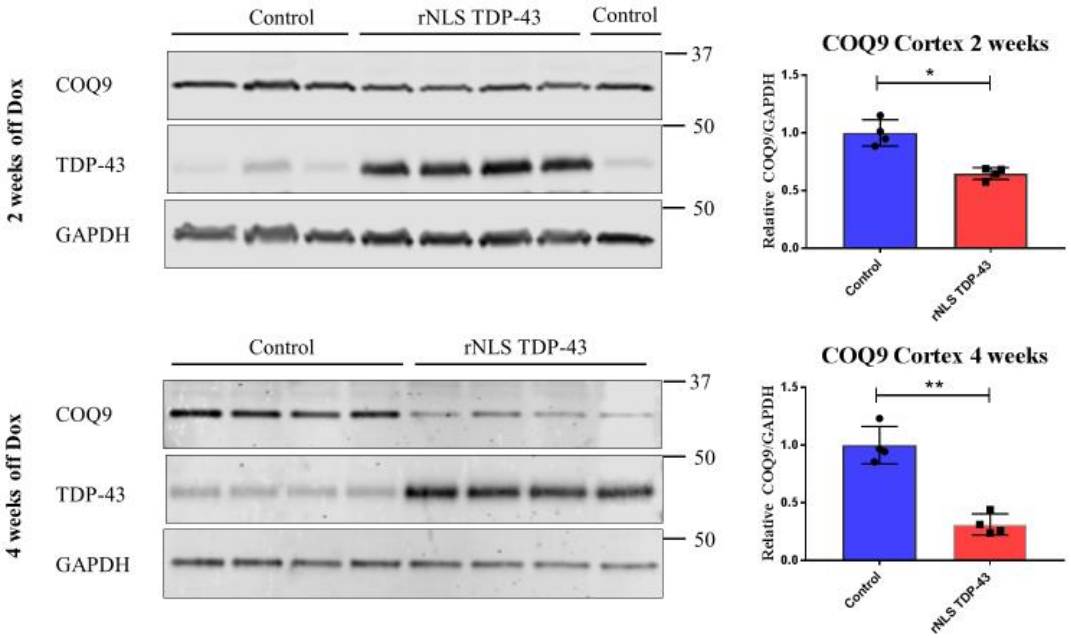

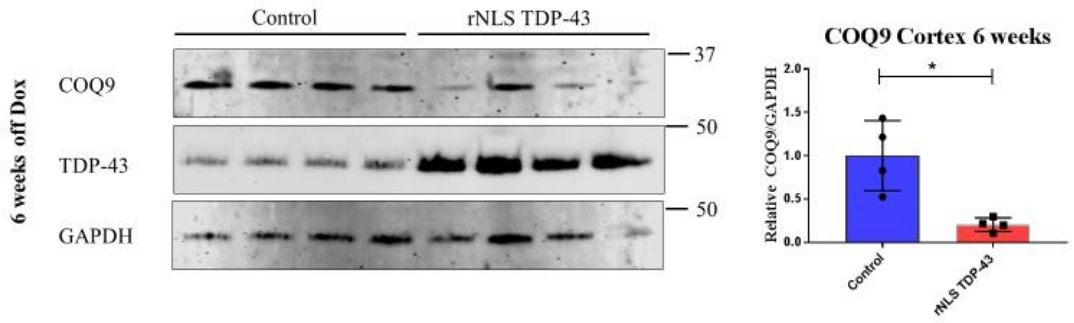

Figure 4.2.34 Validation of COQ9 within *different* mice cohort used for proteomics.

Specific COQ9 antibody was used to validate protein changes using cortex tissue from the different cohort that was used for SWATH MS (litter-matched, sex-matched pairs for control and rNLS) at 2,4 and 6-week timepoints (n=3). Blots were visualised and quantified using the LI-COR Image Studio software. Statistical analysis was conducted using a Paired T-test via GraphPad Prism version 7.02 (not significant=P > 0.05). The molecular weight for COQ9 is 35kDa. For full blots refer to ***Appendix figure 2.4****. For p-values refer to* ***Table 4.2.20****.*

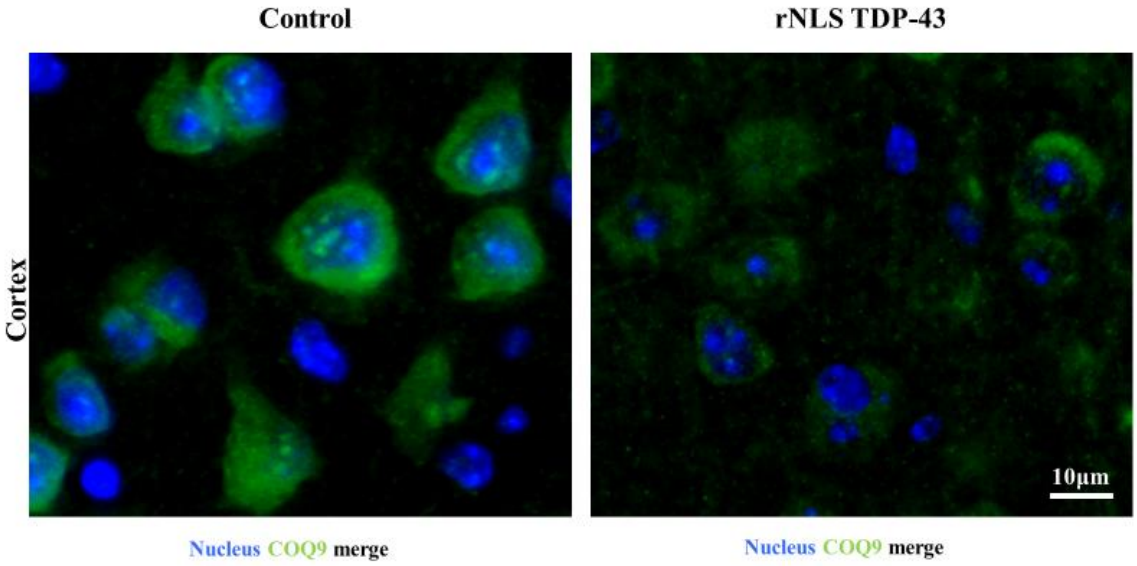

Figure 4.2.35 Visualisation of COQ9 within the cortex.

Specific COQ9 antibody (1/100 concentration) was used to visualise the candidate protein using immunofluorescence imaging of cortex tissue from litter-matched, sex-matched pairs for control and rNLS at 4-week timepoint (2 technical replicates). Imaging was conducted at 40x magnification, using the same exposure time for control and rNLS via the Zeiss Axiolmager upright fluorescence microscope. Blue: nuclear stain DAPI; green: COQ9.

SWHAT MS showed that *VDAC3* was decreased at 2- and 6-weeks disease within the cortex, however western blot analysis showed no significant difference between control and rNLS mice in both the *same* and *different* cohorts of mice (**Figure 4.2.36-37**). The blots also showed a second band for each sample right above the VDAC3 band as can been seen in the full blots (**Appendix figure 2.5 and 3.6**). This may suggest another isoform or the proteins VDAC1-2, and as such validation of VDAC3 needs to be repeated with a different antibody. Immunofluorescence imaging of VDAC3 at 4-week cortex showed nonspecific binding and must be repeated with a different antibody (**Figure 4.2.38**).

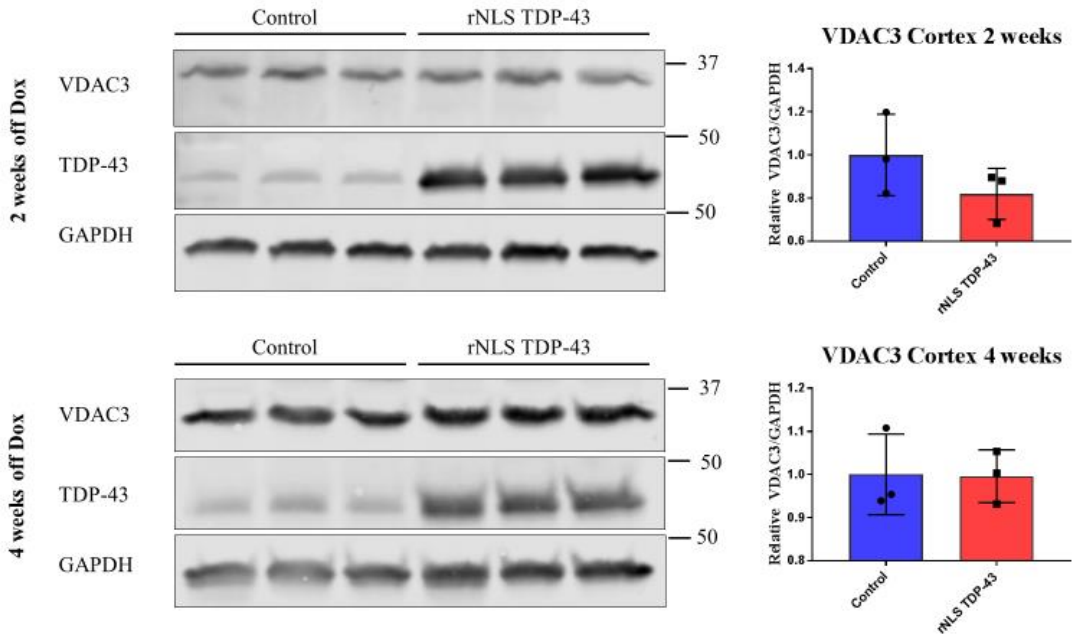

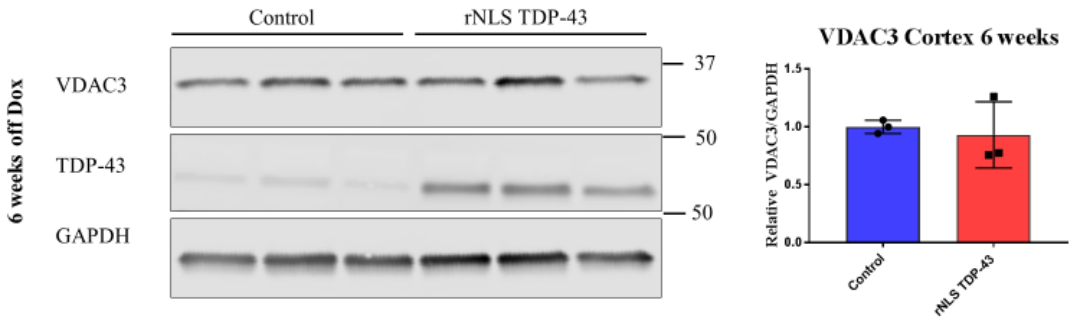

Figure 4.2.36 Validation of VDAC3 within *same* mice cohort used for proteomics.

Specific VDAC3 antibody was used to validate protein changes using cortex tissue from the same cohort that was used for SWATH MS (litter-matched, sex-matched pairs for control and rNLS) at 2,4 and 6-week timepoints (n=3). Blots were visualised and quantified using the LI-COR Image Studio software. Statistical analysis was conducted using a Paired T-test via GraphPad Prism version 7.02 (not significant=P > 0.05). The molecular weight for VDAC is 35kDa. For full blots refer to ***Appendix figure 2.5****. For p-values refer to* ***Table 4.2.20****.*

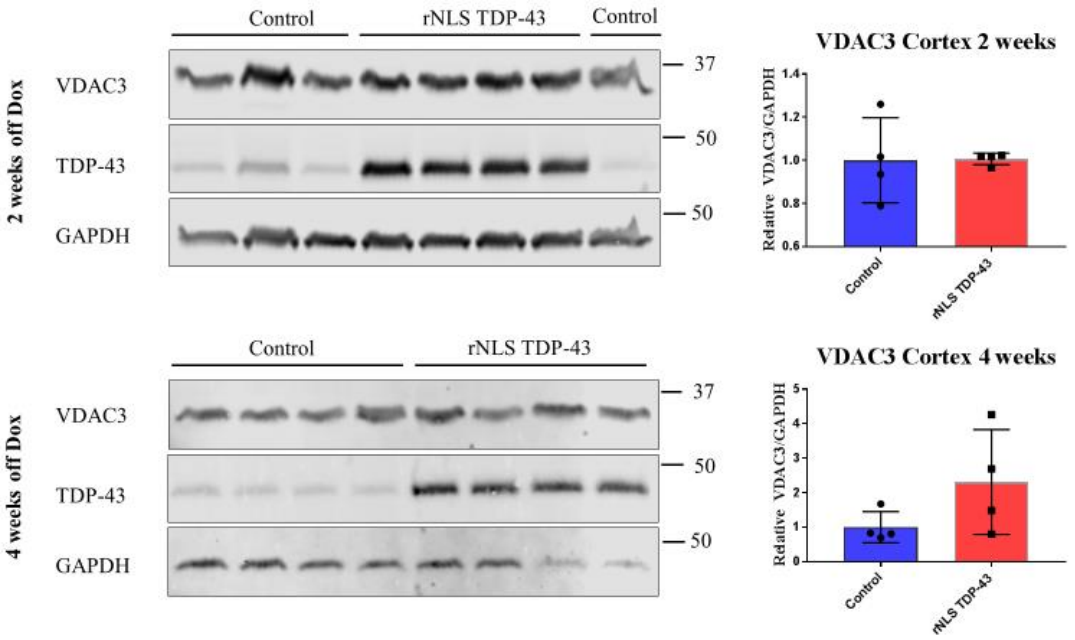

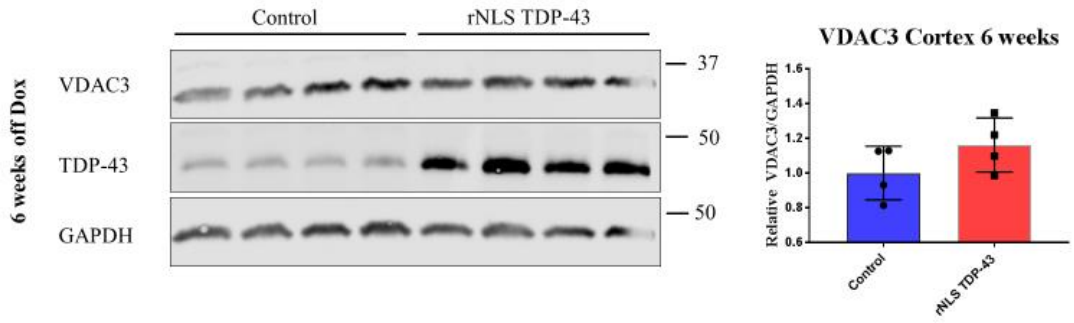

Figure 4.2.37 Validation of VDAC3 within *different* mice cohort used for proteomics.

Specific VDAC3 antibody was used to validate protein changes using cortex tissue from the different cohort that was used for SWATH MS (litter-matched, sex-matched pairs for control and rNLS) at 2,4 and 6-week timepoints (n=3). Blots were visualised and quantified using the LI-COR Image Studio software. Statistical analysis was conducted using a Paired T-test via GraphPad Prism version 7.02 (not significant=P > 0.05). The molecular weight for VDAC is 35kDa. For full blots refer to ***Appendix figure 2.6****. For p-values refer to* ***Table 4.2.20****.*

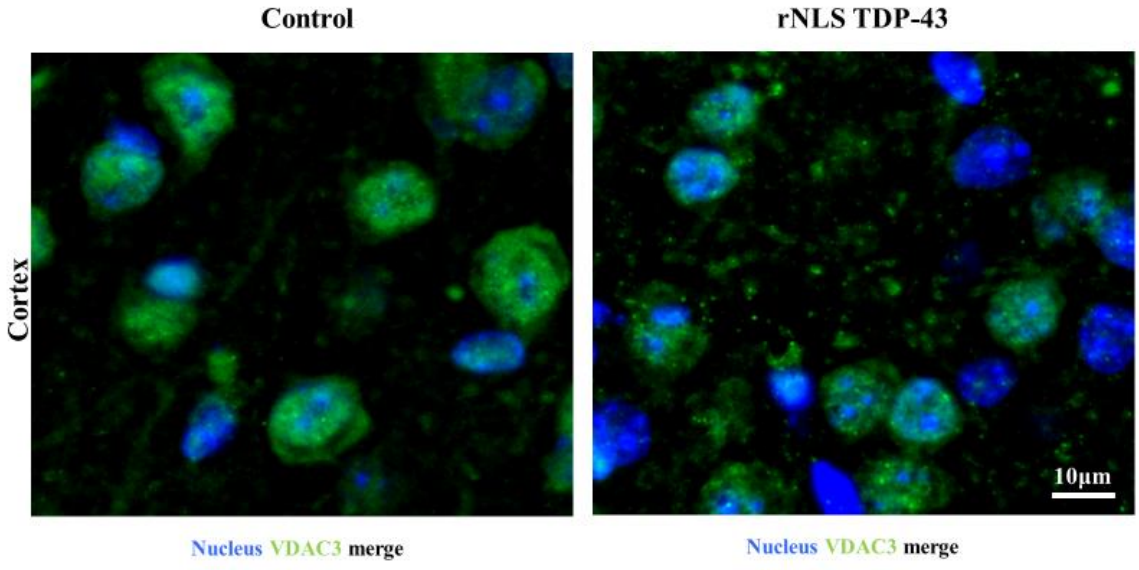

Figure 4.2.38 Visualisation of VDAC3 within the cortex.

Specific VDAC3 antibody (1/100 concentration) was used to visualise the candidate protein using immunofluorescence imaging of cortex tissue from litter-matched, sex-matched pairs for control and rNLS at 4-week timepoint (2 technical replicates). Imaging was conducted at 40x magnification, using the same exposure time for control and rNLS via the Zeiss Axiolmager upright fluorescence microscope. Blue: nuclear stain DAPI; green: VDAC3.

SWATH MS showed an increase in *IMA3* at 4 and 6 weeks disease and western blot analysis of cortex tissue from the *same* cohort of mice also revealed a significant increase at both 4- and 6-week timepoints (**Figure 4.2.39**). The western blot analysis using tissue from *different* cohort of mice revealed a significant increase of IMA3 at all timepoints within the cortex (**Figure 4.2.40**). However, the antibody showed some nonspecific bands that can be seen in the full blots (**Appendix figure 2.7 and 3.8**). Immunofluorescence using the same antibody using cortex tissue at 4-weeks disease also showed an increase in IMA3, however there was some nonspecific binding and as such must be repeated (**Figure 4.2.41**).

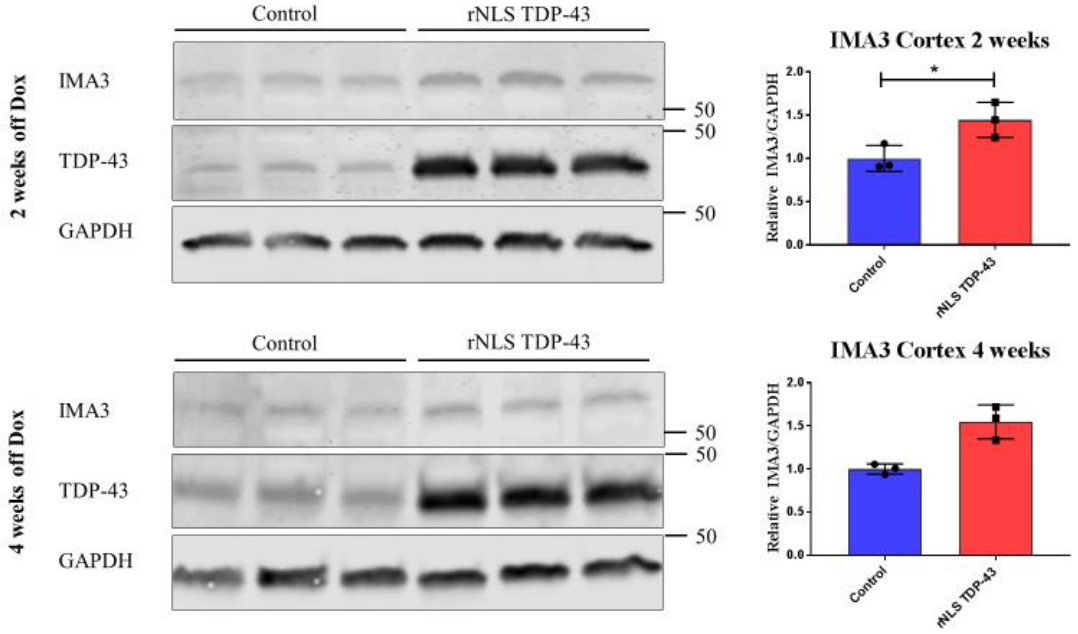

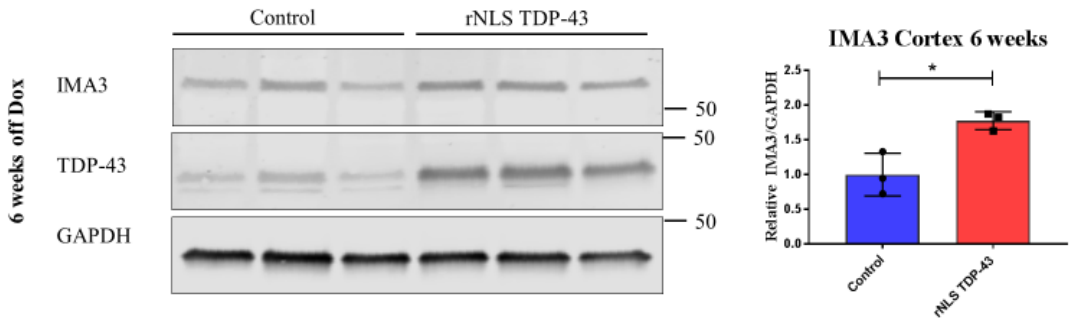

Figure 4.2.39 Validation of IMA3 within *same* mice cohort used for proteomics.

Specific IMA3 antibody was used to validate protein changes using cortex tissue from the same cohort that was used for SWATH MS (litter-matched, sex-matched pairs for control and rNLS) at 2,4 and 6-week timepoints (n=3). Blots were visualised and quantified using the LI-COR Image Studio software. Statistical analysis was conducted using a Paired T-test via GraphPad Prism version 7.02 (not significant=P > 0.05). The molecular weight for IMA3 is 58kDa. For full blots refer to ***Appendix figure 2.7****. For p-values refer to* ***Table 4.2.20****.*

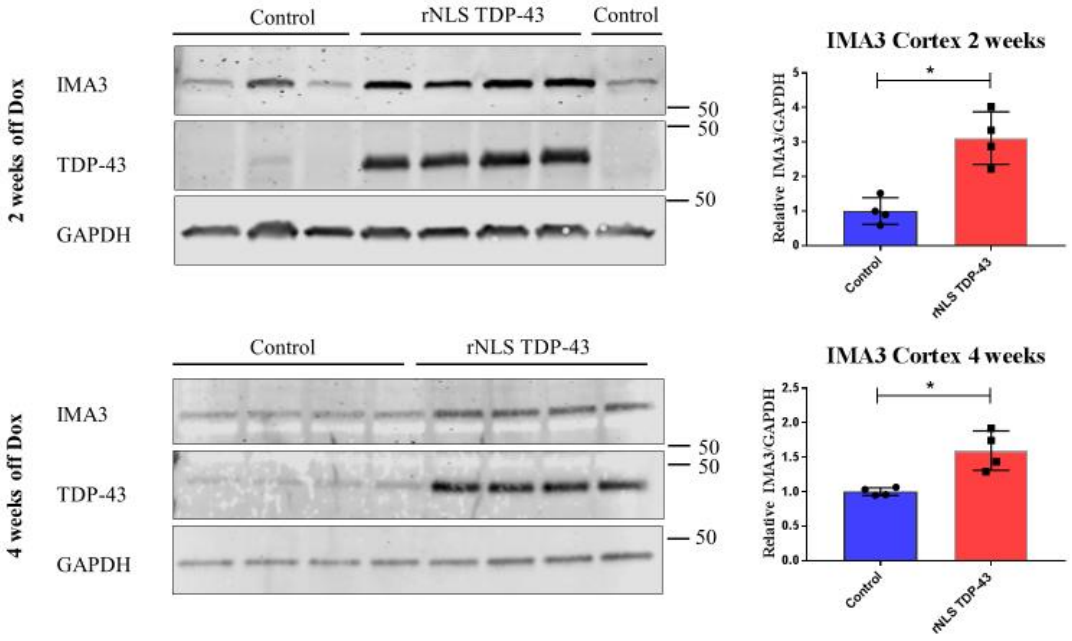

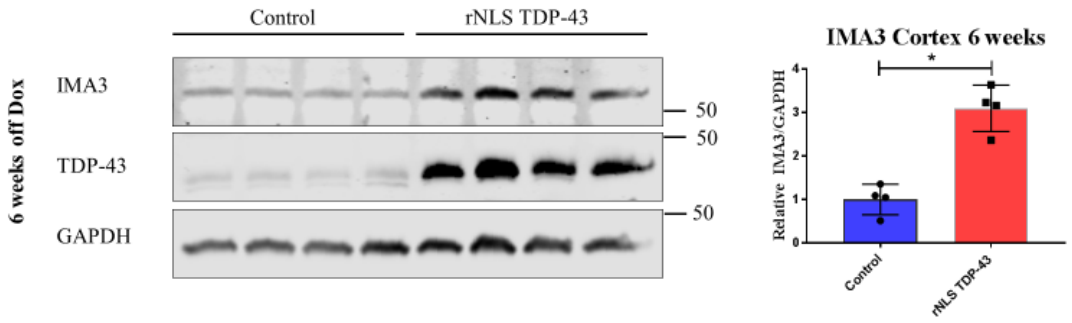

Figure 4.2.40 Validation of IMA3 within *different* mice cohort used for proteomics.

*Specific IMA3 antibody was used to validate protein changes using cortex tissue from the different cohort that was used for SWATH MS (litter-matched, sex-matched pairs for control and rNLS) at 2,4 and 6-week timepoints (n=3). Blots were visualised and quantified using the LI-COR Image Studio software. Statistical analysis was conducted using a Paired T-test via GraphPad Prism version 7.02 (not significant=P > 0.05). The molecular weight for IMA3 is 58kDa. For full blots refer to **Appendix figure 2.8**. For p-values refer to **Table 4.2.20**.*

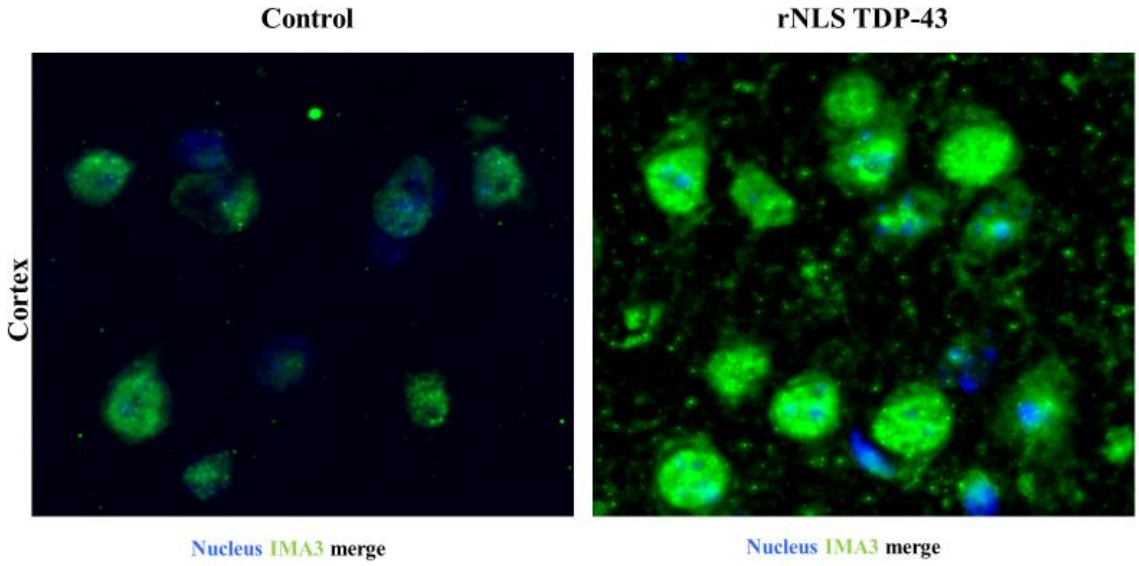

Figure 4.2.41 Visualisation of IMA3 within the cortex.

Specific IMA3 antibody (1/100 concentration) was used to visualise the candidate protein using immunofluorescence imaging of cortex tissue from litter-matched, sex-matched pairs for control and rNLS at 4-week timepoint (2 technical replicates). Imaging was conducted at 40x magnification, using the same exposure time for control and rNLS via the Zeiss Axiolmager upright fluorescence microscope. Blue: nuclear stain DAPI; green: IMA3.

Table 4.2.20 P-values generated from western blot quantification of target proteins.

Western blotting using specific antibodies was used to validate the changes in proteins in two cohorts of mice: Proteomic cohort (same cohort) and a second different cohort of mice. Blots were visualised and quantified using the LI-COR Image Studio software. Statistical analysis was conducted using a Paired T-test via GraphPad Prism version 7.02. Orange: highlights p-value<0.05.

Protein	p-value		
	Week 2	Week 4	Week 6
Same mice cohort			
COQ9	0.0452	0.0007	0.0073
IMA3	0.0207	0.0561	0.0310
VDAC3	0.0996	0.8992	0.6661
Different mice cohort			
COQ9	0.0218	0.0079	0.0351
IMA3	0.0293	0.0396	0.0121
VDAC3	0.9569	0.1726	0.2109

5. DISCUSSION

5.1 Major findings and implications

The most common feature of ALS pathology is the mislocalisation and aggregation of nuclear TDP-43 inclusions within the cytoplasm of cortical and motor neurons[52]. To investigate the proteins and pathways involved in TDP-43-mediated neurodegeneration, a large-scale proteomics study of the cortex and spinal cord of rNLS TDP-43 mice was performed. The current study was conducted to interrogate this dataset, in order to analyse changes in biochemical pathways over the course of disease with particular emphasis on alterations in the early disease stages, and to validate findings using western blotting and immunofluorescence. The major findings of the current study include: the finding that two key proteins (COQ9 and IMA3) involved in two key molecular mechanisms of ALS disease (mitochondrial dysfunction and nucleo-cytoplasmic protein import) are altered early in disease in vivo, and that extensive biochemical pathway analysis of protein profiles of the cortex and lumbar spinal cord of rNLS TDP-43 mice reveals dramatic changes during the course of disease. These biochemical alterations may therefore account for the onset and progression of neurodegeneration in ALS, and further research on these mechanisms is warranted.

This project has also resulted in the establishment of a new bioinformatic analysis pipeline, which had not before been conducted in the Neurodegeneration Pathobiology Laboratory. This analysis pipeline will be used in the future for additional large-scale proteomics studies on neurodegenerative disease, and allows for the consistent and comprehensive functional analysis of large proteomic datasets.

5.1.1 COQ9 decreased within the cortex of rNLS TDP-43 mice

Mitochondria have several essential functions within cells including energy production, biosynthesis of intermediates, and regulation of calcium homeostasis[132]. In addition, mitochondria are also a source of reactive oxygen species (ROS) and control major apoptosis pathways[132]. Expectedly, *mitochondrial dysfunction* is one of the main proposed pathogenic mechanisms for ALS[82]. Both the structure and function of mitochondria are affected within ALS patients as discussed earlier. More specific to TDP-43 pathology, a study has shown that soluble and un-cleaved TDP-43 co-localises to the inner mitochondrial membrane (IMM) of ALS spinal cord neurons[133]. This study also showed that suppression of TDP-43 co-localisation with the IMM prevents neurodegeneration in mutant TDP-43 A315T mice[133]. Specifically, inhibition of TDP-43 mitochondrial localisation prevents the following: mitochondrial dysfunction, neuron loss, phospho-TDP-43 positive inclusions and astrogliosis[133]. Results from the current study now show that these mitochondrial disturbances may also be a feature early in disease in a mouse model that displays more disease-reminiscent features than the TDP-43 A315T mutant mouse, with direct relevance to disease onset and progression in people living with ALS.

An essential component of the mitochondrial respiratory chain that produces 90% of ATP is the lipid Coenzyme Q (CoQ, or ubiquinone)[134]. CoQ shuttles electrons from complex I and II to complex III at the inner mitochondrial membrane (IMM)[135]. CoQ also plays a key role in controlling the mitochondrial permeability transition pore and is an essential antioxidant[135]. The biosynthesis of CoQ requires the CoQ-synthome complex that is formed by proteins COQ1-9 (**Figure 5.1.1**)[135]. COQ9 associates with COQ7 and is involved in the deamination step of the CoQ biosynthesis pathway[134, 135]. COQ9 is a critical component of

the CoQ-synthome as it has been shown that deletion of COQ9 results in separation of the CoQ-synthome[136]. In addition, COQ9 stabilises the CoQ-synthome and increase CoQ biosynthesis[137].

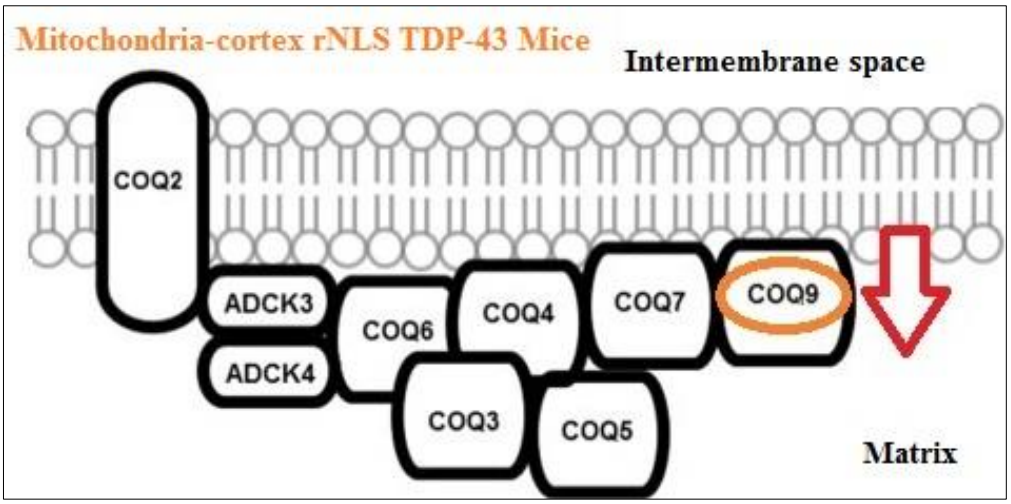

Figure 5.1.1 CoQ-synthome complex for Coenzyme Q biosynthesis involving COQ9.

COQ9 is part of a mitochondrial multi-subunit complex, named the CoQ-synthome, required for biosynthesis of coenzyme Q[136]. COQ9 is decreased within the cortex of rNLS TDP-43 mice during disease course. Illustration adapted from Acosta et. al., 2016[135].

Previous studies using a mutant COQ9 mouse model revealed that impaired COQ9 causes CoQ deficiency resulting in brain-specific dysfunction of mitochondrial bioenergetics[138]. Further investigation revealed that the mitochondrial dysfunction within the mutant COQ9 mice caused an increase in ROS and led to caspase-independent apoptosis[138]. The current study showed that within the cortex of rNLS TDP-43 mice, COQ9 is significantly decreased at early-, mid-, and late stage disease compared to litter-matched, aged-matched controls. This suggests that perhaps COQ9 decrease may be a mediator of mitochondrial dysfunction that can lead to generation of ROS and apoptotic signalling in the

cortex of rNLS TDP-43 mice even early in disease (IPA analysis revealed apoptotic signalling even at the 2-week timepoint).

However, SWATH MS revealed that COQ9 was increased at 2-weeks disease within the spinal cord which may denote that there is an inverse pattern of COQ9 protein expression between the cortex and spinal cord in rNLS TDP-43 mice. Previous studies using samples from sALS patients showed an increase in CoQ within the CSF and plasma which was attributed to the neuroprotective quality of CoQ[139, 140]. This CoQ increase might be explained by an increase of COQ9 within the spinal cord as it has been shown that COQ9 increases CoQ biosynthesis[137]. Although COQ9 levels were not measured in the studies investigating CoQ levels[139, 140]. Exogenous administration of CoQ and its reduced derivative in both SOD1 (G93A) mice and in a Phase II trial did not show any sufficient evidence for neuroprotective ability of CoQ[141, 142]. However, the absence of pharmacological effects in these studies was attributed to low CNS availability of CoQ due to oral administration[141]. Overall, together with previous studies, the findings of the current project demonstrate that an early and sustained alteration in mitochondrial function, in particular COQ9, may underlie TDP-43 pathology and could contribute to ALS pathogenesis.

5.1.2 IMA3 increased within the cortex of rNLS TDP-43 mice

The transport of proteins, such as transcription factors, between the cytoplasm and the nucleus is the key step in signal transduction which is critical for the appropriate regulation of gene expression[143]. Deficits in nucleo-cytoplasmic transport within neurons can lead to impaired function, loss of plasticity, and neurodegeneration [144, 145].

The transport of proteins across the nuclear membrane requires two types of importins: importin-α and importin-β. Importin-α is an adapter protein that binds to proteins

that contain a nuclear localisation sequence (NLS), and importin-β is a receptor for the nuclear envelope (**Figure 5.1.2**)[146]. Together the cargo protein, importin-α and importin-β interact with the nuclear pore complex (NPC) to allow the cargo to cross the nuclear membrane (**Figure 5.1.2**)[146]. Once inside the nucleus RanGTP facilitates the release of the cargo protein and the importins return to the cytoplasm[146].

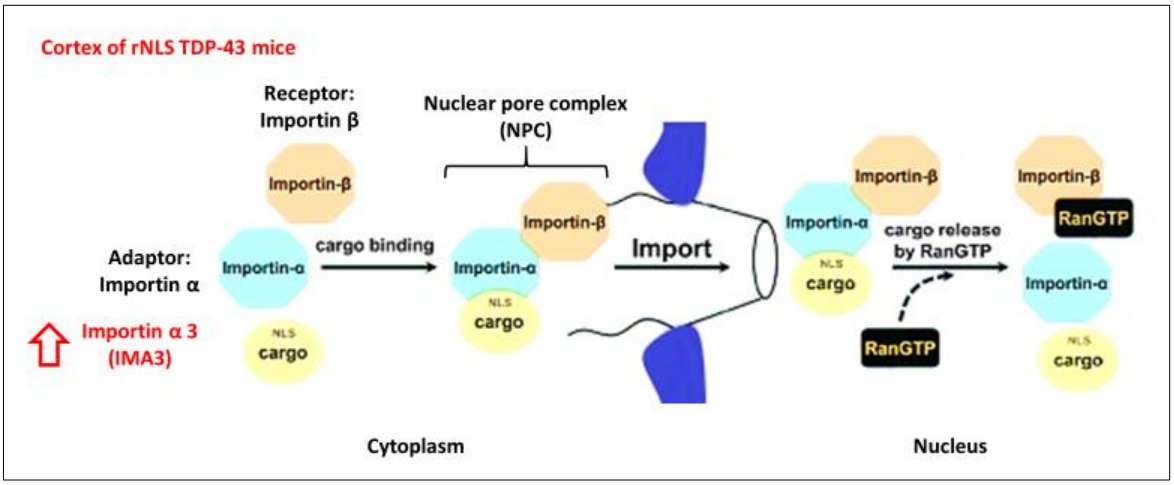

Figure 5.1.2 Simplified model of nuclear import and involvement of IMA3.

Importin α 3 (IMA3) binds to proteins (cargo) with a nuclear localization signal (NLS) and combines with importin β which is the nuclear envelope receptor that facilitates interaction with the nuclear pore complex (NPC) to allow entry into the nucleus. Within the nucleus RanGTP facilitates the release of cargo protein and disassociates from the NPC. Illustration adapted from Patel et. al., 2011[144] and Gorlich, 1998[147].

Increasing evidence suggests that altered nucleo-cytoplasmic transport is a likely pathogenic mechanism of neurogenerative diseases including ALS[144]. A study investigating ALS nucleo-cytoplasmic transport in SOD1(G93A) mice showed an accumulation of importin-β within the cytoplasm, accompanied by a decrease of importin-β within the nucleus, during disease progression in the anterior horn cells[148]. This study does not mention

importin-α despite the necessity of *both* importins for nuclear transport, which may be due to details of the function of the NPC being elucidated after this study. However, from these results it can be proposed that importin-α was also accumulated within the cytoplasm as it requires importin-β to act as the receptor for the nuclear envelope. Within the current study, it was shown that importin-α 3 (IMA3) was increased within the cortex of rNLS TDP-43 at early-, mid, and late-stage disease, although the distribution of IMA3 within cells cannot be deduced from proteomics and therefore needs to be further investigated. It is therefore possible that in addition to changes in level of IMA3, the distribution within neurons may be altered in the presence of TDP-43 pathology, which may contribute to disease.

More recently, one study reported that impaired nuclear import caused TDP-43 accumulation[149]. In this study, it was shown that the knock down of importin-β 1 resulted in the accumulation of TDP-43 within the cytoplasm of human SHSY-5Y and N2a cells as well as primary mouse neurons[149]. Also shown was the binding of TDP-43 to importin-α, confirming that TDP-43 nuclear import is carried out by the classical nuclear import pathway described above[149]. Together, these results suggest that changes in nucleo-cytoplasmic transport may play a role in ALS neurodegeneration.

An additional role of importins within cells is the trafficking of signalling proteins across the cell to reach the nucleus[143]. In neurons, this trafficking of signalling proteins is complicated by their complex, and polarised structure[144]. For example, in response to pathologic stimuli, signals must travel from dendrites or axons to the nucleus to affect transcription[143, 144]. It has been shown by multiple studies that NLS-targeted proteins are retrogradely transported along the axon by the combination of importin-α and importin-β with the motor protein dynein (microtubule retrograde trafficking) within neurons[150-152]. The

importin-α/importin-β/dynein complex provides injured neurons an effective method of communicating retrograde signals from distal neurites to the nucleus[153, 154].

This extra function of importin proteins may be a likely explanation for the increase seen in importin proteins IMA3 and IPO4 within the cortex of rNLS TDP-43 mice within the current study. It is possible that during neuronal stress and the increased signalling (as shown by IPA analysis), importin proteins are up-regulated to assist in the retrograde transport of signalling proteins from distal parts of the neuron to the nucleus. However, this hypothesis needs to be further tested by investigating the binding and co-localisation of IMA3 and IPO4 with dynein using tissue form rNLS TDP-43 cortex and spinal cord. Overall, both previous and the current study provide evidence that warrants the future investigation of the role of nuclear import proteins (both as part of the nuclear pore complex and retrograde trafficking complex) within ALS pathogenesis.

5.1.3 Interpretation of protein changes in rNLS TDP-43 mice

The protein changes within the cortex of rNLS TDP-43 mice can be construed as early-, mid-, and late stage changes of disease. An important early change was the activation of apoptosis signalling at 2-weeks disease predicted by IPA analysis, which was un-expected as it is earlier than the loss of neurons within rNLS TDP-43 mice[108]. This suggests that neurodegeneration is triggered in the rNLS TDP-43 mice even earlier than previously indicated[108]. EIF2a signalling is another early change within the cortex and is involved in stress granule formation and ER stress. The activation of EIF2 signalling at an early timepoint (2 week) indicates that these processes are also occurring before obvious loss of neurons in the cortex, and may contribute to the initial trigger of neurodegeneration.

The increase in biofunction ‘localization of protein’ combined with the decrease in ‘vesicular transport’ was another interesting early-stage disease change within cortex.

Although 'localization of protein' is not strictly defined within IPA, the biofunction is annotated with proteins such as actinin alpha 4 (ACTN4) which is involved in numerous pathways including actin cytoskeleton signalling (inhibited at the 2-week). Cytoskeletal dysfunction is a proposed pathogenic mechanism of ALS[155]. This suggests there may be a link between actin cytoskeleton dysfunction and vesicular transport in rNLS TDP-43 mice. This was shown in a previous study where a mouse model characterised by defects in vesicular transport, developed ALS disease due to harbouring a mutant dynactin p150(Glued) gene (bidirectional intracellular transport protein)[156]. These early findings, again suggest that molecular dysfunction in multiple pathways is occurring much earlier than neuron loss in rNLS TDP-43 mice.

In addition to early changes, there were two interesting patterns of protein changes identified by singular analysis: the '*change-skip-change*' pattern was shown by proteins that were altered at the 2- and 6-week timepoints but did not show any changes during the 4-week timepoint. This infers that there are proteins that change in early-stage disease, recover at mid-stage disease, and are then altered again during late-stage disease. This may suggest that when pathogenesis is triggered, different processes attempt to alleviate the dysfunctions, however after a certain period a 'pathogenic threshold' is passed and systems can no longer prevent the changes. This finding suggests that the proteins involved in this pattern of change may be important for investigating therapeutic targets for ALS.

The second interesting patter of protein change was the '*skip-change-skip*' that included proteins that only changed at the 4-week timepoint but not at 2- and 6-weeks. The proteins that exhibit this change pattern may be very relevant to TDP-43 pathogenesis as the changes are at the mid-point of disease when neuronal loss has been reported in rNLS mice[108]. However, the reason may potentially be technical rather than biological. For the SWATH MS at the 2- and 6-week timepoint for the cortex samples n=4-5 biological

replicates were analysed. However, for the 4-weeks timepoint n=3 biological samples were analysed. As such the 4-week timepoint may have lower power to detect reliable changes. Therefore, these proteins must be validated with specific antibodies.

While the spinal cord is heavily implicated in ALS pathology, only a small number of protein changes were detected at the early- and late-stage disease in this study. This may be attributed to several reasons. Since proteins from motor neurons within the spinal cord make up a small percentage of the total protein isolated by biochemical methods from total spinal cord, protein changes in low abundance proteins specifically in motor neurons may not have been detected by SWATH MS. In the cortex, almost all neurons express hTDP-43ΔNLS in the rNLS mice, and so any proteomic changes in the cortex may be more readily detected using the methods employed here. The small number of protein changes in the spinal cord at late-stage disease may also be due to the demise of most spinal cord motor neurons at this timepoint. And lastly, SWATH MS was conducted on the soluble fraction of proteins, and therefore the insoluble fraction, which would incorporate proteins interacting with aggregated TDP-43, needs to be investigated for further protein changes within the spinal cord. In addition, the results from the 4-week spinal cord samples, which are pending, will also provide insight into the number of protein changes within the spinal cord of rNLS mice.

ALS is a disease affecting both cortex and spinal cord, and the results showing overlap in some protein changes in the SWATH dataset between cortex and spinal cord indicate that findings in either or both regions may be implicated for disease pathogenesis. However, further detailed analysis of spinal cord, such as specific proteomic profiling of isolated motor neurons rather than total protein lysates, will be an interesting area for future research to understand the biochemical changes in disease.

5.2 Methodological considerations

Proteomic studies characterise the proteome of a variety of complex biological systems. In biomedical research, quantitative proteomics reveal the difference in the protein expression between healthy and disease samples to gain understanding of the disease pathology, progression, and to discover potential biomarkers or targets for treatment. This process begins with selecting the disease model and the type of tissue to be sampled for proteomic analysis.

5.2.1 Sample source

Post-mortem tissue

The sample type used in neurodegenerative proteomics is dependent on the research question and can range from human post-mortem or animal tissue to neuronal cell lines. There are benefits, and caveats associated with each sample source. Using human post-mortem brain and spinal cord tissue has led to successful findings in many previous studies of neurodegenerative disease. Two examples include the identification of 17 altered phosphorylated proteins in the hippocampus of AD patients, and the discovery of cytosolic non-specific dipeptidase 2 (CNDP2) overexpression within the substantia nigra of PD subjects leading to neurodegeneration via the oxidative stress pathway [157, 158].

However, using human post-mortem tissue does have limitations. Foremost, using tissue from end stage of disease does not provide insights into its causes and progression which in turn deters from discovering genuine therapeutic targets. It is difficult to interpret if changes in protein quantities directly contribute to pathogenesis or have changed due to overall system dysfunction when studying tissue extracted from end stage of disease. An example is the role of mitochondrial dysfunction in ALS and other neurodegenerative diseases. While it has been shown that there are changes in mitochondrial structure, quantity,

and localisation within human post-mortem tissue of ALS patients, it is not known if mitochondria contribute to pathogenesis, or inversely, is mitochondrial dysfunction a by-product of stressed cells [159, 160].

Lastly, human post-mortem tissue samples are difficult to acquire without access to a comprehensive biobank and consequently most studies have been conducted on small sample sizes. Two recent ALS proteomic studies used human post-mortem tissues from a cohort of only 4 and 10 patients [95, 99]. Furthermore, the tissue samples need to be accompanied with the complete clinical and demographical data to account for the large variability caused by the genetic and clinical heterogeneity of ALS. Nevertheless, post-mortem tissue is still the best choice for confirming findings from non-human sample sources.

Tissue from animal models

An alternative to human post-mortem tissue is using tissue from animal models of ALS. Performing proteomic experiments using animal tissue permits studying disease onset and therefore probable causes and early intervention targets. Animal models also allow for controlling a variety of genetic and phenotypic variables making interpretations more precise. One example of a successful proteomic study using an animal model to study neurodegeneration was conducted on a mouse model of HD during onset and progression of disease [161]. This study found that HD pathology is highly dynamic as was shown by the non-linear alternations in proteins and pathways during disease progression [161]. Examples within ALS include the discovery of Galectin-3 as a potential biomarker, and the characterisation of ALS spinal cord proteome[100, 101]. While proteomic studies of ALS using animal tissue have been successful, they are mainly limited to superoxide dismutase 1 (SOD1) mouse models, which is a genetic mutation with a frequency of two percent of total ALS cases [100, 101, 162].

Although animal tissue samples have benefits, it is a challenge to compare the findings to the human form of the disease. As such, results from animal models will have to be validated using human tissue.

When performing proteomics using whole or sections of brain and spinal cord tissue, either from post-mortem or animal, it is not possible to obtain proteomic changes that are cell-specific to neurons [163, 164]. The complex network of different neurons and glial cells within the brain make it a challenge to distinguish neuron-specific information, particularly when neuron loss occurs in distinct brain regions within neurodegenerative diseases [165, 166]. In the case of ALS, to detect proteins changes within the main affected cells, the upper and lower motor neurons need to be isolated from whole tissue prior to proteomics. The separation of neurons is challenging because they have filamentous axons that are branched within the central nervous system (CNS) which are surrounded by oligodendrocytes (for myelin sheath formation) and other glial cells (for homeostasis, structural support, immune protection) [166]. Because of this dense network, it is not possible to use standard tissue homogenisation techniques or flow cytometry to isolate intact neurons.

Alternatively, laser-capture microdissection (LCM) can be used to separate a subset of cells or single cells from tissue, which can then be examined for specific proteomic changes via western blotting and mass spectrometry [165]. There have been several successful reports of extracting groups of neurons and single neurons (including motoneurons) from both mouse and human tissue [167-169]. Using LCM and subsequently mass spectrometry within neurodegeneration has been applied to AD, although on a small scale [170, 171]. While LCM provides selectivity and precision, it has limitations that prevent it from being used as an isolation method prior to mass spectrometry in large scale studies. Some of the limitations

include the requirement for fresh frozen tissue for protein studies and the interference of LCM stains with proteomic tools like two-dimensional gel electrophoresis (2DE) [172].

The sample source within the current study was from the cortex and spinal cord of a bigenic mouse model that exhibits ALS pathology and phenotype[108]. This model also permits researchers to turn off the disease causing TDP-43 genes, leading the mice to recover, providing a unique insight into the mechanisms required for the functional recovery from neurodegeneration. The sample preparation consisted of protein extraction via traditional homogenisation which resulted in formation of a soluble and an insoluble fraction. The soluble fraction was analysed by mass spectrometry, which reduced the total of number of proteins and enriched for proteins that have low abundance[163]. The insoluble fraction will be investigated in future studies.

Overall, the sample strategy for the current study was very well aligned with the aim of discovering proteins and pathways that mediate TDP-43 pathology in a very relevant *in vivo* model of disease. Being a discovery pipeline aimed at investigating mechanisms of disease onset, it was not feasible to use human post-mortem tissue as that would only show last stage changes in protein quantities. Furthermore, using LCM to separate singular neurons to then perform mass spectrometry is not logistically compatible with large scale nature of the study. However, both human post-mortem tissue and LCM can be used down-stream in the pipeline for validation and mechanistic studies.

5.2.2 Types of Proteomics

A variety of proteomic tools are available to study the quantitative protein changes of cells and tissue; however, all methods follow the general five stages of protein extraction (sample preparation), protein separation, protein identification, and quantification. Protein extraction protocols are designed to align with the type of analytical technique being used and

type of cells or tissue samples [163]. Nevertheless, most protein extractions involve tissue disruption, enzymatic digestion, and lysis with the use of detergents [173]. The main methods used for protein separation are two-dimensional gel electrophoresis (2-DE) combined with difference in gel electrophoresis (DIGE) or liquid chromatography (LC). Gel based separation allows for consistent quantification, while LC methods are beneficial for the separation of whole proteins, and thus must be chosen according to the specific study [174-177].

Mass spectrometry combines protein identification with quantification by separating charged particles based on mass (ionisation) and then using a mass analyser to quantify. The main two types of mass spectrometry instruments used are matrix assisted laser desorption ionisation-time of flight (MALDI-TOF, where MALDI is used for ionisation and TOF is used for mass analysis) and electro spray ionisation (ESI) with tandem analyser (multistage ionisation and mass analyser combined) [163, 178]. First experimental mass values are generated by the mass analyser and are subsequently paired to theoretical mass values within databases generated by genome sequences to identify proteins [163].

Mass spectrometry techniques can be broadly placed into two types based on the identification strategy being applied. The first method is data dependent acquisition (DDA) which first surveys the sample and records a preselected set of ion values (at a given time) that are characteristic of peptides and then uses these spectra to identify proteins via a second stage of mass selection (MS/MS) [179, 180]. DDA is a powerful technique for identification of proteins, however it is biased towards proteins with higher abundance which limits its use for quantitative proteomics [180]. The second method is data independent acquisition (DIA) which scans samples and records all ion values representative of peptides (during multiple cycles) and then performs a second stage mass spectrometry for identification [180, 181]. While DIA is

an unbiased approach, identification of proteins is difficult because the ability to match fragments to intact peptides is lost during the multiple cycles of recording the spectra [180, 181].

The proteomic technique applied within the current study utilises sequential window acquisition of all theoretical mass spectra (SWATH-MS). SWATH-MS combines both DDA and DIA for a technique that can both identify and quantify proteins successfully [182]. First DDA is used to develop a spectral library for identification and next DIA is used to quantify proteins from complex biological samples [180, 182]. SWATH-MS has emerged as the preferred proteomic technique with over 144 publications over four years between 2012 and 2016 [180]. These studies show that SWATH-MS is a powerful method of quantifying large numbers of proteins from very complex biological samples [183-185]. Moreover, SWATH is an emerging method within neuroproteomics making it a suitable method to study AL [186]. Despite the benefits if SWATH MS, the results require validated, which is discussed in section 5.2.4.

5.2.3 Bioinformatic analyses

Proteomic data need to be analysed and interpreted in relation to the research question and known literature to place them within biological context [187, 188]. In early studies, this interpretation of protein lists was based on knowledge attained by consuming a large amount of relevant literature (i.e. expert review) [187, 189]. However, the increasing generation of large and complex proteomic datasets has led to the development of many computational tools and databases that have automated the functional analysis of proteomics data [190-192]. The first layer involves *data processing* which is experiment-specific and results in an ordered or unordered list of proteins. The second stage consists of functional analysis which can be carried out via various methods and tools. In the current study it was shown that while

singular analyses lead to descriptive interpretations, more comprehensive analysis methods lead to more mechanistic interpretations.

The most basic singular analysis approach is searching aggregated databases such as Uniprot to determine the functions and cellular compartments of individual proteins [109, 193]. Singular analysis combined with relevant literature was a valuable first stage of narrowing down candidate proteins of interest from the large dataset of differentiated proteins. However, singular analysis lacks biological contextualisation when applied alone, and this can prevent the elucidation of important proteomic relationships. However, singular analysis can be combined with comprehensive methods for more uniform examination of experimental observations within a biological context. Comprehensive methods applied within the current study were *enrichment analysis* and *protein interaction analysis*.

Enrichment analysis tests proteomic data to determine which functional annotations are most enriched within protein sets by comparing the frequency of functional annotations, such as pathways and cellular processes within an experimental protein list against the annotation frequency of the reference list within a curated database [190]. An annotation's degree of enrichment can be statistically tested using a Fisher's exact test or a hypergeometric distribution with the addition of an appropriate multiple testing correction. Annotated term enrichment results in a complete summary of the significant functional characteristics of a protein list, however it can be an oversimplification of complex realities and can lead to misclassification if curations are incorrect or misleading.

Singular and enrichment analyses, while very informative, are only descriptive. The interpretation of proteomics data by using protein interaction analysis methods can detect the direct and indirect relationship of proteins for a more mechanistic interpretation. The most common protein interaction analysis techniques map protein lists on a pathway and subsequently highlights the direction changes in individual proteins of significance [187, 189].

Despite the drastic increase in the number of analysis tools, there is no platform that provides practical information for the selection of approaches to interpret proteomics data [187, 192, 194]. The available proteomics reviews provide scattered information on available tools [194-197], while others emphasise experimental challenges and broad issues in proteomic bioinformatics [190-192]. The other substantial portion of available literature focuses mainly on transcriptomics [198, 199] for which an assortment of interpretation tools has been established and these are now also used for proteomic analysis [187]. For this reason, it is important to take note of the challenges of analysing proteome data in comparison to other "omics". The proteome has a larger dynamic range, that is more than eight orders of magnitude when compared to the genome [200, 201]. The proteome is not static and consists of processes (post-translational modifications, context-specific protein interactions, and protein networks) that immensely diversify the possible structures of each translational product at any point in time [202].

The proteomic data analysis approach employed within the current study applied singular, enrichment, and protein interaction analysis methods using IPA. This strategy narrowed down both singular protein candidates as well as protein pathways (and the

significant proteins within those pathways) pertinent to ALS. However, care was taken when interpreting functional analysis results as curations are heavily reliant on non-relevant models of disease. For example, the current GO database for ALS is heavily reliant on studies of disease-linked mutant superoxide dismutase (SOD1), which is involved in only ~2-3% of disease, and largely ignores studies focused on the more disease-relevant pathological TDP-43 protein. Overall, the functional analysis within the current study systematically covered descriptive and mechanistic interpretation of protein lists for a thorough global analysis.

5.2.4 Validation studies

The analytical limitations of many proteomic workflows result in variable, incomplete, and biased reporting of the proteome because they consist of separation and identification strategies that have unavoidable intrinsic selectivity for certain protein groups based on characteristics such as size, abundance, and other physicochemical features [203-205]. In addition, in proteomics studies where a small fraction of the proteome is being sampled, biologically meaningful proteins with minor changes remain undetected which leads to biased downstream interpretation [206, 207] Therefore, due to sample complexity and technical limitations, it is pertinent to validate proteomics data using alternative methods of protein quantification. Most common validation methods include quantitative western blotting and ELISA assays.

Within the current study, western blotting using specific antibodies was used to validate protein changes shown by SWATH MS. This revealed that while SWATH MS is successful at identifying and quantifying large numbers of proteins from a complex

sample, the results do need to be validated. However, validation studies using specific antibodies, such as western blotting, are limited to the quality of the antibody. In this study, only 4 antibodies used resulted in visible bands. To overcome this limitation the options are to optimise the western blot protocol to apply different blocking buffers and transfer methods, or search for a more successful antibody within literature.

5.3 Future research

In addition to the already mentioned further investigation of findings, the following future research will be performed. Firstly, to eliminate antibody bias both COQ9 and IMA3 will be validated using different antibodies. Secondly, tissue staining protocol will optimized for each antibody to successfully visualise candidate proteins within rNLS TDP-43 tissue. Once staining is optimised, co-staining of candidate protein with (i) TDP-43 for co-localisation and (ii) motor neuron marker to determine if changes are seen specifically within motor neurons. Thirdly, to determine if protein changes are reflected in RNA, quantitative Real-Time PCR (q-RT PCR) will be used to analyse the RNA from the cortex and spinal cord of rNLS TDP-43 mice. Subsequently protein candidates will be investigated mechanistically to determine which of the protein targets are involved in TDP-43 pathogenesis and neurodegeneration.

Mechanistic studies will involve the use of motor neuron-like NSC-34 cells and primary mouse cortical neurons. The cells will be used either un-transfected or transfected with plasmids for expression of wildtype or cytoplasmically-targeted inclusion forming TDP-43 along with the top candidate protein's plasmids for target over-expression, or siRNA for target knockdown (including experiments for modulation of COQ9 and IMA3 levels). Cells will then be analysed by immunofluorescence and immunoblotting for levels and localization of each target, and for: (i) sub-cellular location of TDP-43, (ii) levels of total, nuclear and cytoplasmic TDP-43, (iii) levels of phosphorylated TDP-43 and percentage of cells bearing TDP-43 inclusions, (iv) levels of soluble versus insoluble TDP-43, (v) markers of relevant biological function of each

target, such as mitochondrial integrity and nucleocytoplasmic transport, and (vi) markers of cell death, including caspase activation and nuclear condensation.

To investigate the proteins and pathways involved in the functional recovery of rNLS TDP-43 mice, the mice will be taken off the DOX diet for 6 weeks to develop disease as shown in this study, and will be placed back on DOX to recover[108]. SWATH MS proteomics will be conducted on 1- and 2-weeks recovery timepoints. The results will then undergo a similar analysis and validation as reported in this study.

IPA analysis revealed mainly motor dysfunction related biological functions, however to control for the protein changes during normal neuronal development in mice, a cohort will be aged and then taken off the DOX diet to develop disease at an older age. Again, SWATH MS proteomics will be performed to identify and quantify protein changes. These results will then be compared to the result within the current study.

Overall, these studies will confirm and extend the findings of the current study, with the goal of identifying upstream pathogenic mechanisms that could be targeted for future therapy for people living with ALS.

5.4 Conclusions

This study, for the first time in world, identified the proteins and pathways which changed during disease course within rNLS TDP-43 mouse model of ALS. Two key proteins, COQ9 and IMA3, which are involved in known mechanisms of ALS pathogenesis were validated using immunoblotting. In addition, the canonical pathways, upstream regulators and biological function involved in rNLS TDP-43 pathology were comprehensively identified. This study provides important insights into TDP-43-mediated ALS neurodegeneration which warrants further investigation.

Appendix 1.

Singular analysis

Appendix Table 1.1 List of protein changes by SWATH MS.

Protein was extracted from the hippocampus, cortex, and lumbar spinal cord of rNLS mice at 2, 4, and 6-week timepoints. SWATH MS was conducted (n=3-5 mice) to identify and quantify proteins that changed in TDP-43 mice compared to control non-bigenic mice. Proteins that showed a fold change of ≥1.5-fold which were determined to be significant (p-value <0.05 or q-value <0.1) were selected for singular analysis: a total of 190 proteins across hippocampus, cortex, and spinal cord were either increased (red) or deceased (green) compared to litter-, sex- and time-matched non-bigenic controls. A UniProt database search was conducted for each individual protein to determine the function(s) and subcellular location(s), and results are summarised. Data for spinal cord at 4 weeks disease is currently being generated. NC: not changed, ND: not detected.

Protein ID (MOUSE)	Protein name	Fold change (disease/control)								Subcellular location	Uniprot functions summary	Uniprot code
		Hippocampus			Cortex			Spinal cord				
		2 weeks	4 weeks	6 weeks	2 weeks	4 weeks	6 weeks	2 weeks	6 weeks			
1433F	14-3-3 protein eta	NC	NC	NC	NC	0.668	NC	NC	NC	Cytoplasm	Adapter protein implicated in the regulation of a large spectrum of both general and specialized signalling pathways.	P68510
3HIDH	3-hydroxyisobutyrate dehydrogenase	NC	NC	NC	NC	1.604	NC	NC	NC	Mitochondrion	Enzyme. Involved in the pathway L-valine degradation,	Q99L13

											which is part of Amino-acid degradation.	
ACADS	Short-chain specific acyl-CoA dehydrogenase	ND	ND	ND	NC	NC	1.531	ND	NC	Mitochondrion matrix	Enzyme. Involved in the pathway mitochondrial fatty acid beta-oxidation, which is part of Lipid metabolism.	Q07417
ACDSB	Short/branched chain specific acyl-CoA dehydrogenase	NC	NC	NC	NC	NC	1.597	ND	NC	Mitochondrion matrix	Enzyme. Involved in the pathway mitochondrial fatty acid beta-oxidation, which is part of Lipid metabolism.	Q9DBL1
ACTZ	Alpha-centractin	NC	NC	NC	1.512	NC	NC	NC	NC	Centrosome	Alpha-centractin. microtubule based vesicle motility. Associated with the centrosome.	P61164
AL9A1	4-trimethylaminobutyraldehyde dehydrogenase	NC	NC	NC	NC	NC	1.574	NC	NC	Cytoplasm	Enzyme. Involved in the pathway carnitine biosynthesis, which is part of Amine and polyamine biosynthesis.	Q9JLJ2
AMPN	Aminopeptidase N	ND	ND	NC	NC	0.492	NC	ND	NC	Membrane, Single-pass type II membrane protein	Enzyme. May be involved in the metabolism of regulatory peptides of neuropeptides.	P97449
ANR63	Ankyrin repeat domain-containing protein 63	ND	ND	ND	NC	NC	0.557	ND	ND	Unknown	Function unknown.	A2ARS0
APMAP	Adipocyte plasma membrane-associated protein	NC	NC	NC	0.655	NC	NC	ND	NC	Membrane; Single-pass type II membrane protein	Adipocyte plasma membrane-associated protein. May play a role in adipocyte differentiation.	Q9D7N9
APOD	Apolipoprotein D	NC	NC	NC	NC	2.028	2.246	ND	NC	Secreted	Able to transport a variety of ligands in a number of different contexts.	P51910

ARHL2	Poly(ADP-ribose) glycohydrolase ARH3	ND	ND	ND	NC	1.514	NC	ND	ND	Nucleus, cytoplasm	Poly(ADP-ribose) id synthesized after DNA damage and is rapidly degraded by poly(ADP-ribose) glycohydrolase. Poly(ADP-ribose) metabolism may be required for maintenance of the normal function of neuronal cells.	Q8CG72
ARMC6	Armadillo repeat-containing protein 6	NC	NC	NC	NC	NC	1.555	ND	NC	Unknown	Hematopoietic progenitor cell differentiation.	Q8BNU0
ARP19	cAMP-regulated phosphoprotein 19	ND	ND	ND	NC	NC	0.634	ND	NC	Cytoplasm	Protein phosphatase inhibitor that specifically inhibits protein phosphatase 2A (PP2A) during mitosis.	P56212
ARPC5	Actin-related protein 2/3 complex subunit 5	NC	NC	0.592	NC	NC	NC	ND	ND	Cytoskeleton	Involved in regulation of actin polymerization.	Q9CPW4
ARSA	Arylsulfatase A (ASA)	NC	NC	NC	NC	NC	1.832	ND	NC	Lysosome	Enzyme. Hydrolyzes cerebroside sulphate.	P50428
ASSY	Argininosuccinate synthase	NC	NC	NC	1.519	2.109	1.988	NC	NC	Myelin sheath, extracellular exosome, mitochondrion	Enzyme. Involved in step 2 of the subpathway that synthesizes L-arginine.	P16460
AT1A1	Sodium/potassium-transporting ATPase subunit alpha-1	NC	NC	NC	NC	NC	0.665	NC	NC	Cell membrane	Enzyme. Hydrolysis of ATP coupled with the exchange of sodium and potassium ions across the plasma membrane.	Q8VDN2
ATIF1	ATPase inhibitor	NC	NC	NC	ND	ND	ND	NC	0.568	Mitochondrion	Limiting ATP depletion when the mitochondrial membrane potential falls below a threshold.	O35143

BRK1	Protein BRICK1	NC	NC	NC	NC	0.576	NC	NC	NC	Cytoskeleton	Involved in regulation of actin and microtubule organization.	Q91VR8
C1QA	Complement C1q subcomponent subunit A	ND	ND	ND	NC	NC	3.277	ND	ND	Secreted	Complement activation pathway.	P98086
C1QB	Complement C1q subcomponent subunit B	NC	NC	NC	NC	NC	1.762	ND	ND	Secreted	Complement activation pathway.	P14106
C1QBP	Complement component 1 Q subcomponent-binding protein	NC	NC	NC	NC	1.677	1.782	NC	NC	Mitochondrion matrix, several subcellular locations	Multifunctional and multicompartmental protein involved in few processes.	O35658
CA2D1	Voltage-dependent calcium channel subunit alpha-2/delta-1	NC	NC	NC	NC	0.609	NC	ND	ND	Membrane	Activation/inactivation kinetics of the calcium channel.	O08532
CACP	Carnitine O-acetyltransferase	NC	NC	NC	NC	NC	1.797	ND	ND	ER, Peroxisome, Mitochondrion membrane	Enzyme. Specific for short chain fatty acids. Affect the flux through the pyruvate dehydrogenase complex.	P47934
CADM2	Cell adhesion molecule 2	NC	NC	0.597	NC	NC	NC	NC	NC	Cell membrane, synapse, axon	Important for synapse organization, providing regulated trans-synaptic adhesion.	Q8BLQ9
CANB1	Calcineurin subunit B type 1	NC	NC	NC	NC	NC	0.646	NC	NC	Cytosol, cell membrane	Regulatory subunit of calcineurin.	Q63810
CATD	Cathepsin D	NC	NC	NC	NC	1.613	1.548	NC	NC	Lysosome	Acid protease active in intracellular protein breakdown.	P18242

CCD53	WASH complex subunit 3	ND	ND	ND	NC	3.797	2.142	ND	ND	Early endosome	Activity in recruiting and activating the Arp2/3 complex to induce actin polymerization. Regulation of the fission of tubules that serve as transport intermediates during endosome sorting.	Q9CR27
CCG8	Voltage-dependent calcium channel gamma-8 subunit	NC	NC	0.609	NC	NC	NC	ND	ND	Membrane, postsynaptic cell membrane	Regulates the trafficking and gating properties of AMPA-selective glutamate receptors.	Q8VHW2
CD9	CD9 antigen	NC	NC	NC	NC	1.625	1.563	ND	ND	Membrane, exosome	Involved in platelet activation and aggregation.	P40240
CDS1	Phosphatidate cytidylyltransferase 1	NC	ND	ND	NC	NC	0.533	ND	ND	Endoplasmic reticulum membrane	Enzyme. Provides CDP-diacylglycerol, an important precursor for the synthesis of phosphatidylinositol. May play an important role in the signal transduction mechanism of retina and neural cells.	P98191
CE051	UPF0600 protein C5orf51 homolog	NC	NC	NC	NC	NC	3.619	ND	ND	Unknown	Function unknown.	Q8BR90
CHCH2	Coiled-coil-helix-coiled-coil-helix domain-containing protein 2	NC	NC	NC	0.501	0.631	0.637	ND	ND	Nucleus, Mitochondrion	Transcription factor- binds to oxygen responsive element of COX4I2 and activates its transcription under hypoxia conditions.	Q9D1L0
CHM4B	Charged multivesicular body protein 4b	NC	NC	NC	NC	NC	NC	NC	0.605	Cytosol, Late endosome membrane	Core component of the endosomal sorting.	Q9D8B3

CK5P3	CDK5 regulatory subunit-associated protein 3	NC	NC	NC	NC	1.811	NC	ND	ND	Nucleus, Centrosome	Tumour suppressor initially identified as a CDK5R1 interactor controlling cell proliferation.	Q99LM2
CMPK2	UMP-CMP kinase 2, mitochondrial	NC	NC	NC	NC	NC	1.798	ND	ND	Mitochondrion	Enzyme. May participate in dUTP and dCTP synthesis in mitochondria.	Q3U5Q7
CNKR2	Connector enhancer of kinase suppressor of ras 2	NC	NC	NC	0.554	0.55	0.668	ND	ND	Cytoplasm, Membrane	May function as an adapter protein or regulator of Ras signalling pathways.	Q80YA9
COMT	Catechol O-methyltransferase	NC	NC	NC	NC	1.573	NC	ND	ND	Cytoplasm (Soluble), Cell membrane (membrane-bound)	Enzyme. Catalyses the O-methylation, and thereby the inactivation, of catecholamine neurotransmitters and catechol hormones. Also shortens the biological half-lives of certain neuroactive drugs, like L-DOPA, alpha-methyl DOPA and isoproterenol.	O88587
COPD	Coatomer subunit delta	ND	ND	ND	1.55	NC	NC	NC	NC	Cytoplasm, Golgi	Biosynthetic protein transport from the ER.	Q5XJY5
COQ9	Ubiquinone biosynthesis protein COQ9	NC	NC	NC	NC	NC	NC	4.302	NC	Mitochondrion	An essential lipid-soluble electron transporter for aerobic cellular respiration.	Q8K1Z0
COTL1	Coactosin-like protein	NC	NC	NC	NC	NC	1.58	NC	NC	Cytoskeleton	Binds to F-actin in a calcium-independent manner. Has no direct effect on actin depolymerisation.	Q9CQI6
CP062	UPF0505 protein C16orf62 homolog	ND	ND	ND	NC	NC	1.785	ND	ND	Membrane	ATP7A trafficking between the trans-Golgi network and vesicles in the cell periphery.	Q8BWQ6

CPLX3	Complexin-3	ND	ND	ND	NC	NC	1.785	ND	ND	Membrane, synapse	Positively regulates a late step in synaptic vesicle exocytosis.	Q8R1B5
CPNS1	Calpain small subunit 1	NC	NC	1.626	NC	NC	NC	NC	NC	Cytoplasm, Cell membrane	Regulatory subunit of thiol-protease which catalyses limited proteolysis of substrates involved in cytoskeletal remodelling and signal transduction.	O88456
DCLK1	Serine/threonine-protein kinase DCLK1	NC	NC	0.64	0.669	0.614	0.64	NC	NC	Postsynaptic density	Enzyme. May be involved in a calcium-signalling pathway controlling neuronal migration in the developing brain	Q9JLM8
DCTN6	Dynactin subunit 6	NC	NC	NC	NC	4.05	NC	ND	NC	Cytoskeleton	May be involved in Dynein binding.	Q9WUB4
DENR	Density-regulated protein (DRP)	NC	NC	NC	NC	NC	NC	NC	0.66	Translation initiation complex	May be involved in the translation of target mRNAs by scanning and recognition of the initiation codon.	Q9CQJ6
DGKB	Diacylglycerol kinase beta	NC	NC	NC	0.519	0.524	0.568	ND	ND	Cytoplasm	Enzyme. Exhibits high phosphorylation activity for long-chain diacylglycerols.	Q6NS52
DGKZ	Diacylglycerol kinase zeta	NC	NC	NC	NC	0.598	0.585	ND	ND	Cytoplasm, Nucleus	Enzyme. Phosphorylation of long chain diacylglycerols. Regulates RASGRP1 activity.	Q80UP3
DHB11	Estradiol 17-beta-dehydrogenase 11	NC	1.586	NC	NC	NC	1.59	NC	NC	Secreted, Cytoplasm	Enzyme. May participate in androgen metabolism during steroidogenesis.	Q9EQ06
DHYS	Deoxyhypusine synthase (DHS)	ND	ND	ND	2.826	NC	1.873	ND	ND	Cytoplasm	Enzyme. Catalyses the NAD-dependent oxidative cleavage of spermidine to form the intermediate deoxyhypusine residue.	Q3TXU5

DIRA2	GTP-binding protein Di-Ras2	NC	NC	NC	NC	NC	0.65	ND	NC	Cell membrane	Displays low GTPase activity and exists predominantly in the GTP-bound form.	Q5PR73
DLG3	Synapse-associated protein 102	NC	NC	NC	0.634	NC	NC	ND	ND	Neuronal cell body, postsynaptic density	Disks large homolog 3. Required for learning most likely through its role in synaptic plasticity following NMDA receptor signalling.	P70175
DNJB5	DnaJ homolog subfamily B member 5 (Heat shock protein Hsp40-3)	ND	ND	ND	2.918	NC	NC	ND	ND	Cytosol, Nucleus	Chaperone binding.	O89114
ECHA	Trifunctional enzyme subunit alpha	NC	NC	1.527	NC	NC	NC	NC	NC	Mitochondrion matrix	Bifunctional subunit. Involved in the pathway fatty acid beta-oxidation.	Q8BMS1
EMB	Embigin	ND	ND	ND	NC	NC	NC		0.635	Cell membrane, synapse	Plays a role in the outgrowth of motoneurons and in the formation of neuromuscular junctions.	P21995
ERF3A	Eukaryotic peptide chain release factor GTP-binding subunit ERF3A	NC	NC	NC	NC	NC	1.852	ND	ND	Cytosol, translation release factor complex	Involved in translation termination in response to the termination codons UAA, UAG and UGA.	Q8R050
ERGI1	Endoplasmic reticulum-Golgi intermediate compartment protein 1	NC	NC	NC	2.056	NC	NC	ND	ND	Endoplasmic reticulum, Golgi intermediate compartment membrane	Possible role in transport between endoplasmic reticulum and Golgi.	Q9DC16

FAK1	Focal adhesion kinase 1 (FADK 1)	ND	ND	ND	NC	0.546	NC	ND	ND	Cell junction, focal adhesion	Enzyme. Regulates axon growth and neuronal cell migration, axon branching and synapse formation; required for normal development of the nervous system.	P34152
FPPS	Farnesyl pyrophosphate synthase (FPP synthase)	NC	NC	NC	NC	NC	0.485	NC	0.637	Cytoplasm	Enzyme. Key enzyme in isoprenoid biosynthesis	Q920E5
FRIH	Ferritin heavy chain (Ferritin H subunit)	ND	ND	ND	NC	NC	1.532	NC	NC	Autolysosome	Stores iron in a soluble, non-toxic, readily available form.	P09528
FRS1L	DOMON domain-containing protein FRRS1L	NC	NC	NC	NC	NC	0.647	ND	ND	Cell membrane, synapse	. Important modulator of glutamate signalling pathway.	B1AXV0
FUCM	Fucose mutarotase	ND	ND	ND	NC	1.626	NC	ND	ND	Unknown	Enzyme. Interconversion between alpha- and beta-L-fucoses.	Q8R2K1
FUND1	FUN14 domain-containing protein 1	ND	ND	ND	NC	1.546	NC	ND	ND	Mitochondrion outer membrane	Acts as an activator of hypoxia-induced mitophagy, an important mechanism for mitochondrial quality control.	Q9DB70
FUND2	FUN14 domain-containing protein 2	NC	NC	NC	NC	1.508	NC	NC	NC	Integral component of mitochondrial outer membrane	Mitophagy.	Q9D6K8
GFAP	Glial fibrillary acidic protein	NC	NC	3.776	1.519	2.091	3.379	NC	NC	Cytoplasm	GFAP, a class-III intermediate filament, is a cell-specific marker that, during the development of the central nervous system, distinguishes astrocytes from other glial cells.	P03995

GNAI1	Guanine nucleotide-binding protein G	NC	NC	0.64	NC	NC	NC	NC	NC	Nucleus, Cytoplasm, Cell membrane	Function as transducers downstream of G protein-coupled receptors (GPCRs) in numerous signalling cascades.	B2RSH2
GOT1B	Vesicle transport protein GOT1B (Golgi transport 1 homolog B)	ND	ND	ND	NC	2.529	2.97	ND	ND	Golgi apparatus membrane	May be involved in fusion of ER-derived transport vesicles with the Golgi complex.	Q9CR60
GPM6A	Neuronal membrane glycoprotein M6-a (M6a)	NC	NC	NC	NC	NC	0.646	ND	ND	Cell membrane, Cell projection (axon, dendritic spine, filopodium)	Involved in neuronal differentiation, including differentiation and migration of neuronal stem cells.	P35802
GPM6B	Neuronal membrane glycoprotein M6-b (M6b)	NC	NC	NC	NC	NC	0.627	NC	NC	Membrane, Cell membrane	May be involved in neural development.	P35803
GRIA3	Glutamate receptor 3	NC	NC	NC	NC	NC	0.652	ND	ND	Postsynaptic cell membrane	Receptor for glutamate that functions as ligand-gated ion channel in the central nervous system.	Q9Z2W9
GRN	Granulins	NC	NC	NC	NC	1.698	1.691	ND	ND	Secreted	Granulins have possible cytokine-like activity.	P28798
GSTO1	Glutathione S-transferase omega-1	NC	NC	NC	NC	1.974	1.937	ND	ND	Cytosol	Enzyme. Exhibits glutathione-dependent thiol transferase and dehydroascorbate reductase activities.	O09131
HCD2	3-hydroxyacyl-CoA dehydrogenase type-2	NC	1.582	NC	NC	NC	NC	NC	NC	Mitochondrion	Enzyme. Functions in mitochondrial tRNA maturation.	O08756
HECW2	E3 ubiquitin-protein ligase	ND	ND	ND	NC	NC	0.464	ND	ND	Cytoplasm	Enzyme. E3 ubiquitin-protein ligase that mediates ubiquitination of TP73.	Q6I6G8

HMGA1	High mobility group protein	NC	NC	NC	NC	NC	2.203	ND	ND	Nucleus, Chromosome	Binds preferentially to the minor groove of A+T rich regions in double-stranded DNA.	P17095
HS105	Heat shock protein 105 kDa (42 degrees C-HSP) (Heat shock 110 kDa protein)	NC	NC	0.627	NC	NC	0.634	NC	NC	Cytoplasm, Nucleus	Prevents the aggregation of denatured proteins in cells under severe stress.	Q61699
HYEP	Epoxide hydrolase 1	NC	NC	NC	NC	NC	1.676	NC	NC	Microsome membrane	Enzyme. Catalyses the hydrolysis of arene and aliphatic epoxides to less reactive and more water soluble dihydrodiols by the trans addition of water.	Q9D379
ICAM5	Intercellular adhesion molecule 5	NC	NC	0.637	NC	NC	NC	ND	ND	Membrane	Intercellular adhesion molecule 5	Q60625
IFIT3	Interferon-induced protein with tetratricopeptide repeats 3 (IFIT-3)	ND	ND	NC	NC	NC	3.349	ND	ND	Cytoplasm, Mitochondrion	Interferon-induced protein with tetratricopeptide repeats 3	Q64345
IMA3	Importin subunit alpha-3 (Importin alpha Q1)	NC	NC	NC	NC	1.729	1.743	ND	ND	Cytoplasm, Nucleus	Functions in nuclear protein import as an adapter protein.	O35343
IP3KA	Inositol-trisphosphate 3-kinase A	NC	NC	0.455	NC	0.616	0.576	ND	ND	Dendritic spine	Enzyme. ATP + 1D-myo-inositol 1,4,5-trisphosphate = ADP + 1D-myo-inositol 1,3,4,5-tetrakisphosphate.	Q8R071
IPO4	Importin-4 (Imp4) (Importin-4a)	NC	NC	NC	NC	1.914	1.605	ND	ND	Cytoplasm, Nucleus	Nuclear protein import as nuclear transport receptor.	Q8VI75
IRGM1	Immunity-related GTPase family M protein 1	NC	NC	NC	NC	NC	1.555	ND	ND	Golgi apparatus membrane, Cell membrane	Regulation of autophagy.	Q60766

ISCA2	Iron-sulfur cluster assembly 2 homolog	NC	NC	NC	NC	1.534	NC	ND	ND	Mitochondrion	Involved in the maturation of mitochondrial 4Fe-4S proteins functioning late in the iron-sulphur cluster assembly pathway.	Q9DCB8
KCC2A	Calcium/calmodulin-dependent protein kinase type II subunit alpha	NC	NC	NC	NC	NC	0.636	NC	NC	Presynaptic cell membrane	Enzyme. May function in long-term potentiation and neurotransmitter release.	P11798
KCC4	Calcium/calmodulin-dependent protein kinase type IV	NC	NC	NC	NC	0.601	0.494	ND	ND	Cytoplasm, Nucleus	Operates in the calcium-triggered CaMKK-CaMK4 signalling cascade and regulates, mainly by phosphorylation, the activity of several transcription activators.	P08414
KCD16	BTB/POZ domain-containing protein KCTD16	ND	ND	ND	NC	NC	0.643	ND	ND	Presynaptic cell membrane	Auxiliary subunit of GABA-B receptors that determine the pharmacology and kinetics of the receptor response.	Q5DTY9
KCMA1	Calcium-activated potassium channel subunit alpha-1	ND	ND	ND	NC	0.659	0.6	ND	ND	Cell membrane	Potassium channel activated by both membrane depolarization or increase in cytosolic Ca2+.	Q08460
KCNA1	Potassium voltage-gated channel subfamily A member 1 (MBK1)	ND	ND	ND	NC	0.64	0.533	ND	ND	Cell membrane, axon, dendrite, synapse	Contributes to the regulation of the membrane potential and nerve signalling, and prevents neuronal hyperexcitability.	P16388
KKCC2	Calcium/calmodulin-dependent protein kinase kinase 2 (CaM-KK 2)	ND	ND	ND	0.507	NC	0.625	ND	ND	Nucleus, Cytoplasm, Cell projection	May play a role in neurite growth. Isoform 2 may promote neurite elongation, while isoform 1 may promoter neurite branching. May be involved in hippocampal activation of CREB1.	Q8C078

KLC1	Kinesin light chain 1 (KLC 1)	NC	NC	NC	0.643	NC	NC	NC	NC	Cell projection	A microtubule-associated force-producing protein that may play a role in organelle transport.	O88447
KPCA	Protein kinase C alpha type (PKC-A)	NC	NC	NC	NC	NC	0.656	ND	ND	Cytoplasm, cell membrane, mitochondrion, nucleus	Enzyme. Depending on the cell type, is involved in many cell functions.	P20444
KPCB	Protein kinase C beta type (PKC-B)	NC	NC	0.546	0.64	0.544	0.531	NC	NC	Cytoplasm, cell membrane, nucleus	Enzyme. Protein kinase C. Depending on the cell type, is involved in many cell functions.	P68404
KS6C1	Ribosomal protein S6 kinase delta-1	ND	ND	ND	NC	1.713		ND	ND	Cytoplasm, Membrane	Enzyme. Maybe involved in transmitting sphingosine-1 phosphate (SPP)-mediated signalling into the cell.	Q8BLK9
LAMP2	Lysosome-associated membrane glycoprotein 2 (LAMP-2)	ND	ND	ND	NC	NC	1.903	ND	ND	Cell membrane and organelle membranes	Lysosome-associated membrane glycoprotein 2	P17047
LEG1	Galectin-1 (Gal-1)	NC	NC	NC	NC	NC	1.935	NC	NC	Secreted, extracellular matrix	Plays a role in regulating apoptosis, cell proliferation and cell differentiation.	P16045
LRC40	Leucine-rich repeat-containing protein 40	ND	ND	ND	2.319	NC	NC	ND	ND	Membrane	Leucine-rich repeat-containing protein 40	Q9CRC8
LYAG	Lysosomal alpha-glucosidase	NC	NC	NC	1.686	NC	NC	ND	ND	Lysosome	Enzyme. Essential for the degradation of glycogen to glucose in lysosomes.	P70699
MA6D1	MAP6 domain-containing protein 1	NC	NC	NC	NC	NC	1.506	NC	NC	Golgi apparatus, cytoskeleton	May have microtubule-stabilizing activity.	Q14BB9

MAAI	Maleylacetoacetate isomerase (MAAI)	NC	NC	NC	NC	1.524	NC	NC	NC	Cytoplasm	Enzyme. This protein is involved in step 5 of the subpathway that synthesizes acetoacetate and fumarate from L-phenylalanine.	Q9WVL0
MACD2	O-acetyl-ADP-ribose deacetylase MACROD2	ND	ND	ND	NC	NC	0.544	ND	ND	Nucleus	Enzyme. Removes ADP-ribose from glutamate residues in proteins bearing a single ADP-ribose moiety.	Q3UYG8
MBB1A	Myb-binding protein 1A	ND	ND	NC	1.706	NC	1.498	ND	ND	Nucleolus, Cytoplasm	May activate or repress transcription via interactions with sequence specific DNA-binding proteins.	Q7TPV4
MCCB	Methylcrotonoyl-CoA carboxylase beta chain	ND	ND	ND	NC	NC	1.642	ND	ND	Mitochondrion matrix	Enzyme. Methylcrotonoyl-CoA carboxylase beta chain.	Q3ULD5
MIC27	MICOS complex subunit Mic27 (Apolipoprotein O-like)	NC	NC	NC	NC	NC	0.602	ND	ND	Mitochondrion inner membrane	A large protein complex of the mitochondrial inner membrane that plays crucial roles in the maintenance of crista junctions, inner membrane architecture, and formation of contact sites to the outer membrane.	Q78IK4
MOES	Moesin (Membrane-organizing extension spike protein)	NC	NC	NC	NC	NC	2.028	NC	NC	Cell membrane, cytoskeleton	Probably involved in connections of major cytoskeletal structures to the plasma membrane.	P26041
MP2K1	Dual specificity mitogen-activated protein kinase kinase 1 (MAP kinase kinase 1)	NC	NC	0.547	NC	NC	NC	NC	NC	Centrosome, spindle pole body	Enzyme. Dual specificity mitogen-activated protein kinase kinase. Signal transduction and transcriptional regulation.	P31938
MYEF2	Myelin expression factor 2 (MEF-2)	NC	NC	NC	NC	NC	NC	2.415	NC	Nucleus	Transcriptional repressor of the myelin basic protein gene (MBP).	Q8C854

MYG	Myoglobin	ND	ND	ND	ND	ND	ND	NC	2.139	Extracellular exosome	Reserve supply of oxygen and facilitates the movement of oxygen within muscles.	P04247
NEUG	Neurogranin (Ng)	NC	NC	NC	NC	0.661	0.604	ND	ND	Cytoplasm, synapse, dendritic spine	Regulates the affinity of calmodulin for calcium. Involved in synaptic plasticity and spatial learning.	P60761
NFH	Neurofilament heavy polypeptide (NF-H)	NC	NC	NC	NC	NC	NC	NC	0.576	Cytoplasm	Important function in mature axons that is not subserved by the two smaller NF proteins.	P19246
NFL	Neurofilament light polypeptide (NF-L)	NC	NC	NC	NC	NC	0.635	NC	NC	Axon, axon cytoplasm	Neurofilament light polypeptide	P08551
NFM	Neurofilament medium polypeptide (NF-M)	NC	NC	NC	NC	NC	0.634	NC	0.664	Axon, myelin sheath, neurofilament	Neurofilament medium polypeptide	P08553
NGEF	Ephexin-1 (Eph-interacting exchange protein)	NC	NC	NC	NC	NC	0.666	ND	ND	Cytoplasm, Membrane	Acts as a guanine nucleotide exchange factor.	Q8CHT1
NHP2	H/ACA ribonucleoprotein complex subunit 2	ND	ND	ND	NC	1.518	NC	ND	ND	Nucleolus, Cajal body	Required for ribosome biogenesis and telomere maintenance.	Q9CRB2
NOE1	Noelin (Neuronal olfactomedin-related ER localized protein)	NC	NC	NC	NC	0.651	NC	ND	ND	Secreted, synapse, Endoplasmic reticulum, axon, Perikaryon	Contributes to the regulation of axonal growth in the embryonic and adult central nervous system by inhibiting interactions between RTN4R and LINGO1.	O88998
NOP58	Nucleolar protein 58	NC	NC	NC	NC	1.519	NC	ND	ND	Nucleolus, nucleoplasm	Required for the biogenesis of box C/D snoRNAs.	Q6DFW4

NP1L1	Nucleosome assembly protein 1-like 1	NC	NC	NC	NC	NC	0.666	ND	ND	Nucleus	May be involved in modulating chromatin formation and contribute to regulation of cell proliferation.	P28656
NPC2	Epididymal secretory protein E1 (mE1)	ND	ND	ND	NC	NC	1.758	ND	ND	Secreted, Endoplasmic reticulum, Lysosome	Intracellular cholesterol transporter	Q9Z0J0
NPY	Pro-neuropeptide Y	ND	ND	ND	NC	0.619		ND	ND	Secreted	NPY is implicated in the control of feeding and in secretion of gonadotrophin-release hormone.	P57774
NSMA2	Sphingomyelin phosphodiesterase 3	ND	ND	ND	NC	NC	0.531	ND	ND	Lipid-anchor in membranes	Enzyme. Involved in the pathway sphingolipid metabolism, which is part of Lipid metabolism.	Q9JJY3
ORN	Oligoribonuclease	NC	ND	ND	NC	NC	1.741	NC	NC	Mitochondrion intermembrane space, Mitochondrion matrix	Enzyme. 3'-5' exonuclease activity.	Q9D8S4
P5CR2	Pyrroline-5-carboxylate reductase 2	NC	NC	NC	NC	1.514	1.608	ND	ND	Cytoplasm, Mitochondrion	Enzyme. Housekeeping enzyme that catalyses the last step in proline biosynthesis.	Q922Q4
PAK1	Serine/threonine-protein kinase PAK 1	NC	NC	NC	NC	0.635	0.662	NC	NC	Cytoplasm (many other locations)	Enzyme. Part of a ternary complex that contains PAK1, DVL1 and MUSK that is important for MUSK-dependent regulation of AChR clustering during the formation of the neuromuscular junction (NMJ).	O88643

PCP4	Calmodulin regulator protein PCP4 (Brain-specific antigen PCP-4)	NC	NC	0.584	NC	NC	0.545	NC	0.58	Cytosol, nucleus	Probable regulator of calmodulin signalling. Maybe involved in synaptic plasticity.	P63054
PCSK1	ProSAAS (IA-4) (Proprotein convertase subtilisin/kexin type 1 inhibitor)	NC	NC	NC	NC	NC	1.708	NC	NC	Secreted, Golgi apparatus, trans-Golgi network	May function in the control of the neuroendocrine secretory pathway.	Q9QXV0
PGM2L	Glucose 1,6-bisphosphate synthase	NC	NC	0.557		0.635		NC	NC	Cytosol	Enzyme. Glucose metabolism pathway.	Q8CAA7
PHAR1	Phosphatase and actin regulator 1	ND	ND	ND	NC	NC	0.585	ND	ND	Cytoplasm, synapse, nucleus	Enzyme. Binds actin monomers (G actin) and plays a role in the reorganization of the actin cytoskeleton and in formation of actin stress fibres.	Q2M3X8
PITC1	Cytoplasmic phosphatidylinositol transfer protein 1	NC	NC	NC	NC	NC	0.668	NC	NC	Cytoplasm	May play a role in the phosphoinositide-mediated signalling in the neural development.	Q8K4R4
PLAK	Junction plakoglobin (Desmoplakin III)	NC	NC	NC	2.036	NC	1.53	ND	ND	Cell junction, adherens junction	Common junctional plaque protein.	Q02257
PLBL2	Putative phospholipase B-like 2	NC	NC	NC	1.747	2.039	1.55	ND	ND	Lysosome lumen	Enzyme. Lipid catabolic process	Q3TCN2
PLXA2	Plexin-A2 (Plex 2)	ND	ND	ND	0.607	NC	NC	ND	ND	Cell membrane	Plays a role in axon guidance, invasive growth and cell migration.	P70207
PNPT1	Polyribonucleotide nucleotidyltransferase 1	ND	ND	ND	NC	NC	1.622	ND	ND	Cytoplasm, Mitochondrion	Enzyme. RNA-binding protein implicated in numerous RNA metabolic processes.	Q8K1R3

PP2BA	Serine/threonine-protein phosphatase 2B catalytic subunit alpha isoform	NC	0.605	0.542	NC	0.664	0.644	NC	NC	Cell membrane, sarcolemma, nucleus	Enzyme. Calcium-dependent, calmodulin-stimulated protein phosphatase.	P63328
PP2BB	Serine/threonine-protein phosphatase 2B catalytic subunit beta isoform	NC	NC	0.567	NC	0.547	NC	NC	NC	Calcineurin complex, cytosol	Enzyme. Calcium-dependent, calmodulin-stimulated protein phosphatase.	P48453
PPCEL	Prolyl endopeptidase-like	NC	NC	NC	NC	NC	1.918	ND	ND	cytosol	Enzyme. Probable serine peptidase whose precise substrate specificity remains unclear.	Q8C167
PPGB	Lysosomal protective protein	ND	ND	ND	NC	1.573	NC	ND	ND	Lysosome	Protective protein appears to be essential for both the activity of beta-galactosidase and neuraminidase.	P16675
PREB	Prolactin regulatory element-binding protein	ND	ND	ND	NC	1.568	NC	ND	ND	Endoplasmic reticulum membrane	Guanine nucleotide exchange factor that specifically activates the small GTPase SAR1B.	Q9WUQ2
PRRT1	Proline-rich transmembrane protein 1	NC	NC	0.652	NC	NC	NC	NC	NC	Cell membrane, synapse	May be involved in response to biotic stimulus.	O35449
PSD3	PH and SEC7 domain-containing protein 3	NC	NC	NC	NC	0.647	NC	ND	ND	Postsynaptic cell membrane	Guanine nucleotide exchange factor for ARF6.	Q2PFD7
PSME2	Proteasome activator complex subunit 2	ND	ND	ND	NC	NC	2.148	ND	ND	Cytoplasm, extracellular exosome	Implicated in immunoproteasome assembly and required for efficient antigen processing.	P97372
PSME3	Proteasome activator complex subunit 3	ND	ND	ND	NC	2.649	NC	ND	ND	Nucleus, Cytoplasm	Proteasome activator complex. proteasome regulator.	P61290

PURB	Transcriptional activator protein Pur-beta	NC	NC	NC	0.502	NC	NC	ND	ND	Nucleus	Transcriptional activator protein. Has capacity to bind repeated elements in single-stranded DNA.	O35295
PYRD	Dihydroorotate dehydrogenase (quinone)	NC	NC	NC	NC	1.598	1.566	ND	ND	Mitochondrion inner membrane	Enzyme. Catalyses the conversion of dihydroorotate to orotate.	O35435
RAP2C	Ras-related protein Rap-2c	NC	NC	NC	NC	1.693	NC	ND	ND	Cytoplasm	Small GTP-binding protein which cycles between a GDP-bound inactive and a GTP-bound active form.	Q8BU31
RB3GP	Rab3 GTPase-activating protein catalytic subunit	NC	NC	NC	NC	NC	0.665	NC	NC	Cytoplasm	Probable catalytic subunit of a GTPase activating protein that has specificity for Rab3 subfamily. Rab3 proteins are involved in regulated exocytosis of neurotransmitters and hormones.	Q80UJ7
RET1	Retinol-binding protein 1	NC	NC	NC	NC	1.507	1.865	ND	ND	Cytoplasm	Intracellular transport of retinol.	Q00915
RGRF2	Ras-specific guanine nucleotide-releasing factor 2 (Ras-GRF2)	ND	ND	ND	NC	NC	0.64	ND	ND	Cytoplasm, Cell membrane, Endoplasmic reticulum membrane	Functions as a calcium-regulated nucleotide exchange factor activating both Ras and RAC1 through the exchange of bound GDP for GTP.	P70392
RHG32	Rho GTPase-activating protein 32	ND	ND	ND	NC	NC	0.619	ND	ND	Synapse, postsynaptic cell membrane dendritic spine	May be involved in the differentiation of neuronal cells during the formation of neurite extensions. Involved in NMDA receptor activity-dependent actin reorganization in dendritic spines.	Q811P8

RIMB2	RIMS-binding protein 2 (RIM-BP2)	NC	NC	NC	NC	0.511	NC	ND	ND	Cell membrane, synapse	Plays a role in the synaptic transmission as bifunctional linker that interacts simultaneously with RIMS1, RIMS2, CACNA1D and CACNA1B.	Q80U40
RU17	U1 small nuclear ribonucleoprotein 70 kDa (U1 snRNP 70 kDa)	ND	ND	ND	NC	NC	1.497	ND	ND	Nucleus speckle, nucleus, nucleoplasm	Component of the spliceosomal U1 snRNP, which is essential for recognition of the pre-mRNA 5' splice-site and the subsequent assembly of the spliceosome.	Q62376
RYR2	Ryanodine receptor 2 (RYR-2)	NC	NC	NC	NC	NC	0.614	ND	ND	Sarcoplasmic reticulum membrane	Calcium channel that mediates the release of Ca2+ from the sarcoplasmic reticulum into the cytoplasm and thereby plays a key role in triggering cardiac muscle contraction.	E9Q401
S2542	Mitochondrial coenzyme A transporter SLC25A42	NC	NC	NC	NC	NC	1.797	ND	ND	Mitochondrion inner membrane	Mitochondrial carrier mediating the transport of coenzyme A	Q8R0Y8
S4A10	Sodium-driven chloride bicarbonate exchanger	NC	NC	NC	NC	0.624	NC	ND	ND	Cell membrane	Electrogenic sodium/bicarbonate cotransporter in exchange for intracellular chloride	Q5DTL9
SAR1B	GTP-binding protein SAR1b	NC	NC	NC	NC	1.594	1.665	NC	NC	Endoplasmic reticulum membrane	Involved in transport from the endoplasmic reticulum to the Golgi apparatus.	Q9CQC9
SCFD1	Sec1 family domain-containing protein 1	NC	NC	1.602	NC	NC	NC	ND	ND	Cytoplasm, Endoplasmic reticulum membrane	Plays a role in SNARE-pin assembly and Golgi-to-ER retrograde transport via its interaction with COG4.	Q8BRF7

SCMC2	Calcium-binding mitochondrial carrier protein	NC	NC	NC	NC		1.549	NC	NC	Mitochondrion inner membrane	Calcium-dependent mitochondrial solute carrier.	A2ASZ8
Sep-08	Septin-8	NC	NC	NC	NC	0.656		NC	NC	Cytoplasm, cytoskeleton	Filament-forming cytoskeletal GTPase.	Q8CHH9
SF01	Splicing factor 1	ND	ND	ND	NC	0.421		ND	ND	Nucleus	Necessary for the ATP-dependent first step of spliceosome assembly.	Q64213
SGPL1	Sphingosine-1-phosphate lyase 1 (S1PL)	ND	ND	ND	NC		1.865	ND	ND	Endoplasmic reticulum membrane	Cleaves phosphorylated sphingoid bases (PSBs), such as sphingosine-1-phosphate, into fatty aldehydes and phosphoethanolamine.	Q8R0X7
SL9A1	Sodium/hydrogen exchanger 1	NC	NC	NC	NC	1.581	1.55	NC	NC	Membrane, Endoplasmic reticulum membrane	Involved in pH regulation to eliminate acids generated by active metabolism or to counter adverse environmental conditions.	Q61165
SNP25	Synaptosomal-associated protein 25 (SNAP-25)	NC	0.494	NC	0.605	0.536	0.582	NC	NC	Cytoplasm, perinuclear region	t-SNARE involved in the molecular regulation of neurotransmitter release. May play an important role in the synaptic function of specific neuronal systems.	P60879
SPEE	Spermidine synthase (SPDSY)	NC	NC	1.52	NC	NC	NC	NC	NC	Unknown	Enzyme. Catalyses the production of spermidine from putrescine and decarboxylated S-adenosylmethionine (dcSAM).	Q64674
SPSY	Spermine synthase (SPMSY)	NC	0.662	NC	NC	NC	NC	NC	NC	Extracellular exosome	Catalyses the production of spermine.	P97355

SRBS1	Sorbin and SH3 domain-containing protein 1 (Ponsin)	NC	NC	NC	NC	NC	1.535	ND	ND	Adherens junction, Cell membrane, cytoplasm, cytoskeleton	Plays a role in tyrosine phosphorylation of CBL by linking CBL to the insulin receptor. Required for insulin-stimulated glucose transport. Involved in formation of actin stress fibres and focal adhesions.	Q62417
SRGP3	SLIT-ROBO Rho GTPase-activating protein 3 (srGAP3)	NC	0.528	NC	0.493	0.635	NC	NC	NC	cytoplasm	GTPase-activating protein for RAC1 and perhaps CDC42, but not for RhoA small GTPase.	Q812A2
STMN1	Stathmin (Leukemia-associated gene protein)	NC	NC	NC	NC	0.665	NC	NC	NC	Cytoplasm, cytoskeleton	Involved in the regulation of the microtubule (MT) filament system by destabilizing microtubules. Phosphorylation at Ser-16 may be required for axon formation during neurogenesis.	P54227
STRBP	Spermatid perinuclear RNA-binding protein	ND	ND	ND	0.503	NC	NC	ND	ND	Cytoplasm, cytoskeleton	Spermatid perinuclear RNA-binding protein	Q91WM1
STRUM	WASH complex subunit 5 (WASH complex subunit strumpellin)	NC	NC	NC	NC	NC	1.585	ND	NC	Cytoplasm, cytosol	May be involved in axonal outgrowth.	Q8C2E7
SV2A	Synaptic vesicle glycoprotein 2A	NC	NC	NC	NC	NC	NC	NC	0.64	Cell junction, synapse	Plays a role in the control of regulated secretion in neural and endocrine cells, enhancing selectively low-frequency neurotransmission.	Q9JIS5
SYUA	Alpha-synuclein (Non-A beta component of AD amyloid)	NC	NC	NC	NC	NC	NC	NC	0.65	Cytoplasm › cytosol	May be involved in the regulation of dopamine release and transport.	O55042

TADBP	**TAR DNA-binding protein 43 (TDP-43)**	9.236	5.98	4.779	7.004	3.956	3.921	2.794	2.621	**Nucleus (mislocated to cytoplasm in rNLS mice)**	**DNA and RNA-binding protein which regulates transcription and splicing.**	**Q921F2**
TAGL2	Transgelin-2 (SM22-beta)	NC	NC	NC	NC	NC	1.499	NC	NC	Cell-cell adherens junction	Cadherin binding involved in cell-cell adhesion	Q9WVA4
TCAL3	Transcription elongation factor A protein-like 3	NC	1.515	NC	NC	NC	NC	NC	NC	Nucleus	May be involved in transcriptional regulation.	Q8R0A5
THEM6	Protein THEM6	NC	NC	NC	2.335	2.634	1.774	ND	ND	Secreted	Functions unknown.	Q80ZW2
TOM34	Mitochondrial import receptor subunit TOM34 (Translocase of outer membrane 34 kDa subunit)	NC	NC	NC	1.621	NC	NC	NC	NC	Cytoplasm	Plays a role in the import of cytosolically synthesized preproteins into mitochondria. May be a chaperone-like protein that helps to keep newly synthesized precursors in an unfolded import compatible state.	Q9CYG7
TPSN	Tapasin (TPN)	ND	ND	ND	NC	NC	3.172	ND	ND	Endoplasmic reticulum membrane	Involved in the association of MHC class I with transporter associated with antigen processing (TAP) and in the assembly of MHC class I with peptide (peptide loading).	Q9R233
TRFE	Serotransferrin (Transferrin)	NC	NC	1.501	NC	NC	NC	NC	NC	Secreted	Transferrins are iron binding transport proteins.	Q921I1
TRI46	Tripartite motif-containing protein 46	NC	NC	NC	1.574	NC	NC	ND	ND	Cytoskeleton, axon	Microtubule-associated protein that is involved in the formation of parallel microtubule bundles linked by cross-bridges in the proximal axon.	Q7TNM2

TRNT1	CCA tRNA nucleotidyltransferase 1	ND	ND	ND	NC	NC	1.511	ND	ND	Mitochondrion	Enzyme. Adds and repairs the conserved 3'-CCA sequence necessary for the attachment of amino acids to the 3' terminus of tRNA molecules, using CTP and ATP as substrates.	Q8K1J6
TY3H	Tyrosine 3-monooxygenase	ND	ND	ND	NC	2.786	NC	ND	ND	Axon	Enzyme. Plays an important role in the physiology of adrenergic neurons.	P24529
UBQL4	Ubiquilin-4 (Ataxin-1 interacting ubiquitin-like protein)	NC	NC	NC	NC	NC	2.168	ND	ND	Nucleus, cytoplasm, endoplasmic reticulum, perinuclear region	Plays a role in the regulation of protein degradation via the ubiquitin-proteasome system (UPS). Mediates the proteasomal targeting of misfolded or accumulated proteins for degradation by binding (via UBA domain) to their polyubiquitin chains and by interacting (via ubiquitin-like domain) with the subunits of the proteasome.	Q99NB8
VAT1	Synaptic vesicle membrane protein VAT-1 homolog	NC	NC	NC	NC	1.672	1.756	NC	NC	Cytoplasm, Mitochondrion outer membrane	Synaptic vesicle membrane protein.	Q62465
VDAC2	Voltage-dependent anion-selective channel protein 2 (VDAC-2)	NC	NC	NC	NC	NC	0.647	NC	NC	Mitochondrion outer membrane	Forms a channel through the mitochondrial outer membrane that allows diffusion of small hydrophilic molecules.	Q60930
VDAC3	Voltage-dependent anion-selective channel protein 3 (VDAC-3)	ND	ND	ND	0.53	NC	0.606	ND	ND	Mitochondrion outer membrane	Forms a channel through the mitochondrial outer membrane that allows diffusion of small hydrophilic molecules.	Q60931

VIME	Vimentin	NC	NC	NC	NC	NC	2.298	NC	NC	Cytoplasm	Vimentin is attached to the nucleus, endoplasmic reticulum, and mitochondria, either laterally or terminally.	P20152
VMA5A	von Willebrand factor A domain-containing protein 5A	NC	NC	NC	NC	NC	1.803	NC	NC	Nucleoplasm, nucleus	May play a role in tumorigenesis as a tumour suppressor.	Q99KC8
VPS35	Vacuolar protein sorting-associated protein 35	NC	NC	NC	NC	NC	NC	NC	1.584	Cytoplasm	Vacuolar protein sorting-associated protein	Q9EQH3
VTI1B	Vesicle transport through interaction with t-SNAREs homolog 1B	NC	NC	NC	NC	NC	0.495	ND	ND	Late endosome membrane	V-SNARE that mediates vesicle transport pathways through interactions with t-SNAREs on the target membrane.	O88384
WASF1	Wiskott-Aldrich syndrome protein family member 1 (WASP family protein member 1)	NC	NC	0.642	NC	NC	NC	NC	NC	Cytoplasm, cytoskeleton, synapse	Effector molecule involved in the transmission of signals from tyrosine kinase receptors and small GTPases to the actin cytoskeleton. Promotes formation of actin filaments. Part of the WAVE complex that regulates lamellipodia formation. The WAVE complex regulates actin filament reorganization via its interaction with the Arp2/3 complex.	Q8R5H6

Appendix 2.

Validation studies

CNKR2 Week 2 Cortex

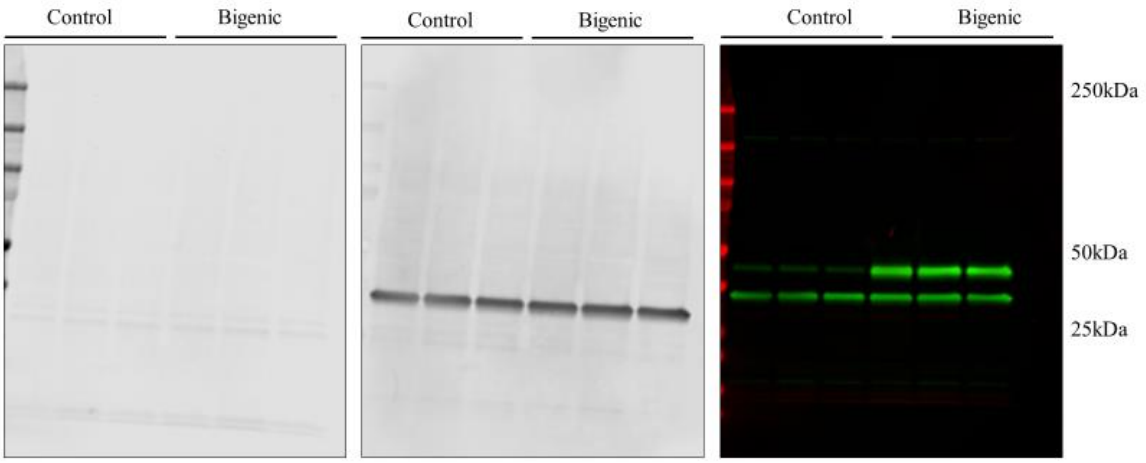

CNKR2 Week 4 Cortex

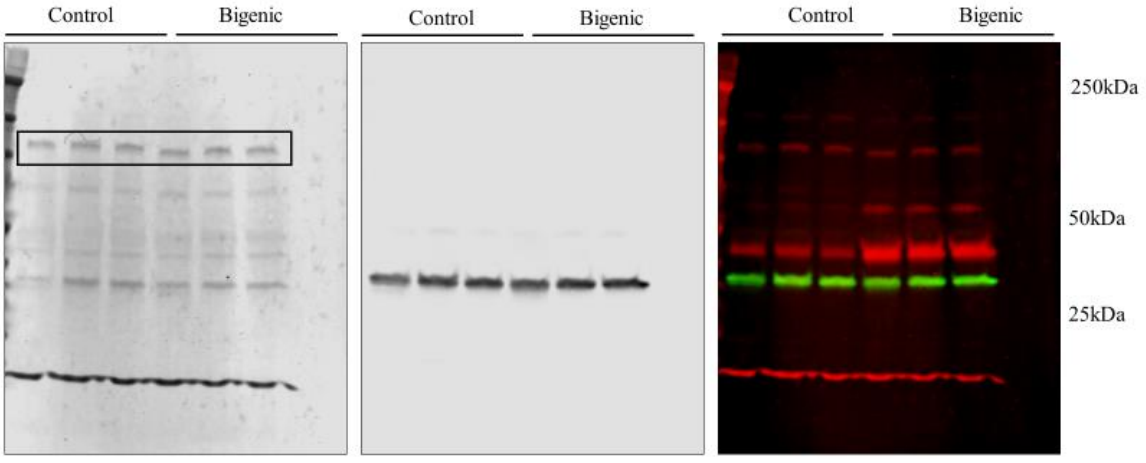

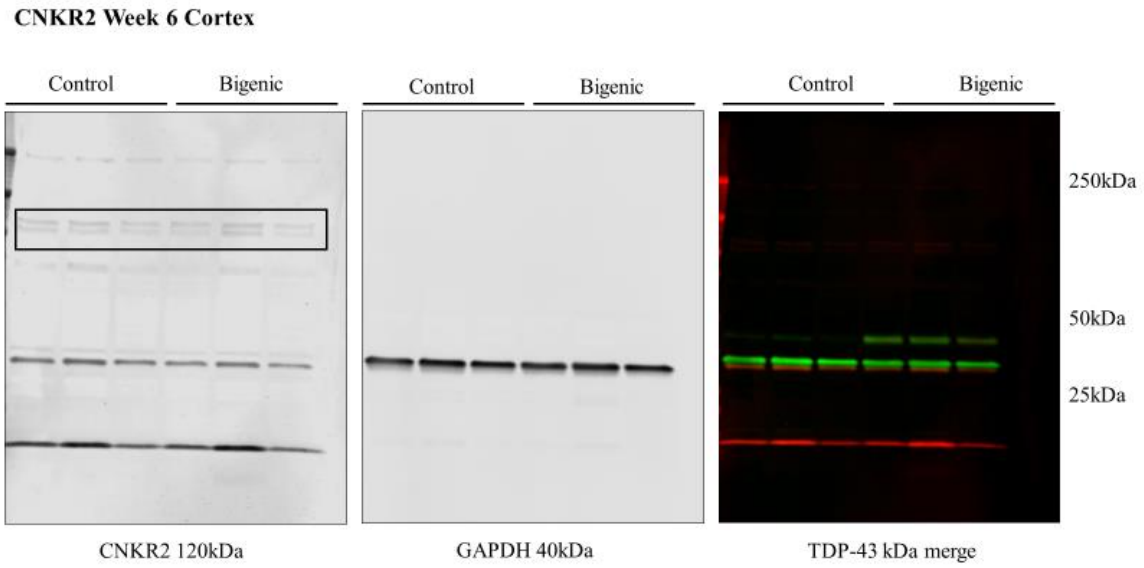

Appendix Figure 2.1 Full western blots for Figure 4.1.7.

Specific CNKR2 antibody was used to validate protein changes using cortex tissue from the same cohort that was used for SWATH MS (litter-matched, sex-matched pairs for control and rNLS) at 2,4 and 6-week timepoints (n=3). Blots were quantified using the LI-COR Image Studio software and analysed using GraphPad Prism version 7.02. The molecular weight for CNKR2 is 120kDa. Week 2 blot did not show a band for CNKR2.

CNKR2 Week 2 Cortex

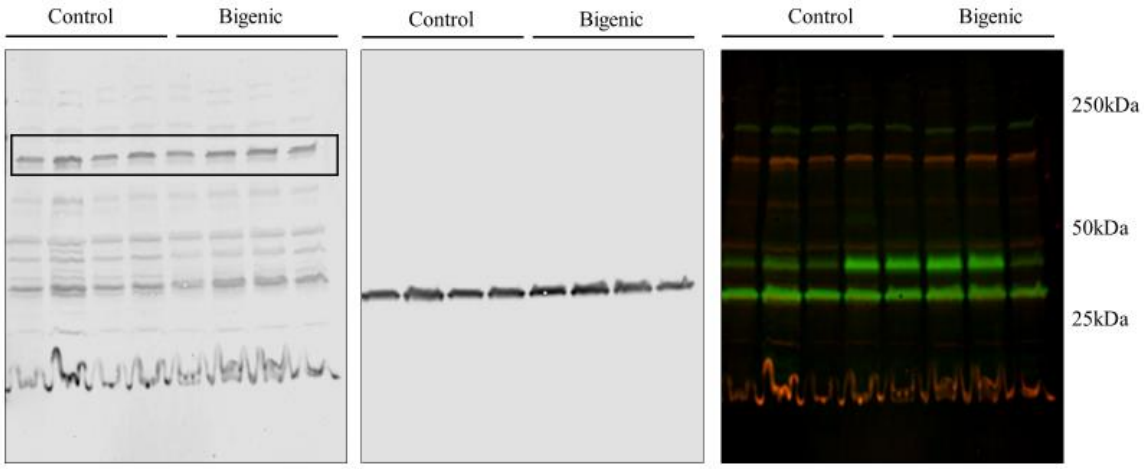

CNKR2 Week 4 Cortex

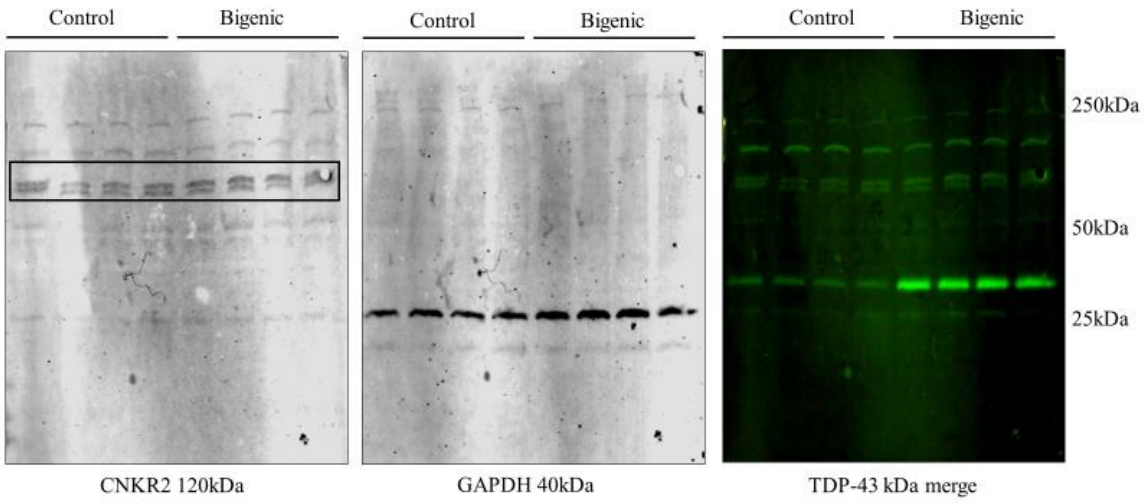

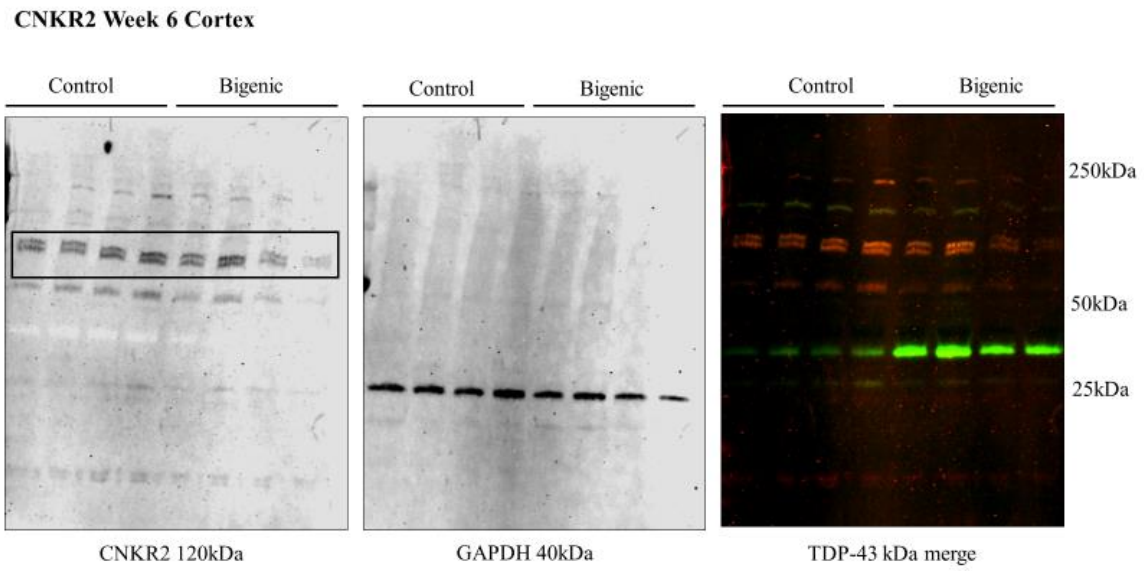

Appendix Figure 2.2 Full western blots for Figure 4.2.33.

Specific COQ9 antibody was used to validate protein changes using cortex tissue from the same cohort that was used for SWATH MS (litter-matched, sex-matched pairs for control and rNLS) at 2,4 and 6-week timepoints (n=3). Blots were visualised and quantified using the LI-COR Image Studio software. Statistical analysis was conducted using a Paired T-test via GraphPad Prism version 7.02 (not significant=P > 0.05). The molecular weight for COQ9 is 35kDa.

COQ9 Week 2 Cortex

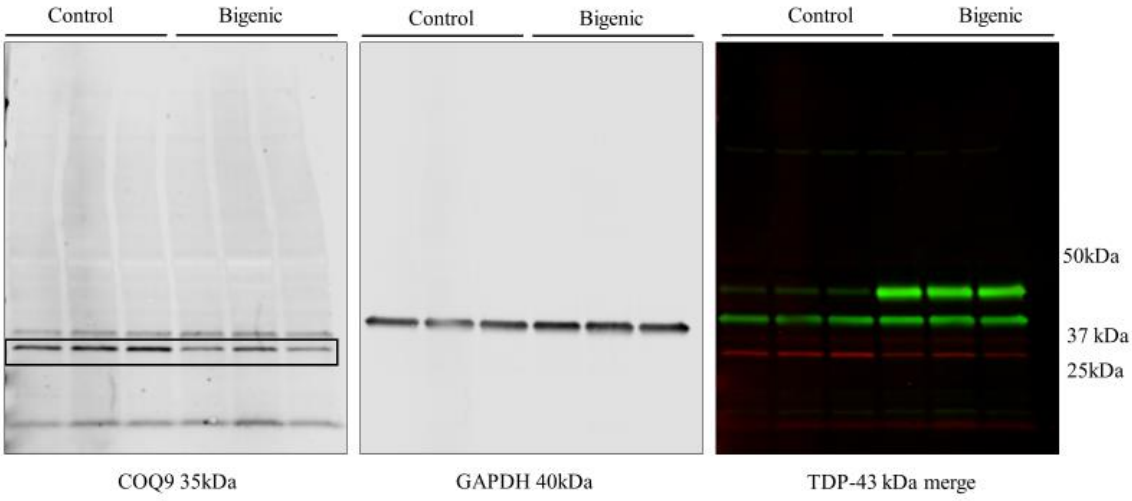

COQ9 Week 4 Cortex

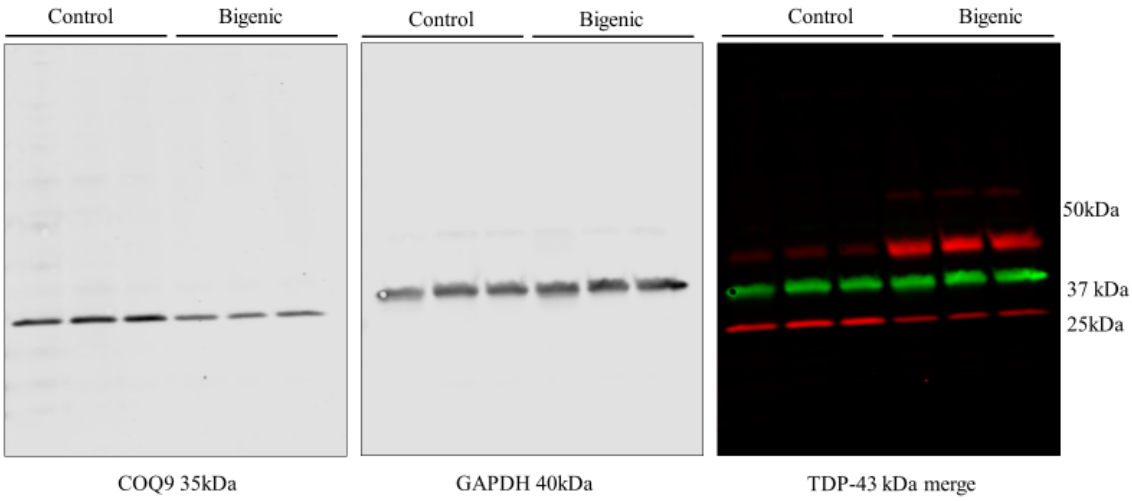

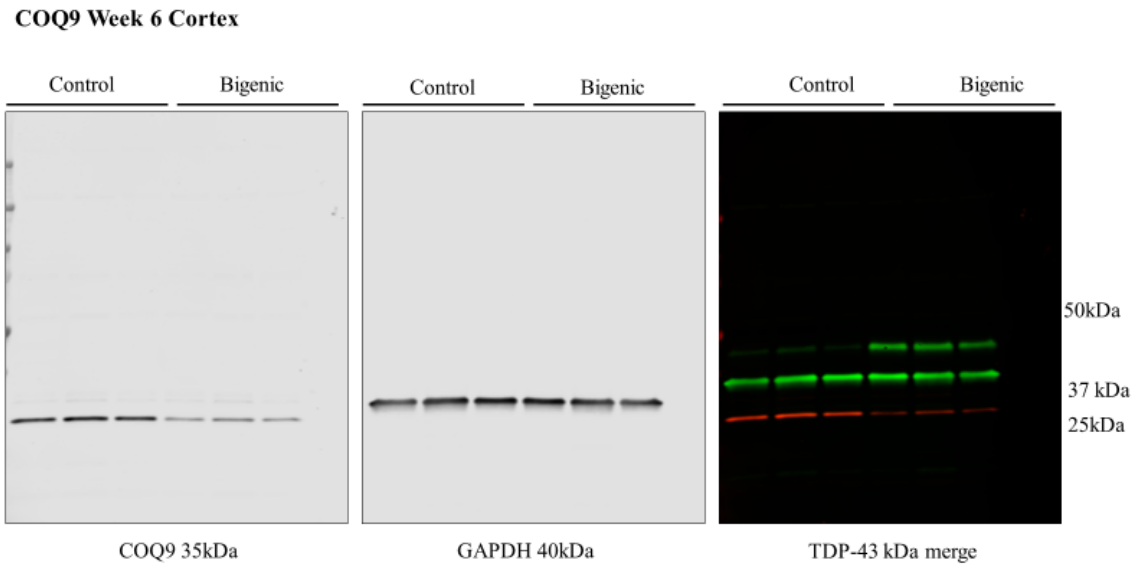

Appendix Figure 2.3 Full western blots for Figure 4.2.33.

Specific COQ9 antibody was used to validate protein changes using cortex tissue from the same cohort that was used for SWATH MS (litter-matched, sex-matched pairs for control and rNLS) at 2,4 and 6-week timepoints (n=3). Blots were visualised and quantified using the LI-COR Image Studio software. Statistical analysis was conducted using a Paired T-test via GraphPad Prism version 7.02 (not significant=P > 0.05). The molecular weight for COQ9 is 35kDa.

COQ9 Week 2 Cortex

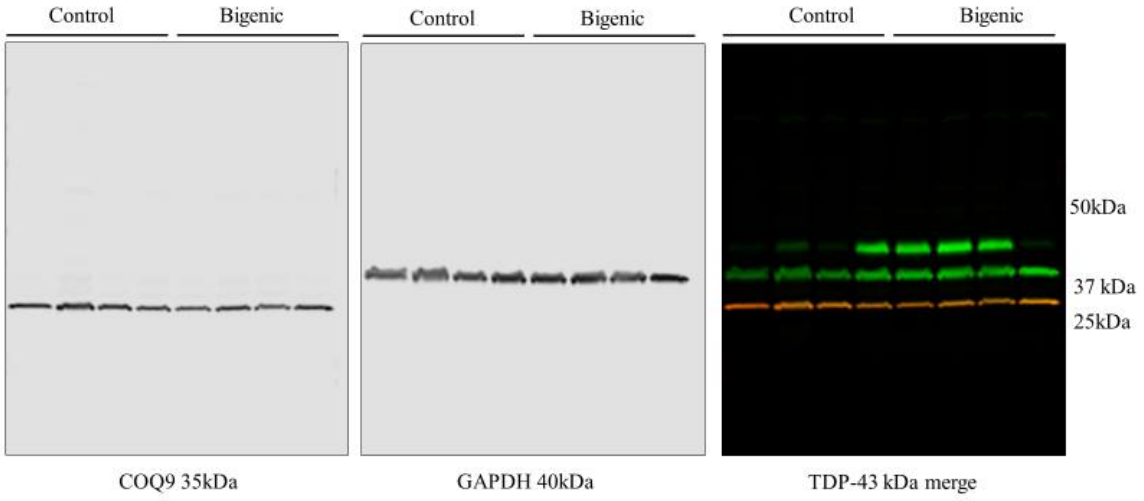

COQ9 Week 4 Cortex

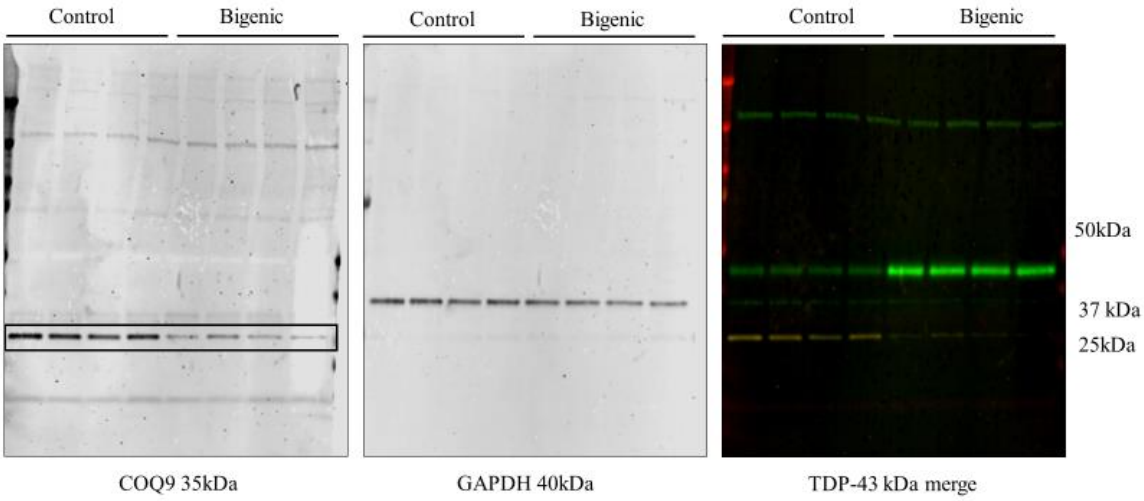

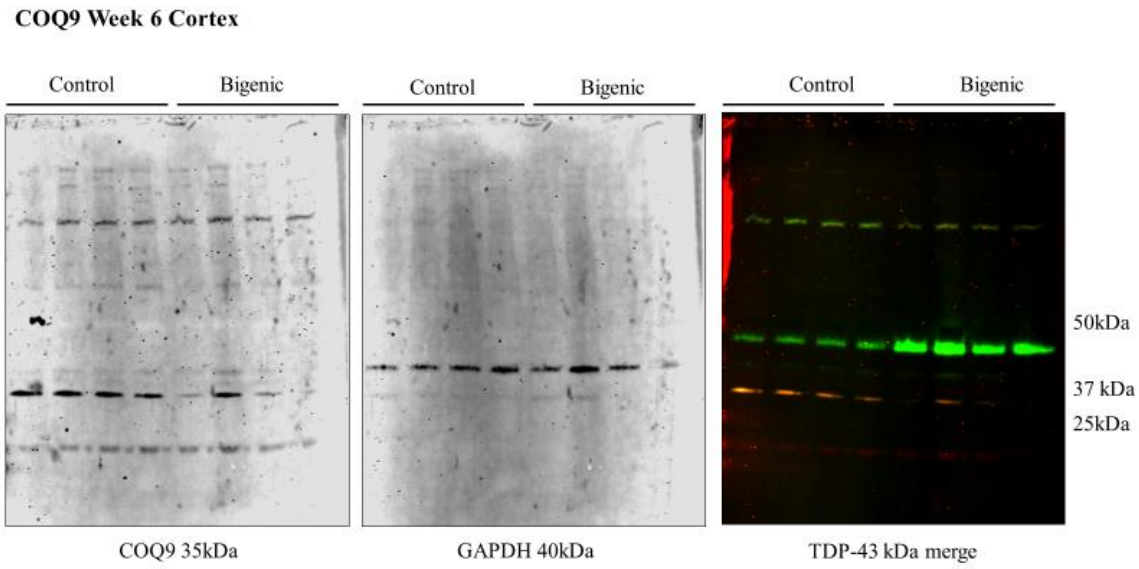

Appendix Figure 2.4 Full western blots for Figure 4.2.34

Specific COQ9 antibody was used to validate protein changes using cortex tissue from the different cohort that was used for SWATH MS (litter-matched, sex-matched pairs for control and rNLS) at 2,4 and 6-week timepoints (n=3). Blots were visualised and quantified using the LI-COR Image Studio software. Statistical analysis was conducted using a Paired T-test via GraphPad Prism version 7.02 (not significant=P > 0.05). The molecular weight for COQ9 is 35kDa.

VDAC3 Week 2 Cortex

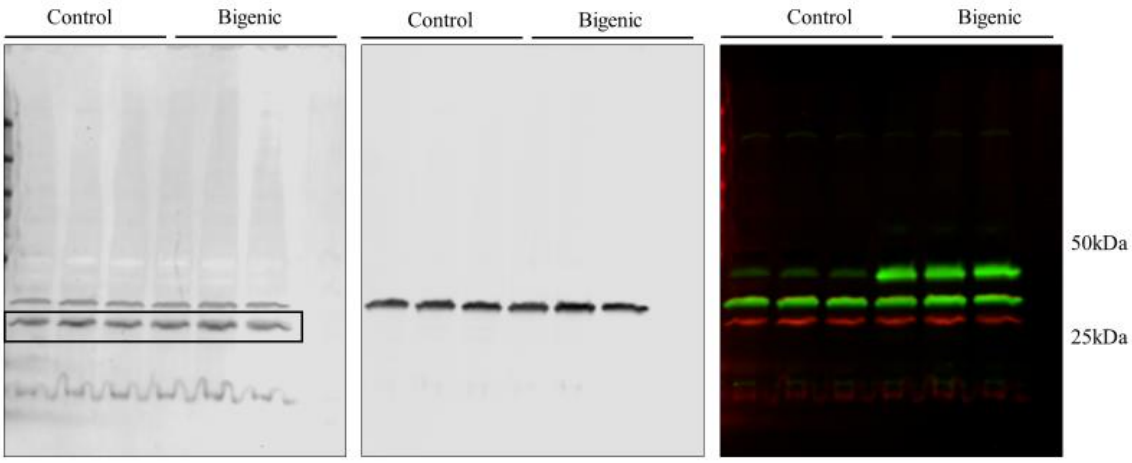

VDAC3 35kDa GAPDH 40kDa TDP-43 kDa merge

VADC3 Week 4 Cortex

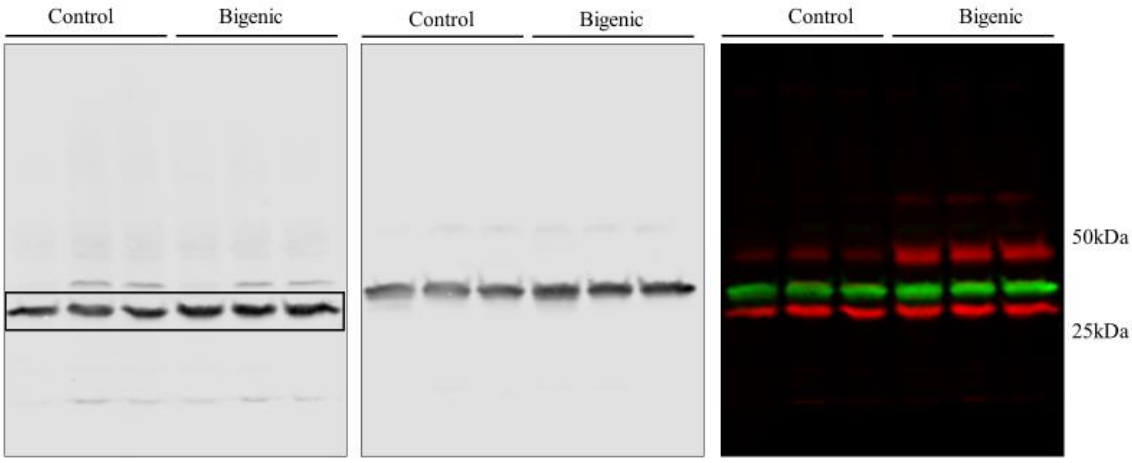

VDAC3 35kDa GAPDH 40kDa TDP-43 kDa merge

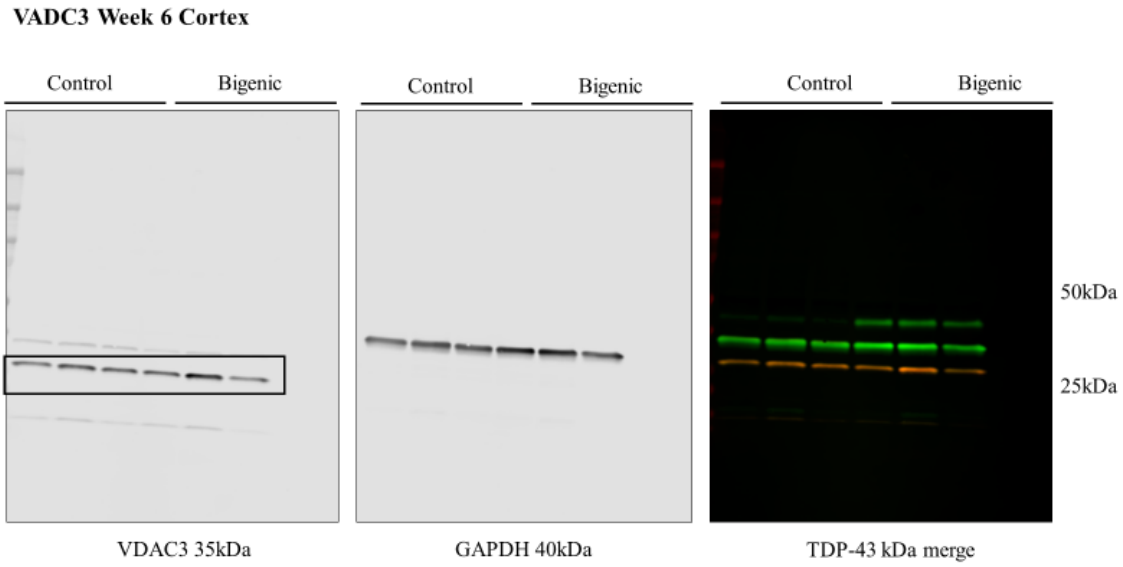

Appendix Figure 2.5 Full western blots for Figure 4.2.36.

Specific VDAC3 antibody was used to validate protein changes using cortex tissue from the same cohort that was used for SWATH MS (litter-matched, sex-matched pairs for control and rNLS) at 2,4 and 6-week timepoints (n=3). Blots were visualised and quantified using the LI-COR Image Studio software. Statistical analysis was conducted using a Paired T-test via GraphPad Prism version 7.02 (not significant=P > 0.05). The molecular weight for VDAC is 35kDa.

VDAC3 Week 2 Cortex

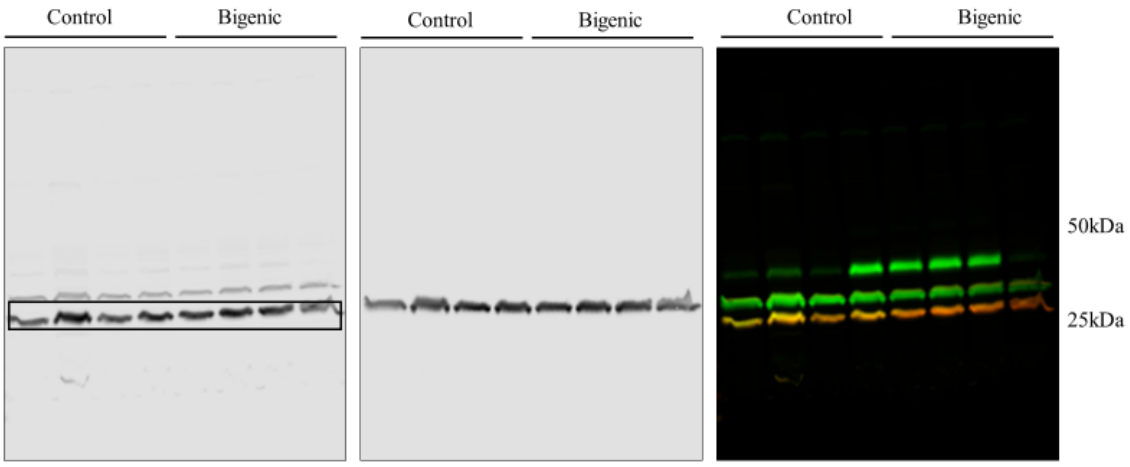

VDAC3 35kDa | GAPDH 40kDa | TDP-43 kDa merge

VADC3 Week 4 Cortex

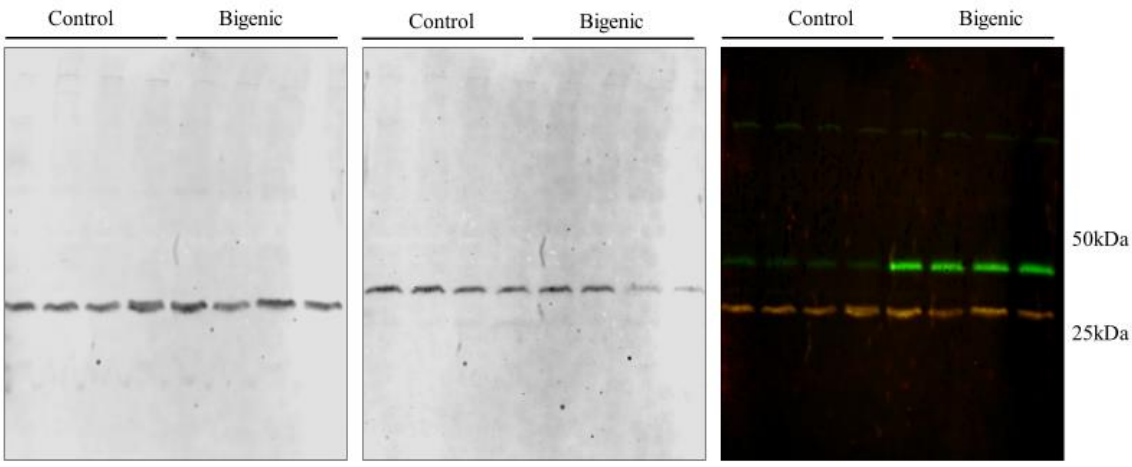

VDAC3 35kDa | GAPDH 40kDa | TDP-43 kDa merge

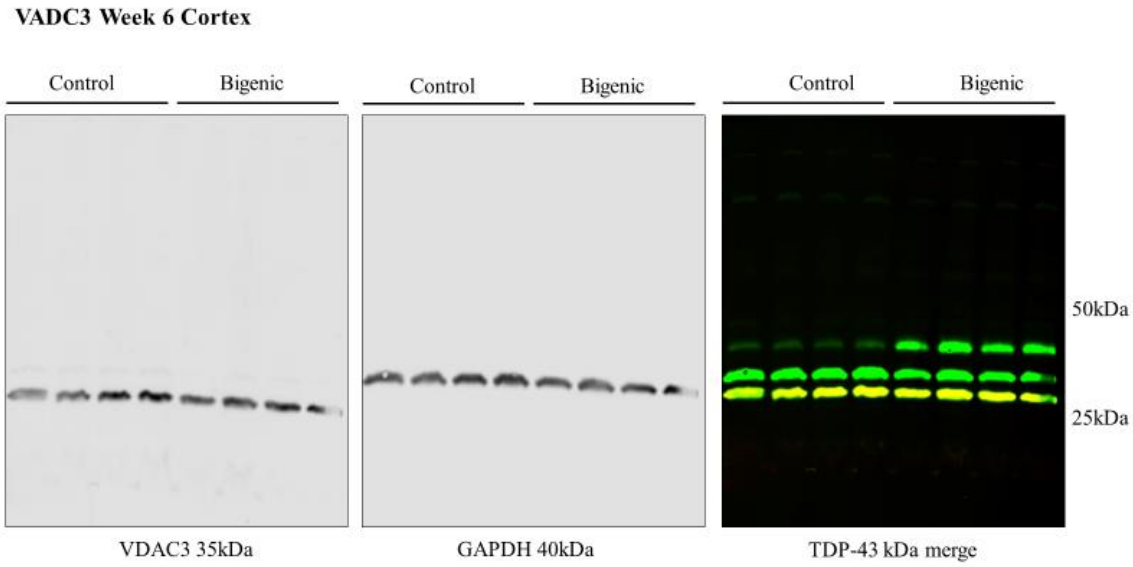

Appendix Figure 2.6 Full western blots for Figure 4.2.37.

Specific VDAC3 antibody was used to validate protein changes using cortex tissue from the different cohort that was used for SWATH MS (litter-matched, sex-matched pairs for control and rNLS) at 2,4 and 6-week timepoints (n=3). Blots were visualised and quantified using the LI-COR Image Studio software. Statistical analysis was conducted using a Paired T-test via GraphPad Prism version 7.02 (not significant=P > 0.05). The molecular weight for VDAC is 35kDa. For full blots refer to ***Appendix figure 3.6****. For p-values refer to* ***Table 4.2.20****.*

IMA3Week 2 Cortex

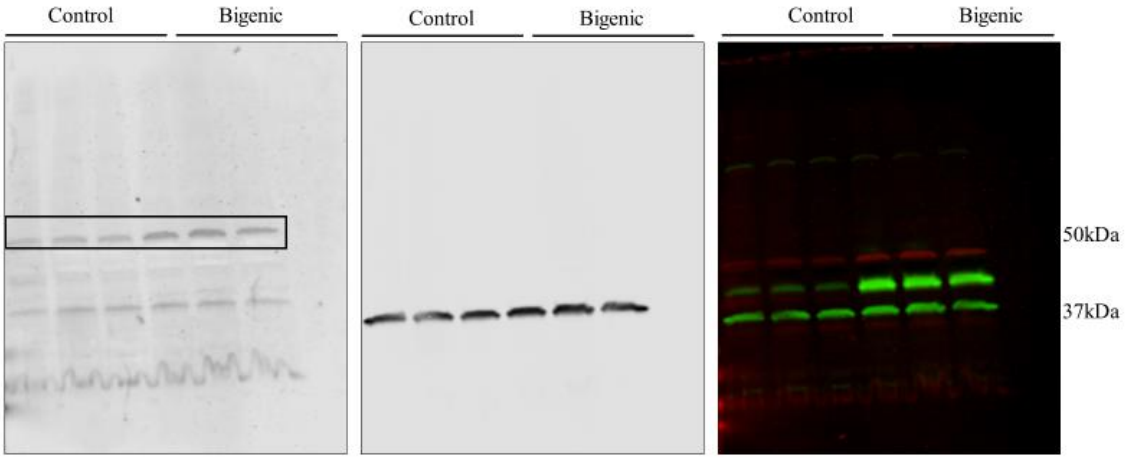

IMA3 58kDa | GAPDH 40kDa | TDP-43 kDa merge

IMA3 Week 4 Cortex

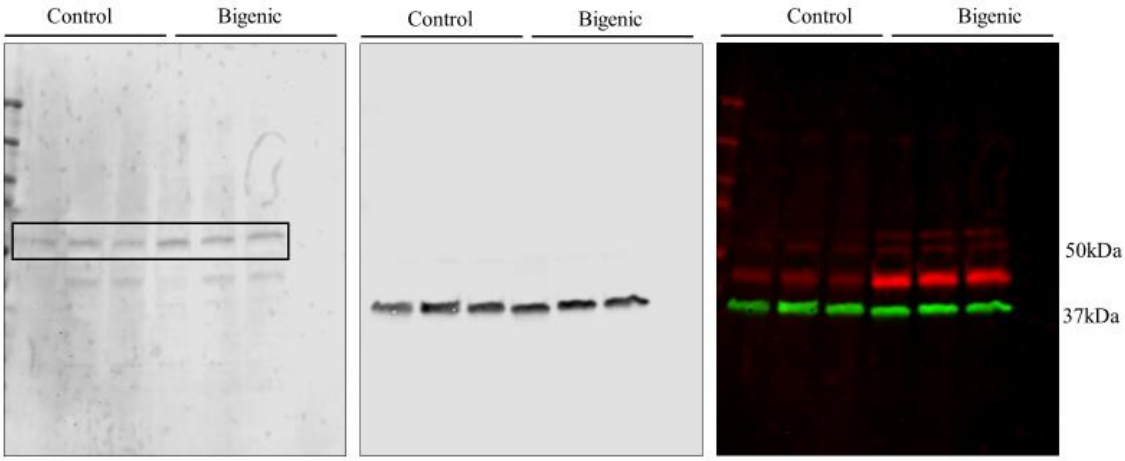

IMA3 58kDa | GAPDH 40kDa | TDP-43 kDa merge

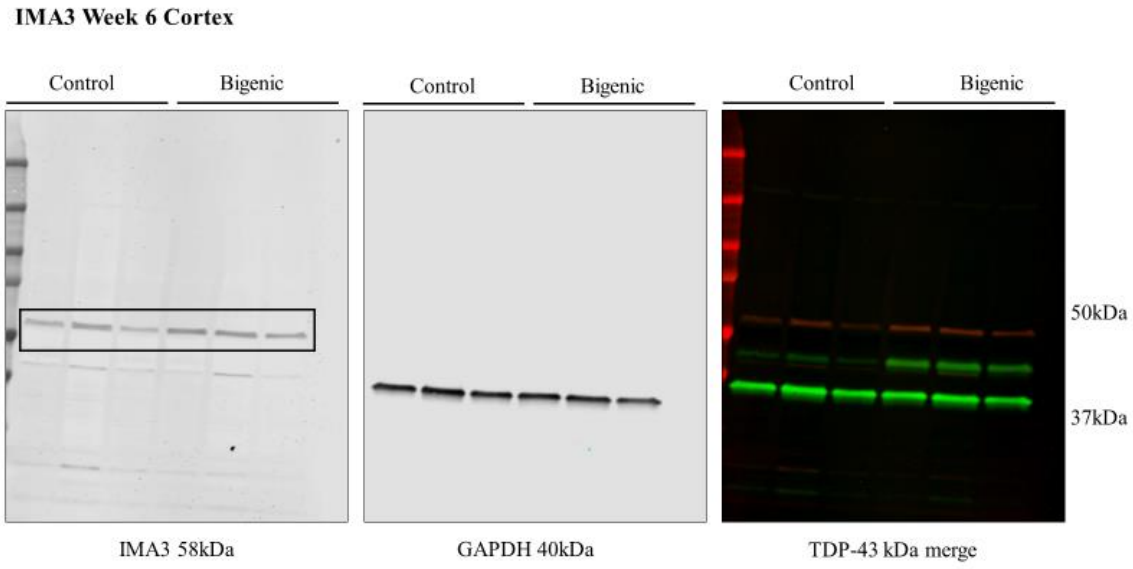

Appendix Figure 2.7 Full western blots for Figure 4.2.39.

Specific IMA3 antibody was used to validate protein changes using cortex tissue from the same cohort that was used for SWATH MS (litter-matched, sex-matched pairs for control and rNLS) at 2,4 and 6-week timepoints (n=3). Blots were visualised and quantified using the LI-COR Image Studio software. Statistical analysis was conducted using a Paired T-test via GraphPad Prism version 7.02 (not significant=P > 0.05). The molecular weight for IMA3 is 58kDa.

IMA3Week 2 Cortex

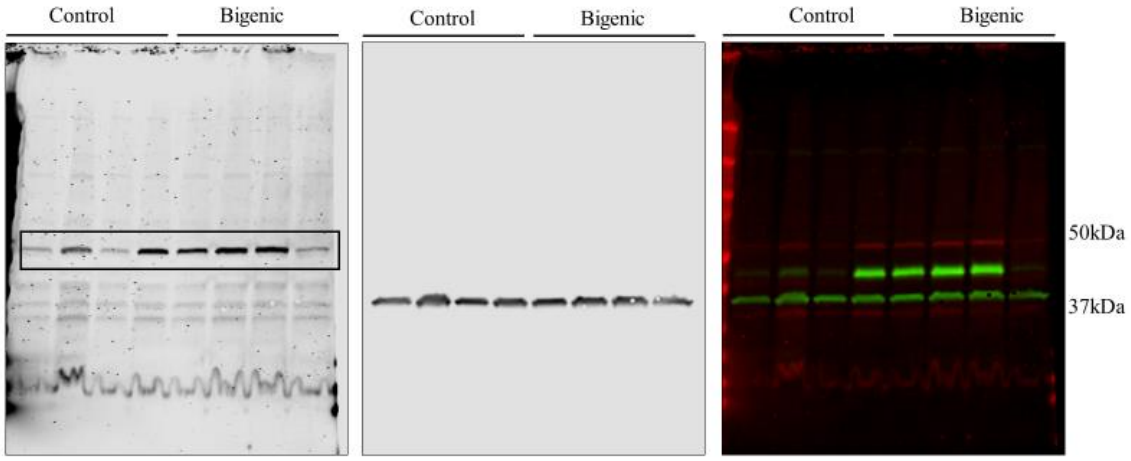

IMA3 58kDa GAPDH 40kDa TDP-43 kDa merge

IMA3 Week 4 Cortex

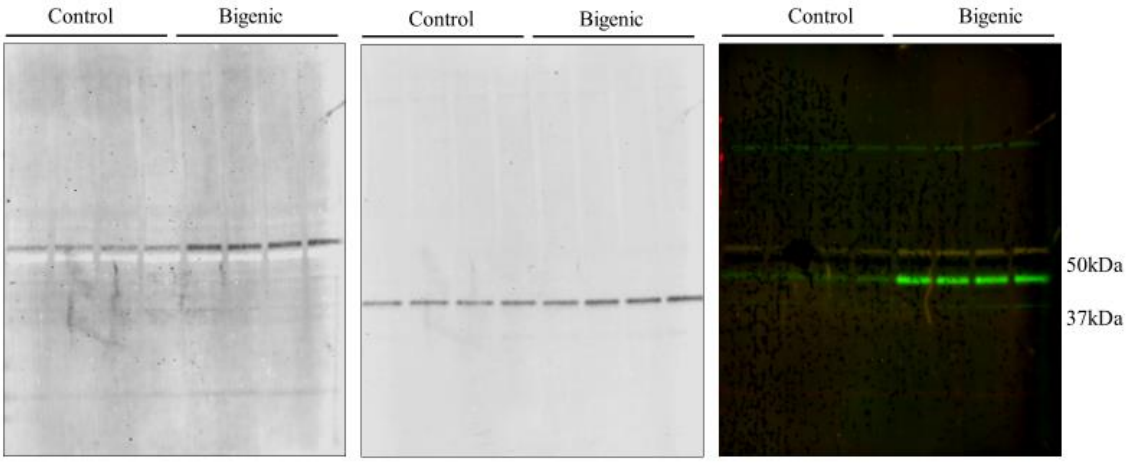

IMA3 58kDa GAPDH 40kDa TDP-43 kDa merge

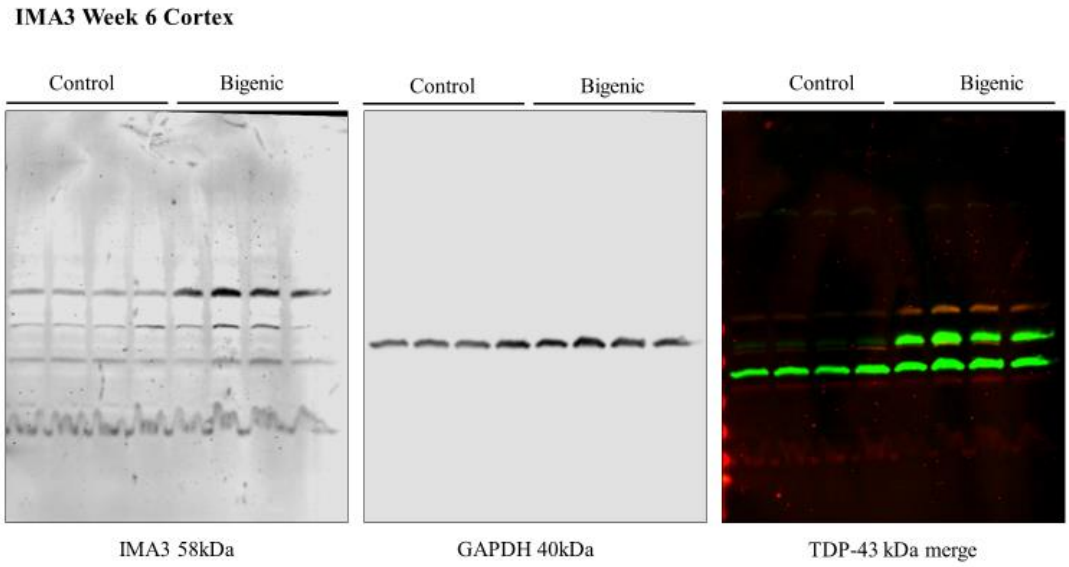

Appendix Figure 2.8 Full western blots for Figure 4.2.40.

Specific IMA3 antibody was used to validate protein changes using cortex tissue from the different cohort that was used for SWATH MS (litter-matched, sex-matched pairs for control and rNLS) at 2,4 and 6-week timepoints (n=3). Blots were visualised and quantified using the LI-COR Image Studio software. Statistical analysis was conducted using a Paired T-test via GraphPad Prism version 7.02 (not significant=P > 0.05). The molecular weight for IMA3 is 58kDa.

Appendix 3. Animal Ethics Approval

Please see next page for a copy of the animal ethic approval provided by Macquarie University.

Appendix 3 of this thesis has been removed as it may contain sensitive/confidential content

References

1. Alonso, A., et al., *Incidence and lifetime risk of motor neuron disease in the United Kingdom: a population-based study.* Eur J Neurol, 2009. **16**(6): p. 745-51.
2. Logroscino, G., et al., *Incidence of amyotrophic lateral sclerosis in Europe.* J Neurol Neurosurg Psychiatry, 2010. **81**(4): p. 385-90.
3. Rowland , L.P. and N.A. Shneider *Amyotrophic Lateral Sclerosis.* New England Journal of Medicine, 2001. **344**(22): p. 1688-1700.
4. Byrne, S., et al., *Rate of familial amyotrophic lateral sclerosis: a systematic review and meta-analysis.* J Neurol Neurosurg Psychiatry, 2011. **82**(6): p. 623-7.
5. Georgoulopoulou, E., et al., *Changing incidence and subtypes of ALS in Modena, Italy: A 10-years prospective study.* Amyotrophic Lateral Sclerosis, 2011. **12**(6): p. 451-457.
6. Riancho, J., et al., *Amyotrophic Lateral Sclerosis in Northern Spain 40 Years Later: What Has Changed?* Neurodegener Dis, 2016. **16**(5-6): p. 337-41.
7. Brown, R.H. and A. Al-Chalabi, *Amyotrophic Lateral Sclerosis.* New England Journal of Medicine, 2017. **377**(2): p. 162-172.
8. Sabatelli, M., A. Conte, and M. Zollino, *Clinical and genetic heterogeneity of amyotrophic lateral sclerosis.* Clinical Genetics, 2013. **83**(5): p. 408-416.
9. Haverkamp, L.J., V. Appel, and S.H. Appel, *Natural history of amyotrophic lateral sclerosis in a database population. Validation of a scoring system and a model for survival prediction.* Brain, 1995. **118 (Pt 3)**: p. 707-19.
10. Gouveia, L.O. and M. de Carvalho, *Young-onset sporadic amyotrophic lateral sclerosis: a distinct nosological entity?* Amyotroph Lateral Scler, 2007. **8**(6): p. 323-7.
11. Logroscino, G., et al., *Incidence of amyotrophic lateral sclerosis in southern Italy: a population based study.* J Neurol Neurosurg Psychiatry, 2005. **76**(8): p. 1094-8.
12. Ravits, J.M. and A.R. La Spada, *ALS motor phenotype heterogeneity, focality, and spread: Deconstructing motor neuron degeneration.* Neurology, 2009. **73**(10): p. 805-811.
13. Wijesekera, L.C. and P.N. Leigh, *Amyotrophic lateral sclerosis.* Orphanet Journal of Rare Diseases, 2009. **4**: p. 3-3.
14. Chen, R., et al., *Motor neuron disease presenting as acute respiratory failure: a clinical and pathological study.* J Neurol Neurosurg Psychiatry, 1996. **60**(4): p. 455-8.
15. de Carvalho, M., et al., *Motor neuron disease presenting with respiratory failure.* J Neurol Sci, 1996. **139 Suppl**: p. 117-22.
16. Norris, F., et al., *Onset, natural history and outcome in idiopathic adult motor neuron disease.* J Neurol Sci, 1993. **118**(1): p. 48-55.
17. Hu, M., et al., *Flail arm syndrome: a distinctive variant of amyotrophic lateral sclerosis.* Journal of Neurology, Neurosurgery, and Psychiatry, 1998. **65**(6): p. 950-951.

18. Katz, J.S., et al., *Brachial amyotrophic diplegia: a slowly progressive motor neuron disorder.* Neurology, 1999. **53**(5): p. 1071-6.
19. Wijesekera, L.C., et al., *Natural history and clinical features of the flail arm and flail leg ALS variants.* Neurology, 2009. **72**(12): p. 1087-1094.
20. Hübers, A., et al., *Clinical features and differential diagnosis of flail arm syndrome.* Journal of Neurology, 2016. **263**(2): p. 390-395.
21. Gordon, P.H., et al., *The natural history of primary lateral sclerosis.* Neurology, 2006. **66**(5): p. 647-53.
22. Tartaglia, M.C., et al., *Differentiation between primary lateral sclerosis and amyotrophic lateral sclerosis: examination of symptoms and signs at disease onset and during follow-up.* Arch Neurol, 2007. **64**(2): p. 232-6.
23. Kim, W.K., et al., *Study of 962 patients indicates progressive muscular atrophy is a form of ALS.* Neurology, 2009. **73**(20): p. 1686-92.
24. van Blitterswijk, M., et al., *Genetic overlap between apparently sporadic motor neuron diseases.* PLoS One, 2012. **7**(11): p. e48983.
25. Zoccolella, S., et al., *Analysis of survival and prognostic factors in amyotrophic lateral sclerosis: a population based study.* J Neurol Neurosurg Psychiatry, 2008. **79**(1): p. 33-7.
26. Martin, S., A. Al Khleifat, and A. Al-Chalabi, *What causes amyotrophic lateral sclerosis?* F1000Research, 2017. **6**: p. 371.
27. Calvo, A., et al., *Factors predicting survival in ALS: a multicenter Italian study.* J Neurol, 2017. **264**(1): p. 54-63.
28. Czaplinski, A., A.A. Yen, and S.H. Appel, *Amyotrophic lateral sclerosis: early predictors of prolonged survival.* J Neurol, 2006. **253**(11): p. 1428-36.
29. Shoesmith, C.L., et al., *Prognosis of amyotrophic lateral sclerosis with respiratory onset.* J Neurol Neurosurg Psychiatry, 2007. **78**(6): p. 629-31.
30. Elamin, M., et al., *Executive dysfunction is a negative prognostic indicator in patients with ALS without dementia.* Neurology, 2011. **76**(14): p. 1263-9.
31. Moura, M.C., et al., *Prognostic Factors in Amyotrophic Lateral Sclerosis: A Population-Based Study.* PLoS One, 2015. **10**(10): p. e0141500.
32. Marin, B., et al., *Population-Based Evidence that Survival in Amyotrophic Lateral Sclerosis is Related to Weight Loss at Diagnosis.* Neurodegener Dis, 2016. **16**(3-4): p. 225-34.
33. Rosen, D.R., et al., *Mutations in Cu/Zn superoxide dismutase gene are associated with familial amyotrophic lateral sclerosis.* Nature, 1993. **362**(6415): p. 59-62.
34. Andersen, P.M., *Amyotrophic lateral sclerosis associated with mutations in the CuZn superoxide dismutase gene.* Curr Neurol Neurosci Rep, 2006. **6**(1): p. 37-46.
35. Chio, A., et al., *Prevalence of SOD1 mutations in the Italian ALS population.* Neurology, 2008. **70**(7): p. 533-7.
36. Chen, S., et al., *Genetics of amyotrophic lateral sclerosis: an update.* Molecular Neurodegeneration, 2013. **8**: p. 28-28.
37. Rakhit, R. and A. Chakrabartty, *Structure, folding, and misfolding of Cu,Zn superoxide dismutase in amyotrophic lateral sclerosis.* Biochimica et Biophysica Acta (BBA) - Molecular Basis of Disease, 2006. **1762**(11): p. 1025-1037.

38. Gurney, M.E., *The use of transgenic mouse models of amyotrophic lateral sclerosis in preclinical drug studies.* J Neurol Sci, 1997. **152 Suppl 1**: p. S67-73.
39. Valentine, J.S., P.A. Doucette, and S. Zittin Potter, *COPPER-ZINC SUPEROXIDE DISMUTASE AND AMYOTROPHIC LATERAL SCLEROSIS.* Annual Review of Biochemistry, 2005. **74**(1): p. 563-593.
40. Bunton-Stasyshyn, R.K.A., et al., *SOD1 Function and Its Implications for Amyotrophic Lateral Sclerosis Pathology.* The Neuroscientist, 2015. **21**(5): p. 519-529.
41. Sreedharan, J., et al., *TDP-43 mutations in familial and sporadic amyotrophic lateral sclerosis.* Science, 2008. **319**(5870): p. 1668-72.
42. Chio, A., et al., *Extensive genetics of ALS: a population-based study in Italy.* Neurology, 2012. **79**(19): p. 1983-9.
43. Harms, M., T. Miller, and R. Baloh, *TARDBP-Related Amyotrophic Lateral Sclerosis*, in *GeneReviews [Internet]*, M. Adam, H. Ardinger, and R. Pagon, Editors. 2009, University of Washington: Seattle (WA).
44. Kabashi, E., et al., *TARDBP mutations in individuals with sporadic and familial amyotrophic lateral sclerosis.* Nat Genet, 2008. **40**(5): p. 572-4.
45. Corcia, P., et al., *Phenotype and genotype analysis in amyotrophic lateral sclerosis with TARDBP gene mutations.* Neurology, 2012. **78**(19): p. 1519-26.
46. Ou, S.H., et al., *Cloning and characterization of a novel cellular protein, TDP-43, that binds to human immunodeficiency virus type 1 TAR DNA sequence motifs.* J Virol, 1995. **69**(6): p. 3584-96.
47. Winton, M.J., et al., *Disturbance of nuclear and cytoplasmic TAR DNA-binding protein (TDP-43) induces disease-like redistribution, sequestration, and aggregate formation.* J Biol Chem, 2008. **283**(19): p. 13302-9.
48. Diaper, D.C., et al., *Loss and gain of Drosophila TDP-43 impair synaptic efficacy and motor control leading to age-related neurodegeneration by loss-of-function phenotypes.* Hum Mol Genet, 2013. **22**(8): p. 1539-57.
49. Ayala, Y.M., et al., *TDP-43 regulates its mRNA levels through a negative feedback loop.* Embo j, 2011. **30**(2): p. 277-88.
50. Polymenidou, M., et al., *Long pre-mRNA depletion and RNA missplicing contribute to neuronal vulnerability from loss of TDP-43.* Nat Neurosci, 2011. **14**(4): p. 459-68.
51. Xu, Z.S., *Does a loss of TDP-43 function cause neurodegeneration?* Mol Neurodegener, 2012. **7**: p. 27.
52. Neumann, M., et al., *Ubiquitinated TDP-43 in frontotemporal lobar degeneration and amyotrophic lateral sclerosis.* Science, 2006. **314**(5796): p. 130-133.
53. McLaughlin, R.L., K.P. Kenna, and O. Hardiman, *Genetics of ALS*, in *Movement Disorder Genetics*, S.A. Schneider and J.M.T. Brás, Editors. 2015, Springer International Publishing: Cham. p. 385-409.
54. Renton, A.E., A. Chio, and B.J. Traynor, *State of play in amyotrophic lateral sclerosis genetics.* Nat Neurosci, 2014. **17**(1): p. 17-23.
55. Kwiatkowski, T.J., Jr., et al., *Mutations in the FUS/TLS gene on chromosome 16 cause familial amyotrophic lateral sclerosis.* Science, 2009. **323**(5918): p. 1205-8.
56. Vance, C., et al., *Mutations in FUS, an RNA processing protein, cause familial amyotrophic lateral sclerosis type 6.* Science, 2009. **323**(5918): p. 1208-1211.

57. Lanson, N.A., Jr. and U.B. Pandey, *FUS-related proteinopathies: lessons from animal models.* Brain Res, 2012. **1462**: p. 44-60.
58. Nolan, M., K. Talbot, and O. Ansorge, *Pathogenesis of FUS-associated ALS and FTD: insights from rodent models.* Acta Neuropathologica Communications, 2016. **4**(1): p. 99.
59. Kabashi, E., et al., *FUS and TARDBP but not SOD1 interact in genetic models of amyotrophic lateral sclerosis.* PLoS Genet, 2011. **7**(8): p. e1002214.
60. DeJesus-Hernandez, M., et al., *Expanded GGGGCC hexanucleotide repeat in noncoding region of C9ORF72 causes chromosome 9p-linked FTD and ALS.* Neuron, 2011. **72**(2): p. 245-56.
61. Renton, A.E., et al., *A hexanucleotide repeat expansion in C9ORF72 is the cause of chromosome 9p21-linked ALS-FTD.* Neuron, 2011. **72**.
62. Majounie, E., et al., *Frequency of the C9orf72 hexanucleotide repeat expansion in patients with amyotrophic lateral sclerosis and frontotemporal dementia: a cross-sectional study.* Lancet Neurol, 2012. **11**(4): p. 323-30.
63. Couratier, P., et al., *ALS and frontotemporal dementia belong to a common disease spectrum.* Rev Neurol (Paris), 2017. **173**(5): p. 273-279.
64. Cooper-Knock, J., P.J. Shaw, and J. Kirby, *The widening spectrum of C9ORF72-related disease; genotype/phenotype correlations and potential modifiers of clinical phenotype.* Acta Neuropathol, 2014. **127**(3): p. 333-45.
65. Haeusler, A.R., C.J. Donnelly, and J.D. Rothstein, *The expanding biology of the C9orf72 nucleotide repeat expansion in neurodegenerative disease.* Nat Rev Neurosci, 2016. **17**(6): p. 383-395.
66. Detmer, S.A. and D.C. Chan, *Functions and dysfunctions of mitochondrial dynamics.* Nat Rev Mol Cell Biol, 2007. **8**(11): p. 870-879.
67. Jaiswal, M.K., *Calcium, mitochondria, and the pathogenesis of ALS: the good, the bad, and the ugly.* Front Cell Neurosci, 2013. **7**: p. 199.
68. Bonafede, R. and R. Mariotti, *ALS Pathogenesis and Therapeutic Approaches: The Role of Mesenchymal Stem Cells and Extracellular Vesicles.* Front Cell Neurosci, 2017. **11**: p. 80.
69. Chung, M.J. and Y.L. Suh, *Ultrastructural changes of mitochondria in the skeletal muscle of patients with amyotrophic lateral sclerosis.* Ultrastruct Pathol, 2002. **26**(1): p. 3-7.
70. Echaniz-Laguna, A., et al., *Mitochondrial respiratory chain function in skeletal muscle of ALS patients.* Ann Neurol, 2002. **52**(5): p. 623-7.
71. Manfredi, G. and Z. Xu, *Mitochondrial dysfunction and its role in motor neuron degeneration in ALS.* Mitochondrion, 2005. **5**(2): p. 77-87.
72. Sasaki, S. and M. Iwata, *Mitochondrial alterations in the spinal cord of patients with sporadic amyotrophic lateral sclerosis.* J Neuropathol Exp Neurol, 2007. **66**(1): p. 10-6.
73. Vielhaber, S., et al., *Visualization of defective mitochondrial function in skeletal muscle fibers of patients with sporadic amyotrophic lateral sclerosis.* J Neurol Sci, 1999. **169**(1-2): p. 133-9.
74. Boillee, S., C. Vande Velde, and D.W. Cleveland, *ALS: a disease of motor neurons and their nonneuronal neighbors.* Neuron, 2006. **52**(1): p. 39-59.

75. Magrane, J. and G. Manfredi, *Mitochondrial function, morphology, and axonal transport in amyotrophic lateral sclerosis.* Antioxid Redox Signal, 2009. **11**(7): p. 1615-26.
76. Niciu, M.J., B. Kelmendi, and G. Sanacora, *Overview of glutamatergic neurotransmission in the nervous system.* Pharmacol Biochem Behav, 2012. **100**(4): p. 656-64.
77. Nakanishi, S., *Molecular diversity of glutamate receptors and implications for brain function.* Science, 1992. **258**(5082): p. 597-603.
78. Meldrum, B.S., *Glutamate as a neurotransmitter in the brain: review of physiology and pathology.* J Nutr, 2000. **130**(4S Suppl): p. 1007s-15s.
79. Shaw, P.J. and C.J. Eggett, *Molecular factors underlying selective vulnerability of motor neurons to neurodegeneration in amyotrophic lateral sclerosis.* J Neurol, 2000. **247 Suppl 1**: p. I17-27.
80. Lin, C.L., et al., *Aberrant RNA processing in a neurodegenerative disease: the cause for absent EAAT2, a glutamate transporter, in amyotrophic lateral sclerosis.* Neuron, 1998. **20**(3): p. 589-602.
81. Trotti, D., et al., *SOD1 mutants linked to amyotrophic lateral sclerosis selectively inactivate a glial glutamate transporter.* Nat Neurosci, 1999. **2**(5): p. 427-33.
82. Zarei, S., et al., *A comprehensive review of amyotrophic lateral sclerosis.* Surg Neurol Int, 2015. **6**: p. 171.
83. Rothstein, J.D., et al., *Abnormal excitatory amino acid metabolism in amyotrophic lateral sclerosis.* Ann Neurol, 1990. **28**(1): p. 18-25.
84. Rothstein, J.D., et al., *Beta-lactam antibiotics offer neuroprotection by increasing glutamate transporter expression.* Nature, 2005. **433**(7021): p. 73-7.
85. Beart, P.M. and R.D. O'Shea, *Transporters for L-glutamate: an update on their molecular pharmacology and pathological involvement.* Br J Pharmacol, 2007. **150**(1): p. 5-17.
86. Vucic, S., J.D. Rothstein, and M.C. Kiernan, *Advances in treating amyotrophic lateral sclerosis: insights from pathophysiological studies.* Trends Neurosci, 2014. **37**(8): p. 433-42.
87. Devasagayam, T.P., et al., *Free radicals and antioxidants in human health: current status and future prospects.* J Assoc Physicians India, 2004. **52**: p. 794-804.
88. Forsberg, K., et al., *Glial nuclear aggregates of superoxide dismutase-1 are regularly present in patients with amyotrophic lateral sclerosis.* Acta Neuropathol, 2011. **121**(5): p. 623-34.
89. Carri, M.T., et al., *Oxidative stress and mitochondrial damage: importance in non-SOD1 ALS.* Front Cell Neurosci, 2015. **9**: p. 41.
90. Simpson, E.P., et al., *Increased lipid peroxidation in sera of ALS patients: a potential biomarker of disease burden.* Neurology, 2004. **62**(10): p. 1758-65.
91. Smith, R.G., et al., *Presence of 4-hydroxynonenal in cerebrospinal fluid of patients with sporadic amyotrophic lateral sclerosis.* Ann Neurol, 1998. **44**(4): p. 696-9.
92. Beckman, J.S., et al., *Superoxide dismutase and the death of motoneurons in ALS.* Trends Neurosci, 2001. **24**(11 Suppl): p. S15-20.

93. Bacman, S.R., W.G. Bradley, and C.T. Moraes, *Mitochondrial involvement in amyotrophic lateral sclerosis: trigger or target?* Mol Neurobiol, 2006. **33**(2): p. 113-31.
94. Tohgi, H., et al., *Remarkable increase in cerebrospinal fluid 3-nitrotyrosine in patients with sporadic amyotrophic lateral sclerosis.* Ann Neurol, 1999. **46**(1): p. 129-31.
95. Engelen-Lee, J., et al., *Proteomic profiling of the spinal cord in ALS: decreased ATP5D levels suggest synaptic dysfunction in ALS pathogenesis.* Amyotroph Lateral Scler Frontotemporal Degener, 2017. **18**(3-4): p. 210-220.
96. Kamelgarn, M., et al., *Proteomic analysis of FUS interacting proteins provides insights into FUS function and its role in ALS.* Biochim Biophys Acta, 2016. **1862**(10): p. 2004-14.
97. Blokhuis, A.M., et al., *Comparative interactomics analysis of different ALS-associated proteins identifies converging molecular pathways.* Acta Neuropathol, 2016. **132**(2): p. 175-96.
98. Chen, Y., et al., *Proteomic analysis of cerebrospinal fluid in amyotrophic lateral sclerosis.* Exp Ther Med, 2016. **11**(6): p. 2095-2106.
99. Hanrieder, J., et al., *MALDI imaging of post-mortem human spinal cord in amyotrophic lateral sclerosis.* J Neurochem, 2013. **124**(5): p. 695-707.
100. Zhou, J.-Y., et al., *Galectin-3 is a candidate biomarker for amyotrophic lateral sclerosis: discovery by a proteomics approach.* Journal of proteome research, 2010. **9**(10): p. 5133-5141.
101. Bergemalm, D., et al., *Changes in the Spinal Cord Proteome of an Amyotrophic Lateral Sclerosis Murine Model Determined by Differential In-gel Electrophoresis.* Molecular & Cellular Proteomics : MCP, 2009. **8**(6): p. 1306-1317.
102. Vucic, S., J.D. Rothstein, and M.C. Kiernan, *Advances in treating amyotrophic lateral sclerosis: insights from pathophysiological studies.* Trends in neurosciences, 2014. **37**(8): p. 433-442.
103. Weishaupt, J.H., T. Hyman, and I. Dikic, *Common Molecular Pathways in Amyotrophic Lateral Sclerosis and Frontotemporal Dementia.* Trends in molecular medicine, 2016. **22**(9): p. 769-783.
104. Arnold, E.S., et al., *ALS-linked TDP-43 mutations produce aberrant RNA splicing and adult-onset motor neuron disease without aggregation or loss of nuclear TDP-43.* Proceedings of the National Academy of Sciences, 2013. **110**(8): p. E736-E745.
105. Igaz, L.M., et al., *Dysregulation of the ALS-associated gene TDP-43 leads to neuronal death and degeneration in mice.* The Journal of clinical investigation, 2011. **121**(2): p. 726-738.
106. Ling, S.-C., M. Polymenidou, and D.W. Cleveland, *Converging mechanisms in ALS and FTD: disrupted RNA and protein homeostasis.* Neuron, 2013. **79**(3): p. 416-438.
107. Tan, R.H., et al., *ALS/FTLD: experimental models and reality.* Acta Neuropathologica, 2017: p. 1-20.

108. Walker, A.K., et al., *Functional recovery in new mouse models of ALS/FTLD after clearance of pathological cytoplasmic TDP-43.* Acta neuropathologica, 2015. **130**(5): p. 643-660.
109. *Reorganizing the protein space at the Universal Protein Resource (UniProt).* Nucleic Acids Res, 2012. **40**(Database issue): p. D71-5.
110. Bardou, P., et al., *jvenn: an interactive Venn diagram viewer.* BMC Bioinformatics, 2014. **15**(1): p. 293.
111. Malsam, J. and T.H. Söllner, *Organization of SNAREs within the Golgi Stack.* Cold Spring Harbor Perspectives in Biology, 2011. **3**(10): p. a005249.
112. Funayama, M., et al., *CHCHD2 mutations in autosomal dominant late-onset Parkinson's disease: a genome-wide linkage and sequencing study.* Lancet Neurol, 2015. **14**(3): p. 274-82.
113. Shen, S., et al., *CHCHD10 mutations in patients with amyotrophic lateral sclerosis in Mainland China.* Neurobiol Aging, 2017. **54**: p. 214.e7-214.e10.
114. Perrone, F., et al., *Investigating the role of ALS genes CHCHD10 and TUBA4A in Belgian FTD-ALS spectrum patients.* Neurobiology of Aging, 2017. **51**(Supplement C): p. 177.e9-177.e16.
115. Woo, J.A., et al., *Loss of function CHCHD10 mutations in cytoplasmic TDP-43 accumulation and synaptic integrity.* Nat Commun, 2017. **8**: p. 15558.
116. Vaags, A.K., et al., *Absent CNKSR2 causes seizures and intellectual, attention, and language deficits.* Ann Neurol, 2014. **76**(5): p. 758-64.
117. Houge, G., I.H. Rasmussen, and R. Hovland, *Loss-of-Function CNKSR2 Mutation Is a Likely Cause of Non-Syndromic X-Linked Intellectual Disability.* Molecular Syndromology, 2012. **2**(2): p. 60-63.
118. Lain, E., et al., *A novel role for embigin to promote sprouting of motor nerve terminals at the neuromuscular junction.* J Biol Chem, 2009. **284**(13): p. 8930-9.
119. Harashima, S., et al., *Purkinje cell protein 4 positively regulates neurite outgrowth and neurotransmitter release.* J Neurosci Res, 2011. **89**(10): p. 1519-30.
120. Recabarren, D. and M. Alarcón, *Gene networks in neurodegenerative disorders.* Life Sciences, 2017. **183**(Supplement C): p. 83-97.
121. Ziai, R., et al., *Isolation, sequence, and developmental profile of a brain-specific polypeptide, PEP-19.* Proceedings of the National Academy of Sciences, 1986. **83**(21): p. 8420-8423.
122. Figueroa-Romero, C., et al., *Identification of epigenetically altered genes in sporadic amyotrophic lateral sclerosis.* PLoS One, 2012. **7**(12): p. e52672.
123. Chin, M.H., et al., *Mitochondrial dysfunction, oxidative stress, and apoptosis revealed by proteomic and transcriptomic analyses of the striata in two mouse models of Parkinson's disease.* J Proteome Res, 2008. **7**(2): p. 666-77.
124. Lederer, C.W., et al., *Pathways and genes differentially expressed in the motor cortex of patients with sporadic amyotrophic lateral sclerosis.* BMC Genomics, 2007. **8**: p. 26-26.
125. Hoogenraad, N.J., L.A. Ward, and M.T. Ryan, *Import and assembly of proteins into mitochondria of mammalian cells.* Biochimica et Biophysica Acta (BBA) - Molecular Cell Research, 2002. **1592**(1): p. 97-105.

126. Wang, C. and R.J. Youle, *The Role of Mitochondria in Apoptosis.* Annual review of genetics, 2009. **43**: p. 95-118.
127. Maglott, D., et al., *Entrez Gene: gene-centered information at NCBI.* Nucleic Acids Res, 2005. **33**(Database issue): p. D54-8.
128. Slemmon, J.R., et al., *Increased levels of hemoglobin-derived and other peptides in Alzheimer's disease cerebellum.* J Neurosci, 1994. **14**(4): p. 2225-35.
129. Adlard, P.A., et al., *Cognitive loss in zinc transporter-3 knock-out mice: a phenocopy for the synaptic and memory deficits of Alzheimer's disease?* J Neurosci, 2010. **30**(5): p. 1631-6.
130. Kuhn, A., et al., *Mutant huntingtin's effects on striatal gene expression in mice recapitulate changes observed in human Huntington's disease brain and do not differ with mutant huntingtin length or wild-type huntingtin dosage.* Hum Mol Genet, 2007. **16**(15): p. 1845-61. Epub 2007 May 21.
131. Cozzolino, M. and M.T. Carri, *Mitochondrial dysfunction in ALS.* Prog Neurobiol, 2012. **97**(2): p. 54-66.
132. Nunnari, J. and A. Suomalainen, *Mitochondria: in sickness and in health.* Cell, 2012. **148**(6): p. 1145-59.
133. Wang, W., et al., *The Inhibition of TDP-43 Mitochondrial Localization Blocks Its Neuronal Toxicity.* Nature medicine, 2016. **22**(8): p. 869-878.
134. Lohman, D.C., et al., *Mitochondrial COQ9 is a lipid-binding protein that associates with COQ7 to enable coenzyme Q biosynthesis.* Proceedings of the National Academy of Sciences of the United States of America, 2014. **111**(44): p. E4697-E4705.
135. Acosta, M.J., et al., *Coenzyme Q biosynthesis in health and disease.* Biochimica et Biophysica Acta (BBA) - Bioenergetics, 2016. **1857**(8): p. 1079-1085.
136. He, C.H., et al., *Yeast Coq9 controls deamination of coenzyme Q intermediates that derive from para-aminobenzoic acid.* Biochim Biophys Acta, 2015. **1851**(9): p. 1227-39.
137. He, C.H., et al., *Human COQ9 Rescues a coq9 Yeast Mutant by Enhancing Coenzyme Q Biosynthesis from 4-Hydroxybenzoic Acid and Stabilizing the CoQ-Synthome.* Front Physiol, 2017. **8**: p. 463.
138. Garcia-Corzo, L., et al., *Dysfunctional Coq9 protein causes predominant encephalomyopathy associated with CoQ deficiency.* Hum Mol Genet, 2013. **22**(6): p. 1233-48.
139. Sohmiya, M., et al., *An increase of oxidized coenzyme Q-10 occurs in the plasma of sporadic ALS patients.* J Neurol Sci, 2005. **228**(1): p. 49-53.
140. Murata, T., C. Ohtsuka, and Y. Terayama, *Increased mitochondrial oxidative damage in patients with sporadic amyotrophic lateral sclerosis.* J Neurol Sci, 2008. **267**(1-2): p. 66-9.
141. Lucchetti, J., et al., *A Mouse Model of Familial ALS Has Increased CNS Levels of Endogenous Ubiquinol(9/10) and Does Not Benefit from Exogenous Administration of Ubiquinol(10).* PLoS ONE, 2013. **8**(7): p. e69540.
142. Kaufmann, P., et al., *Phase II trial of CoQ10 for ALS finds insufficient evidence to justify phase III.* Ann Neurol, 2009. **66**(2): p. 235-44.
143. Bluthgen, N. and S. Legewie, *Robustness of signal transduction pathways.* Cell Mol Life Sci, 2013. **70**(13): p. 2259-69.

144. Patel, V.P. and C.T. Chu, *Nuclear transport, oxidative stress, and neurodegeneration.* International Journal of Clinical and Experimental Pathology, 2011. **4**(3): p. 215-229.
145. Bito, H. and S. Takemoto-Kimura, *Ca(2+)/CREB/CBP-dependent gene regulation: a shared mechanism critical in long-term synaptic plasticity and neuronal survival.* Cell Calcium, 2003. **34**(4-5): p. 425-30.
146. Sorokin, A.V., E.R. Kim, and L.P. Ovchinnikov, *Nucleocytoplasmic transport of proteins.* Biochemistry (Mosc), 2007. **72**(13): p. 1439-57.
147. Gorlich, D., *Transport into and out of the cell nucleus.* Embo j, 1998. **17**(10): p. 2721-7.
148. Zhang, J., et al., *Altered distributions of nucleocytoplasmic transport-related proteins in the spinal cord of a mouse model of amyotrophic lateral sclerosis.* Acta Neuropathol, 2006. **112**(6): p. 673-80.
149. Nishimura, A.L., et al., *Nuclear import impairment causes cytoplasmic trans-activation response DNA-binding protein accumulation and is associated with frontotemporal lobar degeneration.* Brain, 2010. **133**(Pt 6): p. 1763-71.
150. Ambron, R.T., et al., *A signal sequence mediates the retrograde transport of proteins from the axon periphery to the cell body and then into the nucleus.* J Neurosci, 1992. **12**(7): p. 2813-8.
151. Schmied, R., et al., *Endogenous axoplasmic proteins and proteins containing nuclear localization signal sequences use the retrograde axonal transport/nuclear import pathway in Aplysia neurons.* J Neurosci, 1993. **13**(9): p. 4064-71.
152. Hanz, S., et al., *Axoplasmic importins enable retrograde injury signaling in lesioned nerve.* Neuron, 2003. **40**(6): p. 1095-104.
153. Yudin, D., et al., *Localized regulation of axonal RanGTPase controls retrograde injury signaling in peripheral nerve.* Neuron, 2008. **59**(2): p. 241-52.
154. Lever, M.B., A. Karpova, and M.R. Kreutz, *An Importin Code in neuronal transport from synapse-to-nucleus?* Frontiers in Molecular Neuroscience, 2015. **8**: p. 33.
155. Julien, J.P., S. Millecamps, and J. Kriz, *Cytoskeletal defects in amyotrophic lateral sclerosis (motor neuron disease).* Novartis Found Symp, 2005. **264**: p. 183-92; discussion 192-6, 227-30.
156. Laird, F.M., et al., *Motor neuron disease occurring in a mutant dynactin mouse model is characterized by defects in vesicular trafficking.* J Neurosci, 2008. **28**(9): p. 1997-2005.
157. Di Domenico, F., et al., *Quantitative proteomics analysis of phosphorylated proteins in the hippocampus of Alzheimer's disease subjects.* J Proteomics, 2011. **74**(7): p. 1091-103.
158. Licker, V., et al., *Proteomic profiling of the substantia nigra demonstrates CNDP2 overexpression in Parkinson's disease.* J Proteomics, 2012. **75**(15): p. 4656-67.
159. Lin, M.T. and M.F. Beal, *Mitochondrial dysfunction and oxidative stress in neurodegenerative diseases.* Nature, 2006. **443**(7113): p. 787-795.
160. Rodolfo, C., et al., *Proteomic analysis of mitochondrial dysfunction in neurodegenerative diseases.* Expert Rev Proteomics, 2010. **7**(4): p. 519-42.

161. Zabel, C., et al., *A large number of protein expression changes occur early in life and precede phenotype onset in a mouse model for huntington disease.* Mol Cell Proteomics, 2009. **8**(4): p. 720-34.
162. Van Damme, P., W. Robberecht, and L. Van Den Bosch, *Modelling amyotrophic lateral sclerosis: progress and possibilities.* Dis Model Mech, 2017. **10**(5): p. 537-549.
163. Pal, R., et al., *New Insight into Neurodegeneration: the Role of Proteomics.* Molecular Neurobiology, 2014. **49**(3): p. 1181-1199.
164. Pal, R., J.P. Larsen, and S.G. Moller, *The Potential of Proteomics in Understanding Neurodegeneration.* Int Rev Neurobiol, 2015. **121**: p. 25-58.
165. Murray, G.I., *An overview of laser microdissection technologies.* Acta Histochem, 2007. **109**(3): p. 171-6.
166. Plum, S., et al., *Proteomics in neurodegenerative diseases: Methods for obtaining a closer look at the neuronal proteome.* PROTEOMICS – Clinical Applications, 2015. **9**(9-10): p. 848-871.
167. Nardo, G., et al., *Transcriptomic indices of fast and slow disease progression in two mouse models of amyotrophic lateral sclerosis.* Brain, 2013. **136**(11): p. 3305-3332.
168. Woodrow, L., P. Sheppard, and P.F. Gardiner, *Transcriptional changes in rat α-motoneurons resulting from increased physical activity.* Neuroscience, 2013. **255**: p. 45-54.
169. Boone, D.R., S.L. Sell, and H.L. Hellmich, *Laser Capture Microdissection of Enriched Populations of Neurons or Single Neurons for Gene Expression Analysis After Traumatic Brain Injury.* Journal of Visualized Experiments : JoVE, 2013(74): p. 50308.
170. Minjarez, B., et al., *Identification of polypeptides in neurofibrillary tangles and total homogenates of brains with Alzheimer's disease by tandem mass spectrometry.* J Alzheimers Dis, 2013. **34**(1): p. 239-62.
171. Hashimoto, M., et al., *Analysis of microdissected neurons by 18O mass spectrometry reveals altered protein expression in Alzheimer's disease.* J Cell Mol Med, 2012. **16**(8): p. 1686-700.
172. Kunz, G.M., Jr. and D.W. Chan, *The use of laser capture microscopy in proteomics research--a review.* Dis Markers, 2004. **20**(3): p. 155-60.
173. Yu, C. and L. Cohen, *Tissue sample preparation-not the same old grind*. 2004, ADVANSTAR COMMUNICATIONS 131 W FIRST ST, DULUTH, MN 55802 USA.
174. Unlu, M., M.E. Morgan, and J.S. Minden, *Difference gel electrophoresis: a single gel method for detecting changes in protein extracts.* Electrophoresis, 1997. **18**(11): p. 2071-7.
175. Boysen, R.I. and M.T. Hearn, *HPLC of peptides and proteins.* Current Protocols in Protein Science, 2001: p. 8.7. 1-8.7. 40.
176. Boysen, R.I. and M.T.W. Hearn, *HPLC of Peptides and Proteins: Standard Operating Conditions*, in *Current Protocols in Molecular Biology*. 2001, John Wiley & Sons, Inc.
177. Minden, J.S., et al., *Difference gel electrophoresis.* Electrophoresis, 2009. **30 Suppl 1**: p. S156-61.

178. Ho, C.S., et al., *Electrospray ionisation mass spectrometry: principles and clinical applications.* Clin Biochem Rev, 2003. **24**(1): p. 3-12.
179. Mann, M., R.C. Hendrickson, and A. Pandey, *Analysis of proteins and proteomes by mass spectrometry.* Annu Rev Biochem, 2001. **70**: p. 437-73.
180. Anjo, S.I., C. Santa, and B. Manadas, *SWATH-MS as a tool for biomarker discovery: From basic research to clinical applications.* PROTEOMICS, 2017. **17**(3-4): p. 1600278-n/a.
181. Gillet, L.C., et al., *Targeted data extraction of the MS/MS spectra generated by data-independent acquisition: a new concept for consistent and accurate proteome analysis.* Mol Cell Proteomics, 2012. **11**(6): p. O111.016717.
182. Huang, Q., et al., *SWATH enables precise label-free quantification on proteome scale.* PROTEOMICS, 2015. **15**(7): p. 1215-1223.
183. Liu, Y., et al., *Mass spectrometric protein maps for biomarker discovery and clinical research.* Expert Rev Mol Diagn, 2013. **13**(8): p. 811-25.
184. Guo, T., et al., *Rapid mass spectrometric conversion of tissue biopsy samples into permanent quantitative digital proteome maps.* Nat Med, 2015. **21**(4): p. 407-13.
185. Zawadzka, A.M., et al., *Variation and quantification among a target set of phosphopeptides in human plasma by multiple reaction monitoring and SWATH-MS2 data-independent acquisition.* Electrophoresis, 2014. **35**(24): p. 3487-97.
186. Craft, G.E., A. Chen, and A.C. Nairn, *Recent advances in quantitative neuroproteomics.* Methods, 2013. **61**(3): p. 186-218.
187. Laukens, K., S. Naulaerts, and W.V. Berghe, *Bioinformatics approaches for the functional interpretation of protein lists: from ontology term enrichment to network analysis.* Proteomics, 2015. **15**(5-6): p. 981-96.
188. Mirzaei, M., et al., *Applications of Quantitative Proteomics in Plant Research*, in *Agricultural Proteomics Volume 1: Crops, Horticulture, Farm Animals, Food, Insect and Microorganisms*, G.H. Salekdeh, Editor. 2016, Springer International Publishing: Cham. p. 1-29.
189. Kumar, C. and M. Mann, *Bioinformatics analysis of mass spectrometry-based proteomics data sets.* FEBS Lett, 2009. **583**(11): p. 1703-12.
190. Malik, R., et al., *From proteome lists to biological impact--tools and strategies for the analysis of large MS data sets.* Proteomics, 2010. **10**(6): p. 1270-83.
191. Matthiesen, R., et al., *Discussion on common data analysis strategies used in MS-based proteomics.* Proteomics, 2011. **11**(4): p. 604-19.
192. Goh, W.W. and L. Wong, *Computational proteomics: designing a comprehensive analytical strategy.* Drug Discov Today, 2014. **19**(3): p. 266-74.
193. Pruitt, K.D., et al., *RefSeq: an update on mammalian reference sequences.* Nucleic Acids Res, 2014. **42**(Database issue): p. D756-63.
194. Carnielli, C.M., F.V. Winck, and A.F. Paes Leme, *Functional annotation and biological interpretation of proteomics data.* Biochim Biophys Acta, 2015. **1854**(1): p. 46-54.
195. Bessarabova, M., et al., *Knowledge-based analysis of proteomics data.* BMC Bioinformatics, 2012. **13 Suppl 16**: p. S13.
196. Nikolsky, Y., et al., *Functional analysis of OMICs data and small molecule compounds in an integrated "knowledge-based" platform.* Methods Mol Biol, 2009. **563**: p. 177-96.

197. Palagi, P.M., et al., *Proteome informatics I: bioinformatics tools for processing experimental data.* Proteomics, 2006. **6**(20): p. 5435-44.
198. Curtis, R.K., M. Oresic, and A. Vidal-Puig, *Pathways to the analysis of microarray data.* Trends Biotechnol, 2005. **23**(8): p. 429-35.
199. Werner, T., *Bioinformatics applications for pathway analysis of microarray data.* Curr Opin Biotechnol, 2008. **19**(1): p. 50-4.
200. Schwanhausser, B., et al., *Global quantification of mammalian gene expression control.* Nature, 2011. **473**(7347): p. 337-42.
201. Zubarev, R.A., *The challenge of the proteome dynamic range and its implications for in-depth proteomics.* Proteomics, 2013. **13**(5): p. 723-6.
202. Gawron, D., K. Gevaert, and P. Van Damme, *The proteome under translational control.* Proteomics, 2014. **14**(23-24): p. 2647-62.
203. Goh, W.W.B., et al., *How advancement in biological network analysis methods empowers proteomics.* PROTEOMICS, 2012. **12**(4-5): p. 550-563.
204. Goh, W.W.B., et al., *Proteomics Signature Profiling (PSP): A Novel Contextualization Approach for Cancer Proteomics.* Journal of Proteome Research, 2012. **11**(3): p. 1571-1581.
205. Padula, M., et al., *A Comprehensive Guide for Performing Sample Preparation and Top-Down Protein Analysis.* Proteomes, 2017. **5**(2): p. 11.
206. Christoforou, A. and K.S. Lilley, *Taming the isobaric tagging elephant in the room in quantitative proteomics.* Nat Meth, 2011. **8**(11): p. 911-913.
207. Louie, B., R. Higdon, and E. Kolker, *The necessity of adjusting tests of protein category enrichment in discovery proteomics.* Bioinformatics, 2010. **26**(24): p. 3007-11.